A thesis submitted for the degree of Doctor of Philosophy

Discovering the Function of IFI44, a Hallmark Interferon-Stimulated Gene

Elizabeth Horton

Trinity 2024



Wolfson College
Weatherall Institute of Molecular Medicine
University of Oxford

Supervisor: Professor Jan Rehwinkel
Co-supervisor: Professor Hal Drakesmith

Abstract

The innate immune response is the first line of defence against infection, acting to reduce the replication and spread of pathogens throughout the body along with activating and guiding the adaptive immune response. As a part of this, cells induce cell-autonomous immunity whereby they non-specifically sense the presence of intracellular invaders, such as viruses, and respond. One such response is the secretion of interferons (IFNs) – a class of cellular signalling molecules (or cytokines) that can mediate multiple anti-viral effects. The anti-viral effects of type I IFNs are predominantly mediated by a class of genes called IFN-stimulated genes (ISGs). The protein products of some ISGs inhibit virus entry, replication or egress. ISGs thus play a vital role in the immune response against viral pathogens. However, while there are hundreds of ISGs, only a few have been well-characterised.

IFI44 is a prototypical ISG, conserved from molluscs to humans. *IFI44* is highly expressed in most cell types in response to type I IFN stimulation, such as during pathogen infection and in patients with type I interferonopathies. As such, *IFI44* is used as a biomarker for systemic lupus erythematosus (SLE). Next to *IFI44* on chromosome one is *IFI44L*, which likely arose as a consequence of gene duplication, and is also highly conserved. *IFI44L* shows the same expression patterns as *IFI44* and has an equally undefined role. These observations indicate that the IFI44 and IFI44L proteins have important, yet unknown, molecular functions. In this study, I discovered a surprising role for IFI44 in mediating erythrocyte, and therefore iron, homeostasis. I further observed that vaccinia virus cleaves IFI44 and IFI44L, which may indicate viral antagonism of an uncharacterised antiviral activity.

Using a total *Ifi44* and *Ifi44l* knock-out mouse model through deleting *Ifi44* in C57BL/6 mice which naturally lack *Ifi44l*, I identified that *Ifi44l* knock-out results in the dysregulation of iron biosynthesis and iron recycling. Genes involved in the haem biosynthetic pathway (e.g. *Urod*, *Uros*, *Sptb*) and in erythroid homeostasis (e.g. *Hmox1*, *Slc40a1*, *Cd163*) were downregulated in *Ifi44*$^{-/-}$ splenocytes. In addition, *Ifi44*$^{-/-}$ mice displayed a mild microcytic anaemia. This could not be attributed to defective erythropoiesis, as the

erythroid precursor populations of *Ifi44*$^{-/-}$ mice remained indistinguishable from those of *Ifi44*$^{+/+}$ mice. However, *Ifi44*$^{-/-}$ mice showed a marked reduction in splenic erythrophagocytic red pulp macrophage (RPM) populations, and *Ifi44*$^{-/-}$ RPMs expressed significantly less surface CD163. As CD163 is a haem scavenger receptor, this indicated that *Ifi44*$^{-/-}$ RPMs were less efficient at recycling erythrocytes, and therefore iron. I hypothesised that a reduction in erythrophagocytosis would lead to increased intravascular haemolysis, and consequently splenic iron loading. Confirming this, *Ifi44*$^{-/-}$ mice had increased insoluble iron deposits in their spleens. Hydroxyl radicals can result from iron catalysing the Fenton reaction, and this can induce cell death. Interestingly, bone marrow derived macrophages (BMDMs) from *Ifi44*$^{-/-}$ mice were more susceptible to cell death induced by haem *in vitro*, indicating that *Ifi44* is protective against oxidative stress-induced cell death in macrophages. Finally, I found that *Ifi44*$^{-/-}$ mice had a delayed recovery in response to experimentally induced haemolytic anaemia.

Taken together, I postulate that IFI44 may be protective against ferroptosis in RPMs, and when IFI44 is not present, there is a dysregulation of iron recycling. This work contributes to fundamental knowledge of systemic iron homeostasis, and I identified a previously uncharacterised role for an ISG in mediating iron homeostasis.

This thesis has a word count of 40,798 words.

Acknowledgements

First and foremost, I would like to acknowledge my overall supervisor, Jan Rehwinkel. Jan has provided me with expert guidance on not only how to thrive as a D.Phil student, but how to flourish and grow as a scientist. Jan is endlessly patient, kind, and an exceptionally committed mentor and role model, without whom this project, and my development as a scientist, would not be where it is today. I thank Jan for the freedom to drive my own project, along with guidance and support for when I was unsure. Jan has created an environment within his lab built on collaboration, respect and trust – and it has been a tremendous pleasure to carry out my D.Phil here.

Next, I acknowledge my day-to-day supervisor Rachel Rigby, who provided me with the tools and skills necessary for completion of a D.Phil in immunology, along with friendship. I will carry Rachel's "lab hacks" with me into my next positions, alongside everything else she taught me.

Further, I'd like to acknowledge Rehwinkel lab members, past (Jonny Hertzog, Natalia Sampaio, Rachel Rigby, Henry Blest, Valerie Odon, Isobel Davis and Sarah Choi) and present (Anne Bridgeman, Anna Rozina, Svea Wupper, Tanja Davis, Alex Fedorov, Alex Redmond and Gerissa Fowler) for their wonderful support and camaraderie. Everyone in the lab contributed direct scientific inputs to my work, both intellectually and physically. In particular, I'd like to thank Rachel, Anne, Alex R and Tanja for help with *in vivo* studies and Rachel, Tanja and Alex F for bioinformatic analysis. Tanja, my bench-mate, is an exceptionally talented scientist and provided much technical advice (and buffers) throughout. Gerissa started her D.Phil at the same time as me, and has been a true friend and sounding board from start to finish. Anne is a beacon of knowledge for any and every technique, and has provided invaluable insight, advice and aid. Henry helped to both generate hypotheses and methods to test them, and has very much been missed since he graduated. I am grateful to have been able to supervise Isobel Davis, a very talented MSc student, and Sarah Choi, a dedicated undergraduate student. Both Isobel and Sarah contributed key experiments to the project: Sarah in validating knock-down cell lines, and Isobel in cloning IFI44/L into pcDNA vectors and performing many immunoprecipitations

to determine whether they interact. I am very grateful for their dedication and effort.

To Hal Drakesmith, my co-supervisor, who is a Professor in Iron Biology and provided invaluable advice and guidance on the iron-related experiments that I performed. Hal and his lab, namely Megan Teh, Dana Costigan, Alexandra Preston, Andrew Armitage, Shamsideen Yusuf and Hannah Murray, were integral to aiding me in navigating haematological waters through supply of protocols, reagents, technical advice and interpretation of results. Hal was additionally on my thesis committee, along with Lynn Dustin, both of whom provided scientific input, advice and encouragement throughout.

Collaboration is integral to driving forward scientific research, and I have been very lucky to collaborate with some remarkable scientists. Adan Pinto Fernandez, who collaborated on the ISGylation experiments and mass spectrometry experiment. Iolanda Vendrell, Roman Fischer and Benedikt Kessler at the Target Discovery Institute also contributed to these mass spectroscopy experiments. Tiong (Jack) Tan and Alain Townsend provided IAV/X-31, training in microneutralisation assays and *in vivo* infections. Nasullah Khalid Alham performed quantification of histological staining. Geoff Smith provided VACV mutant viruses, alongside intellectual input and insight into optimising these experiments. Petr Broz and Vanessa Mack very kindly performed bacterial challenge assays in our BMDMs. To all these scientists, I am very thankful for their contributions.

I would like to thank the WIMM DPhil Studentship, and by proxy the MRC, for funding myself and my tuition, and allowing me to undertake this DPhil.

Next, I'd like to thank the IMMposters band, who have provided an outlet for creativity and energy, and also provided academic insights and career advice during rehearsals. The IMMposters are Doug Higgs, Chris Norbury, Steve Kelly, Alex Sternberg, Paul Bowness, Paul Klenerman, Olana Peters and Richard Wheeler.

A strong support network is integral for success, and I am very grateful for mine. Specifically, I'd like to thank my Wolfson friends Catherine Wormald, Jan Grohn, Munim Syed, Jessica Rahardjo and Oana Diaconescu, University of Sheffield friends Georgie Simpson, Kerrie Harbidge and Katie Coxon, my school friend Kirsty Mitchell and my best friend since I was five years old, Juliana Hauswirth along with her husband, Kai Hauswirth and her mum, Victoria Sawma. Particularly, I'd like to thank my flatmate Nameerah Khan, who has witnessed every high and every low and provided advice, friendship and support throughout - as well as expert formatting advice and solutions. In addition, I'd like to thank my sisters, Helena Horton and Becky Hands, my brother-in-law Nick Hands, and my nephew, Barnabas Hands for providing unconditional love, support, sanity, encouragement, proof-reading and food (pre-chewed in the case of Barney).

Finally, I'd like to dedicate this thesis to my parents, Claire and Robin Horton. My

parents are a source of comfort and stability, and they believe in my abilities even when I doubt them myself. They are my constant cheerleaders. Their uplifting support and encouragement have enabled me to navigate the hardships and celebrate the wins. They lead by example, and I hope I can follow in their footsteps throughout my life.

COVID-19 Statement

This study commenced during the COVID-19 pandemic in October 2020. Numerous governmental lockdowns and restrictions resulted in reduced access to the lab, limited hands-on supervision and a lack of face-to-face meetings with my supervisors and peers. This culminated in experiments taking longer to complete, acquiring skills being more difficult and reduced access to timely feedback. As such, during the first year and a half of my D.Phil, my scientific development was much slower than if there were not these restrictions in place, and there was less progress made with my project. To this end, at the end of my D.Phil, time was a very limiting factor. Due to this, some experiments could not be repeated three times, as I had to prioritise certain assays and experiments over others.

Acronyms

Absent in melanoma 2 (AIM2)-like receptors - ALRs
Adenosine deaminase acting on RNA 1 - ADAR1
Amyotrophic lateral sclerosis – ALS
Anaemia of inflammation - AoI
Antioxidant response element - ARE
Autism spectrum disorder - ASD
Baby hamster kidney cells - BHKs
Biliverdin reductase - BVR
Bone morphogenetic protein - BMP
Bone marrow derived macrophages - BMDMs
BTB domain and CNC homologue 1 - BACH1
C-type lectin receptors – CLRs
Carboxy-terminal domain – CTD
Caspase activation and recruitment domains - CARDs
Crystal violet – CV
Cyclic GMP-AMP – cGAMP Danger-associated molecular patterns – DAMPs
Dendritic cells – DCs
Deoxynucleoside triphosphates – dNTPs
Disintegrin and metalloproteinase 17 - ADAM17
Drebrin - DBN1
Dulbecco's modified Eagle medium - DMEM
Empty vector – EV
Encephalomyocarditis virus - EMCV
Endoplasmic reticulum – ER
Endosomal sorting complexes required for transport III - ESCRT-III
Erythroblastic islands – EBIs
Erythropoietin - EPO
Erythropoietin receptor – EPOR
Ferroportin - FPN

Ferroptosis suppressor protein 1 - FSP1
FK506 binding protein 51 - FKBP5 Gamma-activated sequences - GASs
Glutathione peroxidase 4 - GPX4
Green fluorescent protein – GFP
Guansine-5'-triphosphate - GTP
Haematopoietic stem and progenitor cells - HSPCs
Haematopoietic stem cells - HSCs
Heme Oxygenase 1 - HMOX1 Heme-responsive gene 1 - HRG1
Human embryonic kidney - HEK
Hepatitis C virus – HCV
Herpes simplex virus – HSV
Horse radish peroxidase (HRP)
Human embryonic kidney – HEK
Human foreskin fibroblasts – HFFs
Human immunodeficiency virus 1 - HIV-1
IL-1R-activated kinase-4 - IRAK4
Immunoglobulin G - IgG
Immunoprecipitation – IP
Influenza A Virus – IAV
Interferon – IFN
Interferon response elements - ISREs
Interferon-induced protein 44 - IFI44
Interferon-induced protein 44-like - IFI44L
Interferon-induced protein with tetratricopeptide repeats – IFIT
Interferon-induced transmembrane – IFITM
Interferon-stimulated genes - ISGs
Interleukin-10 - IL-10
Iron-regulatory protein - IRP
Iron-responsive element - IRE
Janus kinase–signal transducer and activator of transcription – JAK-STAT
Kaposi's Sarcoma-Associated Herpesvirus – KSHV
Kelch-like ECH-associated protein 1 - KEAP1
Kupffer Cells – KCs
Lactate dehydrogenase - LDH
Laboratory of genetics and physiology 2 - LGP2
Leucine-rich repeat - LRR
Lipopolysaccharide – LPS
Lower respiratory tract infections - LRTIs

Lymphocyte antigen 6 complex, locus C1 - Ly6C
Lymphocytic choriomeningitis virus - LCMV
Mammalian/mechanistic target of rapamycin - mTOR
Mean corpuscular haemoglobin - MCH
Mean corpuscular volume - MCV
Melanoma differentiation-associated protein 5 - MDA5
Mitochondrial antiviral signalling protein – MAVS
Mitogen-activated protein kinase/extracellular signal-regulated kinase -MAPK/ERK
Mouse embryonic fibroblasts – MEFs
MTOR-associated protein, eak-7 homolog - MEAK7
Multiplicity of infection - MOI
Myeloid differentiation primary response 88 - MyD88
Myxovirus resistance – Mx
Natural Killer cells – NKs
NOD-like receptors - NLRs
Nuclear factor erythroid 2-related factor 2 - NRF2
Nuclear factor kappa-light-chain-enhancer of activated B cells (NF-κB)
Nuclear receptor coactivator protein 7 - NCOA7
Nucleic acids – NAs
Oligoadenylate synthetase - OAS
Oxidation Resistance 1 - OXR1
Pattern recognition receptors - PRRs
Pattern-associated molecular patterns – PAMPs
Polyethylenimine - PEI
Peripheral blood mononuclear cells - PBMCs
Peroxiredoxin 2 - PRDX2
Phenylhydrazine hydrochloride – PHZ
Phosphatidylserine - PS
Polymerase chain reaction – PCR
Polyriboinosinic:polyribocytidylic acid- poly I:C
Proliferator-activated receptor gamma - PPARγ
Reactive oxygen species - ROS
Red blood cell – RBC
Red pulp macrophages – RPM
Reduction-oxidation - Redox
Retinoic acid-inducible gene I - RIG-I
Retinoic acid-inducible gene I–like receptors - RLRs
Ribonuclease L – RnaseL

Roswell Park Memorial Institute – RPMI
Sendai virus - SeV
Sialic acid-binding immunoglobulin-type lectin-1 - SIGLEC1
Signal regulatory protein a - SIRPa
Single nucleotide polymorphisms - SNPs
Small musculoaponeurotic fibrosarcoma oncogene homologue - sMAF
Sterile alpha motif and histidine/aspartic acid domain-containing protein 1 – SAMHD1
Stimulator of interferon genes – STING
Stress erythroid progenitors - SEPs
Supramolecular organising centres - SMOCs
Systemic lupus erythematosus – SLE
TIR domain-containing adapter molecule 1 – TRIF
TNF receptor-associated factor 6 - TRAF6
Toll-IL-1 receptor resistance – TIR
Toll-like receptors – TLRs
Transferrin receptor protein 1 - TFRC, TfR1
Transforming growth factor (TGF)B-activated kinase 1 - TAK1
Tre2/Bub2/Cdc16 Lysine Motif Domain Catalytic - TLDc
Tricarboxylic acid - TCA
Tripartite motif-containing – TRIM
Tumour necrosis factor - TNF
Two-dimensional – 2D
Ubiquitin-specific protease 18 - USP18
Vaccinia virus - VACV
Vascular cell adhesion molecule 1 - VCAM-1
Vesicular stomatitis - VSV
Wild-type - WT
Zika Virus – ZIKV

Contents

1 Introduction **1**
1.1 Self vs nonself recognition . . . 2
1.1.1 Toll-like receptors . . . 3
1.1.2 Sensing of cytosolic DNA . . . 6
1.1.3 Sensing of cytosolic RNA . . . 8
1.1.4 Downstream signalling . . . 11
1.2 The Interferon Response . . . 12
1.2.1 Type I IFNs . . . 13
1.2.2 Type II IFNs . . . 16
1.2.3 Type III IFNs . . . 17
1.2.4 Interferon-stimulated genes . . . 17
1.3 Interferon-induced protein 44 (IFI44) and IFI44-like protein (IFI44L) . . . 21
1.3.1 GTPase Domain . . . 22
1.3.2 Tre2/Bub2/Cdc16 Lysine Motif Domain Catalytic (TLDc) Domain 22
1.4 Iron Metabolism . . . 25
1.4.1 Cellular Iron Homeostasis . . . 27
1.4.2 Systemic Iron Homeostasis . . . 33
1.4.3 Erythrocyte Homeostasis . . . 35
1.5 Objective of this Study . . . 45
References for Chapter 1 . . . 47

2 Materials and Methods **84**
2.1 Materials . . . 84
2.1.1 Cells . . . 84
2.1.2 Viruses . . . 85
2.1.3 Plasmids . . . 87
2.1.4 Oligonucleotides . . . 89
2.1.5 Antibodies . . . 94
2.1.6 Mice . . . 96

2.2 Methods . . . 97
2.2.1 Cloning . . . 97
2.2.2 Lentiviral Particles . . . 99
2.2.3 *In vitro* virus infection . . . 100
2.2.4 Plaque assay . . . 102
2.2.5 Immunoblotting . . . 102
2.2.6 Immunoprecipitation . . . 103
2.2.7 Immunofluorescence . . . 103
2.2.8 RT-qPCR . . . 104
2.2.9 *In vivo* infection, organ harvesting and downstream processing . . . 104
2.2.10 Microneutralisation assay . . . 106
2.2.11 Pearl's Prussian Blue Staining . . . 106
2.2.12 Serum iron quantification . . . 107
2.2.13 Flow Cytometry . . . 107
2.2.14 IL-1β ELISA . . . 108
2.2.15 Bacterial PAMP Stimulation Assays . . . 108
2.2.16 Hemin Stimulation Assay . . . 110
2.2.17 Cell-titre Glo Assay . . . 110
2.2.18 ROS Glo Assay . . . 110
2.2.19 Mass Spectrometry . . . 110
2.2.20 RNA Sequencing . . . 111
2.3 Data analysis and software . . . 112
References for Chapter 2 . . . 113

3 IFI44 and IFI44L are Prototypical Interferon-Stimulated Genes 115
3.1 The expression kinetics of IFI44 and IFI44L . . . 118
3.2 Generation of *Ifi44*$^{-/-}$ mice . . . 118
3.3 IFI44 does not have antiproliforative activity *in vitro*, *in vivo* or *ex vivo* . . . 123
3.4 Localisation of IFI44 and IFI44L . . . 124
3.5 Functionality of the TLDc Domain in IFI44 and IFI44L . . . 126
3.6 Binding Partners of IFI44 and IFI44L . . . 129
3.7 Summary for Chapter 3 . . . 133
References for Chapter 3 . . . 136

4 The role of IFI44 in the Immune Response 141
4.1 IFI44 is not a regulator of the interferon response . . . 142
4.2 IFI44 is ISGylated . . . 143
4.3 IFI44/L overexpression does not affect virus infectivity *in vitro* . . . 145
4.4 VACV cleaves IFI44 and IFI44L . . . 149

4.5 IFI44 does not affect lentiviral infectivity *in vivo* . . . 151
4.6 IFI44 does not affect IAV infectivity *in vivo* . . . 153
4.7 There are no overt differences in the myeloid compartment in the spleen of *Ifi44*$^{-/-}$ mice . . . 158
4.8 IFI44 does not play a role in bacterial infection *ex vivo* . . . 158
4.9 Summary for Chapter 4 . . . 160
References for Chapter 4 . . . 162

5 IFI44 and Erythrocyte Homeostasis 166
5.1 Genes associated with iron recycling are significantly downregulated in *Ifi44*$^{-/-}$ spleens . . . 166
5.2 *Ifi44*$^{-/-}$ mice have microcytic RBCs . . . 168
5.3 Erythroid progenitor populations in the bone marrow and spleen from *Ifi44*$^{-/-}$ mice are indistinguishable from those in wild-type mice . . . 173
5.4 *Ifi44*$^{-/-}$ spleens contain fewer tissue-resident RPMs due to increased ferroptosis 175
5.5 *Ifi44*$^{-/-}$;*Adar1*$^{mZa/mZa}$ mice phenocopy *Ifi44*$^{-/-}$ mice in their blood profile, erythroid progenitor populations and RPM population . . . 178
5.6 *Ifi44*$^{-/-}$ exhibit a delayed recovery in response to acute haemolytic anaemia 178
5.7 Summary for Chapter 5 . . . 185
References for Chapter 5 . . . 187

6 Discussion 191
6.1 IFI44 and virus infection . . . 191
6.1.1 IFI44 and *in vivo* infection . . . 195
6.2 *Ifi44* and cell cycle control . . . 196
6.3 *Ifi44* and erythrocyte homeostasis . . . 197
6.3.1 The role of the TLDc domain of IFI44/L in ferroptosis and endosome acidification . . . 199
6.3.2 IFI44 and parasitic infection . . . 200
6.4 IFI44: the interface of IFN signalling and iron homeostasis . . . 201
References for Chapter 6 . . . 205

Supplementary Information 213

List of Figures

1.1 LPS-induced activation of the NFκB signalling pathway. 4
1.2 Multiple TLR family members can detect PAMPs on individual microorganisms. 5
1.3 The cGAS–STING pathway of cytosolic DNA sensing. 7
1.4 RIG-I-like Receptors. 10
1.5 Phosphorylation of innate immune adaptor proteins licenses IRF3 activation. 13
1.6 SMOC formation for TLRs, RLRs and NLRs. 14
1.7 Type I IFN signalling. 16
1.8 Interferon-stimulated genes inhibit viral infection and replication. 18
1.9 Protein domains and predicted structure of human IFI44 and IFI44L. . . . 23
1.10 TLDc Domain-containing proteins and their homology to IFI44/L. 26
1.11 Cellular iron uptake pathways. 28
1.12 The general mechanism of ferroptosis. 32
1.13 NRF2/KEAP1 regulatory axis. 33
1.14 Hepcidin control of cellular iron efflux through ferroportin. 36
1.15 Erythrocyte homeostasis. 37
1.16 Erythropoiesis. 38
1.17 Erythrocyte recycling by red pulp macrophages. 41

3.1 *IFI44* and *IFI44L* are 'core' ISGs expressed in response to all subtypes of type I IFN, in most cell types in PBMCs. 117
3.2 *IFI44* and *IFI44L* are expressed after IFN stimulation across a variety of human cell lines, and at baseline in PMA treated THP-1 cells. 119
3.3 *IFI44* and *IFI44L* are late ISGs. 120
3.4 *IFI44* and *IFI44L* expression gradually decreases after interferon stimulation is removed. 121
3.5 Generation of an *Ifi44*$^{-/-}$ mouse on a C57 BL/6N background, which naturally lack *Ifi44l*. 122
3.6 IFI44 and IFI44L are not antiproliferative in mouse splenocytes or HEK293T cells. 125

3.7 The sub-cellular localisation of IFI44 and IFI44L is non-conclusive. 126
3.8 The TLDc domain of IFI44 and IFI44L does not protect against hydrogen peroxide- or arsenic- induced cell death, nor does it bind to any tested V-ATPase subunit. 128
3.9 Immunoprecipitation of IFI44 and IFI44L and silver nitrate staining reveals multiple binding partners. 131
3.10 Binding partners of IFI44. 132
3.11 IFI44 and IFI44L interact. 134

4.1 IFI44 is not a regulator of the interferon response. 144
4.2 IFI44 is ISGylated. 145
4.3 HSV-1 and VACV infection of *Ifi44*$^{-/-}$MEFs and IFI44-V5 overexpressing HEK293T cells. 147
4.4 Neither IFI44 nor IFI44L confer protection or susceptibility to a panel of different viruses. 149
4.5 Overexpression of IFI44 and IFI44L does not confer protection or susceptibility to HSV-1 or VACV. 150
4.6 IFI44 and IFI44L are cleaved by VACV, in a proteasome-independent manner. 152
4.7 There is no difference in lentiviral infectivity in *Ifi44*$^{-/-}$ mice. 153
4.8 There is no difference in IAV infectivity in *Ifi44*$^{-/-}$ mice. 155
4.9 There is no difference in the adaptive immune response to IAV in *Ifi44*$^{-/-}$ mice. 156
4.10 *Ifi44*$^{-/-}$; *Adar1*$^{mZa/mZa}$ mice display an interferon signature. 157
4.11 There are no overt differences in the myeloid compartment in the spleen of *Ifi44*$^{-/-}$ mice. 159
4.12 *Ifi44* is not involved in the response to bacterial infection. 160

5.1 Differentially expressed genes in spleens and livers from *Ifi44*$^{-/-}$ mice. . . . 167
5.2 Genes involved in erythrocyte homeostasis are downregulated in *Ifi44*$^{-/-}$ mice. 169
5.3 *Ifi44*$^{-/-}$ mice display a mild, microcytic anaemia, which is unchanged in IAV/X-31 infection. 170
5.4 *Ifi44*$^{-/-}$ mice do not show signs of AI. 172
5.5 Erythroid progenitor populations are indistinguishable in the bone marrow of *Ifi44*$^{-/-}$ and *Ifi44*$^{+/+}$ mice. 173
5.6 Erythroid progenitor populations are indistinguishable in the spleen of *Ifi44*$^{-/-}$ and *Ifi44*$^{+/+}$ mice. 174
5.7 *Ifi44*$^{-/-}$ spleens have fewer RPMs displaying reduced expression of the haem-scavenging receptor CD163. 176
5.8 *Ifi44*$^{-/-}$ mice have more tissue iron loading in their splenic compartments. . 177

5.9 The reduced number of splenic RPMs in *Ifi44*$^{-/-}$ mice may be due to increased ferroptosis. . . . 179
5.10 *Ifi44*$^{-/-}$;*Adar1*$^{mZa/mZa}$ mice phenocopy *Ifi44*$^{-/-}$ mice. . . . 180
5.11 *Ifi44*$^{-/-}$ mice display delayed recovery after induced acute haemolytic anaemia. 182
5.12 *Ifi44*$^{-/-}$ mice do not expand their RPM compartment during acute haemolytic stress. . . . 183
5.13 PHZ treatment increases erythrophagocytosis in C57BL/6 mice. . . . 184
5.14 Erythroid progenitor populations in the bone marrow and spleen are indistinguishable in *Ifi44*$^{-/-}$ and *Ifi44*$^{+/+}$ mice during acute haemolytic anaemia. 185
5.15 *Ifi44* maintains erythrocyte homeostasis. . . . 186

6.1 IFI44/L are cleaved by VACV. . . . 194
6.2 The working hypothesis model. . . . 204
S1 ImmPres Database. . . . 213
S2 *IFI44* and *IFI44L* are highly expressed in most cell types in response to all subtypes of type I IFN. . . . 214
S3 Single-cell expression of *IFI44L* in PBMCs. . . . 214
S4 *IFI44* and *IFI44L* are late ISGs. . . . 215
S5 Plasmid maps for pLenti6.3 constructs. . . . 215
S6 Differentially expressed genes in *Ifi44*$^{-/-}$ mice shared between spleens and livers. . . . 216
S7 Immunoprecipitation of IFI44 and IFI44L with gentle NP40-based lysis buffer gives rise to inconsistent results. . . . 217
S8 *Ifi44*$^{-/-}$ organs do not display an ISG signature. . . . 218
S9 IFI44 is ISGylated. . . . 219
S10 The role of mouse *Ifi44* in EMCV infection is inconclusive. . . . 219
S11 Overexpression of IFI44/L does not affect HSV-1 viral protein expression. . 220
S12 Overexpression of IFI44/L does not affect PR8 viral protein expression. . . 221
S13 VACV degrades IFI44 and IFI44L. . . . 222
S14 Overexpression of IFI44/L does not affect HIV-1 viral protein expression. . 223
S15 Gating strategy in murine lung and spleen samples for tetramer-specific CD8$^+$ T cells. . . . 223
S16 X-31 infected *Ifi44*$^{-/-}$ mice show no differences in the T cell compartment. . 224
S17 Gene ontology analysis on downregulated genes in *Ifi44*$^{-/-}$ livers. . . . 225
S18 Gene ontology analysis on upregulated genes in *Ifi44*$^{-/-}$ livers. . . . 226
S19 Gene ontology analysis on downregulated genes in *Ifi44*$^{-/-}$ spleens. . . . 227
S20 Gene ontology analysis on upregulated genes in *Ifi44*$^{-/-}$ spleens. . . . 228

S21 Haemoglobin genes are downregulated in *Ifi44*$^{-/-}$ spleens, but RBCs are loaded with similar levels of haem relative to their size. 229
S22 The International Mouse Phenotyping Consortium. 230
S23 Gating strategy for RPMs. 231
S24 Splenic erythropoiesis gating strategy. 231

Chapter 1

Introduction

Innate immunity is one of the two branches of modern immunology. Innate immunity arose around one billion years ago, with all multicellular animals, plants and protozoans evolving innate immune defences (1, 2). Indeed, many of these organisms singularly rely upon their innate immune system for pathogenic defence. In humans, the innate immune system provides a robust first line of defence against invading pathogens, acting to reduce replication and spread while activating and guiding the adaptive response. The innate immune system comprises of physical barriers, such as the epithelia at mucosal surfaces, biological barriers, such as anti-microbial peptides and chemical barriers, such as low pH (3). For those pathogens that breach these barriers, a complex web of host innate immune mechanisms awaits them. Waiting to engulf and/or destroy are a plethora of innate immune cells: circulating monocytes, tissue-resident macrophages, natural killer (NK) cells, neutrophils, dendritic cells (DCs), basophils, eosinophils and mast cells. These cells have pattern recognition receptors (PRRs) on their cell surface, capable of recognising conserved pathogen-associated molecular patterns (PAMPs) associated with pathogens (4, 5). Alternatively, PRRs can sense danger-associated molecular patterns (DAMPs), the products of damaged tissue, which arise as a result of infection (6). Once engaged, PRRs can trigger cellular maturation, induce co-stimulatory molecules and increase antigen presentation (5). Certainly, it is not just specialised immune cells that can sense PAMPs and DAMPs. All cells have a mechanism to sense and respond to intracellular invaders, a process called cell-autonomous immunity (7). One such response is the secretion of cytokines which acts to attract, polarise and activate innate immune cells (8, 9). In addition, cytokines can mediate physiological processes such as vasodilation and fever. Further to recruiting and activating immune cells, a family of cytokines termed interferons (IFNs) prevent pathogen infection and replication. Indeed, IFNs were discovered because of - and are termed for - their ability to interfere with virus infection (10). Therefore, PRR

engagement can lead to the direct restriction of viruses. If intracellular pathogens are able to evade all of these host defences, the final resistance is regulated cell death, whereby a cell undergoes inflammatory death to produce more PAMPs and DAMPs alongside eliminating the replicative niche of the pathogen, thus limiting pathogen replication (11). This is often mediated by the inflammasome, a multiprotein complex involving one of several PRRs that forms in the cytosol (12, 13). When formed, it proteolytically cleaves pro-caspase-1 to a catalytically active form. Caspase-1 then processes and activates the cytokines IL-1β and IL-18, which are released through pores in the cell formed by gasdermin D (14). This results in an inflammatory form of cell death, termed pyroptosis (15). Similarly for extracellular pathogens, the complement system awaits, discovered by Jules Bordet as a heat-liable component of plasma (16). It consists of a chain of proteolytic cascades and results in the opsonisation and lysis of pathogens, alongside the production of proinflammatory molecules (17). These innate immune features are germline-encoded and act rapidly to provide host defence, while activating and guiding the slower adaptive response through cytokine secretion and antigen presentation.

1.1 Self vs nonself recognition

Self/nonself recognition is a common innate immune mechanism conserved over billions of years which is essential for the recognition and destruction of pathogens. This is achieved through germline-encoded PRRs, a term coined by Charles Janeway Jr in 1989 who connected innate immune sensing with control over inducible immune molecules, which go on to stimulate the adaptive immune response (4). Janeway postulated that PRRs are selected during evolution to detect microbial PAMPs, and as these are not produced by multicellular hosts, they can efficiently discriminate self and nonself. Matzinger furthered this in 1994 and postulated that PRRs are detecting danger – from pathogens, or from cell damage (6). During the 1990s, there was a boom in the discovery of various PRRs and their cognate ligands. The first example of PRRs were initially discovered in *Drosophila* (18-21) and as such named toll-like receptors (TLRs) after the *Drosophila* Toll protein. There are four other classes of PRRs, based on protein domain homology: retinoic acid-inducible gene I–like receptors (RLRs), NOD-like receptors (NLRs), absent in melanoma 2 (AIM2)-like receptors (ALRs) and C-type lectin receptors (CLRs). These PRRs are expressed on plasma membranes, endosomal membranes and cytosolically. After recognition of cognate ligands, they activate downstream signalling to produce an innate immune response.

1.1.1 Toll-like receptors

TLRs are type 1 transmembrane glycoproteins and are structurally characterised by an extracellular leucine-rich repeat (LRR) and an intracellular Toll-IL-1 receptor resistance (TIR) homology domain. The extracellular domain mediates PAMP binding, whereas the intracellular domain facilitates downstream signalling through interaction with different receptor adaptor proteins (22). The protein Toll was discovered in *Drosophila* as it was shown to have a homologous cytosolic domain to that of human IL-1 receptor, now termed TIR domain, but with an extracellular LRR domain (as opposed to immunoglobulins) (23). Mutant Toll flies were found to be highly susceptible to fungal infections, yet resistant to gram-negative bacterial infections (21). Shortly thereafter, the first human homologue, TLR4, was discovered (24) and subsequently its ligand, bacterial lipopolysaccharide (LPS) (25). TLR4 was shown to activate the nuclear factor kappa-light-chain-enhancer of activated B cells (NF-κB) pathway, and result in the expression of costimulatory molecule B7 (CD80) (24). This was a foundationally important link of the innate TLR to the adaptive response, proving Janeway's original hypothesis correct (4). The seminal importance of this work is shown through the 2011 Nobel Prize in medicine, awarded to Jules Hoffman and Bruce Beutler for uncovering Toll as an innate sensor in flies and TLR4 as the receptor for LPS in mice, respectively. Ralph Steinman was jointly awarded this Prize for his discovery of dendritic cells.

We now know that humans encode 10 TLRs and mice 12, which are found either at plasma or endosomal membranes (26). Depending on their adaptor usage, these signal via a Myeloid differentiation primary response 88 (MyD88)-dependent or TIR domain-containing adapter molecule 1 (TRIF)-dependent pathway (27). In the case of TLR4, MyD88 functions alongside MyD88 adaptor-like (MAL or TIRAP) to drive NF-κB signalling (28). NF-κB is a family of transcription factors which coordinate immunity and inflammation. When activated, NF-κB translocates to the nucleus, where it drives the expression of genes encoding inflammatory cytokines (29) (Figure 1.1). MyD88 contains a death domain, mediating interactions with IL-1R-activated kinase-4 (IRAK4), which in turn activates IRAK1 and 2. Subsequently, TNF receptor-associated factor 6 (TRAF6) is recruited to the complex where it initiates the formation of K63 ubiquitin chains, forming scaffolds for the recruitment of transforming growth factor (TGF)β activated kinase 1 (TAK1). Next, NF-κB is released from its inhibited state by the IKK complex, such that it can translocate to the nucleus (30).

Typically, TLRs present in the plasma membrane detect bacterial cell surface components: TLR4 binds LPS (25, 31), TLR5 binds flagellin (32) and TLRs 1, 2 and 6 bacterial lipoproteins (33, 34). Conversely, TLRs present in endosomes detect nucleic acids (NAs): TLR3 detects dsRNA (35), TLR7 and 8 detect ssRNA (36-38), TLR9 detects unmethy-

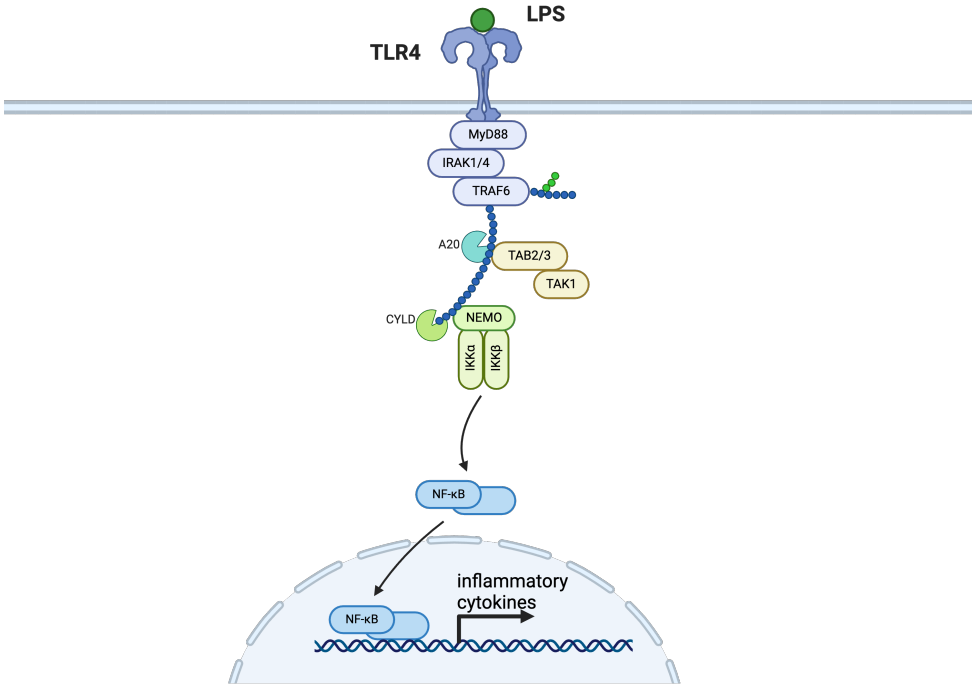


Figure 1.1: LPS-induced activation of the NFκB signalling pathway.

The canonical NFκB pathway acts downstream of TLR4 engagement with LPS. Adaptor protein Myeloid differentiation primary response 88 (MyD88) is recruited first, where it interacts with and activates IL-1R-activated kinase-4 (IRAK4), and subsequently IRAK1 and 2. Subsequently, TNF receptor-associated factor 6 (TRAF6) is recruited to the complex where it initiates the formation of K63 ubiquitin chains, forming scaffolds for the recruitment of transforming growth factor (TGF)B-activated kinase 1 (TAK1). Next, a multi-subunit IκB kinase (IKK) complex is recruited, which degrades IκB proteins. IKK is composed of two catalytic subunits, IKKα and IKKβ, and a regulatory subunit named NF-κB essential modulator (NEMO). As IκB proteins bind to and inhibit NFκB in the cytosol, NFκB is then freed to translocate to the nucleus and induce the transcription of genes encoding inflammatory cytokines.

lated CpG ssDNA (39) and TLR13 detects bacterial ribosomal RNA (Figure 1.2) (40). NAs are not uniquely microbial, and as such TLRs sensing these are restricted to endosomes (41). In addition, TLRs sensing NAs require cleavage by endosomal proteases to be functional (42) and their cognate ligand NAs require processing by endosomal nucleases to create high affinity ligands (43). None of these regulatory steps are important for the detection of bacterial cell wall components. This leads us to the paradigm of NA sensing. Janeway emphasised that the premise of PRR-PAMP recognition is to recognise molecules specific and unique to cellular invaders (4). However, while pathogenic NAs may contain certain unique elements, such as unmethylated CpG DNA (44), self-NAs are found intrinsically. Indeed, aberrant activation of NA sensors can lead to an array of autoimmune diseases (45-50). In contrast, TLRs detecting microbial cell surface components

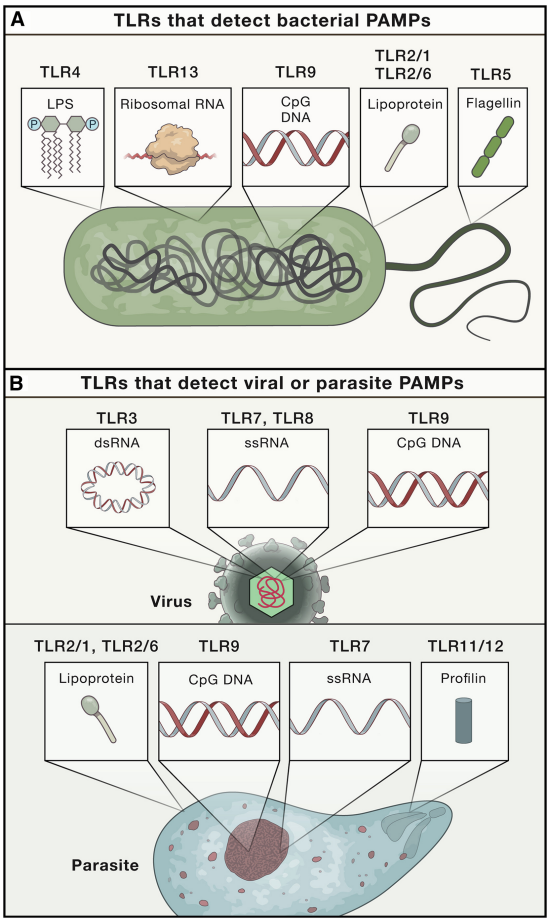


Figure 1.2: Multiple TLR family members can detect PAMPs on individual microorganisms. *Taken From Figure 1 of Fitzgerald, K. A. and J. C. Kagan (2020). Toll-like Receptors and the Control of Immunity." Cell 180(6): 1044-1066.* A bacterium **(A)**, virus, or parasite **(B)** are depicted. Insets display PAMPs and the TLRs that are responsible for their detection. The TLR names represent those found in mice, as genetic evidence is available to support the importance of each TLR-PAMP interaction indicated.

are rarely implicated in autoimmunity. Despite the risks associated with using NA as a PAMP, this mechanism is an ancient form of cellular defence, found in virtually all multicellular organisms (51-53). NA sensing is of particular importance in regard to sensing intracellular invaders, specifically viruses, as viruses originate from eukaryotic cells and lack the presence of prokaryotic molecular patterns. An important way to discriminate then, between self and nonself NAs, is the (mis)localisation of NA ligands. Detection of NAs in a compartment where they should not be present, for example in endosomes by TLR3/7/9/13, initiates downstream signalling. In vertebrates, NA sensing results in antiviral defence through the production of type I IFNs, amongst other mechanisms (54). Herein, I will be outlining the NA sensing mechanisms, and subsequent downstream signalling, as they relate to viruses.

1.1.2 Sensing of cytosolic DNA

DNA is not only the molecule conveying the information of life, but also a key driver of inflammation and immunity when outside of the nucleus and mitochondria. This is an error-prone process, and self-DNA escape to the cytosol is associated with autoimmune diseases such as systemic lupus erythematosus (SLE) (55). Cytosolic double-stranded DNA has been known to trigger immune responses since long before the concept of pattern recognition was introduced: as far back as 1928, Frederick Griffith demonstrated that there was a 'transforming principle' activating the immune system, which turned out to be DNA (56). Eventually, it was understood that the presence of cytosolic DNA would trigger a type I IFN response (55, 57-59), however the responsible sensor had not been uncovered. Endosomal DNA sensor TLR9 was discovered first (39), but this did not satisfy the question of how cytosolic DNA is immunostimulatory. In 2009, AIM2 was shown to bind DNA in the cytoplasm, and subsequently to engage the caspase-1 activating adaptor ASC to form a caspase-1 activating inflammasome (60-62). While this was a transformative discovery, it did not answer how the type I IFN pathway is activated in response to cytosolic DNA. Adaptor protein stimulator of interferon genes (STING) was discovered next and shown to induce type I IFN, along with a potent antiviral state, when overexpressed (63). Mechanistically, STING activates the kinase TBK1, which phosphorylates transcription factor IRF3, leading to its translocation to the nucleus and driving the expression of type I IFNs (64, 65). STING was thought to be a putative DNA sensor, in lieu of any further discoveries and after the finding that STING knock-out mice are severely impaired after DNA virus challenge (64). This was until Russel Vance's 2011 paper with the surprising discovery that STING senses neither DNA nor protein, but unique molecules called cyclic dinucleotides, which act as conserved signalling molecules in bacteria (66). In 2013, Zhijian (James) Chen's team put two and two together in the landmark discovery that cytosolic DNA elicits the production of the cyclic dinucleotide cyclic GMP-AMP (cGAMP), which binds to and activates STING (67). In a back-to-back article, Chen also describes the enzyme responsible for cGAMP catalysis, cGAMP synthase (cGAS) (68). Chen demonstrated that cGAS directly binds cytosolic DNA, undergoes a conformational change, and produces cGAMP from cellular ATP and GTP. In the same year, cGAMP was shown by other groups to have a unique linkage chemistry, rendering it an exceptionally potent activator of human STING (69-72). Since then, cGAS has been accepted by the field as a central mechanism of antiviral immunity – at least, in response to DNA or DNA viruses (Figure 1.3). The cGAS-STING pathway has also been shown to act as a crucial mediator of antitumour immunity (73), alongside being a driver of inflammatory diseases (74).

By way of mechanism, cGAS recognises DNA in a sequence-independent manner through

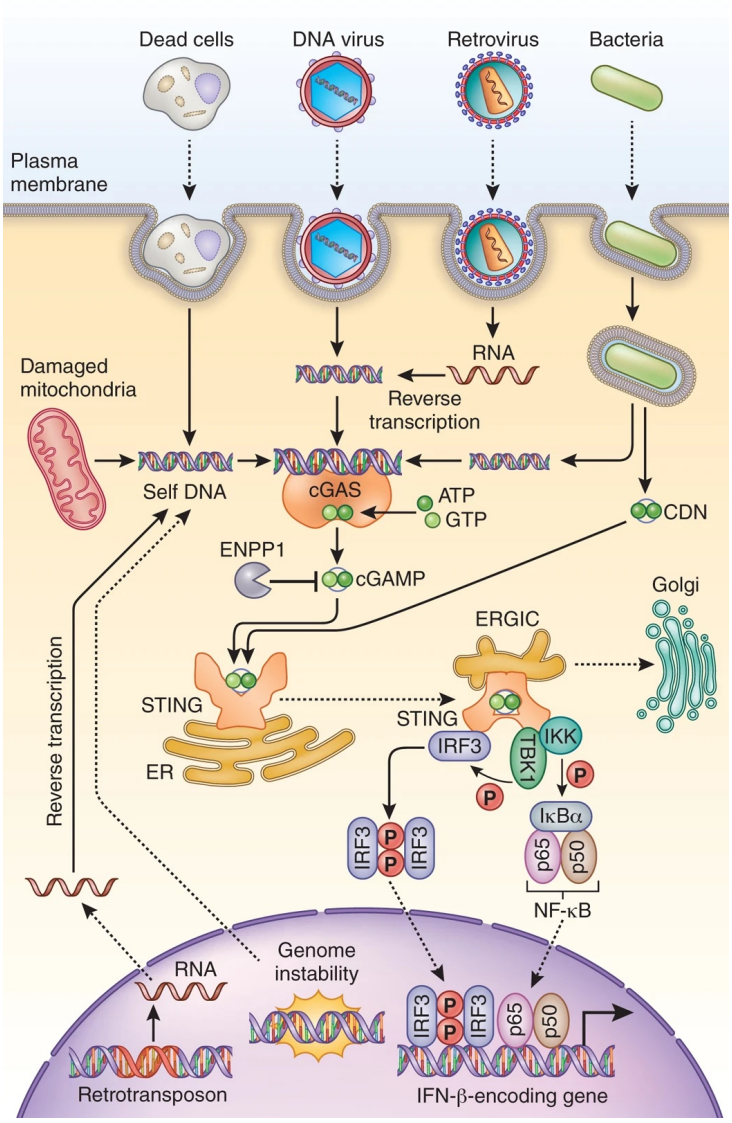


Figure 1.3: The cGAS–STING pathway of cytosolic DNA sensing.

Taken From Figure 1 of Chen, Q., et al. (2016). "Regulation and function of the cGAS–STING pathway of cytosolic DNA sensing." Nature Immunology 17(10): 1142-1149. DNA is a PAMP when it is delivered to the host cytoplasm by microbial infection and is a DAMP when it enters the cytoplasm from the nucleus (e.g. through DNA damage and reverse transcription of retroelements), mitochondria or dead cells. Cytosolic DNA binds to and activates cGAS, which catalyses the synthesis of cGAMP from ATP and GTP. cGAMP binds to the ER adaptor STING, which traffics to the ER-Golgi intermediate compartment (ERGIC) and the Golgi apparatus. STING then activates IKK and TBK1. TBK1 phosphorylates STING, which in turn recruits IRF3 for phosphorylation by TBK1. Phosphorylated IRF3 dimerises and then enters the nucleus, where it functions with NF-κB to turn on the expression of type I IFNs and other immunomodulatory molecules.

interacting with the sugar-phosphate backbone. DNA binding induces a conformational change, allowing ATP and GTP to access the catalytic site (75). A complex forms in which two cGAS molecules bind two DNA molecules, resulting in ladder-like structures, and explaining the increased potency of long dsDNA in activating cGAS (76). DNA binding to cGAS induces phase separation *in vitro* (77), and a recent review postulates that phase separation is a new form of innate immune regulation (78). The second messenger cGAMP binds STING on the endoplasmic reticulum (ER) membrane which induces a conformational change and subsequent translocation of STING to the Golgi (74). At the Golgi, TBK1 and IRF3 are recruited to STING, all three are phosphorylated and the resulting IRF3 dimer detaches and translocates to the nucleus. STING can also activate the kinase IKK, which in turn phosphorylates IκB proteins (63). Phosphorylated IκB proteins are degraded through the ubiquitin-proteasome pathway, which releases NF-κB such that it can enter the nucleus and result in the expression of inflammatory cytokines. Activation of cGAS by DNA can be bypassed through the arrival of cGAMP directly into the cytosol. This can occur through gap junctions (79), being packaged into new virions which transport cGAMP between cells (80, 81), and also through a variety of channels (82), some of which are targeted for degradation by viruses (83). This process is inhibited by ENPP1 and ENPP3, extracellular membrane proteins that degrade cGAMP, providing a layer of regulation to the pathway (84, 85). Alongside being activated by viral dsDNA in the cytoplasm, cGAS can be activated by engulfed extracellular DNA, for example neutrophil extracellular traps (NETs), turnover of apoptotic cell corpses or non-apoptotic cell death (86). Cell-intrinsic mitochondrial DNA is also a potent cGAS activator, arising directly from pathogens which perturb mitochondrial integrity (87-89), as a result of inflammatory cytokine signalling (90), or from defective mitophagy (91). Lastly, cell-intrinsic genomic DNA has the potential to activate cGAS when mislocalised (92-95).

Autoactivation of cytosolic DNA sensors is prevented through the degradation of DNA by TREX1 (92, 96). Some viruses use this to their advantage, relying on TREX1 as a host-dependency factor to degrade inflammatory DNA (89). Mutations in TREX1, gain-of-function mutations in STING and DNase II deficiency all lead to a subset of autoimmune diseases called type I interferonopathies (47, 74).

1.1.3 Sensing of cytosolic RNA

Cytosolic RNA is sensed by RLRs, which activate the type I IFN system to induce an anti-viral state (97). Similar to DNA sensing, both viral and host RNAs can trigger RLR sensing and lead to an inflammatory response. There are three members of the RLR family: Retinoic acid-inducible gene I (RIG-I) (98), melanoma differentiation-associated

protein 5 (MDA5) (99) and laboratory of genetics and physiology 2 (LGP2). While all RLRs contain a carboxy-terminal domain (CTD) and central helicase domain, only RIG-I and MDA5 have caspase activation and recruitment domains (CARDs), which mediate downstream signalling. For RIG-I, the CARDs are sequestered by the helicase domain at steady state; then, 5'triphosphate-RNA binding induces a major conformational change where the helicase and CTD bind RNA thus exposing the CARD domains (100). Active RIG-I can also oligomerise into larger complexes in the presence of ATP (101, 102). MDA5 adopts a more open conformation in the absence of ligand, and assembles into helical filaments upon ligand binding (103). The exposed CARD domains of MDA5 and RIG-I interact with CARD domains of the adaptor protein mitochondrial antiviral signalling protein (MAVS) on the mitochondrial membrane, which recruits and activates TBK1 and IκB kinase-ϵ (IKKϵ), which in turn activate IRF3 and IRF7. IRF3 and 7, along with NFκB, induce the transcription of genes encoding IFNs (Figure 1.4) (97). RLRs themselves are induced by IFN signalling, resulting in a feedforward loop.

RIG-I and MDA5 have differential preferences for their RNA ligands: RIG-I favours short blunt-ended RNAs with a 5' triphosphate group (104-106) or diphosphate group (107), whereas MDA5 prefers long dsRNA. The agonists for RIG-I are very much characteristic of viral RNAs produced, for example, by influenza virus (108), but are usually absent in uninfected cells due to mRNA processing, as cellular pre-mRNAs gain a 5' cap prior to export to the cytosol. This 7-methylguanylate cap, further modified by a 2'-O-methyl group, prevents endogenous mRNAs activating RIG-I (109). Synthetic RNA polyriboinosinic:polyribocytidylic acid (poly I:C) was the first ligand shown to activate MDA5, denoting that long dsRNA is its ligand (99, 110). Where these long dsRNA species come from in physiological settings is an open question. There is some evidence that they are host-derived, for example mitochondrial RNA (111) or endogenous reteroelements (112). Indeed, it has been shown that RIG-I can be activated by host cellular RNAs over the course of an infection, and this explains how restriction of dsDNA viruses is partially dependent on RLRs (113-115). Both RNA and DNA viruses alike result in MDA5 activation and signalling, with varying degrees of reliance on the protein for antiviral resistance. For example, MDA5 signalling is essential to mount a type I IFN response during *Picornaviridae* infection (116-118), whereas it only plays a partial role in other infections, due to redundancy with RIG-I and cytosolic DNA sensors (119-122).

Constitutive activation of RLRs leads to autoimmune diseases, either through spontaneous signalling in the absence of infection, or due to alterations in RNA metabolism, generating stimulatory RNAs. Gain-of-function mutations in the gene encoding MDA5, *IFIH1*, lead to type I interferonopathies (123, 124). Similarly, gain-of-function mutations in *DDX58*, encoding RIG-I, lead to an autoimmune disease (125). Interestingly, single nucleotide

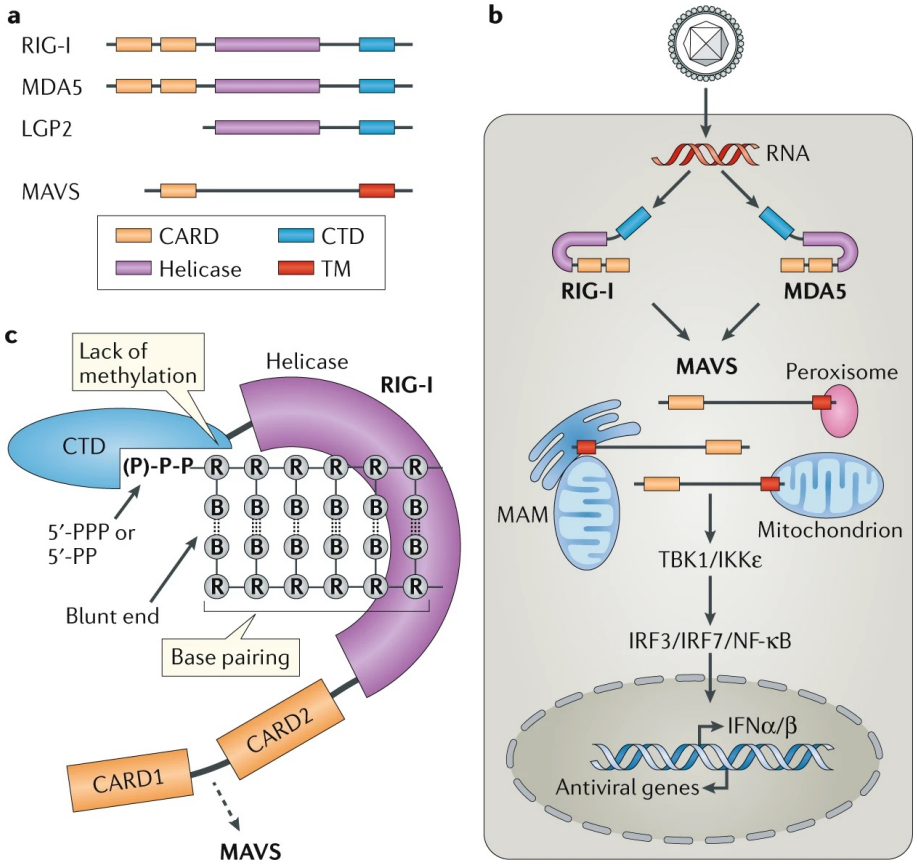


Figure 1.4: RIG-I-like Receptors.

Taken From Figure 2 of Rehwinkel, J. and M. U. Gack (2020). "RIG-I-like receptors: their regulation and roles in RNA sensing." Nat Rev Immunol 20(9): 537-551 **a.** Domain architecture of retinoic acid-inducible gene I (RIG-I)-like receptors (RLRs) and mitochondrial antiviral-signalling protein (MAVS). The three members of the RLR family have a central helicase domain and form a subfamily of SF2 helicases. An additional RNA-binding fold, called the carboxy-terminal domain (CTD), is also found in all RLRs. RIG-I and melanoma differentiation-associated protein 5 (MDA5) contain two caspase activation and recruitment domains (CARDs) in tandem orientation at their N termini. The signalling adaptor protein MAVS also has a CARD as well as a C-terminal transmembrane domain (TM). **b.** RLR signalling pathway. RIG-I and MDA5 are activated by immunostimulatory RNA, for example, viral RNAs. They then undergo conformational changes that expose and multimerize their CARDs (not shown for simplicity), which allows homotypic CARD–CARD interactions with MAVS. MAVS is anchored with its TM domain into mitochondria, mitochondrial-associated membranes (MAMs) and peroxisomes, and relays the signal to TANK-binding kinase 1 (TBK1) and IκB kinase-ϵ (IKKϵ). These in turn activate interferon regulatory factor 3 (IRF3) and IRF7, which together with the transcription factor nuclear factor-κB (NF-κB) induce the expression of type I IFNs and other genes. **c.** RIG-I is shown in its active conformation, bound to an immunostimulatory RNA.

polymorphisms (SNPs) in *IFIH1* are associated with type 1 diabetes, psoriasis, rheumatoid arthritis and multiple sclerosis (126-130). This is thought to be due to heightened type I IFN levels, but the mechanistic basis of this remains to be understood. In addition, changes in RNA metabolism may create new ligands in the cytosol. Under homeostatic conditions, the enzyme adenosine deaminase acting on RNA 1 (ADAR1) catalyses A-to-I editing of self-RNA, preventing autoactivation of RLRs (131, 132). Mutations in *ADAR1* causes chronic IFN production and inflammation in an MDA5-dependent manner (133, 134).

Stringent and efficient self/nonself recognition is a crucial part of this pathway, to allow a rapid response in the case of PAMP/DAMP presence, while sterile activation of RLRs is prevented. One mechanism of regulation of RLRs is achieved through post-translational modification (PTM). There are over 200 types of PTM, and many of these have been shown to dynamically control proteins involved in NA sensing. For example, K63-linked polyubiquitin chains stabilise RIG-I CARD domains in a signalling-active, oligomeric, 'lock-washer' conformation (135, 136). This polyubiquitination is mediated by TRIM25 (137), which is directly antagonised by multiple viral pathogens (138-141). As such, redundancy exists in the pathway, and Riplet has also been shown to mediate K63-linked ubiquitination of RIG-I (142). In addition to ubiquitination, RIG-I and MDA5 are controlled by SUMOylation (143), dephosphorylation (144, 145) and MDA5 requires ISGylation for oligomerisation and subsequent signal transduction (146).

1.1.4 Downstream signalling

I have outlined separate mechanisms of action for receptor activation and signalling by TLRs, cGAS and RIG-I/MDA5. However, these pathways converge and have much overlap – proteins and domains are shared between these systems, along with many shared mechanisms throughout different PRR signalling pathways.

Downstream, there are shared outcomes from PRR signalling such as NFκB activation, cytokine maturation, cell death, and IFN induction through IRF3. RIG-I-MAVS, cGAS-STING and TLR3/4-TRIF all achieve IRF3 activation through a common signalling mechanism: phosphorylation at a shared C-terminal consensus motif, pLxIS (Figure 1.5) (147). This pLxIS motif is found in MAVS, STING, TRIF and IRF3, where p denotes a hydrophilic residue and x is any residue. The pLxIS motif is phosphorylated on the S residue by TBK1 (MAVS, STING and IRF3) or IKK (MAVS) and allows the interaction of adaptor proteins with IRF3 and subsequent activation (147). This pLxIS motif seems to be more widely shared than originally thought, with roles in activating TRAF6 ubiquitin ligase along with IκB kinases (148, 149).

A proposed general mechanism for signal transduction involves activation of a receptor by presence of ligand, which overcomes autoinhibition and allows for oligomerisation. The oligomerised receptor can then act as a scaffold for adaptor proteins to form filaments, which relay the signal downstream. Examples of this can be found in the inflammasome, with adaptor protein ASC forming filaments on caspase-1 (150-152), and in RNA-sensing, with RLR adaptor MAVS forming helical structures after RIG-I/MDA5 activation (101, 103, 153, 154). In both cases, CARD domains on ASC and RIG-I/MDA5/MAVS facilitates this oligomerisation. CARD domains are part of the death domain (DD) superfamily, which is one of the largest and most widely distributed domain superfamilies (155). The DD superfamily is present in multiple signal transduction pathways across innate immunity and is found in caspases, kinases and adaptor proteins (155, 156). Homotypic interactions between proteins with DDs allows for the cooperative formation of higher order oligomeric complexes termed signalosomes or SMOCs (157-160). These allow for a rapid and amplified response to small amounts of stimuli through clustering key proteins and initiating proximity-induced activation of the effector enzymes. This is a conserved theme throughout PRR signal transduction as the interactions required for enzymatic activation are intrinsically weak allosteric interactions, and require close proximity for effectiveness – which in turn provides another layer of regulation to the pathway (157).

SMOCs have been observed in almost every PRR pathway (Figure 1.6) (161-164). Perhaps a good example of DD-induced SMOCs is the inflammasome. Several receptors initiating inflammasome activation (including, amongst others, AIM2 and NLRP3) contain a DD superfamily domain known as a pyrin domain (PYD). After activation (e.g. by dsDNA in the case of AIM2), the adaptor protein (ASC) is recruited, which contains both a PYD and a CARD. Homotypic interactions form between PYD:PYD of AIM2:ASC and CARD:CARD of ASC:caspase-1, allowing for large oligomeric complex formation which in turn facilitates proximity-induced enzyme activation (152, 165-168). Other signal transduction mechanisms, e.g. cGAMP, complement some of these SMOC based mechanisms for a stringent innate response.

1.2 The Interferon Response

IFNs are a class of cellular signalling molecules, secreted by an infected cell upon detection of foreign NAs (46, 169-171). After their discovery in 1957 (10), it was clear that IFNs are critically important to human health and disease. By the 1980s, lab-made IFNs were introduced as a pharmaceutical therapeutic for certain types of cancer, and later for hepatitis infection and multiple sclerosis (172).

There are three types of IFN: types I, II and III. All cells can secrete type I IFN, however

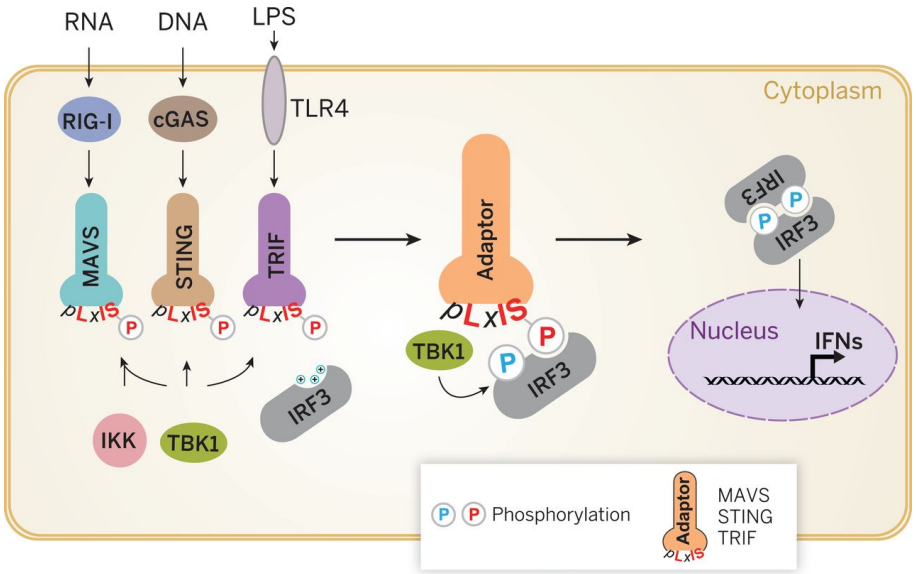


Figure 1.5: Phosphorylation of innate immune adaptor proteins licenses IRF3 activation.
Taken from graphical abstract of Liu, S., et al. (2015). "Phosphorylation of innate immune adaptor proteins MAVS, STING, and TRIF induces IRF3 activation." Science 347(6227): aaa2630. MAVS, STING, and TRIF—which are activated by viral RNA, cytosolic DNA, and bacterial LPS, respectively—activate the kinases IKK and TBK1. These kinases then phosphorylate the adaptor proteins, which in turn recruit IRF3, thereby licensing IRF3 for phosphorylation (P) by TBK1. Phosphorylated IRF3 dissociates from the adaptor proteins, dimerises, and then enters the nucleus to induce IFNs.

type II and III IFN secretion is largely restricted to cells of the immune system (173). IFNs are secreted by cells into the extracellular milieu, from where they can bind their cognate receptor on the same cell, or neighbouring cells. After receptor engagement, signal transduction is mediated by Janus kinase–signal transducer and activator of transcription (JAK-STAT) signalling (174). IFN signalling induces the transcription of IFN-stimulated genes (ISGs), the protein products of which can induce a cellular anti-viral state through various mechanisms (175). This includes inhibition of virus entry, inhibition of virus replication and inhibition of viral egress alongside encoding proteins involved in antigen presentation. IFNs and ISGs thus play a vital role in the immune response against viral pathogens. (175).

1.2.1 Type I IFNs

Type I IFN is the largest family of IFN proteins, with a common structure composed of five α-helices. Type I IFNs are produced by all cells after detection of virus infection and instigate ISG expression through binding to the type I IFN receptor, IFNAR (Figure 1.7). IFNAR is comprised of two subunits, IFNAR1 and IFNAR2, and is present on all nucleated cells. The different IFNAR subunits are thought to be monomeric at baseline, then

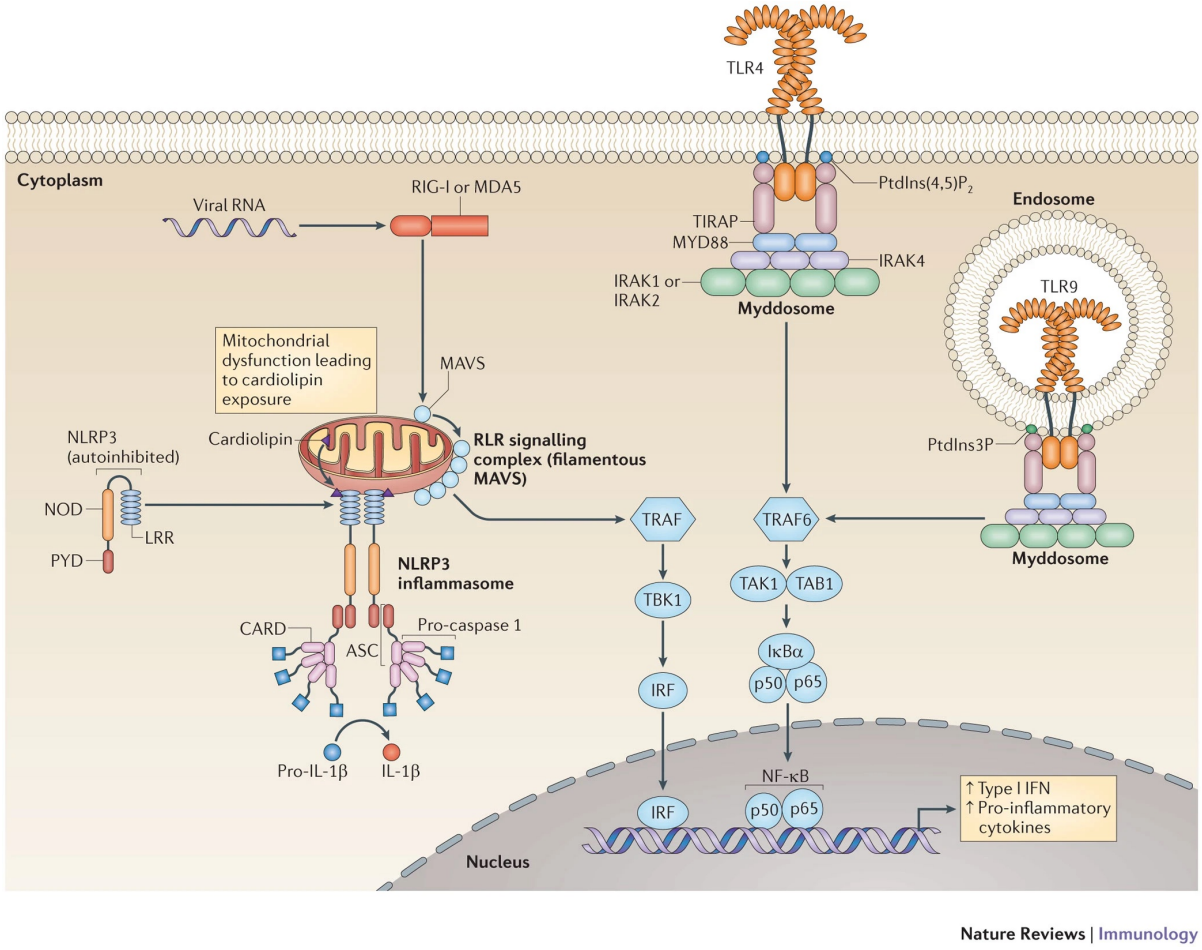


Figure 1.6: SMOC formation for TLRs, RLRs and NLRs.

Taken from Figure 1 of Kagan, J. C., et al. (2014). "SMOCs: supramolecular organizing centres that control innate immunity." Nature Reviews Immunology 14(12): 821-826. Depicted are the best-studied SMOCs, including the ligands and regulatory proteins that promote their assembly, and the downstream biological activities induced by these protein complexes. The figure does not show the exact stoichiometry of the protein components in each signalling complex. Binding of LPS (not shown) activates Toll-like receptor 4 (TLR4), leading to assembly of a Myddosome on the plasma membrane. By contrast, unmethylated CpG-containing DNA oligonucleotides (not shown) promote TLR9 to assemble an endosomal Myddosome. TIRAP facilitates Myddosome assembly and also has an amino-terminal lipid-binding domain that interacts promiscuously with acidic phosphoinositides and phosphatidylserine. For example, TIRAP is depicted as binding phosphatidylinositol-3-phosphate and phosphatidylinositol-4,5-bisphosphate on the endosomal membrane and the plasma membrane, respectively. Binding of cardiolipin, which translocates to the outer mitochondrial membrane upon mitochondrial dysfunction, relieves the autoinhibited state of NLRP3. This in turn may promote NLRP3 inflammasome assembly through downstream PYD–PYD and CARD–CARD interactions. Activation of RLRs — RIG-I or MDA5 — leads to the formation of higher-order oligomers of MAVS.

high-affinity interaction of type I IFNs with IFNAR2 causes the recruitment of IFNAR1 and signalling initiation (176, 177). All subtypes of type I IFN genes are intronless and cluster together on a conserved locus in amniotes (178-180). In humans, this region is on chromosome nine, and in mice on chromosome four. In humans, type I IFNs consist of 13 subtypes of IFNα, as well as a single IFNβ, IFNω, IFNκ and IFNϵ. These differ in expression (181, 182), kinetics and potency (183, 184). How shared IFN receptors decipher the complexity of IFN signalling inputs remains elusive, but ligand binding affinities and receptor distribution are thought to play a role (177, 185). To date, the evolutionary advantage of maintaining this number of type I IFN genes is poorly understood.

IFN gene expression relies upon the transcription factors IRF3 and IRF7. When activated and phosphorylated, these can form homodimers or heterodimers. IRF3 is constitutively abundant, whereas IRF7 requires upregulation after IFN signalling, resulting in a positive feedback loop (186, 187). As IRF3 has preferential affinity for the *IFNB1* gene, IFNβ is the major subtype produced early in infection (188).

Type I IFNs are made and secreted by cells, and then bind the IFNAR heterodimer (176). JAKs (TYK2 and JAK1) are found associated with the intracellular domains of IFNAR 1 and 2, respectively. Heterodimerisation brings these JAKs into close proximity, where they can trans-phosphorylate (174). This creates a scaffold for the recruitment of STAT1 and STAT2, which are phosphorylated by the JAKs, dimerise, and recruit IRF9. This complex translocates to the nucleus, where it binds to IFN response elements (ISREs) in the promoter regions of ISGs, inducing gene expression (189). Some of the proteins encoded by ISGs provide signal amplification, for example, RIG-I, MDA5 and MAVS are all encoded by ISGs, along with IRF7. In addition, proteins encoded by ISGs can also provide negative regulation – for example, ubiquitin-specific protease 18 (USP18) specifically renders the IFNAR complex insensitive to IFNα, possibly through preventing IFNα from recruiting IFNAR1 to the receptor complex (190-192).

Due to the importance of the type I IFN pathway in viral restriction, it is not surprising that patients with inborn errors in this pathway are more susceptible to virus infection (193-195). There are many examples of this, and to name a few, mutations in *TLR3* have been associated with increased risk of fatal IAV infection (196), acute respiratory distress syndrome (197) and life-threatening COVID-19 (193), while mutations in *DDX58* are associated with severe influenza infection (198). Mutations in *IRF3* are associated with herpes simplex encephalitis in children (199) and mutations in *IRF7* life-threatening influenza (200), and both are associated with severe life-threatening COVID-19 (193). Thus, the type I IFN system is crucial for innate defence against virus infection.

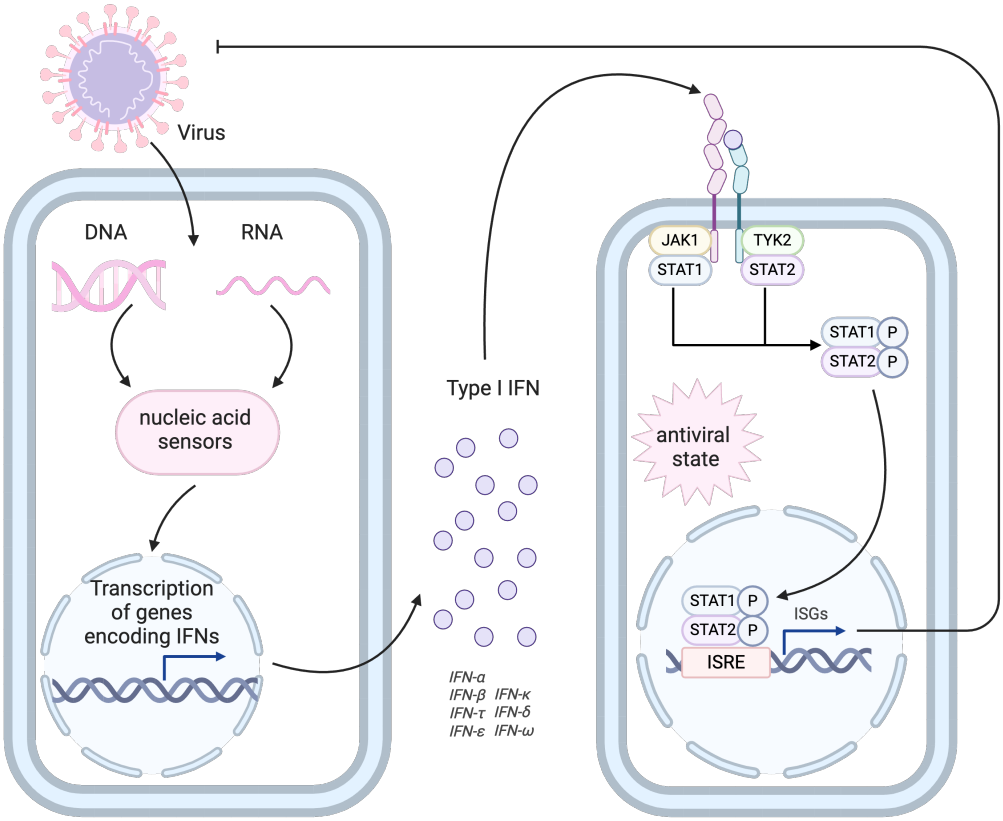


Figure 1.7: Type I IFN signalling.

Based on Figure 1 of Rehwinkel, J. and M. U. Gack (2020). "RIG-I-like receptors: their regulation and roles in RNA sensing." Nat Rev Immunol 20(9): 537-551. After infection, viral NAs are detected in the cytosol by cytosolic NA receptors. This leads to the transcription of genes encoding type I interferons (IFNs). Type I IFNs are made, secreted, and bind to the type I IFN receptor (IFNAR) on the same cell or neighbouring cells. IFN binding to IFNAR results in dimerisation and activation of the JAK-STAT signalling pathway. Phosphorylated STAT dimers translocate to the nucleus, where they bind interferon response elements (ISREs) in the promotor regions of target genes. This results in the transcription of a subset of genes termed interferon stimulated genes (ISGs). The protein products of ISGs act alone or in concert to prevent viral infection and replication.

1.2.2 Type II IFNs

The type II IFN subfamily has just one member, IFNγ, with distant amino-acid sequence homology to type I IFNs. Like type I IFNs, IFNγ binds two class II cytokine receptor proteins, IFNGR1 and IFNGR2. IFNGR1 has a JAK1 binding domain and a STAT1 docking site, while IFNGR2 contains a JAK2 binding domain (201). IFNGR1 is constitutively present on all cells, whereas the expression of IFNGR2 is tightly regulated and IFNGR2 is less widely expressed (201). IFNGR signalling results in STAT1 activation, which

binds gamma-activated sequences (GASs) in the promoter regions of target genes (201). IFNγ expression is tightly regulated by epigenetic, transcriptional, post-transcriptional and post-translational mechanisms (202). As a result, IFNγ is only expressed by cells of the immune system, including antigen-presenting cells (203). This expression pattern means IFNγ has a complex interplay with the adaptive immune system, and can mediate many effects including the amplification of antigen presentation, enhancing antigen recognition and increasing the production of reactive oxygen species (ROS) in macrophages (204, 205). As such, IFNγ is of importance in anti-tumour immunity (206) and infection (205).

1.2.3 Type III IFNs

There are four subtypes of type III IFNs, with IFNλ1, IFNλ2 and IFNλ3 discovered in 2003 (207, 208). These were shown to be structurally related to interleukin-10 (IL-10). The genes encoding these cytokines are found clustered on chromosome 19 and are all inducible by virus infection and demonstrate antiviral activity (207, 208). IFNλ4 was discovered in 2013 through RNA sequencing of human hepatocytes activated with poly(I:C) (209). The identification of IFNλ4 was delayed into the 2010s because not all humans express it. IFNλ4 is controlled by a heritable dinucleotide frameshift variant, *IFNL4-*$\Delta G/TT$ (rs368234815), whereby the *IFNL4-*ΔG allele creates an open reading frame for the full-length protein, and the alternative allele does not (209). Interestingly, IFNλ4 is associated with failure to clear hepatitis C virus (HCV) infection (210).

Type III IFNs also signal through a heterodimeric receptor, formed from IFNλR1 which binds the ligand and IL-10R2, which forms an accessory chain. While the receptor is distinct from that of type I IFNs, the downstream signalling cascade, and resulting gene expression, is analogous (211). IFNλR1 expression is largely restricted to cells of epithelial origin, including epidermal, bronchial and gastrointestinal epithelial cells along with hepatocytes (212, 213). Most leukocytes do not express IFNλR1 (214). As such, type III IFNs have a more limited functional range than type I IFNs, and have evolved to specifically protect the epithelium, which may be the first point of viral entry (215).

1.2.4 Interferon-stimulated genes

ISGs are the set of genes whose transcription is induced by IFN and are the cellular factors mediating the antiviral defence induced by IFN (Figure 1.8) (216-220). It was first realised that IFN could result in transcriptional changes in the 1980s (221), and since then the antiviral functions of some ISGs have been characterised. An overexpression screen in 2011 revealed that some ISGs display broad antiviral activity, whereas some

display virus-specificity (216). Further, there seems to be an 'add-on' effect with some ISGs, whereby the intensity of the antiviral effect is correlated with the number of ISGs present (216). Contrary to this, other ISGs work in isolation to carry out their antiviral function. ISGs can be expressed at baseline and have their expression increased by IFN (for example, *DDX58* and *IRF9*), while some ISGs are entirely dependent on IFN for their expression (for example, *interferon-induced protein 44-like* (*IFI44L*)). The transcriptional profile of ISGs expressed by a cell after IFN signalling varies depending on the type of IFN binding the receptor and the cell type itself (183). Despite this, there is a subset of 'core' ISGs, expressed in every cell type in response to any subtype of type I IFN (183).

ISGs play a vital role in the innate immune response against viral pathogens; however, while there are hundreds of ISGs, only a few have been well-characterised (216, 222).

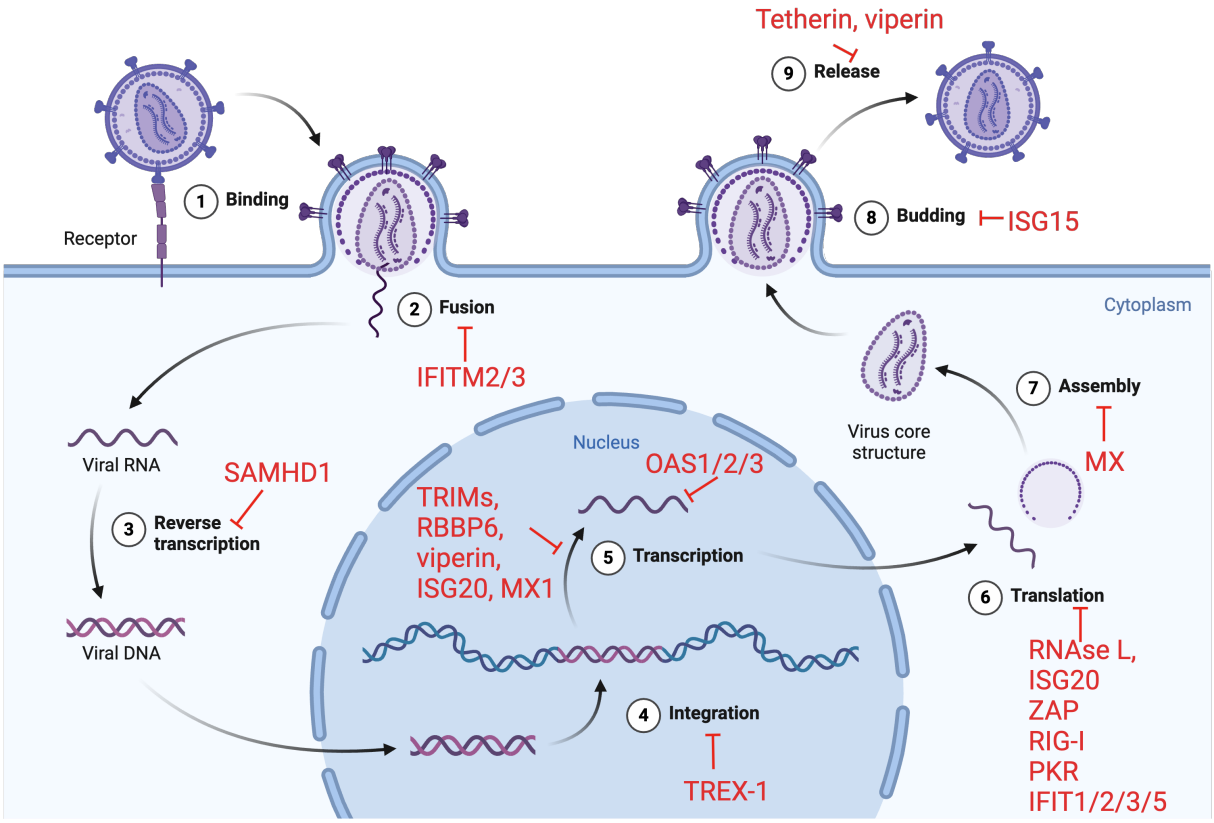


Figure 1.8: Interferon-stimulated genes inhibit viral infection and replication.

Interferon-stimulated genes (ISGs) can inhibit every stage in a viral replication cycle. Depicted here is the HIV lifecycle, and in red are ISGs known to antagonise HIV replication.

Enhancing PAMP detection

As previously mentioned in section 1.1, many PRRs are encoded by ISGs. While they are expressed at baseline, their expression is boosted through IFN signalling. This results

in an intuitive self-regulatory mechanism: the presence of PAMP leads to signalling, IFN and increased levels of PRR, however in the absence of PAMP, these PRRs will not be engaged to signal, resulting in a decrease in their expression.

Oligoadenylate synthetase (OAS) is a protein family comprising of strongly inducible ISGs. OAS proteins can detect cytosolic RNA, and binding leads to the synthesis of 2'-5'-oligoadenylates, which act as second messengers to activate latent ribonuclease L (RNaseL). RNaseL then cleaves both host and viral RNA, which produces new PAMPs to activate other cytosolic RNA sensors (223, 224).

Antiviral effectors

Many ISGs encode direct antiviral effectors that can target every stage of a virus lifecycle. Here, I will outline one example for each stage of a typical lentiviral lifecycle, although this is a non-exhaustive list of all of the human immunodeficiency virus (HIV) restriction factors.

The immediate stages of HIV infection are receptor binding, endocytosis and membrane fusion. This process is inhibited by interferon-induced transmembrane (IFITM) proteins. IFITM proteins are encoded by strongly induced ISGs, limiting the infection of multiple viruses *in vitro* (225, 226). Their anti-viral activity targets endocytosis or they prevent virus-induced cell-cell fusion in the case of HIV-1 (227) and also Kaposi's Sarcoma-Associated Herpesvirus (KSHV) (228). This is thought to be mediated through IFITM3 engaging with endosomes and enhancing their trafficking to lysosomes (229). In addition, IFITM proteins have been shown to decrease cell membrane fluidity, which is thought to limit fusion of viral envelopes to cellular membranes (230-232).

After membrane fusion and release of the viral capsid, viral RNA is converted to DNA through reverse transcription. This is inhibited by sterile alpha motif and histidine/aspartic acid domain-containing protein 1 (SAMHD1), a triphosphohydrolase that depletes the cellular pool of deoxynucleoside triphosphates (dNTPs) through conversion into nucleosides and inorganic triphosplate (233, 234). This directly inhibits reverse transcription of HIV *in vitro* and *in vivo* (234, 235). To counteract this, HIV-2 encodes a protein to antagonise SAMHD1, Vpx (236, 237).

Lentiviruses such as HIV then integrate their viral DNA into the host genome in the nucleus. TREX-1 is an ISG we met in section 1.1.2. It is a cytosolic 3' to 5' exonuclease, and metabolises reverse-transcribed DNA before it can enter the nuclear compartment (238). The expression of TREX-1 can be activated by DNA damaging agents such as UV, hydrogen peroxide and gamma radiation alongside responding to both type I IFN and IFN-γ (239). As such, there is a fluctuating level of TREX-1 present, depending on the

physiological status of the cell.

Once DNA has been synthesised and integrated, transcription occurs to generate viral mRNAs. This can be inhibited by some members of the tripartite motif-containing (TRIM) protein family. The entire TRIM superfamily are ISGs, which are involved in many different aspects of innate antiviral defence (240, 241). Specifically, TRIM22 suppresses retroviral transcription by regulating binding of the transcription factor Sp1 to the long terminal repeats and by interfering with trafficking of the viral Gag protein to the plasma membrane (242, 243).

The lentiviral transcript itself is targeted by many ISGs, including *interferon-stimulated gene 20* (*ISG20*). *ISG20* encodes a 3' to 5' exonuclease with specificity for single-stranded RNA, and so it can degrade lentiviral transcripts (244). To subvert this, HIV-1 induces 2' O-methylation of its genome by recruiting the cellular FTSJ3 methyltransferase, thereby impairing detection by both ISG20 and RNase L (245). As discussed in section 1.2.4, OAS proteins are encoded by ISGs and activate RNaseL, further resulting in RNA degradation. This is non-discriminatory, and reduces transcripts made by the host, which may lead to regulated cell death activation (246, 247).

The viral transcript is then translated, a process which can be inhibited by interferon-induced protein with tetratricopeptide repeats (IFIT) proteins. IFIT1 inhibits translation of viral transcripts at the initiation stage, by competing with the cap-binding initiation factor complex, eIF4F (248). Due to this, mechanistically IFIT1 can only restrict infection by viruses that possess "nonself" cap0-mRNAs. So-called cap0 RNAs lack methylation on the first and second cap-proximal nucleotides, modifications that distinguish self from nonself (248). However, IFIT1b can recognise cap1-mRNAs, and IFIT5 can recognise 5'triphosphate mRNAs, covering a larger range of viruses (249).

Viral assembly and capsid formation are antagonised by Myxovirus resistance (MX) protein 2/B (250-254). MX proteins are IFN-induced dynamin-like large GTPases, present in all vertebrates. Most mammals have two MX genes that arose by gene duplication. MX2/B binds to the lentiviral capsid assemblies and oligomerises, resulting in viral restriction (253, 255). This process is reinforced by MB2/B GTP hydrolysis (253).

Finally, assembled virion capsids bud from the cell. This release is inhibited by the ISG *BST2*, encoding tetherin (256). Tetherin is a type II single-pass transmembrane protein and mediates its antiviral effect by tethering nascent enveloped virions to infected cell surfaces through two membrane anchors (256). It is in turn antagonised by the HIV-1 protein Vpu (257).

IRF3-dependent interferon-independent ISGs

Alongside promoting the transcription of type I IFN mRNAs, IRF3 can independently activate the transcription of several ISGs. Schoggins discovered that delivery of cGAS *in vitro* triggers a STING-dependent, IRF3-mediated antiviral programme that functions independently of canonical JAK/STAT signalling (219). This has been found to occur in response to cytomegalovirus (258) and SARS-CoV-2 (259), and includes the transcripts of key anti-viral ISGs such as *IFIT*, *MX*, *IFITM* and *DDX58*. Direct induction of antiviral ISGs by IRF3 surpasses the requirement for IFNAR, and therefore provides a more rapid anti-viral response. In addition, many viruses encode proteins that are able to inhibit IFN signalling, for example VACV encodes a type I IFN decoy receptor to sequester IFN binding to IFNAR (260) and NS5 of flaviviruses can degrade STAT2 (261).

1.3 Interferon-induced protein 44 (IFI44) and IFI44-like protein (IFI44L)

ISGs play a vital role in the innate immune response against pathogens; however, while there are hundreds of ISGs, only a few have been well characterised. Here, I will outline two ISGs of unknown function: *interferon-induced protein 44* (*IFI44*) and *IFI44L*.

IFI44 is a 50 kDa protein encoded by the gene *IFI44*, and as its name suggests, expression is strongly induced by type I IFN. Indeed, *IFI44* mRNA levels are often used to assess IFN production in an 'IFN score', including in clinical settings (262, 263). IFI44 has two protein domains: a GTP-binding domain (specifically, a P-loop NTPase with GTP-specificity), albeit with no homology to any known GTPases, and a TLDc domain, which (when present in other proteins) is thought to confer resistance to oxidative stress (264, 265) (Figure 1.9A). IFI44 was first discovered as microtubule-associated aggregates in hepatocytes of HCV infected Chimpanzees (266). Since then, IFI44 has been implicated in restricting virus infection (267-271), restricting parasitic infection (272), restricting bacterial (273) and viral (274) infection in shellfish, exhibiting anti-proliferative activity (267, 275), implicated in certain cancers (276-278), as a biomarker of some autoimmune diseases (279-282) and as a diagnostic tool in others (283, 284). In contrast, IFI44 has also been reported to act as a negative regulator of the IFN response, supporting virus replication (285). Near to *IFI44* on chromosome 1 is *IFI44L*, which is conserved from oysters to humans (286). Human IFI44 and IFI44L share 44% amino acid similarity, and both contain the same protein domains (Figure 1.9 A, C, D). *IFI44L* is also an ISG, and has been implicated in restricting HCV infection (216), HBV infection (287) and JEV infection (288), has anti-proliferative activities (267), is also a biomarker for SLE (289-296), is expressed during the DNA-damage induced immune response (297) and in pulmonary

arterial hypertension (298), is a biomarker for proliferative diabetic retinopathy (299) and is involved in certain cancers (278, 300-306). In addition, IFI44L is a potential drug target in rheumatoid arthritis and periodontitis (307). The wide range of pathologies involving *IFI44L* may be due to the strong ISREs present in its promotor region: *IFI44L* has two ISREs, which can be activated by both type I IFN and type II IFN, which will occur across a range of disease and inflammatory states (308). *IFI44L* has an annotated SNP, *rs273259*, which is associated with increased susceptibility to SLE (309) febrile seizures following MMR vaccination (310), is involved in measles-specific humoral immunity (311, 312), and affects the rate of respiratory tract infections in children (313). In addition, presence of *IFI44L* can distinguish between viral and bacterial infections in children (314, 315). *IFI44* and *IFI44L* have also been shown to be upregulated in an IFN-independent, IRF3-dependent manner (219, 259) and *IFI44L* promotor transcription may be upregulated by HIV-1 in an ISRE-independent manner (308). Further, epigenetic regulation of *IFI44L* has also been linked with certain pathologies. *IFI44L* is hypomethylated in COVID-19 patients (316), rheumatoid arthritis (290), SLE (291, 293, 317-319) - in a STAT3-dependent manner (320) - and in patients with severe vs mild Aicardi-Goutières syndrome (321). While there is therefore much evidence that these two proteins are important players in the type I IFN response, their biochemical activities and molecular functions remain largely unknown.

1.3.1 GTPase Domain

IFI44 and IFI44L encode a P-Loop NTPase domain, with predicted specificity for guansine-5'-triphosphate (GTP), however there is no sequence homology with known GTPases or G proteins (275). In fact, only the GTP binding motif (GXXXXGKS) is shared between the groups (275). Mx proteins are ISGs with GTPase activity and their antiviral capacity was described in section 1.2.4. Sequence alignment shows that there is only 22% sequence homology between MX1 and IFI44, with both sharing the GTP binding motif (Figure 1.9 B). Whether IFI44/L can hydrolyse GTP, and how binding or hydrolysis might contribute towards their molecular functions, remain unknown.

1.3.2 Tre2/Bub2/Cdc16 Lysine Motif Domain Catalytic (TLDc) Domain

Bioinformatic analysis of human IFI44 and IFI44L revealed a predicted N-terminal Tre2/Bub2/Cdc16 Lysine Motif Domain Catalytic (TLDc) domain. In mammals, the TLDc domain is shared by only five other proteins (OXR1, NCOA7, TBC1D24, TLDC1 and TLDC2), in which it provides protection against oxidative stress (264, 322). The TLDc-domain containing family is highly conserved, first reported in *Escherichia coli* in

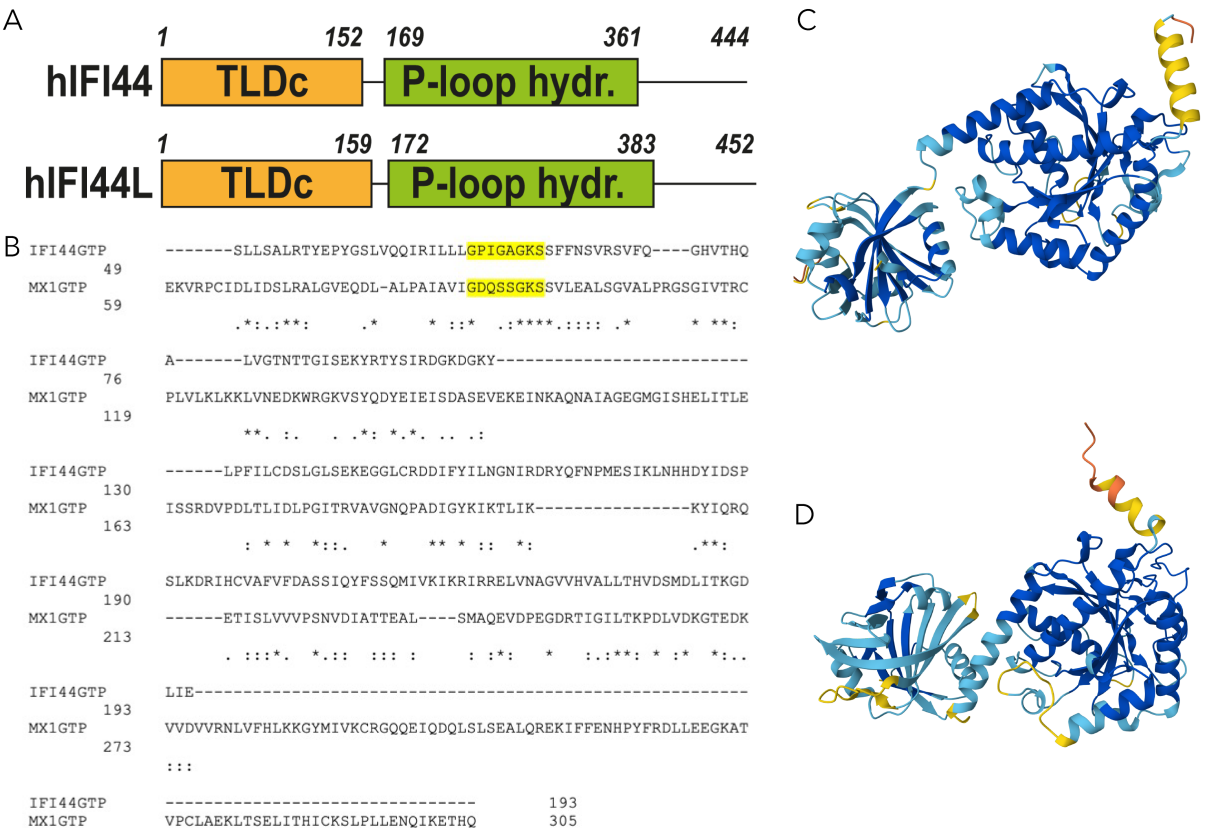


Figure 1.9: Protein domains and predicted structure of human IFI44 and IFI44L.

A. Human IFI44 and IFI44L have two proteins domains, a TLDc domain and a P-loop hydrolase domain, with predicted affinity for GTP. **B.** Amino acid alignment of IFI44 GTP binding domain and that of MX1. There is 22% homology. The GTP binding motif of IFI44 and MX1 is highlighted in yellow. **C.** The AlphaFold predicted structure of human IFI44. **D.** The AlphaFold predicted structure of human IFI44L (598, 599).

2000 (323), and since confirmed in almost all eukaryotes (324). The structure of the TLDc domain is unique, not resembling any other enzymes involved in the detoxification of reactive oxygen species (ROS) (325, 326). The molecular mechanism of action of the TLDc domain is unknown, and under current investigation.

The most well-characterised protein from this group is Oxidation Resistance 1 (OXR1). This protein has been shown to be involved in many pathways relating to oxidative stress resistance, including regulation of the expression and/or function of antioxidant enzymes (327, 328), regulation of the p53 signalling pathway (329), aging (330, 331), mitochondrial integrity (332, 333), DNA integrity (334), resistance to hyperoxic challenge (335) and prevention of neurodegeneration and neuroinflammation (331, 334, 336-340). Overexpression of *Oxr1* in amyotrophic lateral sclerosis (ALS) delayed neuroinflammatory phenotype onset in mice (337, 339, 341). The TLDc domain of OXR1 has been found to be essential

for its function (322, 338, 342, 343), albeit through elusive means. Indeed, OXR1 has a short isoform, OXR1-C, which contains almost exclusively the TLDc domain, and yet is still able to protect against oxidative stress (324, 338). The disruption or deletion of OXR1 can result in a reduced life span in yeast, flies and mice (328, 330, 338, 341, 344), and can cause a range of inherited human neurological disorders (331, 342, 345, 346).

TBC1D24 also plays an important role in normal brain function, specifically the maturation and oxidative stress resistance of neurons (347). Loss-of-function mutations in *TBC1D24* leads to familial myoclonic epilepsy (348-350), familial malignant migrating partial seizures of infancy (351), neurodegeneration and learning disabilities (352, 353), hearing loss (354, 355), and epileptic encephalopathy (356-358), shown to be due to exacerbated oxidative stress sensitivity in a humanised fly model (357).

Nuclear receptor coactivator protein 7 (NCOA7) is also expressed in the brain, where it enhances the transcriptional activities of nuclear receptors, such as the oestrogen receptor (359). NCOA7 expression correlates with prognosis of certain cancers (360-362) and has been shown to prevent growth and metastasis of clear cell renal cell carcinoma by inhibiting the mitogen-activated protein kinase/extracellular signal-regulated kinase (MAPK/ERK) pathway, which regulates epithelial-mesenchymal transformation and apoptosis (363). NCOA7 interacts with the cytoplasmic domain of the vacuolar (V)-ATPase in the brain and was shown to be required for normal assembly and activity in a knock-out mouse model (364). Further, *Ncoa7* deletion in mice resulted in a downregulation of the V-ATPase and less efficient urine acidification (365). Neurones lacking *Ncoa7* exhibited defective lysosomal formation and function, and knock-out mice displayed subsequent social defects (364). In humans, genetic mutations in *NCOA7* have been linked with autism spectrum disorder (ASD) (366). The human *NCOA7* gene encodes several mRNA isoforms, with isoform 4 being produced through an alternative start site, thusly termed *NCOA7-AS*. This transcript is induced by type I IFN but not by oxidative stress (367). The protein product of *NCOA7-AS* contains just the C-terminal TLDc domain of NCOA7 (325, 367). NCOA7-AS is a direct antagonist of viruses entering the cell via the endocytic route, such as influenza A virus, and HCV – a role that is fitting for an IFN-induced factor (368). Mechanistically, NCOA7-AS interacts with the V-ATPase and promotes vesicle acidification, which in turn prevents viral membrane fusion and promotes degradation of endocytosed material (368).

TLDC1, also known as MTOR-associated protein, eak-7 homolog (MEAK7) (47), is an evolutionarily conserved lysosomal membrane protein that promotes cell proliferation and migration (369). It is also expressed in the brain, and expression in mice reduces neuronal cell death (322). TLDC1 is thought to mediate the activation of mammalian/mechanistic target of rapamycin (mTOR) pathway through an alternative complex (369, 370).

Dysregulation of mTOR pathways leads to cancer development, and *TLDC1* mRNA is overexpressed in certain cancers (371). In addition, *TLDC1* mRNA was found to be significantly increased in peripheral blood mononuclear cells (PBMCs) of children with ASD (372).

Very little is known about the last member, TLDC2, except for that it has been shown to protect against oxidative stress *in vitro*, much like the other TLDc-domain containing proteins (322), but there is no *in vivo* data nor human genetic data hinting at the underlying mechanism.

Recently, TLDc domains for all the family members (except IFI44 and IFI44L) have been shown to interact with the cellular V-ATPase (265, 364, 373-378). This may provide us a clue as to the domain's mechanism of action, since the V-ATPase itself can protect against oxidative stress (379). The V-ATPase is a large multi-subunit proton pump found on the endomembrane system of specialised organelles and at the plasma membrane. V-ATPase mediated acidification of intracellular vesicles is important for endocytosis, autophagy, protein degradation and antigen processing (380). The exact influence of each TLDc domain-containing protein on the V-ATPase is contested, with some studies showing that they are important for its assembly (364), and others for its disassembly (with the exception of TLDC1) (374, 378). However, clear themes for all arise: they are seemingly active and important in the brain, they interact with the V-ATPase and protect against oxidative stress, and loss of just one of these proteins can cause neuropathological disease and cancer.

IFI44 and IFI44L are the most evolutionarily distinct proteins in the group, with sequence homology of the TLDc domain to that of the other proteins in the family ranging from 12% to 18% (Figure 1.10). However, structural prediction analyses reveals that they are remarkably similar in structure (Figure 1.10). Since the TLDc domain and the protein family are highly conserved, I hypothesise that the TLDc domains of IFI44 and IFI44L retain functionality.

1.4 Iron Metabolism

In the course of my experimental investigations, an unexpected role for IFI44 in iron recycling for erythropoiesis was revealed. To provide background for these experiments, here I will describe how iron trafficking is controlled and how this relates to red blood cell (RBC) production.

Iron is essential for almost all forms of life. This is true in the most literal sense, that life on Earth likely required iron to develop (381). Indeed, before oxygen was present in

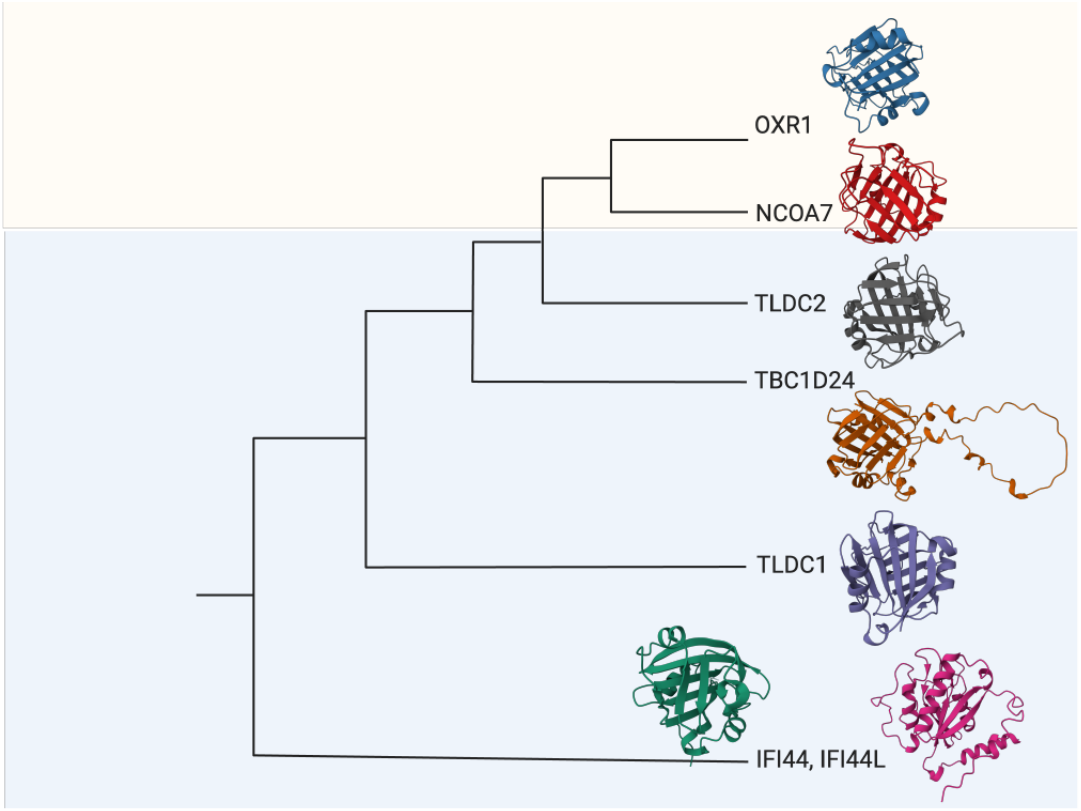


Figure 1.10: TLDc Domain-containing proteins and their homology to IFI44/L.
IFI44 and IFI44L are the most phylogenenetically distant members of the TLDc family, according to their amino acid sequences. However, the AlphaFold predicted structures of the TLDc domains of all these proteins are very highly conserved (598, 599).

Earth's atmosphere, iron as Fe^{2+} was soluble in sea water, and abundant for usage by the earliest life forms. When the Great Oxygenation Event occurred from ≈2.5 billion years ago, oxidised iron (Fe^{3+}), insoluble in water, became a scarce nutrient and so life adapted in kind by developing mechanisms to obtain, store and recycle iron through infection, symbiosis and multicellularity (381). As such, iron is thought to be both an important catalyst for life and a driver of evolution.

In mammals, iron is essential for delivery of oxygen to tissues, mitochondrial function, DNA synthesis and repair and for the activity of hundreds of enzymes (382). Consequently, iron deficiency in humans can cause a wide range of pathologies, one of the most common presentations being anaemia which has 1.2 billion cases worldwide (383). As such, controlling iron-deficiency anaemia is a global health priority. Absolute iron deficiency can be caused by insufficient dietary uptake, impaired absorption or blood loss, while chronic inflammation can result in tissue sequestration of iron, causing functional iron deficiency (384).

Iron is ideal for cellular functionality due to its ability to transiently bind gaseous ligands and to efficiently catalyse reduction-oxidation (redox) reactions by interconverting between Fe^{2+} and Fe^{3+} valence states. However, these properties also lead to toxicity when iron is in excess, as Fenton reactions drive the generation of reactive oxygen species (ROS) (385). ROS can damage DNA, lipids and proteins and ultimately lead to inflammatory cell death termed ferroptosis (386). Due to this, and also due to the fact that many pathogens scavenge iron, mammalian iron homeostasis is tightly regulated (387, 388).

1.4.1 Cellular Iron Homeostasis

As free iron is harmful, it is chaperoned by transferrin, lactoferrin and ferritin (387, 389). Plasma iron is predominantly found bound to transferrin, and this is ubiquitously taken up by transferrin receptor protein 1 (TFRC, TfR1) through clathrin-mediated endocytosis (390) (Figure 1.11a). Serum transferrin is principally produced by hepatocytes, and transferrin deficiency in humans and mice leads to tissue iron overload (391). Once endocytosed, maturing endosomes are acidified by the V-ATPase, resulting in the release of iron from transferrin. Iron is reduced from Fe^{3+} to ferrous iron, Fe^{2+} (392), and transferred into the cytosol by divalent metal transporters (388). Non-transferrin bound iron can enter cells through zinc transporters ZIP8 (393) and ZIP14 (394), and iron bound to hyaluronan can enter through CD44 (395) (Figure 1.11b, c). Further, cells can take up extracellular ferritin iron through receptor-mediated endocytosis involving scavenger receptor class A members (396). Uptake of ferritin iron is an important immunomodulatory process, as extracellular ferritin has been shown to play a direct role in the inflammatory response, triggering NET-mediated cytokine storms (397, 398). Free haem can also cause harmful inflammation through generating ROS, or through direct activation of TLR4 (399). As such, free haem in the bloodstream is scavenged by haptoglobin and hemopexin, which are then endocytosed by CD91 and CD163 respectively (400) (Figure 1.11d). Following cellular entry, iron is either utilised, stored or exported. For usage, iron can be coordinated as an ion via amino acid side chains into proteins or trafficked to the mitochondria, where haem and iron-sulphur (Fe-S) cluster biosynthesis occurs. The precise biochemical roles iron plays in the cell have been reviewed extensively elsewhere (382, 388). Iron that is not metabolised or exported is stored as ferritin (382). Ferritin is a cytosolic 24-subunit cage-like protein complex, which can store up to 4300 iron atoms (401). Ferritin acts to control the cellular iron levels, storing in times of plenty, and releasing when it is scarce (388). Ferric iron is released from ferritin stores by a process called ferritinophagy: a ferritin-specific autophagic pathway initiated by NCOA4 (402). Oxidation-responsive transcription factor nuclear factor erythroid 2-related factor 2 (NRF2) induces the transcription of *HERC2*,

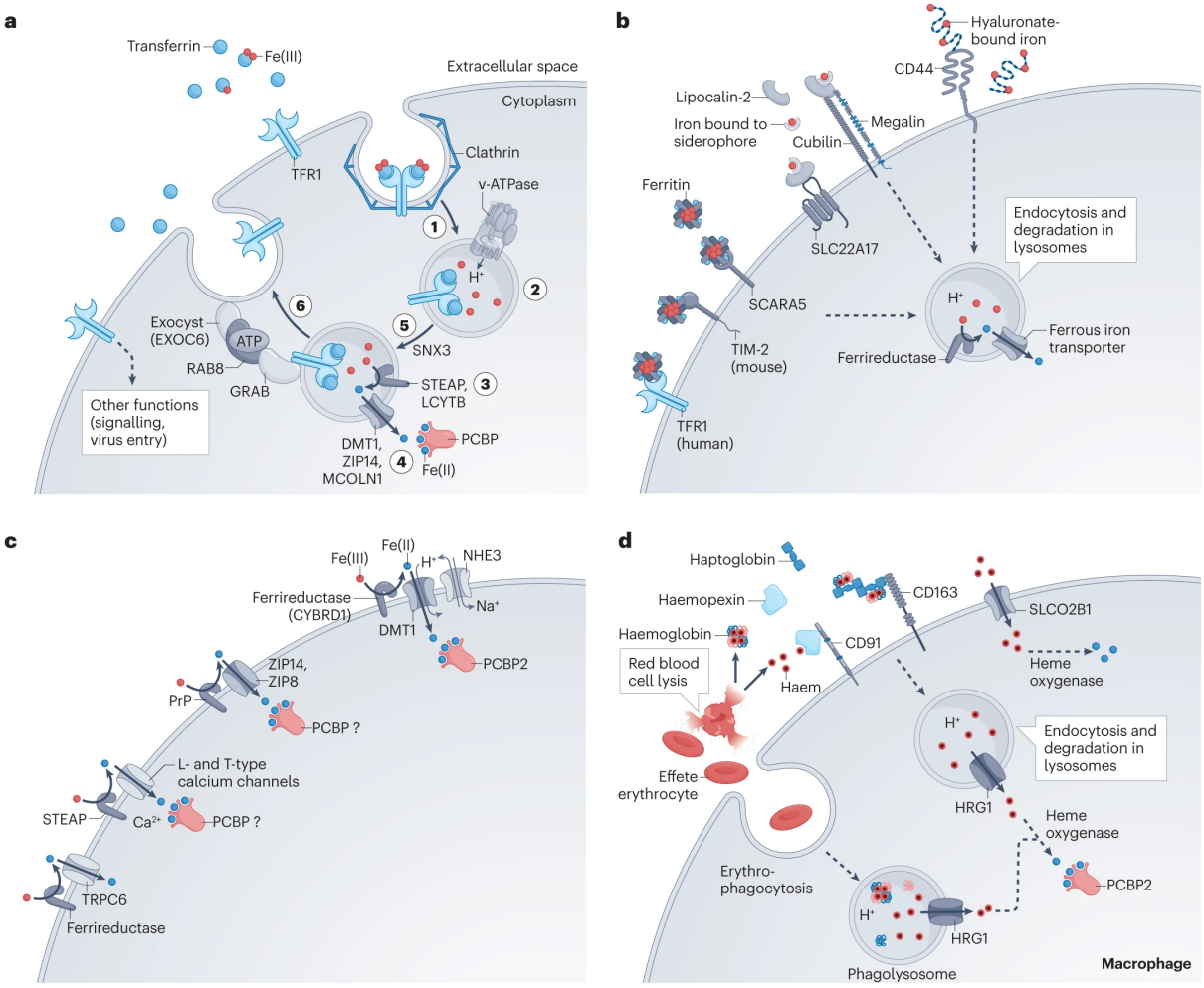


Figure 1.11: Cellular iron uptake pathways. ***Taken from Figure 2 of Galy, B., Conrad, M. and Muckenthaler, M. Mechanisms controlling cellular and systemic iron homeostasis. Nat Rev Mol Cell Biol 25, 133–155 (2024).***

a. Acquisition of transferrin-bound iron (TBI). **b.** Uptake of other forms of iron via receptor-mediated endocytosis. **c.** Uptake of non-transferrin-bound iron ions. **d.** Acquisition of haem iron. For full figure legend, see Figure 2 of *Galy, B., Conrad, M. and Muckenthaler, M. Mechanisms controlling cellular and systemic iron homeostasis. Nat Rev Mol Cell Biol 25, 133–155 (2024)* (388).

an E3 ubiquitin ligase which targets NCOA4 for degradation – meaning this reversal predominantly occurs in conditions of low ROS (and, speculatively, low iron) (403). In addition, ferritin can act as an iron carrier, controlling iron efflux from enterocytes (404) and delivering iron to mitochondria in precursor erythrocytes (405).

Cellular iron export is similarly well-controlled, providing iron to the bloodstream and protecting cells from toxic iron excess. Elemental ferrous iron has only one known exporter, ferroportin (FPN), encoded by *SLC40A1*. FPN exports iron from absorptive enterocytes, iron-recycling macrophages and hepatocytes (406, 407). One study found that FPN can

also mobilise iron from renal proximal tubule epithelial cells during a mouse model of malaria infection (408). In this way, FPN can reduce toxic intracellular iron accumulation and oxidative stress (409, 410). Indeed, a gain-of-function mutation in FPN in African populations provided resistance against anaemia, haemolysis and iron deficiency, but not severe malaria (411). FPN also has been seen to have roles in muscle repair (412), maternal-foetal iron transfer (413) and tubular iron reabsorption (414). Conversely, intracellular ferritin-iron can be directly expelled through the non-canonical routes of secretory autophagy or endosomal microautophagy (415-417).

Intracellular Iron Regulation

Iron acquisition, storage and efflux are carefully controlled to achieve homeostasis through a series of senso-regulatory systems that are heavily intertwined. If this process fails, both iron deficiency and overload can have pathological effects (382, 386, 418, 419). Intracellular iron is regulated through the iron-regulatory protein (IRP)- iron-responsive element (IRE) axis (420). The IRP-IRE axis regulates the post-transcriptional expression of key iron metabolism genes after activation by sensing low cellular iron. Low cellular iron is sensed by IRPs through the presence or absence of Fe-S clusters (420). Mechanistically, IRPs bind to IREs, which are stem-loop structures found in transcripts encoding important proteins involved in iron uptake and storage. IRP binding to IREs can either stabilise the transcript through blocking RNase activity or prevent protein translation through excluding ribosome binding (420), in a manner depending on whether the IRE is present in the 3' or 5' UTR (420). Other proteins involved in control of intracellular iron include hypoxia inducible factor (HIF) proteins (421, 422), which react to the presence or absence of iron ions. When iron (or oxygen) is limiting, HIF proteins can no longer be hydroxylated, a process reliant on iron and oxygen. This stabilises the HIF protein, allowing translocation to the nucleus where it binds coactivators to modulate the expression of target genes, generating broad metabolic changes in the cell (422). Other proteins that sense and respond to cellular iron levels include haem-regulated inhibitor (HIR) and tristetraprolin (TTP) (382). Therefore, low iron is sensed by different pathways that monitor Fe-S clusters, iron ions and haem iron, and results in metabolic changes in the cell.

Ferroptosis

Ferroptosis is a genetically distinct form of regulated cell death, catalysed by membrane lipid peroxidation, the aberrant movement of ions across the plasma membrane, cell swelling and plasma membrane rupture (Figure 1.12) (423, 424). Thus, this form of cell death is intrinsically linked to ROS levels, and cells expressing high levels of ROS scavenging proteins are less likely to undergo lipid peroxidation and ferroptosis (425,

426). Indeed, sensitivity to ferroptosis is governed by hundreds of enzymes, reactions and molecules (427). Unlike other non-apoptotic forms of regulated cell death, there is little evidence that ferroptosis requires specific pore-forming proteins (428, 429). Instead, the execution of ferroptosis involves the peroxidation of phospholipids and the formation of lipid hydroperoxides (430). These lipid hydroperoxides, in turn, react with iron to generate highly reactive lipid radicals and result in plasma membrane rupture through breaking lipid quality control (431). Increased membrane tension resulting from increased lipid peroxidation activates PIEZO1, a mechanosensitive ion channel protein, which opens to allow Ca^{2+} and Na^{+} influx and K^{+} efflux (424, 432). Simultaneously, the plasma membrane Na^{+}/K^{+} ATPase is inactivated, and the loss of ionic homeostasis results in osmotic swelling and plasma membrane rupture (424). The exact biological players involved, and the relative importance of each, remain open questions (433-438).

Thought to be the main cellular defence against ferroptosis is the enzyme glutathione peroxidase 4 (GPX4), which reduces lipid hydroperoxides to lipid alcohols (439-441). This prevents the accumulation of lipid peroxides necessary to initiate ferroptosis. GPX4 is one of 25 selenoproteins in humans, and its expression is therefore regulated by selenium availability (442). Despite this, GPX4 is constitutively expressed in most tissues and organs. In addition, ferroptosis suppressor protein 1 (FSP1) can inhibit lipid peroxidation through an alternative mechanism, reducing coenzyme Q_{10}, which is a powerful antioxidant that can prevent lipid peroxidation (443, 444). Ferroptosis can also be inhibited through membrane repair - endosomal sorting complexes required for transport III (ESCRT-III) can locally repair the plasma membrane and prevent ferroptosis (445). In addition, plasma membrane proteins can inhibit ferroptosis, for example, the lipid flippase SLC47A1 (446) or cystine/glutamate antiporter subunits SLC7A11 and SLC3A2 (447). This is likely due to their transport functionality, as iron or metabolite trafficking is an important component in ferroptosis. An example of this is Prominin2, which facilitates the formation of ferritin-containing multivesicular bodies and exosomes that transport iron out of the cell, inhibiting ferroptosis (416). The role of specific cellular organelles in modulating ferroptosis has been extensively reviewed elsewhere (386).

Ferroptosis has physiologically relevant roles – namely in tumour suppression (447), immune surveillance (448), neuroprotection (449), erythrocyte maturation and iron homeostasis (450, 451). Akin to this, *Gpx4* deficiency and subsequent predisposition to ferroptosis is embryonically lethal in mice (452), results in impaired antiviral defences (453), neurodegeneration (441) and enhanced ischemia/reperfusion injury (440). Further, *Gpx4* ablation in the haematopoietic system of mice results in failed reticulocyte maturation and subsequent anaemia, along with systemic hepatic iron overload and high erythropoietin levels in the plasma (454). Thus, ferroptosis inhibition plays a key role in ery-

thropoiesis (454). Ferroptosis also acts in erythrocyte recycling, as increased uptake of senescent erythrocytes by splenic macrophages induces ferroptosis in mice (450) and gain-of-function mutations in PIEZO1 results in systemic iron overload and interference with iron metabolism (455). Lastly, ferroptosis provides protection against severe disease in a mouse model of *Plasmodium falciparum* infection (456, 457). This suggests a key link between erythrocyte homeostasis, iron homeostasis and ferroptosis. While much is known about the interplay of iron metabolism and ferroptosis (451), there have not yet been major discoveries on the interplay between erythrocyte homeostasis and ferroptosis (458).

Sensing Iron Redox

Cells have inherent mechanisms to protect themselves from the harm that free radicals cause. One example of this is through the NRF2 regulatory hub (Figure 1.13) (388, 459, 460). During homeostasis, NRF2 is bound by Kelch-like ECH-associated protein 1 (KEAP1), which is an adaptor protein of E3 ubiquitin ligase, and promotes NRF2 ubiquitination and proteasomal degradation (388). Oxidative stress disrupts this interaction, and NRF2 is then free to translocate to the nucleus, where it heterodimerises with small musculoaponeurotic fibrosarcoma oncogene homologue (sMAF) and induces the expression of antioxidant response element (ARE)-containing genes. The protein products of ARE-containing genes have key roles in detoxification and antioxidant activity (388). Thus, NRF2-KEAP1 axis is thought of as a thiol-driven master switch, used for system-wide oxidative stress responses (461, 462). NRF2 controls cellular redox status directly, through regulating the transcription of genes involved in the synthesis of NADPH – a critical cofactor involved in antioxidant reactions (463), regulating genes involved in the use of reduced glutathione (464) and regulating the redoxin family of proteins (465). NRF2-KEAP1 regulates both cytosolic and mitochondrial ROS production through its control of NADPH oxidase (466). BTB domain and CNC homologue 1 (BACH1) negatively controls the expression of ARE-containing genes, including haem oxygenase 1 (*HMOX1*) (467). The protein product, HO-1, converts intracellular haem to ferrous iron, carbon dioxide and biliverdin in iron recycling macrophages. NRF2 also regulates the expression of biliverdin reductase (BVR), which generates antioxidant bilirubin from biliverdin (468). The transcriptional activation site of *HMOX1* is competed for by NRF2 and BACH1. When haem is present, it binds BACH1 and promotes its ubiquitination and degradation, freeing up the site for NRF2 binding (388). This system provides an extra layer of regulation for certain important transcripts.

NRF2 also plays a role in regulating the innate immune response, with the *NRF2* transcript being most abundant in monocytes and granulocytes (460). *Nrf2* has been shown

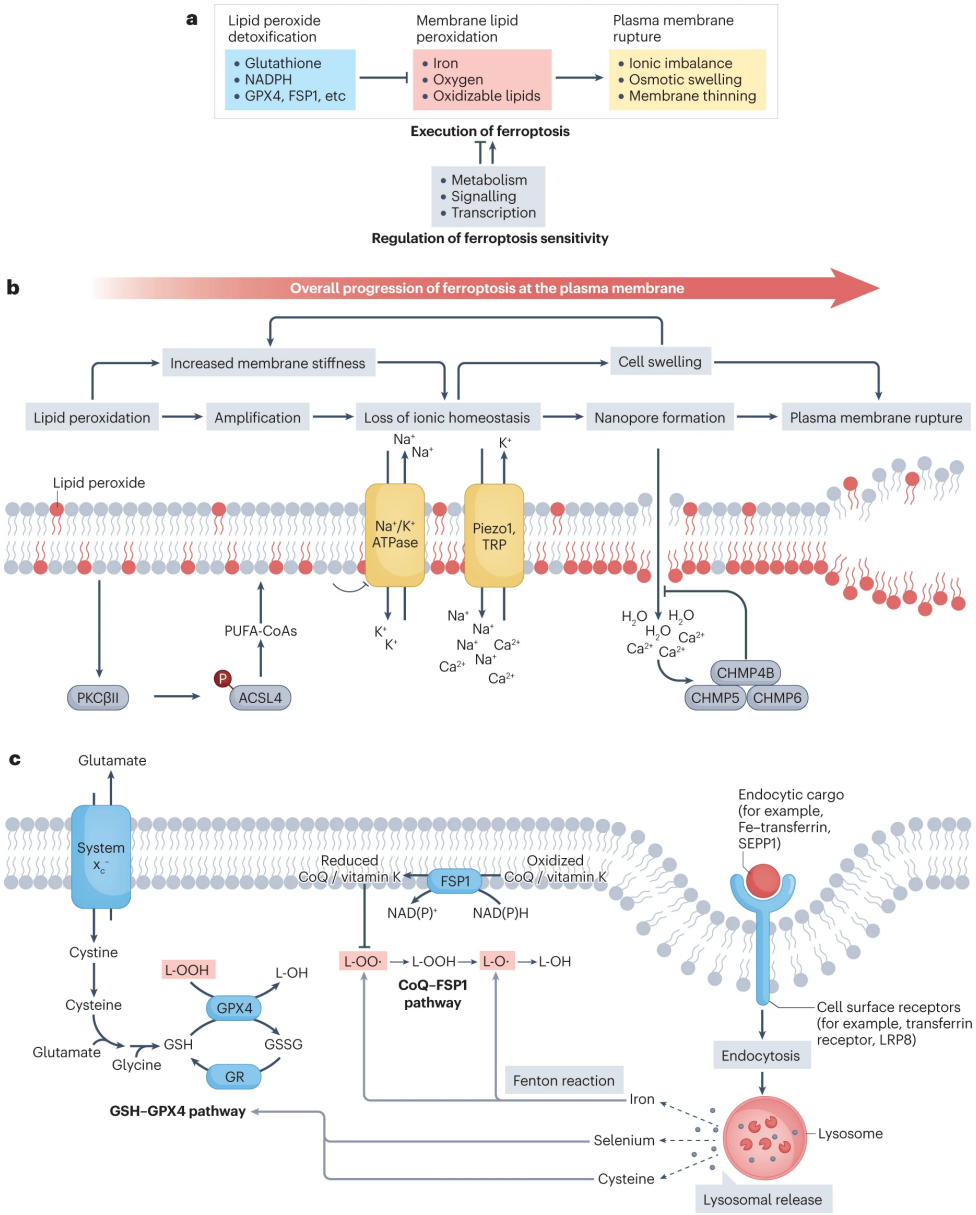


Figure 1.12: The general mechanism of ferroptosis. ***Taken from Figure 1 of Dixon, S. J. and J. A. Olzmann (2024). "The cell biology of ferroptosis." Nature Reviews Molecular Cell Biology 25(6): 424-442.***

a. Ferroptosis execution can be distinguished from the regulation of ferroptosis sensitivity. **b.** Plasma membrane rupture is the key event that results in cell death during ferroptosis. **c.** Important ferroptosis defence mechanisms localise to the plasma membrane. For full figure legend, see Figure 1 of *Dixon, S. J. and J. A. Olzmann (2024). "The cell biology of ferroptosis." Nature Reviews Molecular Cell Biology 25(6): 424-442* (386).

to be critical to survival through suppressing inflammation in mouse models of sepsis (469, 470), important in wound healing (471) and able to repress the expression of pro-inflammatory cytokines in murine macrophages, specifically interfering with IL-6 produc-

tion *in vivo* (472). In humans, mutations in the *NRF2* promoter are associated with ulcerative colitis onset (473) and *Helicobacter* infection (474). This could be due to cross talk with NF-kβ: while NF-kβ may promote the expression of *NRF2* (475), KEAP1 has been shown to inhibit NF-kβ, possibly by degrading IκB kinase-β (476). Finally, NRF2 is implicated in the IFN response, negatively regulating STING through decreasing mRNA stability when activated by a tricarboxylic acid (TCA)-cycle metabolite downstream of TLR engagement (477). NRF2 has also been shown to disrupt the IFN response in vesicular stomatitis (VSV) infection (478). As such, NRF2 is involved in a wealth of human diseases, which have been comprehensively reviewed elsewhere (460).

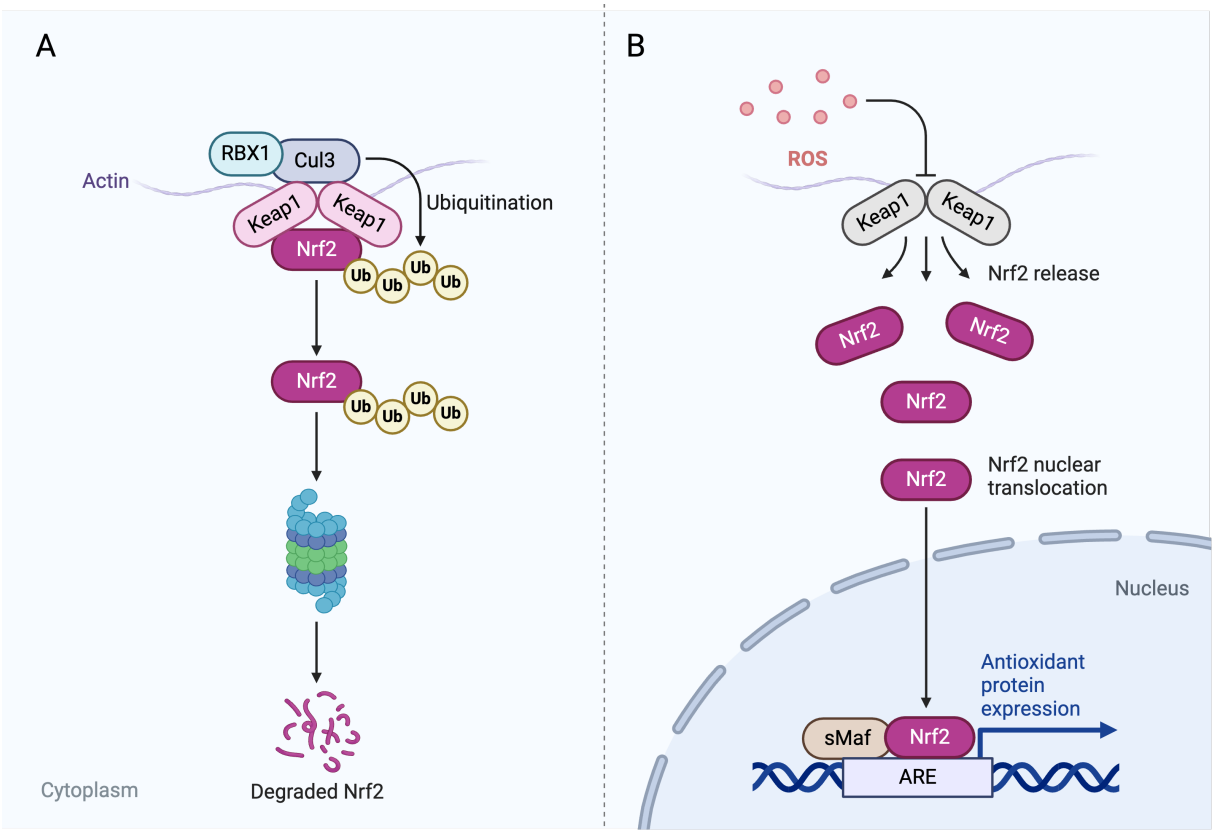


Figure 1.13: NRF2/KEAP1 regulatory axis.

A. Under homeostasis, KEAP1 binds to NRF2 and induces its ubiquitination and proteasomal degradation. **B.** Reactive oxygen species (ROS) presence disrupts this interaction, leaving NRF2 free to translocate to the nucleus, where it heterodimerises with small musculoaponeurotic fibrosarcoma oncogene homologue (sMAF) and induces the expression of antioxidant response element (ARE)-containing genes.

1.4.2 Systemic Iron Homeostasis

Systemic iron homeostasis refers to the control of iron in plasma and organs at large. While I am discussing it as a separate section here, systemic and cellular iron homeostasis

are intrinsically interlinked (388).

The iron hormone hepcidin and its receptor and cellular iron exporter FPN control the major fluxes of iron into blood plasma, which includes intestinal iron absorption, the delivery of recycled iron from macrophages and the release of stored iron from hepatocytes. This is termed the hepcidin-FPN axis (Figure 1.14). Hepcidin is regulated by both iron metabolism, plasma iron concentration, erythropoietic demand for iron, and by inflammatory signals, such as IL-6 and type I IFN (387). Mechanistically, hepcidin binds FPN and induces its ubiquitination and subsequent internalisation and degradation (479, 480). Healthy erythrocytes do not have the full ubiquitination machinery (481), and as such in these cells, hepcidin can directly occlude FPN (482). Hepcidin inhibition of FPN results in the limitation of dietary iron absorption by enterocytes and iron recycling from senescent erythrocytes by macrophages. Transcription of FPN mRNA, *SLC40A1*, is induced by NRF2 and HIF2 (see section 1.4.1). *SLC40A1* expression can be directly repressed by TLR2/6 activation in a mouse model, resulting in a decrease in FPN protein expression and a reduction in plasma iron (483). This is likely a mechanism to prevent the replication of bacterial pathogens, which require iron. In addition, low plasma iron can free transferrin for binding labile iron that is released due to tissue injury and haemolysis during infection. Thus, transient low plasma iron (hypoferremia) can be thought of as a conserved inflammatory response, protecting against infection. Appropriate regulation of hepcidin synthesis is critical to maintain iron homeostasis. Indeed, hepcidin knockout mice become rapidly iron-loaded (484), as do humans with FPN variants that resist hepcidin control (485). Further, hepcidin deficiency causes pathological iron overload in hereditary haemochromatosis (486) and β-thalassaemia (487). As mentioned previously, hepcidin is produced in the liver, which is able to sense and integrate systemic and organ-specific signals, inflammatory cues, metabolic states or erythropoietic activity to regulate the expression of its transcript *Hamp1* (388). Specifically, hepcidin levels are suppressed when erythropoiesis is stimulated or during hypoxia, and enhanced in times of iron abundance (387, 488) or inflammation (489, 490). Its regulation in response to iron is controlled by bone morphogenetic protein (BMP)/SMAD signalling and *Bmp6* expression (491). In turn, BMP6 is regulated by the NRF2-KEAP1-BACH1 system in response to iron-induced mitochondrial reactive lipid species and haem (462).

Hepcidin is upregulated during blood-stage parasitaemia likely because of inflammation, mediating iron redistribution (492). Hepcidin is also upregulated in response to influenza A virus infection, likely through STAT3 signalling (493). Generally, infections or stimuli that invoke a systemic inflammatory response are likely to induce liver hepcidin expression, reduce serum iron, and increase iron accumulation in reticuloendothelial cells (387).

While transient hypoferremia can protect against some pathogens, when prolonged it can

inhibit erythropoiesis and granulopoiesis, influencing the monocyte-to-neutrophil ratio and neutrophil activity (494). In addition, serum iron levels impact the efficacy of the adaptive immune response, with high hepcidin activity resulting in impairment of B-cell responses to immunisation and proliferation of $CD8^+$ and $CD4^+$ T-cells (495, 496). Chronic inflammatory disorders can drive long-lasting hypoferremia, termed anaemia of inflammation (AoI), which is explored further in section 1.4.3.

1.4.3 Erythrocyte Homeostasis

Mammals have evolved to require relatively little dietary iron to survive. In fact, 90% of a human's iron requirements comes from the recycling of senescent red blood cells (RBCs, also called erythrocytes) (Figure 1.15) (497). The iron generated from recycling, diet and freed from hepatic stores forms the plasma iron pool. The plasma iron pool is predominantly utilised during the production of RBCs, in a process called erythropoiesis. Erythropoiesis produces around two and a half million new RBCs per second, which circulate in the blood stream for approximately 120 days in humans (40 days in mice), delivering oxygen and removing carbon dioxide around the body. Oxygen and carbon dioxide are bound within the RBC by haem as part of a protein called haemoglobin. In fact, 70% of mammalian iron is found in complex with haem to carry out this vital process. Erythropoiesis coordinates iron acquisition, synthesis of haem and translation of the globin polypeptides, to generate haemoglobin, a protein composed of two α- and two β-globin chains, which each bind one haem (498-500). Haemoglobin makes up $\geq$98% of total protein content of mature RBCs (501), which have lost all key cellular organelles to make this possible (502). As you would expect from oxygen-transporting cells, RBCs acquire much oxidative damage throughout their lifespan (503), despite carrying antioxidant enzymes and expressing high levels of FPN (409). This is because these transcripts are in limiting supply: RBCs have no capacity for further transcription. Oxidative stress accumulation or RBC damage results in the removal of RBCs from circulation by reticuloendothelial macrophages. Two to three million senescent RBCs are recycled per second by these specialised macrophages in a process termed erythrophagocytosis, giving rise to 25 mg of iron daily (497). This process occurs primarily in the spleen, by tissue-resident red pulp macrophages (RPMs) or in the liver by tissue-resident Kupffer cells (KCs). These are generally the only two organs accepted to be involved in recycling iron: the bone marrow has little to no capacity to engulf senescent RBCs (450). However, one study has shown that during life-threatening malarial anaemia, proximal tubule epithelial cells in the kidney recycle iron through a non-canonical mechanism, contributing towards disease tolerance (408).

Over 60 years in humans, around 400 kg of senescent RBCs are recycled for their iron by

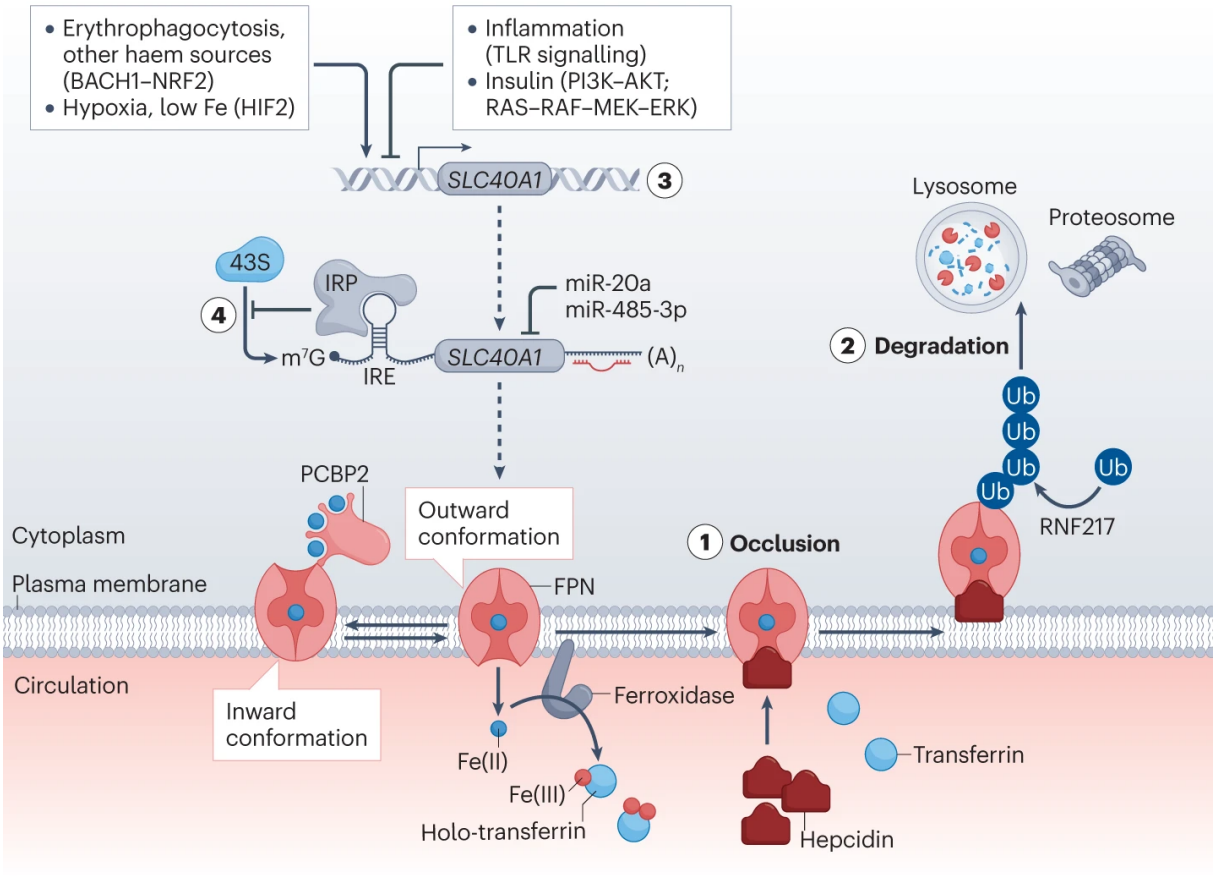


Figure 1.14: Hepcidin control of cellular iron efflux through ferroportin. ***Taken from Figure 6 of Galy, B., et al. (2024). "Mechanisms controlling cellular and systemic iron homeostasis." Nature Reviews Molecular Cell Biology 25(2): 133-155.***

Hepcidin interacts with ferroportin (FPN) channels that actively transport iron out of the cell. Hepcidin binding to FPN can directly obstruct the iron channel **(1)** and/or induce ubiquitination of FPN and internalisation of the FPN–hepcidin complex, which targets FPN for lysosomal or proteasomal degradation **(2)**. The E3 ubiquitin ligase ring finger protein 217 (RNF217) has been identified as responsible for the ubiquitination of FPN. FPN is subject to additional layers of regulation prior to insertion into the membrane. Transcription of the gene encoding FPN (*SLC40A1*) is enhanced by haem (through the BACH1–NRF2 pathway) and hypoxia-inducible factor 2 (HIF2) and repressed by inflammation (through Toll-like receptor (TLR) signalling)) and insulin signalling (PI3K–AKT, RAS–RAF–MEK–ERK) **(3)**. *SLC40A1* translation is inhibited by iron-regulatory proteins (IRPs) binding to iron-responsive elements (IREs) in its 5-prime untranslated region (UTR), whereas microRNAs (miRs) reduce *SLC40A1* mRNA stability (4).

splenic and liver macrophages (497). Therefore, RBC recycling is a fundamental process of vital importance in maintaining the labile iron pool.

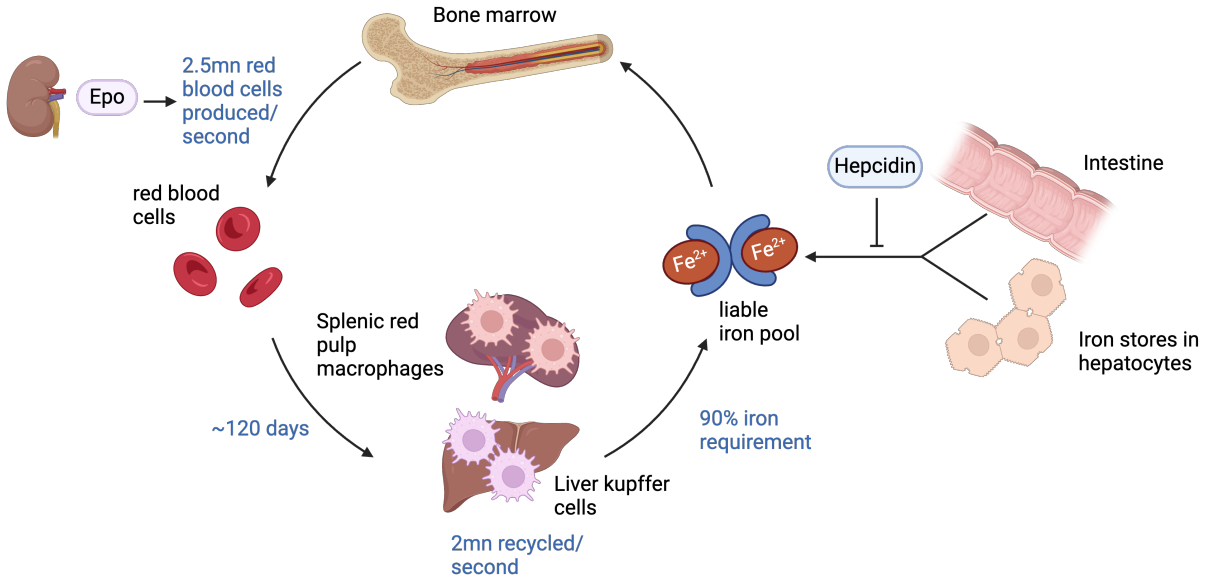


Figure 1.15: Erythrocyte homeostasis.

Red blood cells (RBCs) are produced in the bone marrow at a rate of 2.5 million per second, stimulated by the kidney-produced protein Epo. Mature RBCs circulate in the bloodstream for approximately 120 days, before they become senescent and are phagocytosed by splenic red pulp macrophages (RPMs) or liver Kupffer cells (KCs). Two million are recycled per second, meeting 90% of human's iron requirements. That, plus iron absorbed from diet and stores released from hepatocytes, form the transferrin-iron pool in plasma. Iron release from intestines and hepatocytes can be inhibited by the liver-generated hormone hepcidin. The plasma iron pool is predominantly used in the bone marrow, to create new RBCs.

Erythropoiesis

Erythropoiesis is a multistep process occurring in the bone marrow, lasting around 14 days in humans (Figure 1.16). Multipotential haematopoietic stem and progenitor cells (HSPCs) give rise to erythroid-committed progenitors, which mature into erythroid precursors, enucleated reticulocytes and finally undergo terminal differentiation into RBCs in circulation (502). Initially, erythroid-committed progenitors called burst-forming unit erythroid (BFU-E) cells are produced from HSPCs, which go on to differentiate into colony forming unit erythroid (CFU-E) cells in a developmental continuum (504). The second phase of erythroid maturation is the differentiation of proerythroblasts, the first morphologically distinguishable cells. These then go through multiple rounds of differentiation distinguishable by morphology and cell surface markers (505, 506), including basophilic erythroblasts, polychromatophilic erythroblasts and orthochromatic erythroblasts. In the final steps, the nucleus condenses and extrudes, giving rise to reticulocytes which are released into the peripheral blood. These then fully mature into functional RBCs: losing volume, becoming biconcave and acquiring flexibility, in a process partly

reliant on the presence of RPMs (507). These steps are proposed to be a continuum, based on single-cell RNA sequencing data (508). While each population is clearly defined in flow cytometry (505, 506, 509), there is heterogeneity and overlap between the differentiation states (510). Failure to undergo complete erythropoiesis can result in inflammation. Defective mitophagy results in mature RBCs retaining their mitochondria, and when phagocytosed by RPMs in the spleen, this leads to cGAS/STING activation, type I IFN production and contributed towards the pathology of SLE (511, 512).

The kidney-derived cytokine erythropoietin (EPO) is crucial for erythropoiesis (513-515), and the erythropoietin receptor (EPOR) is expressed on erythroid cells, decreasing with terminal differentiation, as well as in other cells of the haematopoietic lineage (516). The EPO promotor contains a hypoxia-responsive element, which HIFs can bind to and induce its expression (see section 1.4.1) (517). As such, erythropoiesis is driven in times of hypoxia. Alongside EPO, insulin (518), IL-3 (519, 520) and transforming growth factor β superfamily members (521) also stimulate erythropoiesis. Erythropoiesis is additionally controlled on a transcriptional level and a post-transcriptional level (502).

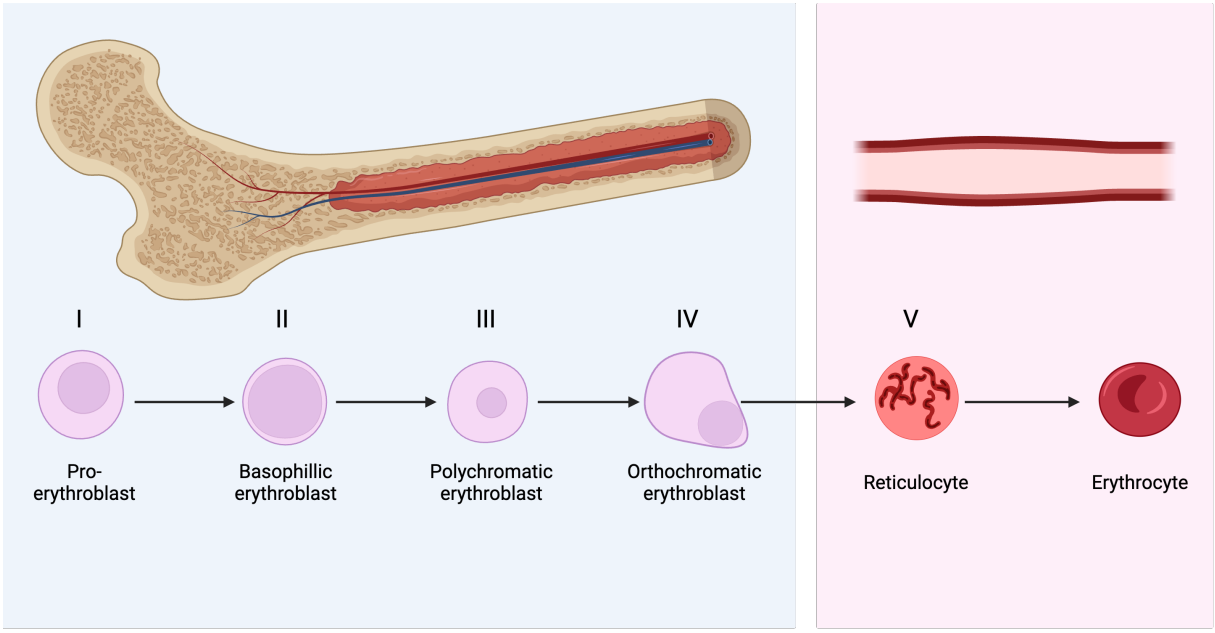


Figure 1.16: Erythropoiesis.

Erythropoiesis predominantly occurs in the bone marrow, whereby erythroid progenitor cells undergo various morphologically distinguishable stages of differentiation, until enucleated reticulocytes are released to the bloodstream, and undergo final maturation to red blood cells.

Erythroblastic Islands

Every step of erythropoiesis, including enucleation, occurs in dedicated areas of the bone marrow called erythroblastic islands (EBIs). Within an EBI, clusters of up to 20 erythroid precursors at varying degrees of maturity surround a central ferritin-rich macrophage, called the EBI macrophage (522, 523). EBI macrophages are tissue-resident macrophages, developing in an identical way to RPMs, and expressing similar surface markers – although, RPMs do not express CD169, while EBI macrophages do (524). EBI macrophages enhance erythropoiesis by promoting survival and proliferation through cell-cell contacts, providing growth factors (525), iron ions (526), and engulfing the extruded nuclei (527). CD169, otherwise known as sialic acid-binding immunoglobulin-type lectin-1 (SIGLEC1) and vascular cell adhesion molecule 1 (VCAM-1), can interact with $\alpha 4\beta 1$ integrins (528), and CD163, which can scavenge haemoglobin-haptoglobin complexes (529) can interact with RBCs (530). Interactions between RBCs and the EBI macrophage allow the provision of nutrients and signals to regulate proliferation and differentiation (531).

EBIs are found in other compartments with facilitate erythropoiesis – for example, the yolk sac, foetal liver and splenic red pulp. However, erythropoiesis only occurs in the former two during development, and only occurs in the latter in times of anaemia or inflammation (532, 533). Bone marrow EBI macrophages can sense inflammatory signals and cause the arrest of medullary erythropoiesis during infection - LPS injection suppresses erythropoiesis, likely due to TLR engagement of the EBI macrophage (534). When medullary erythropoiesis ceases or slows, extramedullary erythropoiesis (so-called stress erythropoiesis) can compensate. Exactly why humans and mice have evolved a system whereby bone marrow erythropoiesis shuts off and splenic erythropoiesis increases during inflammation is an open question. The answers may lay in the fundamental differences in the erythropoietic process itself, with bone marrow erythropoiesis producing a constant rate of RBCs, and extramedullary erythropoiesis producing a bolus of new cells, as discussed below. In addition, as the spleen is the site of iron recycling, splenic RPMs may have a greater capacity for delivering iron to erythropoietic precursors.

Stress Erythropoiesis

Erythropoiesis in the bone marrow produces erythrocytes at a constant rate, balancing the turnover of senescent erythrocytes in the spleen. In mice, when homeostatic erythropoiesis cannot keep up with the erythrocytic demand, stress erythropoiesis predominates which occurs in the spleen (535) and often results in splenomegaly (536, 537). Stress erythropoiesis produces a bolus of new erythrocytes derived from the synchronous differentiation of progenitor cells, unlike the constant steady state production in the bone marrow. This is achieved through deriving stress erythroid progenitors (SEPs) directly from short-term

reconstituting haematopoietic stem cells (HSCs), which migrate from the bone marrow to the spleen. In the spleen, BMP4 and hedgehog result in their commitment to SEPs (538). An increase in serum EPO then allows these SEPs to differentiate, generating a wave of new RBCs (538). The exact mechanisms regulating the proliferation of SEPs, and how they respond to proinflammatory cytokines, are not well understood.

Stress erythropoiesis was first discovered in phenylhydrazine (PHZ)-treated mice recovering from acute anaemia, and likely evolved to relieve acute blood loss and anaemia resulting from inflammation. Indeed, stress erythropoiesis is linked with infection and inflammation. Inflammatory signals such as IFNγ and tumour necrosis factor (TNF)-α inhibit homeostatic bone marrow erythropoiesis (539, 540), increase erythrocyte turnover (539, 541, 542) and enhance stress erythropoiesis (532, 543). TLR engagement along with inflammatory cytokines, particularly IL-6, result in a shift from erythropoiesis to myelopoiesis (539, 544, 545). We additionally saw in section 1.4.2 that inflammation can increase hepcidin levels, resulting in decreased iron bioavailability – both for pathogens and for erythropoiesis. Together, this results in the onset of a type of anaemia termed anaemia of inflammation (AoI). This is the second most common anaemia after iron deficiency anaemia. While there is an initial onset of anaemia in patients and mouse models during infection, eventually splenic stress erythropoiesis compensates and results in recovery (546, 547). This is dependent upon increased EPO levels, driven by innate immune signalling adaptor proteins MyD88 and TRIF (546). However, in patients with chronic inflammatory and autoimmune disorders, AoI will persist (548). Patients with AoI have characteristic changes in systemic iron homeostasis: hypoferremia and hyperferritinemia. It has also been proposed that EBI macrophages are key effectors of AoI, through sensing immune stimuli and shifting their function to mediating an inflammatory response and decreasing bone marrow erythropoiesis (534).

Red Pulp Macrophages

After ≈120 days in circulation, RBCs acquire oxidative damage and become less flexible, meaning they can no longer pass through the narrow endothelial slits in the splenic cords of the red pulp venous sinusoids (549). It is here that they get trapped, opsonised by naturally occurring antibodies and engulfed by specialised macrophages; erythrophagocytic tissue-resident RPMs or RPM-like lymphocyte antigen 6 complex, locus C (Ly6C)$^{\text{hi}}$ monocytes (Figure 1.17) (450, 550). Loss of RBC elasticity occurs not only in aged RBCs, but also in a range of genetic disorders such as sickle cell disease, and certain infections such as malaria. Engulfment is actively repressed in young RBCs through expression of CD47, which binds to signal regulatory protein α (SIRPα) receptor on macrophages and prevents phagocytosis (551, 552). Indeed, malaria parasites preferentially infect young

CD47-expressing RBCs to avoid clearance (553). As RBCs age, they gradually lose CD47 expression (554), and CD47 expression alone is not sufficient to overcome phagocytosis when the RBC has accumulated oxidative stress and is rigid (555, 556). Further, senescent or damaged RBCs express phosphatidylserine (PS), which can be recognised by macrophages which express high levels of PS scavenger receptors (497), alongside through their Fc receptors binding to the opsonised product.

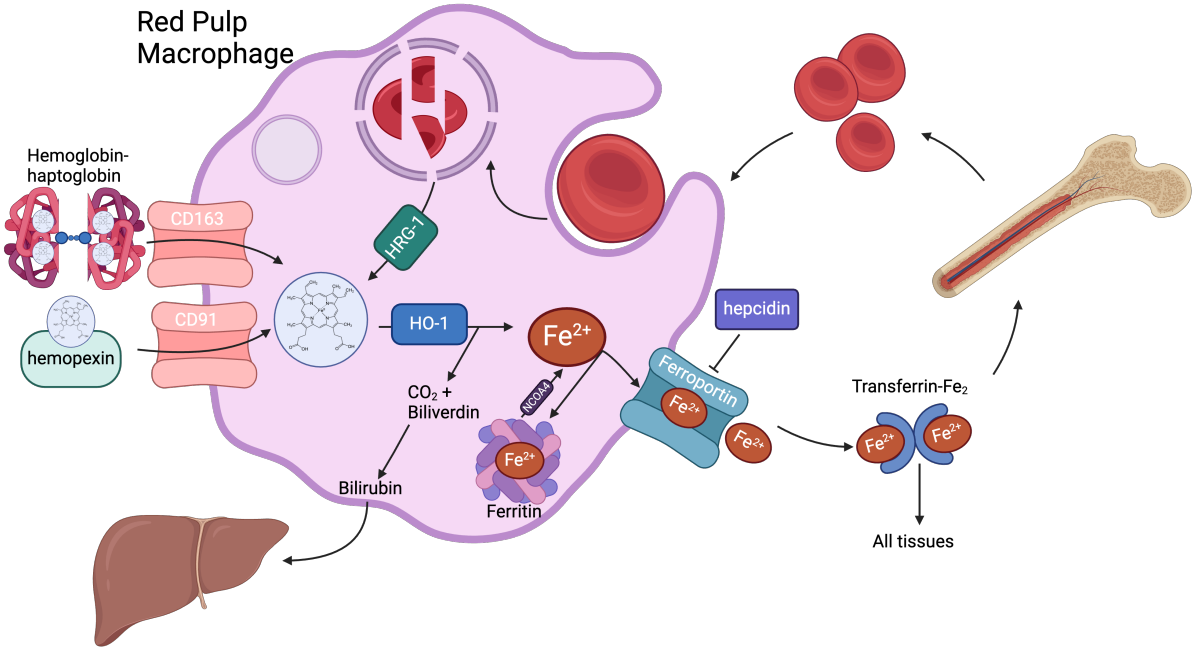


Figure 1.17: Erythrocyte recycling by red pulp macrophages.

Once engulfed, RBCs are rapidly degraded in phagolysosomes, globins are hydrolysed, and their haem is released to the cytoplasm through the transporter HRG-1. Free haem in complex with haptoglobin or haemopexin can additionally be taken up directly through receptor-mediated endocytosis of CD163 or CD91, respectively. Intracellular haem is converted to ferric iron by the enzyme haem oxygenase 1 (HO-1). Ferric iron is exported out of the cell through ferroportin, which is upregulated after erythrophagocytosis, where it can go to the bone marrow to aid erythropoiesis. Alternatively, liver-derived hormone hepcidin can inhibit ferroportin, and ferric iron can be stored in the cell as ferritin. Ferritin can be converted back to ferric iron through the enzyme NCOA4.

If aged RBCs are not taken up by macrophages, they undergo haemolysis, releasing free haemoglobin into the vasculature. Excessive haemolysis contributes towards pathology in many diseases including sickle cell disease and autoimmune haemolytic anaemia. Free haemoglobin is rapidly sequestered by haptoglobin, and the complex is taken up into splenic macrophages through CD163-mediated endocytosis (529, 557). Indeed, CD163 is highly expressed on RPMs and is a marker of highly specialised erythrophagocytic cells (558). Free haem is also scavenged by haemopexin, and haem-haemopexin is taken up

by these macrophages through CD91 (559). One study has additionally proposed RBC haemolysis as the predominant mechanism of RBC uptake in the spleen (558). This is due to the observation of 'erythrocyte ghosts' – RBCs devoid of haemoglobin, which are preferentially taken up by macrophages. Exactly how many RBCs are engulfed whole vs erythrocyte ghosts as a percentage of the total remains to be seen.

Once engulfed, RBCs are rapidly degraded in phagolysosomes, globins are hydrolysed, and their haem is released to the cytoplasm through the transporter HRG-1 (560, 561). HRG-1 was shown to interact with the V-ATPase in yeast, and suppression of HRG-1 lead to a decrease in V-ATPase assembly and a lack of endosomal acidification (562). In mice, HRG-1 deficiency lead to a massive retention of haem in lysosomes, which were 10-100 times larger than usual, and resulted in the formation of the haem crystal haemozoin (563). HRG-1 is thus essential for haem transport from the phagolysosome, and in iron recycling more generally.

Haem in the cytoplasm is rapidly degraded by haem-inducible enzyme HO-1 to carbon dioxide, biliverdin and ferrous iron (561). RPMs express high levels of HO-1, which is essential to their function. As such, approximately 80% of *Hmox1*$^{-/-}$ mice are embryonically lethal (564). As the surviving mice age, they display a progressive loss of CD163^{+} iron recycling macrophages due to cell death following erythrophagocytosis (565). This ultimately results in pathological iron overload in tissues, unregulated macrophage activation, endothelial cell dysfunction and subsequent anaemia, all culminating in systemic inflammatory response syndrome – in both mouse models and human patients with mutations in HO-1 (566, 567). Once released from haem by HO-1, ferric iron is converted to ferritin or exported via FPN, depending on the cellular and tissue-wide iron demand. As *SLC40A1* is a haem-responsive gene, it is induced by erythrophagocytosis and highly expressed in RPMs, meaning under normoxic conditions iron is exported after retrieval from RBCs.

The rate of erythrophagocytosis, and therefore the lifespan of RBCs, can be altered through extracellular signals. For example, there is a recently discovered role for neudesin (a neurotrophic factor, albeit with widespread expression) in suppressing erythrophagocytosis. *Neudesin* deficient macrophages showed increased erythrophagocytosis, while the mice displayed a shortened lifespan of RBCs, increased iron stores in the red pulp, and severe anaemia at 24 weeks of age (568). Conversely, erythrophagocytosis is increased after RPM activation with inflammatory cytokines such as IFNγ (541) and IL-4 (542), or direct PAMP activation (543)

RPMs are tissue-resident macrophages, developing prenatally from yolk-sac progenitors and undergoing expansion driven by proliferator-activated receptor gamma (PPARγ) tran-

scription factor (524). In adulthood, their survival is dependent upon a haem-responsive transcription factor, SPI-C (569, 570). The final step of RPM differentiation is reliant on cytokine IL-33 which is found inside RBCs and released upon their haemolysis (571, 572). RPMs have vast self-renewal capacity, and 12% express proliferation marker Ki-67, locally renewing for longevity within the spleen (573).

During certain pathologies, the embryonically seeded RPM pool may decrease – for example, in cases of hypoxia (574), infections such as malaria (575), or genetic diseases (576). In other instances, acute anaemia may result in excess haemolysis that tissue-resident RPMs alone cannot manage (450). In these cases, Ly6C^{hi} monocytes infiltrate the spleen from the bone marrow and differentiate into RPM-like cells to increase the erythrophagocytic and erythropoietic capacity (536, 575). This is achieved by either recycling RBCs or acting as an EBI macrophage (536, 577). During a mouse model of malaria, the majority of embryonically seeded RPMs are replaced by bone marrow-derived progenitors, which very gradually differentiate into F4/80^{hi}CD11b^{lo} RPMs (575). These monocytes differentiate from monocyte-like (Ly6C^{hi}F4/80^{lo}CD11b^{hi}), to pre-RPM (Ly6C^{lo}F4/80^{lo}CD11b^{hi}) and finally RPM, albeit with a few notable differences to tissue resident RPMs (536). This differentiation process can be driven by TLR7 and TLR9 signalling during sterile inflammation and in a mouse model of malaria (578). Notably, this was not induced by TLR4, TLR3, interleukin-1β, or IFN-γ (578). Further, during induced haem stress, transcription factor NRF2 polarises bone marrow cultures *ex vivo* to become RPM-like cells, and skews fate trajectories away from dendritic cells (459), which was reproduced in a haemolytic mouse model.

As tissue-resident RPMs possess self-renewal capacity and continually process iron, they are susceptible to an age-dependent decline in mice (579). Wild-type female mice of 11 months showed iron loading in RPMs due to a loss of FPN, a lack of erythrophagocytic capacity and subsequent ferroptotic cell death. This leads to a retention of senescent RBCs in the spleen and iron and haem rich extracellular protein aggregates – all of which is rescued through a low-iron diet (579). Therefore, RPM erythrophagocytic capacity decreases with age. As aging often presents as an inflammatory phenotype, excess haem and extracellular iron could represent contributing factors.

RPMs also play a role in innate immunity. They produce type I IFN during malaria infection (580), and cross-prime CD8$^+$ T cell responses during viral infection (581). However, at steady state, RPMs have been reported to release immunosuppressive cytokines such as IL-10, regulating CD4$^+$ T cells (582). In addition, haem-responsive transcription factor SPI-C has a role in fine-tuning the macrophage response to infection, suppressing inflammatory responses while promoting *Fpn* expression (583). Therefore, RPMs likely sense disturbances in iron homeostasis, and respond accordingly through the secretion of

cytokines.

Kupffer Cells

When RPMs within the spleen cannot remove all defective or aged RBCs from circulation, KCs in the liver can perform this role as well. Indeed, *SpiC*$^{-/-}$ mice have no RPMs but normal KCs, and they show normal haematological parameters and serum iron levels, likely due to increased erythrophagocytic function of the liver (570). How RBCs are physically trapped in the liver is less well known, but it is thought that the narrow lumen of liver sinusoidal endothelial cells is packed with KCs (584). Additionally, KCs can aid erythropoiesis in times of acute anaemic stress, developing into EBIs so that extramedullary erythropoiesis can occur (585). KCs are very similar to RPMs in that they are tissue-resident and develop prenatally in the foetal liver. They express the same receptors for recognising RBCs as RPMs, including CD163, and recycle iron from RBCs in the same way (497). In *Hmox1*$^{-/-}$ mice, KCs are gradually lost alongside RPMs, contributing to the total loss of iron recycling capacity and subsequent pathology (565-567). KCs have also been shown to play an important immunomodulatory and anti-inflammatory role after erythrophagocytosis, in a process reliant on haem and NRF2 (586).

The liver displays an on-demand mechanism to clear RBCs and recycle iron in many different pathophysiological conditions (587). Mechanistically, Ly6C^{hi} monocytes accumulate in the liver in response to chemotactic cues and differentiate into FPN-expressing macrophages, recycling defective and senescent RBCs. Importantly, these are distinct from tissue-resident KCs, dependent on transcription factor NRF2 and transient. Therefore, the liver supports rapid RBC removal and iron recycling in acute and chronic anaemic stress, maintaining iron homeostasis.

CD163

As mentioned in section 1.4.3, CD163 is a transmembrane haem scavenger receptor, and is highly expressed on iron-recycling macrophages. It binds haemoglobin-hemopexin complexes, but also has low affinity for free haemoglobin (588), and is pertinent to the clearance of cell-free haemoglobin. It undergoes constitutive, ligand-independent internalisation and recycling between the cell surface and early endosomes (557). It can aid erythropoiesis by mediating interaction between the EBI macrophage and RBCs (530), and it is also a macrophage receptor for bacteria (589). CD163 is predominantly expressed by M2 anti-inflammatory macrophages and as such it is regarded as a marker for M2 macrophages (590). Accordingly, CD163^{+} macrophages are thought to have anti-inflammatory functions, as they produce anti-inflammatory metabolites following haemoglobin detoxifica-

tion, and CD163 expression is potently induced by IL-10, while being downregulated by inflammatory stimuli (590).

Interestingly, a soluble form of CD163 (sCD163) has been identified in plasma (591) as a result of cellular shedding (592, 593). This shedding is inflammation-dependent, requiring TLR engagement, and sCD163 is elevated in a number of inflammatory disorders which have been reviewed previously (590, 594). In humans and non-human primates, proteolytic cleavage of CD163 is similar to that of TNFα, which is mediated by disintegrin and metalloproteinase 17 (ADAM17) (593). ADAM17 is inflammation-responsive, explaining why human sCD163 increases dramatically upon inflammation, and concomitant shedding with TNFα may explain the prevalence of sCD163 in inflammatory disorders (593). Shedding of CD163 allows for the instant downregulation of surface expression, inhibiting further haemoglobin uptake and protecting the macrophage from ferroptotic cell death. The soluble receptor can then scavenge extracellular haemoglobin, acting as a sponge – an idea supported by the fact that some sCD163 is associated with exosomes (595). Free sCD163 bound to haemoglobin can additionally interact with plasma immunoglobulin G (IgG), which bridges the complex to Fc receptors and initiates endocytosis (596). The role of sCD163 specifically in viral disease has been comprehensively reviewed elsewhere (590, 597).

1.5 Objective of this Study

ISGs play a vital role in the innate immune response against viral pathogens; however, while there are hundreds of ISGs, only a few have been well-characterised. *IFI44* and *IFI44L* are prototypical ISGs, induced by IFN and expressed in the early response to infection. Their expression pattern and known implications in antiviral immunity, autoimmune diseases and cancers suggest that they may be important players in the innate antiviral response. Despite this, their biochemical activities and molecular functionalities remain elusive.

In this study, I aim to uncover the molecular function(s) of IFI44 and IFI44L. I investigate their expression kinetics both *in vitro* and *in vivo*, along with uncovering tissue-restriction in their expression. I study whether either protein possess a protective or permissive function during infection with a panel of different viruses, and whether any viruses can antagonise their function. I uncover protein binding partners to provide clues as to cellular functionality. I examine the phenotype of an *Ifi44*$^{-/-}$ mouse model on an *Ifi44l*-deficient background, using RNA-sequencing as an unbiased hypothesis generating approach. Finally, I discover a novel, surprising phenotype of *Ifi44*$^{-/-}$ mice, and characterise haematological abnormalities along with flow-cytometry based immunophenotyping. I aim to

define on a molecular level the exact role IFI44 plays in the innate immune response, and present *Ifi44* as a gene interlinking the IFN response and erythrocyte homeostasis.

References for Chapter 1

1. K. Buchmann, Evolution of Innate Immunity: Clues from Invertebrates via Fish to Mammals. Front Immunol 5, 459 (2014).
2. T. Wein, R. Sorek, Bacterial origins of human cell-autonomous innate immune mechanisms. Nature Reviews Immunology 22, 629-638 (2022).
3. S. Carpenter, L. A. J. O'Neill, From periphery to center stage: 50 years of advancements in innate immunity. Cell 187, 2030-2051 (2024).
4. C. A. Janeway, Jr., Approaching the asymptote? Evolution and revolution in immunology. Cold Spring Harb Symp Quant Biol 54 Pt 1, 1-13 (1989).
5. D. Li, M. Wu, Pattern recognition receptors in health and diseases. Signal Transduction and Targeted Therapy 6, 291 (2021).
6. P. Matzinger, Tolerance, danger, and the extended family. Annu Rev Immunol 12, 991-1045 (1994).
7. F. Randow, J. D. MacMicking, L. C. James, Cellular Self-Defense: How Cell-Autonomous Immunity Protects Against Pathogens. Science 340, 701-706 (2013).
8. S. Kany, J. T. Vollrath, B. Relja, Cytokines in Inflammatory Disease. Int J Mol Sci 20, (2019).
9. J. Deckers et al., Engineering cytokine therapeutics. Nature Reviews Bioengineering 1, 286-303 (2023).
10. A. Isaacs, J. Lindenmann, C. H. Andrewes, Virus interference. I. The interferon. Proceedings of the Royal Society of London. Series B - Biological Sciences 147, 258-267 (1957).
11. D. Tang, R. Kang, T. V. Berghe, P. Vandenabeele, G. Kroemer, The molecular machinery of regulated cell death. Cell Research 29, 347-364 (2019).
12. F. Martinon, K. Burns, J. Tschopp, The Inflammasome: A Molecular Platform Triggering Activation of Inflammatory Caspases and Processing of proIL-β. Molecular Cell 10, 417-426 (2002).
13. J. Fu, K. Schroder, H. Wu, Mechanistic insights from inflammasome structures. Nature Reviews Immunology 24, 518-535 (2024).
14. C. L. Evavold et al., The Pore-Forming Protein Gasdermin D Regulates Interleukin-1 Secretion from Living Macrophages. Immunity 48, 35-44.e36 (2018).
15. P. Yu et al., Pyroptosis: mechanisms and diseases. Signal Transduction and Targeted Therapy 6, 128 (2021).
16. J. Bordet, Les leucocytes et les propriétés actives du sérum chez les vaccinés. Ann Inst Pasteur 9, 462-506 (1895).
17. D. C. Mastellos, G. Hajishengallis, J. D. Lambris, A guide to complement biology, pathology and therapeutic opportunity. Nature Reviews Immunology 24, 118-141 (2024).

18. D. S. Schneider, K. L. Hudson, T. Y. Lin, K. V. Anderson, Dominant and recessive mutations define functional domains of Toll, a transmembrane protein required for dorsal-ventral polarity in the Drosophila embryo. Genes Dev 5, 797-807 (1991).
19. N. J. Gay, F. J. Keith, Drosophila Toll and IL-1 receptor. Nature 351, 355-356 (1991).
20. M. Rosetto, Y. Engstrom, C. T. Baldari, J. L. Telford, D. Hultmark, Signals from the IL-1 receptor homolog, Toll, can activate an immune response in a Drosophila hemocyte cell line. Biochem Biophys Res Commun 209, 111-116 (1995).
21. B. Lemaitre, E. Nicolas, L. Michaut, J.-M. Reichhart, J. A. Hoffmann, The Dorsoventral Regulatory Gene Cassette spätzle/Toll/cactus Controls the Potent Antifungal Response in Drosophila Adults. Cell 86, 973-983 (1996).
22. Y. Xu et al., Structural basis for signal transduction by the Toll/interleukin-1 receptor domains. Nature 408, 111-115 (2000).
23. C. Hashimoto, K. L. Hudson, K. V. Anderson, The Toll gene of Drosophila, required for dorsal-ventral embryonic polarity, appears to encode a transmembrane protein. Cell 52, 269-279 (1988).
24. R. Medzhitov, P. Preston-Hurlburt, C. A. Janeway, A human homologue of the Drosophila Toll protein signals activation of adaptive immunity. Nature 388, 394-397 (1997).
25. A. Poltorak et al., Defective LPS signaling in C3H/HeJ and C57BL/10ScCr mice: mutations in Tlr4 gene. Science 282, 2085-2088 (1998).
26. K. A. Fitzgerald, J. C. Kagan, Toll-like Receptors and the Control of Immunity. Cell 180, 1044-1066 (2020).
27. T. Kawasaki, T. Kawai, Toll-like receptor signaling pathways. Front Immunol 5, 461 (2014).
28. T. Horng, G. M. Barton, R. A. Flavell, R. Medzhitov, The adaptor molecule TIRAP provides signalling specificity for Toll-like receptors. Nature 420, 329-333 (2002).
29. D. Capece et al., NF-Kβ: blending metabolism, immunity, and inflammation. Trends in Immunology 43, 757-775 (2022).
30. N. J. Gay, M. F. Symmons, M. Gangloff, C. E. Bryant, Assembly and localization of Toll-like receptor signalling complexes. Nature Reviews Immunology 14, 546-558 (2014).
31. K. Hoshino et al., Cutting edge: Toll-like receptor 4 (TLR4)-deficient mice are hyporesponsive to lipopolysaccharide: evidence for TLR4 as the Lps gene product. J Immunol 162, 3749-3752 (1999).
32. F. Hayashi et al., The innate immune response to bacterial flagellin is mediated by Toll-like receptor 5. Nature 410, 1099-1103 (2001).
33. J. Y. Kang et al., Recognition of lipopeptide patterns by Toll-like receptor 2-Toll-like receptor 6 heterodimer. Immunity 31, 873-884 (2009).
34. O. Takeuchi et al., Cutting edge: role of Toll-like receptor 1 in mediating immune

response to microbial lipoproteins. J Immunol 169, 10-14 (2002).
35. L. Alexopoulou, A. C. Holt, R. Medzhitov, R. A. Flavell, Recognition of double-stranded RNA and activation of NF-kappaB by Toll-like receptor 3. Nature 413, 732-738 (2001).
36. F. Heil et al., Species-specific recognition of single-stranded RNA via toll-like receptor 7 and 8. Science 303, 1526-1529 (2004).
37. W. Greulich et al., TLR8 Is a Sensor of RNase T2 Degradation Products. Cell 179, 1264-1275 e1213 (2019).
38. S. S. Diebold, T. Kaisho, H. Hemmi, S. Akira, C. Reis e Sousa, Innate antiviral responses by means of TLR7-mediated recognition of single-stranded RNA. Science 303, 1529-1531 (2004).
39. H. Hemmi et al., A Toll-like receptor recognizes bacterial DNA. Nature 408, 740-745 (2000).
40. A. Hidmark, A. von Saint Paul, A. H. Dalpke, Cutting edge: TLR13 is a receptor for bacterial RNA. J Immunol 189, 2717-2721 (2012).
41. G. M. Barton, J. C. Kagan, R. Medzhitov, Intracellular localization of Toll-like receptor 9 prevents recognition of self DNA but facilitates access to viral DNA. Nat Immunol 7, 49-56 (2006).
42. M. E. Peter, A. V. Kubarenko, A. N. Weber, A. H. Dalpke, Identification of an N-terminal recognition site in TLR9 that contributes to CpG-DNA-mediated receptor activation. J Immunol 182, 7690-7697 (2009).
43. M. P. Chan et al., DNase II-dependent DNA digestion is required for DNA sensing by TLR9. Nat Commun 6, 5853 (2015).
44. W. Oda et al., Development of potent unmethylated CpG DNA hydrogel by introducing i-motifs into long single-stranded DNA. International Journal of Pharmaceutics 646, 123438 (2023).
45. Y. J. Crow, Type I interferonopathies: mendelian type I interferon up-regulation. Curr Opin Immunol 32, 7-12 (2015).
46. M. K. Crow, L. Ronnblom, Type I interferons in host defence and inflammatory diseases. Lupus Sci Med 6, e000336 (2019).
47. Y. J. Crow, D. B. Stetson, The type I interferonopathies: 10 years on. Nat Rev Immunol 22, 471-483 (2022).
48. A. Gall et al., Autoimmunity initiates in nonhematopoietic cells and progresses via lymphocytes in an interferon-dependent autoimmune disease. Immunity 36, 120-131 (2012).
49. D. Gao et al., Activation of cyclic GMP-AMP synthase by self-DNA causes autoimmune diseases. Proc Natl Acad Sci U S A 112, E5699-5705 (2015).
50. E. E. Gray, P. M. Treuting, J. J. Woodward, D. B. Stetson, Cutting Edge: cGAS Is

Required for Lethal Autoimmune Disease in the Trex1-Deficient Mouse Model of Aicardi-Goutieres Syndrome. J Immunol 195, 1939-1943 (2015).
51. T. Aoki, J. Hikima, S. D. Hwang, T. S. Jung, Innate immunity of finfish: primordial conservation and function of viral RNA sensors in teleosts. Fish Shellfish Immunol 35, 1689-1702 (2013).
52. M. Schlee, G. Hartmann, Discriminating self from non-self in nucleic acid sensing. Nat Rev Immunol 16, 566-580 (2016).
53. M. Heil, I. Vega-Muñoz, in International Review of Cell and Molecular Biology, C. Vanpouille-Box, L. Galluzzi, Eds. (Academic Press, 2019), vol. 345, pp. 225-285.
54. F. McNab, K. Mayer-Barber, A. Sher, A. Wack, A. O'Garra, Type I interferons in infectious disease. Nature Reviews Immunology 15, 87-103 (2015).
55. C. Soni, B. Reizis, Self-DNA at the Epicenter of SLE: Immunogenic Forms, Regulation, and Effects. Front Immunol 10, 1601 (2019).
56. F. Griffith, The Significance of Pneumococcal Types. Journal of Hygiene 27, 113-159 (1928).
57. K. J. Ishii et al., A Toll-like receptor–independent antiviral response induced by double-stranded B-form DNA. Nature Immunology 7, 40-48 (2006).
58. H. Yoshida, Y. Okabe, K. Kawane, H. Fukuyama, S. Nagata, Lethal anemia caused by interferon-β produced in mouse embryos carrying undigested DNA. Nature Immunology 6, 49-56 (2005).
59. D. B. Stetson, R. Medzhitov, Recognition of cytosolic DNA activates an IRF3-dependent innate immune response. Immunity 24, 93-103 (2006).
60. V. A. K. Rathinam et al., The AIM2 inflammasome is essential for host defense against cytosolic bacteria and DNA viruses. Nature Immunology 11, 395-402 (2010).
61. T. L. Roberts et al., HIN-200 proteins regulate caspase activation in response to foreign cytoplasmic DNA. Science 323, 1057-1060 (2009).
62. V. Hornung et al., AIM2 recognizes cytosolic dsDNA and forms a caspase-1-activating inflammasome with ASC. Nature 458, 514-518 (2009).
63. H. Ishikawa, G. N. Barber, STING is an endoplasmic reticulum adaptor that facilitates innate immune signalling. Nature 455, 674-678 (2008).
64. H. Ishikawa, Z. Ma, G. N. Barber, STING regulates intracellular DNA-mediated, type I interferon-dependent innate immunity. Nature 461, 788-792 (2009).
65. B. Zhong et al., The Adaptor Protein MITA Links Virus-Sensing Receptors to IRF3 Transcription Factor Activation. Immunity 29, 538-550 (2008).
66. D. L. Burdette et al., STING is a direct innate immune sensor of cyclic di-GMP. Nature 478, 515-518 (2011).
67. J. Wu et al., Cyclic GMP-AMP Is an Endogenous Second Messenger in Innate Immune Signaling by Cytosolic DNA. Science 339, 826-830 (2013).

68. L. Sun, J. Wu, F. Du, X. Chen, Z. J. Chen, Cyclic GMP-AMP Synthase Is a Cytosolic DNA Sensor That Activates the Type I Interferon Pathway. Science 339, 786-791 (2013).
69. A. Ablasser et al., cGAS produces a 2-5-linked cyclic dinucleotide second messenger that activates STING. Nature 498, 380-384 (2013).
70. E. J. Diner et al., The innate immune DNA sensor cGAS produces a noncanonical cyclic dinucleotide that activates human STING. Cell Rep 3, 1355-1361 (2013).
71. P. Gao et al., Cyclic G(2',5')pA(3',5') is the metazoan second messenger produced by DNA-activated cyclic GMP-AMP synthase. Cell 153, 1094-1107 (2013).
72. X. Zhang et al., Cyclic GMP-AMP containing mixed phosphodiester linkages is an endogenous high-affinity ligand for STING. Mol Cell 51, 226-235 (2013).
73. N. Samson, A. Ablasser, The cGAS–STING pathway and cancer. Nature Cancer 3, 1452-1463 (2022).
74. A. Decout, J. D. Katz, S. Venkatraman, A. Ablasser, The cGAS–STING pathway as a therapeutic target in inflammatory diseases. Nature Reviews Immunology 21, 548-569 (2021).
75. F. Civril et al., Structural mechanism of cytosolic DNA sensing by cGAS. Nature 498, 332-337 (2013).
76. L. Andreeva et al., cGAS senses long and HMGB/TFAM-bound U-turn DNA by forming protein–DNA ladders. Nature 549, 394-398 (2017).
77. M. Du, Z. J. Chen, DNA-induced liquid phase condensation of cGAS activates innate immune signaling. Science 361, 704-709 (2018).
78. L. Wang, W. Zhou, Phase separation as a new form of regulation in innate immunity. Molecular Cell.
79. A. Ablasser et al., Cell intrinsic immunity spreads to bystander cells via the intercellular transfer of cGAMP. Nature 503, 530-534 (2013).
80. A. Bridgeman et al., Viruses transfer the antiviral second messenger cGAMP between cells. Science 349, 1228-1232 (2015).
81. M. Gentili et al., Transmission of innate immune signaling by packaging of cGAMP in viral particles. Science 349, 1232-1236 (2015).
82. H. T. W. Blest, L. Chauveau, cGAMP the travelling messenger. Front Immunol 14, 1150705 (2023).
83. H. T. W. Blest et al., HSV-1 employs UL56 to antagonize expression and function of cGAMP channels. Cell Reports 43, (2024).
84. J. A. Carozza et al., ENPP1's regulation of extracellular cGAMP is a ubiquitous mechanism of attenuating STING signaling. Proceedings of the National Academy of Sciences 119, e2119189119 (2022).
85. R. Mardjuki et al., Identification of the extracellular membrane protein ENPP3 as a major cGAMP hydrolase and innate immune checkpoint. Cell Reports 43, (2024).

86. C. Lood et al., Neutrophil extracellular traps enriched in oxidized mitochondrial DNA are interferogenic and contribute to lupus-like disease. Nat Med 22, 146-153 (2016).
87. A. P. West et al., Mitochondrial DNA stress primes the antiviral innate immune response. Nature 520, 553-557 (2015).
88. S. Aguirre et al., Dengue virus NS2B protein targets cGAS for degradation and prevents mitochondrial DNA sensing during infection. Nat Microbiol 2, 17037 (2017).
89. C. R. King et al., Pathogen-driven CRISPR screens identify TREX1 as a regulator of DNA self-sensing during influenza virus infection. Cell Host and Microbe 31, 1552-1567.e1558 (2023).
90. L. D. Aarreberg et al., Interleukin-1β Induces mtDNA Release to Activate Innate Immune Signaling via cGAS-STING. Mol Cell 74, 801-815.e806 (2019).
91. D. A. Sliter et al., Parkin and PINK1 mitigate STING-induced inflammation. Nature 561, 258-262 (2018).
92. D. B. Stetson, J. S. Ko, T. Heidmann, R. Medzhitov, Trex1 prevents cell-intrinsic initiation of autoimmunity. Cell 134, 587-598 (2008).
93. C. A. Thomas et al., Modeling of TREX1-Dependent Autoimmune Disease using Human Stem Cells Highlights L1 Accumulation as a Source of Neuroinflammation. Cell Stem Cell 21, 319-331.e318 (2017).
94. M. De Cecco et al., L1 drives IFN in senescent cells and promotes age-associated inflammation. Nature 566, 73-78 (2019).
95. A. Härtlova et al., DNA damage primes the type I interferon system via the cytosolic DNA sensor STING to promote anti-microbial innate immunity. Immunity 42, 332-343 (2015).
96. W. Zhou, L. Mohr, J. Maciejowski, P. J. Kranzusch, cGAS phase separation inhibits TREX1-mediated DNA degradation and enhances cytosolic DNA sensing. Mol Cell 81, 739-755 e737 (2021).
97. J. Rehwinkel, M. U. Gack, RIG-I-like receptors: their regulation and roles in RNA sensing. Nat Rev Immunol 20, 537-551 (2020).
98. M. Yoneyama et al., The RNA helicase RIG-I has an essential function in double-stranded RNA-induced innate antiviral responses. Nat Immunol 5, 730-737 (2004).
99. J. Andrejeva et al., The V proteins of paramyxoviruses bind the IFN-inducible RNA helicase, mda-5, and inhibit its activation of the IFN-beta promoter. Proc Natl Acad Sci U S A 101, 17264-17269 (2004).
100. E. Kowalinski et al., Structural basis for the activation of innate immune pattern-recognition receptor RIG-I by viral RNA. Cell 147, 423-435 (2011).
101. A. Peisley, B. Wu, H. Yao, T. Walz, S. Hur, RIG-I forms signaling-competent filaments in an ATP-dependent, ubiquitin-independent manner. Mol Cell 51, 573-583 (2013).
102. M. Binder et al., Molecular mechanism of signal perception and integration by the

innate immune sensor retinoic acid-inducible gene-I (RIG-I). J Biol Chem 286, 27278-27287 (2011).
103. I. C. Berke, Y. Modis, MDA5 cooperatively forms dimers and ATP-sensitive filaments upon binding double-stranded RNA. Embo j 31, 1714-1726 (2012).
104. V. Hornung et al., 5'-Triphosphate RNA is the ligand for RIG-I. Science 314, 994-997 (2006).
105. M. Schlee et al., Recognition of 5' triphosphate by RIG-I helicase requires short blunt double-stranded RNA as contained in panhandle of negative-strand virus. Immunity 31, 25-34 (2009).
106. A. Pichlmair et al., RIG-I-mediated antiviral responses to single-stranded RNA bearing 5'-phosphates. Science 314, 997-1001 (2006).
107. D. Goubau et al., Antiviral immunity via RIG-I-mediated recognition of RNA bearing 5'-diphosphates. Nature 514, 372-375 (2014).
108. J. Rehwinkel et al., RIG-I detects viral genomic RNA during negative-strand RNA virus infection. Cell 140, 397-408 (2010).
109. S. C. Devarkar et al., Structural basis for m7G recognition and 2-O-methyl discrimination in capped RNAs by the innate immune receptor RIG-I. Proceedings of the National Academy of Sciences 113, 596-601 (2016).
110. L. Gitlin et al., Essential role of mda-5 in type I IFN responses to polyriboinosinic:polyribocytidylic acid and encephalomyocarditis picornavirus. Proceedings of the National Academy of Sciences 103, 8459-8464 (2006).
111. A. Dhir et al., Mitochondrial double-stranded RNA triggers antiviral signalling in humans. Nature 560, 238-242 (2018).
112. S. Ahmad et al., Breaching Self-Tolerance to Alu Duplex RNA Underlies MDA5-Mediated Inflammation. Cell 172, 797-810.e713 (2018).
113. Y. Zhao, X. Ye, W. Dunker, Y. Song, J. Karijolich, RIG-I like receptor sensing of host RNAs facilitates the cell-intrinsic immune response to KSHV infection. Nat Commun 9, 4841 (2018).
114. J. J. Chiang et al., Viral unmasking of cellular 5S rRNA pseudogene transcripts induces RIG-I-mediated immunity. Nat Immunol 19, 53-62 (2018).
115. K. Malathi, B. Dong, M. Gale, R. H. Silverman, Small self-RNA generated by RNase L amplifies antiviral innate immunity. Nature 448, 816-819 (2007).
116. J. P. Wang et al., MDA5 and MAVS Mediate Type I Interferon Responses to Coxsackie B Virus. Journal of Virology 84, 254-260 (2010).
117. L. Slater et al., Co-ordinated role of TLR3, RIG-I and MDA5 in the innate response to rhinovirus in bronchial epithelium. PLoS Pathog 6, e1001178 (2010).
118. Q. Feng et al., MDA5 Detects the Double-Stranded RNA Replicative Form in Picornavirus-Infected Cells. Cell Reports 2, 1187-1196 (2012).

119. L. Gitlin et al., Melanoma differentiation-associated gene 5 (MDA5) is involved in the innate immune response to Paramyxoviridae infection *in vivo*. PLoS Pathog 6, e1000734 (2010).
120. Z. B. Zalinger, R. Elliott, K. M. Rose, S. R. Weiss, MDA5 Is Critical to Host Defense during Infection with Murine Coronavirus. Journal of Virology 89, 12330-12340 (2015).
121. A. Pichlmair et al., Activation of MDA5 Requires Higher-Order RNA Structures Generated during Virus Infection. Journal of Virology 83, 10761-10769 (2009).
122. J. Melchjorsen et al., Early Innate Recognition of Herpes Simplex Virus in Human Primary Macrophages Is Mediated via the MDA5/MAVS-Dependent and MDA5/MAVS/RNA Polymerase III-Independent Pathways. Journal of Virology 84, 11350-11358 (2010).
123. H. Oda et al., Aicardi-Goutières syndrome is caused by *IFIH1* mutations. Am J Hum Genet 95, 121-125 (2014).
124. G. I. Rice et al., Gain-of-function mutations in *IFIH1* cause a spectrum of human disease phenotypes associated with upregulated type I interferon signaling. Nat Genet 46, 503-509 (2014).
125. M. A. Jang et al., Mutations in *DDX58*, which encodes RIG-I, cause atypical Singleton-Merten syndrome. Am J Hum Genet 96, 266-274 (2015).
126. D. J. Smyth et al., A genome-wide association study of nonsynonymous SNPs identifies a type 1 diabetes locus in the interferon-induced helicase (*IFIH1*) region. Nature Genetics 38, 617-619 (2006).
127. Y. Sheng et al., Sequencing-based approach identified three new susceptibility loci for psoriasis. Nature Communications 5, 4331 (2014).
128. A. Martinez et al., Association of the *IFIH1*-GCA-KCNH7 chromosomal region with rheumatoid arthritis. Ann Rheum Dis 67, 137-138 (2008).
129. Y. Jin et al., Genome-wide association analyses identify 13 new susceptibility loci for generalized vitiligo. Nature Genetics 44, 676-680 (2012).
130. C. Enevold et al., Multiple sclerosis and polymorphisms of innate pattern recognition receptors *TLR1-10*, *NOD1-2*, *DDX58*, and *IFIH1*. Journal of Neuroimmunology 212, 125-131 (2009).
131. R. de Reuver, J. Maelfait, Novel insights into double-stranded RNA-mediated immunopathology. Nat Rev Immunol 24, 235-249 (2024).
132. Y. Zhong et al., Zalpha domain proteins mediate the immune response. Front Immunol 14, 1241694 (2023).
133. K. Pestal et al., Isoforms of RNA-Editing Enzyme ADAR1 Independently Control Nucleic Acid Sensor MDA5-Driven Autoimmunity and Multi-organ Development. Immunity 43, 933-944 (2015).
134. H. Chung et al., Human ADAR1 Prevents Endogenous RNA from Triggering Trans-

lational Shutdown. Cell 172, 811-824.e814 (2018).
135. A. Peisley, B. Wu, H. Xu, Z. J. Chen, S. Hur, Structural basis for ubiquitin-mediated antiviral signal activation by RIG-I. Nature 509, 110-114 (2014).
136. W. Zeng et al., Reconstitution of the RIG-I pathway reveals a signaling role of unanchored polyubiquitin chains in innate immunity. Cell 141, 315-330 (2010).
137. M. U. Gack et al., TRIM25 RING-finger E3 ubiquitin ligase is essential for RIG-I-mediated antiviral activity. Nature 446, 916-920 (2007).
138. M. G. Koliopoulos et al., Molecular mechanism of influenza A NS1-mediated TRIM25 recognition and inhibition. Nat Commun 9, 1820 (2018).
139. C. Chiang et al., The Human Papillomavirus E6 Oncoprotein Targets USP15 and TRIM25 To Suppress RIG-I-Mediated Innate Immune Signaling. J Virol 92, (2018).
140. S. Gupta et al., Herpesvirus deconjugases inhibit the IFN response by promoting TRIM25 autoubiquitination and functional inactivation of the RIG-I signalosome. PLoS Pathog 14, e1006852 (2018).
141. G. Manokaran et al., Dengue subgenomic RNA binds TRIM25 to inhibit interferon expression for epidemiological fitness. Science 350, 217-221 (2015).
142. H. Oshiumi et al., The ubiquitin ligase Riplet is essential for RIG-I-dependent innate immune responses to RNA virus infection. Cell Host Microbe 8, 496-509 (2010).
143. M. M. Hu, C. Y. Liao, Q. Yang, X. Q. Xie, H. B. Shu, Innate immunity to RNA virus is regulated by temporal and reversible sumoylation of RIG-I and MDA5. J Exp Med 214, 973-989 (2017).
144. E. Wies et al., Dephosphorylation of the RNA sensors RIG-I and MDA5 by the phosphatase PP1 is essential for innate immune signaling. Immunity 38, 437-449 (2013).
145. D. Acharya et al., Actin cytoskeleton remodeling primes RIG-I-like receptor activation. Cell 185, 3588-3602 e3521 (2022).
146. G. Liu et al., ISG15-dependent activation of the sensor MDA5 is antagonized by the SARS-CoV-2 papain-like protease to evade host innate immunity. Nat Microbiol 6, 467-478 (2021).
147. S. Liu et al., Phosphorylation of innate immune adaptor proteins MAVS, STING, and TRIF induces IRF3 activation. Science 347, aaa2630 (2015).
148. L. M. Landau et al., pLxIS-containing domains are biochemically flexible regulators of interferons and metabolism. Mol Cell 84, 2436-2454.e2410 (2024).
149. L. X. Heinz et al., TASL is the SLC15A4-associated adaptor for IRF5 activation by TLR7-9. Nature 581, 316-322 (2020).
150. X. Cai et al., Prion-like polymerization underlies signal transduction in antiviral immune defense and inflammasome activation. Cell 156, 1207-1222 (2014).
151. A. Lu, V. Kabaleeswaran, T. Fu, V. G. Magupalli, H. Wu, Crystal structure of the F27G AIM2 PYD mutant and similarities of its self-association to DED/DED interac-

tions. J Mol Biol 426, 1420-1427 (2014).
152. M. S. Dick, L. Sborgi, S. Rühl, S. Hiller, P. Broz, ASC filament formation serves as a signal amplification mechanism for inflammasomes. Nature Communications 7, 11929 (2016).
153. F. Hou et al., MAVS forms functional prion-like aggregates to activate and propagate antiviral innate immune response. Cell 146, 448-461 (2011).
154. R. B. Seth, L. Sun, C. K. Ea, Z. J. Chen, Identification and characterization of MAVS, a mitochondrial antiviral signaling protein that activates NF-kappaB and IRF 3. Cell 122, 669-682 (2005).
155. H. H. Park et al., The death domain superfamily in intracellular signaling of apoptosis and inflammation. Annu Rev Immunol 25, 561-586 (2007).
156. J. D. Nanson, B. Kobe, T. Ve, Death, TIR, and RHIM: Self-assembling domains involved in innate immunity and cell-death signaling. Journal of Leukocyte Biology 105, 363-375 (2019).
157. J. C. Kagan, V. G. Magupalli, H. Wu, SMOCs: supramolecular organizing centres that control innate immunity. Nature Reviews Immunology 14, 821-826 (2014).
158. Q. Yin, T.-M. Fu, J. Li, H. Wu, Structural Biology of Innate Immunity. Annual Review of Immunology 33, 393-416 (2015).
159. P. R. Vajjhala, T. Ve, A. Bentham, K. J. Stacey, B. Kobe, The molecular mechanisms of signaling by cooperative assembly formation in innate immunity pathways. Molecular Immunology 86, 23-37 (2017).
160. H. Wu, Higher-Order Assemblies in a New Paradigm of Signal Transduction. Cell 153, 287-292 (2013).
161. A. V. Hauenstein, L. Zhang, H. Wu, The hierarchical structural architecture of inflammasomes, supramolecular inflammatory machines. Current Opinion in Structural Biology 31, 75-83 (2015).
162. S. Nimma, T. Ve, S. J. Williams, B. Kobe, Towards the structure of the TIR-domain signalosome. Current Opinion in Structural Biology 43, 122-130 (2017).
163. T. Ve et al., Structural basis of TIR-domain-assembly formation in MAL- and MyD88-dependent TLR4 signaling. Nature Structural and Molecular Biology 24, 743-751 (2017).
164. H. Xu et al., Structural Basis for the Prion-Like Mavs Filaments in Antiviral Innate Immunity. Biophysical Journal 106, 684a (2014).
165. J. Masumoto et al., ASC, a novel 22-kDa protein, aggregates during apoptosis of human promyelocytic leukemia HL-60 cells. J Biol Chem 274, 33835-33838 (1999).
166. E. Liepinsh et al., The death-domain fold of the ASC PYRIN domain, presenting a basis for PYRIN/PYRIN recognition. J Mol Biol 332, 1155-1163 (2003).
167. S. M. Srinivasula et al., The PYRIN-CARD protein ASC is an activating adaptor

for caspase-1. J Biol Chem 277, 21119-21122 (2002).
168. D. Zheng, T. Liwinski, E. Elinav, Inflammasome activation and regulation: toward a better understanding of complex mechanisms. Cell Discovery 6, 36 (2020).
169. C. Cai, Y. D. Tang, G. Xu, C. Zheng, The crosstalk between viral RNA- and DNA-sensing mechanisms. Cell Mol Life Sci, 1-8 (2021).
170. G. Schreiber, The Role of Type I Interferons in the Pathogenesis and Treatment of COVID-19. Frontiers in Immunology 11, (2020).
171. M. Carty, C. Guy, A. G. Bowie, Detection of Viral Infections by Innate Immunity. Biochem Pharmacol 183, 114316 (2021).
172. Ö. Strannegård, Interferons and their Therapeutic Applications. Ejifcc 11, 52-58 (1999).
173. E. C. Borden et al., Interferons at age 50: past, current and future impact on biomedicine. Nature Reviews Drug Discovery 6, 975-990 (2007).
174. X. Hu, J. li, M. Fu, X. Zhao, W. Wang, The JAK/STAT signaling pathway: from bench to clinic. Signal Transduction and Targeted Therapy 6, 402 (2021).
175. J. W. Schoggins, Interferon-Stimulated Genes: What Do They All Do? Annual Review of Virology 6, 567-584 (2019).
176. J. Piehler, C. Thomas, K. C. Garcia, G. Schreiber, Structural and dynamic determinants of type I interferon receptor assembly and their functional interpretation. Immunol Rev 250, 317-334 (2012).
177. N. A. de Weerd et al., Structural basis of a unique interferon-beta signaling axis mediated via the receptor IFNAR1. Nat Immunol 14, 901-907 (2013).
178. C. J. Secombes, J. Zou, Evolution of Interferons and Interferon Receptors. Front Immunol 8, 209 (2017).
179. Z. Gan et al., Unique Composition of Intronless and Intron-Containing Type I IFNs in the Tibetan Frog Nanorana parkeri Provides New Evidence To Support Independent Retroposition Hypothesis for Type I IFN Genes in Amphibians. J Immunol 201, 3329-3342 (2018).
180. Z. Gan, S. N. Chen, B. Huang, J. Hou, P. Nie, Intronless and intron-containing type I IFN genes coexist in amphibian Xenopus tropicalis: Insights into the origin and evolution of type I IFNs in vertebrates. Dev Comp Immunol 67, 166-176 (2017).
181. D. W. LaFleur et al., Interferon-kappa, a novel type I interferon expressed in human keratinocytes. J Biol Chem 276, 39765-39771 (2001).
182. M. P. Hardy, C. M. Owczarek, L. S. Jermiin, M. Ejdebäck, P. J. Hertzog, Characterization of the type I interferon locus and identification of novel genes. Genomics 84, 331-345 (2004).
183. R. E. Rigby, K. Rue-Albrecht, D. Sims, J. Rehwinkel, Single-cell analysis of signalling and transcriptional responses to type I interferons. bioRxiv, 2023.2007.2003.547491

(2023).
184. T. B. Lavoie et al., Binding and activity of all human alpha interferon subtypes. Cytokine 56, 282-289 (2011).
185. G. Schreiber, The molecular basis for differential type I interferon signaling. J Biol Chem 292, 7285-7294 (2017).
186. S. Ning, J. S. Pagano, G. N. Barber, IRF7: activation, regulation, modification and function. Genes and Immunity 12, 399-414 (2011).
187. I. Marié, J. E. Durbin, D. E. Levy, Differential viral induction of distinct interferon-alpha genes by positive feedback through interferon regulatory factor-7. Embo j 17, 6660-6669 (1998).
188. K. Honda, A. Takaoka, T. Taniguchi, Type I interferon [corrected] gene induction by the interferon regulatory factor family of transcription factors. Immunity 25, 349-360 (2006).
189. E. V. Mesev, R. A. LeDesma, A. Ploss, Decoding type I and III interferon signalling during viral infection. Nat Microbiol 4, 914-924 (2019).
190. O. A. Malakhova et al., UBP43 is a novel regulator of interferon signaling independent of its ISG15 isopeptidase activity. Embo j 25, 2358-2367 (2006).
191. V. François-Newton et al., USP18-based negative feedback control is induced by type I and type III interferons and specifically inactivates interferon response. PLoS One 6, e22200 (2011).
192. S. Wilmes et al., Receptor dimerization dynamics as a regulatory valve for plasticity of type I interferon signaling. J Cell Biol 209, 579-593 (2015).
193. Q. Zhang et al., Inborn errors of type I IFN immunity in patients with life-threatening COVID-19. Science 370, eabd4570 (2020).
194. D. Munnur et al., Altered ISGylation drives aberrant macrophage-dependent immune responses during SARS-CoV-2 infection. Nat Immunol 22, 1416-1427 (2021).
195. M. Bourdon, C. Manet, X. Montagutelli, Host genetic susceptibility to viral infections: the role of type I interferon induction. Genes and Immunity 21, 365-379 (2020).
196. N. Lee et al., *IFITM3*, *TLR3*, and *CD55* Gene SNPs and Cumulative Genetic Risks for Severe Outcomes in Chinese Patients With H7N9/H1N1pdm09 Influenza. J Infect Dis 216, 97-104 (2017).
197. H. K. Lim et al., Severe influenza pneumonitis in children with inherited TLR3 deficiency. J Exp Med 216, 2038-2056 (2019).
198. S. E. Jørgensen et al., Defective RNA sensing by RIG-I in severe influenza virus infection. Clin Exp Immunol 192, 366-376 (2018).
199. L. L. Andersen et al., Functional IRF3 deficiency in a patient with herpes simplex encephalitis. J Exp Med 212, 1371-1379 (2015).
200. M. J. Ciancanelli et al., Infectious disease. Life-threatening influenza and impaired

interferon amplification in human IRF7 deficiency. Science 348, 448-453 (2015).
201. L. C. Platanias, Mechanisms of type-I- and type-II-interferon-mediated signalling. Nature Reviews Immunology 5, 375-386 (2005).
202. M. Soutto, W. Zhou, T. M. Aune, Cutting edge: distal regulatory elements are required to achieve selective expression of IFN-gamma in Th1/Tc1 effector cells. J Immunol 169, 6664-6667 (2002).
203. H. A. Young, J. F. Dray, W. L. Farrar, Expression of transfected human interferon-gamma DNA: evidence for cell-specific regulation. J Immunol 136, 4700-4703 (1986).
204. C. F. Nathan, H. W. Murray, M. E. Wiebe, B. Y. Rubin, Identification of interferon-gamma as the lymphokine that activates human macrophage oxidative metabolism and antimicrobial activity. J Exp Med 158, 670-689 (1983).
205. G. Kak, M. Raza, B. K. Tiwari, Interferon-gamma (IFN-γ): Exploring its implications in infectious diseases. Biomol Concepts 9, 64-79 (2018).
206. A. M. Gocher, C. J. Workman, D. A. A. Vignali, Interferon-γ: teammate or opponent in the tumour microenvironment? Nature Reviews Immunology 22, 158-172 (2022).
207. S. V. Kotenko et al., IFN-λs mediate antiviral protection through a distinct class II cytokine receptor complex. Nature Immunology 4, 69-77 (2003).
208. P. Sheppard et al., IL-28, IL-29 and their class II cytokine receptor IL-28R. Nature Immunology 4, 63-68 (2003).
209. L. Prokunina-Olsson et al., A variant upstream of IFNL3 (IL28B) creating a new interferon gene *IFNL4* is associated with impaired clearance of hepatitis C virus. Nat Genet 45, 164-171 (2013).
210. T. R. O'Brien, L. Prokunina-Olsson, R. P. Donnelly, IFN-λ4: The Paradoxical New Member of the Interferon Lambda Family. Journal of Interferon and Cytokine Research 34, 829-838 (2014).
211. S. E. Doyle et al., Interleukin-29 uses a type 1 interferon-like program to promote antiviral responses in human hepatocytes. Hepatology 44, 896-906 (2006).
212. C. Sommereyns, S. Paul, P. Staeheli, T. Michiels, IFN-lambda (IFN-lambda) is expressed in a tissue-dependent fashion and primarily acts on epithelial cells *in vivo*. PLoS Pathog 4, e1000017 (2008).
213. M. Mordstein et al., Lambda interferon renders epithelial cells of the respiratory and gastrointestinal tracts resistant to viral infections. J Virol 84, 5670-5677 (2010).
214. H. Dickensheets, F. Sheikh, O. Park, B. Gao, R. P. Donnelly, Interferon-lambda (IFN-λ) induces signal transduction and gene expression in human hepatocytes, but not in lymphocytes or monocytes. J Leukoc Biol 93, 377-385 (2013).
215. N. Ank et al., Lambda interferon (IFN-lambda), a type III IFN, is induced by viruses and IFNs and displays potent antiviral activity against select virus infections *in vivo*. J Virol 80, 4501-4509 (2006).

216. J. W. Schoggins et al., A diverse range of gene products are effectors of the type I interferon antiviral response. Nature 472, 481-485 (2011).
217. J. W. Schoggins, C. M. Rice, Interferon-stimulated genes and their antiviral effector functions. Curr Opin Virol 1, 519-525 (2011).
218. J. W. Schoggins, Interferon-Stimulated Genes: What Do They All Do? Annu Rev Virol 6, 567-584 (2019).
219. J. W. Schoggins et al., Pan-viral specificity of IFN-induced genes reveals new roles for cGAS in innate immunity. Nature 505, 691-695 (2014).
220. P. Hubel et al., A protein-interaction network of interferon-stimulated genes extends the innate immune system landscape. Nat Immunol 20, 493-502 (2019).
221. E. Knight, B. D. Korant, Fibroblast interferon induces synthesis of four proteins in human fibroblast cells. Proceedings of the National Academy of Sciences 76, 1824-1827 (1979).
222. C. E. Jones, W. S. Tan, F. Grey, D. J. Hughes, Discovering antiviral restriction factors and pathways using genetic screens. J Gen Virol 102, (2021).
223. S. N. Sarkar, M. K. Harioudh, L. Shao, J. Perez, A. Ghosh, The Many Faces of Oligoadenylate Synthetases. J Interferon Cytokine Res 43, 487-494 (2023).
224. V. Rex, M. Stempel, S. Halle, M. M. Brinkmann, The two faces of oligoadenylate synthetase-like: effective antiviral protein and negative regulator of innate immunity. Curr Opin Virol 60, 101329 (2023).
225. A. L. Brass et al., The IFITM Proteins Mediate Cellular Resistance to Influenza A H1N1 Virus, West Nile Virus, and Dengue Virus. Cell 139, 1243-1254 (2009).
226. C. C. Bailey, G. Zhong, I.-C. Huang, M. Farzan, IFITM-Family Proteins: The Cell and apos;s First Line of Antiviral Defense. Annual Review of Virology 1, 261-283 (2014).
227. J. Lu et al., The IFITM proteins inhibit HIV-1 infection. J Virol 85, 2126-2137 (2011).
228. B. F. Hörnich, A. K. Großkopf, C. J. Dcosta, S. Schlagowski, A. S. Hahn, Interferon-Induced Transmembrane Proteins Inhibit Infection by the Kaposi's Sarcoma-Associated Herpesvirus and the Related Rhesus Monkey Rhadinovirus in a Cell-Specific Manner. mBio 12, e0211321 (2021).
229. J. S. Spence et al., IFITM3 directly engages and shuttles incoming virus particles to lysosomes. Nature Chemical Biology 15, 259-268 (2019).
230. K. Li et al., IFITM proteins restrict viral membrane hemifusion. PLoS Pathog 9, e1003124 (2013).
231. S. Amini-Bavil-Olyaee et al., The antiviral effector IFITM3 disrupts intracellular cholesterol homeostasis to block viral entry. Cell Host Microbe 13, 452-464 (2013).
232. T. M. Desai et al., IFITM3 restricts influenza A virus entry by blocking the formation of fusion pores following virus-endosome hemifusion. PLoS Pathog 10, e1004048

(2014).
233. D. C. Goldstone et al., HIV-1 restriction factor SAMHD1 is a deoxynucleoside triphosphate triphosphohydrolase. Nature 480, 379-382 (2011).
234. C. H. Yu et al., Nucleic acid binding by SAMHD1 contributes to the antiretroviral activity and is enhanced by the GpsN modification. Nature Communications 12, 731 (2021).
235. J. Rehwinkel et al., SAMHD1-dependent retroviral control and escape in mice. The EMBO Journal 32, 2454-2462 (2013).
236. K. Hrecka et al., Vpx relieves inhibition of HIV-1 infection of macrophages mediated by the SAMHD1 protein. Nature 474, 658-661 (2011).
237. N. Laguette et al., SAMHD1 is the dendritic- and myeloid-cell-specific HIV-1 restriction factor counteracted by Vpx. Nature 474, 654-657 (2011).
238. N. Yan, A. D. Regalado-Magdos, B. Stiggelbout, M. A. Lee-Kirsch, J. Lieberman, The cytosolic exonuclease TREX1 inhibits the innate immune response to human immunodeficiency virus type 1. Nat Immunol 11, 1005-1013 (2010).
239. S. R. Simpson, W. O. Hemphill, T. Hudson, F. W. Perrino, TREX1 - Apex predator of cytosolic DNA metabolism. DNA Repair (Amst) 94, 102894 (2020).
240. K. Ozato, D.-M. Shin, T.-H. Chang, H. C. Morse, TRIM family proteins and their emerging roles in innate immunity. Nature Reviews Immunology 8, 849-860 (2008).
241. M. van Gent, K. M. J. Sparrer, M. U. Gack, TRIM Proteins and Their Roles in Antiviral Host Defenses. Annu Rev Virol 5, 385-405 (2018).
242. F. Turrini et al., HIV-1 transcriptional silencing caused by TRIM22 inhibition of Sp1 binding to the viral promoter. Retrovirology 12, 104 (2015).
243. A. Kajaste-Rudnitski et al., TRIM22 inhibits HIV-1 transcription independently of its E3 ubiquitin ligase activity, Tat, and NF-kappaB-responsive long terminal repeat elements. J Virol 85, 5183-5196 (2011).
244. L. Espert et al., ISG20, a new interferon-induced RNase specific for single-stranded RNA, defines an alternative antiviral pathway against RNA genomic viruses. J Biol Chem 278, 16151-16158 (2003).
245. P. El Kazzi et al., Internal RNA 2'O-methylation in the HIV-1 genome counteracts ISG20 nuclease-mediated antiviral effect. Nucleic Acids Res 51, 2501-2515 (2023).
246. H. Yin, Z. Jiang, S. Wang, P. Zhang, IFN-γ restores the impaired function of RNase L and induces mitochondria-mediated apoptosis in lung cancer. Cell Death and Disease 10, 642 (2019).
247. Y. Li et al., Ribonuclease L mediates the cell-lethal phenotype of double-stranded RNA editing enzyme ADAR1 deficiency in a human cell line. eLife 6, e25687 (2017).
248. H. V. Mears, T. R. Sweeney, Mouse Ifit1b is a cap1-RNA–binding protein that inhibits mouse coronavirus translation and is regulated by complexing with Ifit1c. Journal

of Biological Chemistry 295, 17781-17801 (2020).
249. P. Kumar et al., Inhibition of translation by IFIT family members is determined by their ability to interact selectively with the 5'-terminal regions of cap0-, cap1- and 5'ppp- mRNAs. Nucleic Acids Res 42, 3228-3245 (2014).
250. O. Haller, Dynamins Are Forever: MxB Inhibits HIV-1. Cell Host and Microbe 14, 371-373 (2013).
251. G. Betancor et al., The GTPase Domain of MX2 Interacts with the HIV-1 Capsid, Enabling Its Short Isoform to Moderate Antiviral Restriction. Cell Rep 29, 1923-1933.e1923 (2019).
252. Z. Liu et al., The interferon-inducible MxB protein inhibits HIV-1 infection. Cell Host Microbe 14, 398-410 (2013).
253. F. J. D. Alvarez et al., CryoEM structure of MxB reveals a novel oligomerization interface critical for HIV restriction. Science Advances 3, (2017).
254. Jennifer L. Fribourgh et al., Structural Insight into HIV-1 Restriction by MxB. Cell Host and Microbe 16, 627-638 (2014).
255. C. Goujon et al., Human MX2 is an interferon-induced post-entry inhibitor of HIV-1 infection. Nature 502, 559-562 (2013).
256. D. Perez-Caballero et al., Tetherin inhibits HIV-1 release by directly tethering virions to cells. Cell 139, 499-511 (2009).
257. N. Van Damme et al., The interferon-induced protein BST-2 restricts HIV-1 release and is downregulated from the cell surface by the viral Vpu protein. Cell Host Microbe 3, 245-252 (2008).
258. C. L. Ashley, A. Abendroth, B. P. McSharry, B. Slobedman, Interferon-Independent Innate Responses to Cytomegalovirus. Front Immunol 10, 2751 (2019).
259. S.-D. Cho, H. Shin, S. Kim, H. J. Kim, Insights on interferon-independent induction of interferon-stimulated genes shaping the lung's response in early SARS-CoV-2 infection. Heliyon 9, e22997 (2023).
260. B. Hernáez et al., A virus-encoded type I interferon decoy receptor enables evasion of host immunity through cell-surface binding. Nature Communications 9, 5440 (2018).
261. B. Wang et al., Structural basis for STAT2 suppression by flavivirus NS5. Nat Struct Mol Biol 27, 875-885 (2020).
262. G. I. Rice et al., Assessment of interferon-related biomarkers in Aicardi-Goutières syndrome associated with mutations in TREX1, RNASEH2A, RNASEH2B, RNASEH2C, SAMHD1, and ADAR: a case-control study. Lancet Neurol 12, 1159-1169 (2013).
263. R. J. Critchley-Thorne et al., Down-Regulation of the Interferon Signaling Pathway in T Lymphocytes from Patients with Metastatic Melanoma. PLOS Medicine 4, e176 (2007).
264. M. J. Finelli, P. L. Oliver, TLDc proteins: new players in the oxidative stress re-

sponse and neurological disease. Mammalian Genome 28, 395-406 (2017).
265. A. F. Eaton, D. Brown, M. Merkulova, The evolutionary conserved TLDc domain defines a new class of (H(+))V-ATPase interacting proteins. Sci Rep 11, 22654 (2021).
266. Y. Honda et al., Isolation and purification of a non-A, non-B hepatitis-associated microtubular aggregates protein. J Gen Virol 71 (Pt 9), 1999-2004 (1990).
267. D. C. Busse et al., Interferon-Induced Protein 44 and Interferon-Induced Protein 44-Like Restrict Replication of Respiratory Syncytial Virus. J Virol 94, (2020).
268. L. Li, Y. A. Ni, Z. Song, Z. Yi, F. Wang, Identification of pathogenic genes and transcription factors in respiratory syncytial virus. BMC Pediatr 21, 27 (2021).
269. C. Carlton-Smith, R. M. Elliott, Viperin, MTAP44, and Protein Kinase R Contribute to the Interferon-Induced Inhibition of Bunyamwera Orthobunyavirus Replication. Journal of Virology 86, 11548-11557 (2012).
270. D. Power et al., IFI44 suppresses HIV-1 LTR promoter activity and facilitates its latency. Virology 481, 142-150 (2015).
271. M. Sun et al., Screening Host Antiviral Proteins under the Enhanced Immune Responses Induced by a Variant Strain of Porcine Epidemic Diarrhea Virus. Microbiol Spectr 10, e0066122 (2022).
272. X. Xue et al., Protein regulation strategies of the mouse spleen in response to Babesia microti infection. Parasit Vectors 14, 61 (2021).
273. X. Qu et al., Potential roles of IFI44 genes in high resistance to Vibrio in hybrids of Argopecten scallops. Fish Shellfish Immunol, 108702 (2023).
274. M. Rey-Campos, A. Saco, B. Novoa, A. Figueras, Transcriptomic and functional analysis of the antiviral response of mussels after a poly I:C stimulation. Fish Shellfish Immunol, 109867 (2024).
275. L. C. Hallen et al., Antiproliferative activity of the human IFN-alpha-inducible protein IFI44. J Interferon Cytokine Res 27, 675-680 (2007).
276. X. Wu et al., Identification of a Novel Signature and Construction of a Nomogram Predicting Overall Survival in Clear Cell Renal Cell Carcinoma. Front Genet 11, 1017 (2020).
277. H. Pan et al., Interferon-Induced Protein 44 Correlated With Immune Infiltration Serves as a Potential Prognostic Indicator in Head and Neck Squamous Cell Carcinoma. Front Oncol 10, 557157 (2020).
278. D. Rupa et al., ACSL4 upregulates IFI44 and IFI44L expression and promotes the proliferation and invasiveness of head and neck squamous cell carcinoma cells. Cancer Sci, (2024).
279. H. Xu, J. Chen, Y. Wang, Y. Wu, Y. Liang, SELL and IFI44 as potential biomarkers of Sjögren's syndrome and their correlation with immune cell infiltration. Genes Genet Syst, (2021).

280. X. Zhao et al., Identification of key biomarkers and immune infiltration in systemic lupus erythematosus by integrated bioinformatics analysis. J Transl Med 19, 35 (2021).
281. L. Shen et al., Identification and Validation of IFI44 as Key Biomarker in Lupus Nephritis. Front Med (Lausanne) 8, 762848 (2021).
282. Y. Wang et al., Identification and Clinical Correlation Analysis of IFI44 in Systemic Lupus Erythematosus Combined with Bioinformatics and Immune Infiltration Analysis. J Inflamm Res 16, 3219-3231 (2023).
283. S. Elsayed Ramadan Genena et al., Interferon-induced protein 44 (IFI44) and interferon regulatory factor 4 (IRF4) gene expression in rheumatoid arthritis. J Immunoassay Immunochem, 1-20 (2024).
284. M. Shen et al., Identification of key interferon-stimulated genes for indicating the condition of patients with systemic lupus erythematosus. Front Immunol 13, 962393 (2022).
285. M. L. DeDiego, A. Nogales, L. Martinez-Sobrido, D. J. Topham, Interferon-Induced Protein 44 Interacts with Cellular FK506-Binding Protein 5, Negatively Regulates Host Antiviral Responses, and Supports Virus Replication. mBio 10, (2019).
286. X. Qiao et al., The involvement of an interferon-induced protein 44-like (CgIFI44L) in the antiviral immune response of Crassostrea gigas. Fish Shellfish Immunol 129, 96-105 (2022).
287. T. Nosaka et al., Regulatory function of interferon-inducible 44-like for hepatitis B virus covalently closed circular DNA in primary human hepatocytes. Hepatol Res 52, 141-152 (2022).
288. P. Bian et al., RIPK3 Promotes JEV Replication in Neurons via Downregulation of IFI44L. Frontiers in Microbiology 11, (2020).
289. Y. Wang et al., Identification of IFI44L as a new candidate molecular marker for systemic lupus erythematosus. Clin Exp Rheumatol, (2022).
290. M. Salesi, M. H. Dehabadi, R. Salehi, A. Salehi, B. Pakzad, Differentially methylation of *IFI44L* gene promoter in Iranian patients with systemic lupus erythematosus and rheumatoid arthritis. Mol Biol Rep 49, 3065-3072 (2022).
291. B. Zhang, T. Zhou, H. Wu, M. Zhao, Q. Lu, Difference of *IFI44L* methylation and serum IFN-a1 level among patients with discoid and systemic lupus erythematosus and healthy individuals. J Transl Autoimmun 4, 100092 (2021).
292. B. Zhang et al., A simple and highly efficient method of *IFI44L* methylation detection for the diagnosis of systemic lupus erythematosus. Clin Immunol 221, 108612 (2020).
293. M. Karimifar et al., *Interferon-induced protein 44-like* gene promoter is differentially methylated in peripheral blood mononuclear cells of systemic lupus erythematosus patients. J Res Med Sci 24, 99 (2019).
294. M. Zhao et al., *IFI44L* promoter methylation as a blood biomarker for systemic

lupus erythematosus. Ann Rheum Dis 75, 1998-2006 (2016).
295. Y. Cui et al., Exploring the shared molecular mechanisms between systemic lupus erythematosus and primary Sjögren's syndrome based on integrated bioinformatics and single-cell RNA-seq analysis. Front Immunol 14, 1212330 (2023).
296. Y. Wang et al., Identification of *IFI44L* as a new candidate molecular marker for systemic lupus erythematosus. Clin Exp Rheumatol 41, 48-59 (2023).
297. J. Yan et al., DNA damage response-related immune activation signature predicts the response to immune checkpoint inhibitors: from gastrointestinal cancer analysis to pan-cancer validation. Cancer Biol Med 21, 252-266 (2023).
298. H. Yang et al., Integrated weighted gene co-expression network analysis uncovers STAT1(signal transducer and activator of transcription 1) and IFI44L (interferon-induced protein 44-like) as key genes in pulmonary arterial hypertension. Bioengineered 12, 6021-6034 (2021).
299. M. Shang, Y. Zhang, T. Zhang, IFI44L and C1QTNF5 as promising biomarkers of proliferative diabetic retinopathy. Medicine (Baltimore) 101, e31961 (2022).
300. H. Li et al., Integrated expression profiles analysis reveals novel predictive biomarker in pancreatic ductal adenocarcinoma. Oncotarget 8, 52571-52583 (2017).
301. Y. Zeng et al., Comprehensive Analysis of Immune Implication and Prognostic Value of IFI44L in Non-Small Cell Lung Cancer. Frontiers in Oncology 11, (2022).
302. D. Ou, Y. Wu, The prognostic and clinical significance of IFI44L aberrant downregulation in patients with oral squamous cell carcinoma. BMC Cancer 21, 1327 (2021).
303. A. Reyimu et al., Identification of latent biomarkers in connection with progression and prognosis in oral cancer by comprehensive bioinformatics analysis. World J Surg Oncol 19, 240 (2021).
304. J. Y. Wang, J. Q. Wang, S. B. Lu, miR-628-5p promotes growth and migration of osteosarcoma by targeting IFI44L. Biochem Cell Biol 98, 99-105 (2020).
305. W.-C. Huang, S.-L. Tung, Y.-L. Chen, P.-M. Chen, P.-Y. Chu, IFI44L is a novel tumor suppressor in human hepatocellular carcinoma affecting cancer stemness, metastasis, and drug resistance via regulating met/Src signaling pathway. BMC Cancer 18, 609-609 (2018).
306. Y. Takashima et al., Reciprocal expression of the immune response genes CXCR3 and IFI44L as module hubs are associated with patient survivals in primary central nervous system lymphoma. Int J Clin Oncol 28, 468-481 (2023).
307. P. K. Yadalam et al., Gene Interaction Network Analysis Reveals IFI44L as a Drug Target in Rheumatoid Arthritis and Periodontitis. Molecules 27, (2022).
308. Y. Li et al., IFI44L expression is regulated by IRF-1 and HIV-1. FEBS Open Bio 11, 105-113 (2021).
309. Q. Zhang, R. Wu, Y. Tan, J. Huang, S. Luo, Novel polymorphism of *IFI44L* asso-

ciated with the susceptibility and clinical characteristics of systemic lupus erythematosus in a Chinese population. Int Immunopharmacol 117, 109979 (2023).
310. B. Feenstra et al., Common variants associated with general and MMR vaccine-related febrile seizures. Nat Genet 46, 1274-1282 (2014).
311. I. H. Haralambieva et al., Genome-wide associations of *CD46* and *IFI44L* genetic variants with neutralizing antibody response to measles vaccine. Human Genetics 136, 421-435 (2017).
312. I. H. Haralambieva, R. B. Kennedy, I. G. Ovsyannikova, D. J. Schaid, G. A. Poland, Current perspectives in assessing humoral immunity after measles vaccination. Expert Rev Vaccines 18, 75-87 (2019).
313. J. Lempainen et al., Associations Between *IFI44L* Gene Variants and Rates of Respiratory Tract Infections During Early Childhood. J Infect Dis 223, 157-165 (2021).
314. J. A. Herberg et al., Diagnostic Test Accuracy of a 2-Transcript Host RNA Signature for Discriminating Bacterial vs Viral Infection in Febrile Children. Jama 316, 835-845 (2016).
315. S. Tian et al., *FAM89A* and *IFI44L* for distinguishing between viral and bacterial infections in children with febrile illness. Pediatr Investig 5, 195-202 (2021).
316. Y. Lee et al., EWAS of post-COVID-19 patients shows methylation differences in the immune-response associated gene, *IFI44L*, three months after COVID-19 infection. Sci Rep 12, 11478 (2022).
317. E. Weeding, A. H. Sawalha, Deoxyribonucleic Acid Methylation in Systemic Lupus Erythematosus: Implications for Future Clinical Practice. Front Immunol 9, 875 (2018).
318. J. Wang et al., DNA methylation of *IFI44L* as a potential blood biomarker for childhood-onset systemic lupus erythematosus. Pediatric Research, (2024).
319. X. Huang, Y. Tan, R. Wu, Q. Li, S. Luo, MicroRNA-98-5p Inhibits IFI44L-Mediated Differentiation of Dendritic Cells and Activation of Interferon Pathway in Systemic Lupus Erythematosus. Immunol Invest 53, 475-489 (2024).
320. S. Luo, R. Wu, Q. Li, G. Zhang, Epigenetic Regulation of *IFI44L* Expression in Monocytes Affects the Functions of Monocyte-Derived Dendritic Cells in Systemic Lupus Erythematosus. J Immunol Res 2022, 4053038 (2022).
321. J. Garau et al., Altered DNA methylation and gene expression predict disease severity in patients with Aicardi-Goutières syndrome. Clin Immunol 249, 109299 (2023).
322. M. J. Finelli, L. Sanchez-Pulido, K. X. Liu, K. E. Davies, P. L. Oliver, The Evolutionarily Conserved Tre2/Bub2/Cdc16 (TBC), Lysin Motif (LysM), Domain Catalytic (TLDc) Domain Is Neuroprotective against Oxidative Stress. The Journal of biological chemistry 291, 2751-2763 (2016).
323. M. R. Volkert, N. A. Elliott, D. E. Housman, Functional genomics reveals a family of eukaryotic oxidation protection genes. Proc Natl Acad Sci U S A 97, 14530-14535 (2000).

324. M. J. Finelli, L. Sanchez-Pulido, K. X. Liu, K. E. Davies, P. L. Oliver, The Evolutionarily Conserved Tre2/Bub2/Cdc16 (TBC), Lysin Motif (LysM), Domain Catalytic (TLDc) Domain Is Neuroprotective against Oxidative Stress. J Biol Chem 291, 2751-2763 (2016).
325. M. Arnaud-Arnould, M. Tauziet, O. Moncorge, C. Goujon, M. Blaise, Crystal structure of the TLDc domain of human NCOA7-AS. Acta Crystallogr F Struct Biol Commun 77, 230-237 (2021).
326. M. Blaise et al., Crystal structure of the TLDc domain of oxidation resistance protein 2 from zebrafish. Proteins 80, 1694-1698 (2012).
327. D. M. Svistunova et al., Oxidation resistance 1 regulates post-translational modifications of peroxiredoxin 2 in the cerebellum. Free Radic Biol Med 130, 151-162 (2019).
328. G. Jaramillo-Gutierrez, A. Molina-Cruz, S. Kumar, C. Barillas-Mury, The Anopheles gambiae Oxidation Resistance 1 (OXR1) Gene Regulates Expression of Enzymes That Detoxify Reactive Oxygen Species. PLOS ONE 5, e11168 (2010).
329. M. Yang et al., Transcriptome analysis of human OXR1 depleted cells reveals its role in regulating the p53 signaling pathway. Sci Rep 5, 17409 (2015).
330. Y. Sanada et al., Oxidation resistance 1 is essential for protection against oxidative stress and participates in the regulation of aging in *Caenorhabditis elegans*. Free Radical Research 48, 919-928 (2014).
331. K. A. Wilson et al., OXR1 maintains the retromer to delay brain aging under dietary restriction. Nature Communications 15, 467 (2024).
332. N. A. Elliott, M. R. Volkert, Stress induction and mitochondrial localization of Oxr1 proteins in yeast and humans. Mol Cell Biol 24, 3180-3187 (2004).
333. Y. Wu, K. E. Davies, P. L. Oliver, The antioxidant protein Oxr1 influences aspects of mitochondrial morphology. Free Radic Biol Med 95, 255-267 (2016).
334. M. Yang et al., Human OXR1 maintains mitochondrial DNA integrity and counteracts hydrogen peroxide-induced oxidative stress by regulating antioxidant pathways involving p21. Free Radic Biol Med 77, 41-48 (2014).
335. R. Natoli, J. Provis, K. Valter, J. Stone, Expression and role of the early-response gene Oxr1 in the hyperoxia-challenged mouse retina. Invest Ophthalmol Vis Sci 49, 4561-4567 (2008).
336. M. R. Volkert, D. J. Crowley, Preventing Neurodegeneration by Controlling Oxidative Stress: The Role of OXR1. Front Neurosci 14, 611904 (2020).
337. M. J. Finelli, K. X. Liu, Y. Wu, P. L. Oliver, K. E. Davies, Oxr1 improves pathogenic cellular features of ALS-associated FUS and TDP-43 mutations. Hum Mol Genet 24, 3529-3544 (2015).
338. P. L. Oliver et al., Oxr1 is essential for protection against oxidative stress-induced neurodegeneration. PLoS Genet 7, e1002338 (2011).

339. M. G. Williamson et al., Neuronal over-expression of Oxr1 is protective against ALS-associated mutant TDP-43 mislocalisation in motor neurons and neuromuscular defects *in vivo*. Hum Mol Genet 28, 3584-3599 (2019).
340. Y. Jiang et al., Serum secreted miR-137-containing exosomes affects oxidative stress of neurons by regulating OXR1 in Parkinson's disease. Brain Res 1722, 146331 (2019).
341. K. X. Liu et al., Neuron-specific antioxidant OXR1 extends survival of a mouse model of amyotrophic lateral sclerosis. Brain 138, 1167-1181 (2015).
342. J. Wang et al., Loss of Oxidation Resistance 1, OXR1, Is Associated with an Autosomal-Recessive Neurological Disease with Cerebellar Atrophy and Lysosomal Dysfunction. Am J Hum Genet 105, 1237-1253 (2019).
343. Z. Wang, C. D. Berkey, P. I. Watnick, The Drosophila protein mustard tailors the innate immune response activated by the immune deficiency pathway. J Immunol 188, 3993-4000 (2012).
344. V. Uytterhoeven, S. Kuenen, J. Kasprowicz, K. Miskiewicz, P. Verstreken, Loss of Skywalker Reveals Synaptic Endosomes as Sorting Stations for Synaptic Vesicle Proteins. Cell 145, 117-132 (2011).
345. X. Lin et al., A loss-of-function mutation in human *Oxidation Resistance 1* disrupts the spatial–temporal regulation of histone arginine methylation in neurodevelopment. Genome Biology 24, 216 (2023).
346. Y. Li et al., A novel recessive mutation in *OXR1* is identified in patient with hearing loss recapitulated by the knockdown zebrafish. Human Molecular Genetics 32, 764-772 (2022).
347. M. J. Finelli et al., The epilepsy-associated protein TBC1D24 is required for normal development, survival and vesicle trafficking in mammalian neurons. Human Molecular Genetics 28, 584-597 (2018).
348. A. Guven, A. Tolun, TBC1D24 truncating mutation resulting in severe neurodegeneration. Journal of Medical Genetics 50, 199-202 (2013).
349. A.-L. Poulat et al., Homozygous *TBC1D24* mutation in two siblings with familial infantile myoclonic epilepsy (FIME) and moderate intellectual disability. Epilepsy Research 111, 72-77 (2015).
350. A. Falace et al., TBC1D24, an ARF6-Interacting Protein, Is Mutated in Familial Infantile Myoclonic Epilepsy. The American Journal of Human Genetics 87, 365-370 (2010).
351. M. Milh et al., Novel Compound Heterozygous Mutations in TBC1D24 Cause Familial Malignant Migrating Partial Seizures of Infancy. Human Mutation 34, 869-872 (2013).
352. A. Guven, A. Tolun, TBC1D24 truncating mutation resulting in severe neurodegeneration. J Med Genet 50, 199-202 (2013).
353. M. A. Corbett et al., A focal epilepsy and intellectual disability syndrome is due to a mutation in TBC1D24. Am J Hum Genet 87, 371-375 (2010).

354. A. U. Rehman et al., Mutations in TBC1D24, a gene associated with epilepsy, also cause nonsyndromic deafness DFNB86. Am J Hum Genet 94, 144-152 (2014).
355. D. Oziębło et al., TBC1D24 emerges as an important contributor to progressive postlingual dominant hearing loss. Scientific Reports 11, 10300 (2021).
356. H. F. Lee, C. S. Chi, C. R. Tsai, Intrafamilial phenotypic variability in *TBC1D24*-TLDc homozygous pathogenic variant-related developmental and epileptic encephalopathy. Clin Neurol Neurosurg 214, 107142 (2022).
357. K. Lüthy et al., TBC1D24-TLDc-related epilepsy exercise-induced dystonia: rescue by antioxidants in a disease model. Brain 142, 2319-2335 (2019).
358. S. Balestrini et al., TBC1D24 genotype-phenotype correlation: Epilepsies and other neurologic features. Neurology 87, 77-85 (2016).
359. W. Shao, S. Halachmi, M. Brown, ERAP140, a conserved tissue-specific nuclear receptor coactivator. Mol Cell Biol 22, 3358-3372 (2002).
360. H. Arai et al., ERAP140/Nbla10993 is a novel favorable prognostic indicator for neuroblastoma induced in response to retinoic acid. Oncol Rep 19, 1381-1388 (2008).
361. J. Lu et al., Establishment and evaluation of module-based immune-associated gene signature to predict overall survival in patients of colon adenocarcinoma. J Biomed Sci 29, 81 (2022).
362. K. S. Higginbotham et al., A multistage association study identifies a breast cancer genetic locus at NCOA7. Cancer Res 71, 3881-3888 (2011).
363. J. Guo et al., NCOA7 Regulates Growth and Metastasis of Clear Cell Renal Cell Carcinoma via MAPK/ERK Signaling Pathway. Int J Mol Sci 24, (2023).
364. E. Castroflorio et al., The *Ncoa7* locus regulates V-ATPase formation and function, neurodevelopment and behaviour. Cell Mol Life Sci 78, 3503-3524 (2021).
365. M. Merkulova et al., Targeted deletion of the *Ncoa7* gene results in incomplete distal renal tubular acidosis in mice. American Journal of Physiology-Renal Physiology 315, F173-F185 (2018).
366. R. N. Doan et al., Recessive gene disruptions in autism spectrum disorder. Nature Genetics 51, 1092-1098 (2019).
367. L. Yu et al., Induction of a Unique Isoform of the NCOA7 Oxidation Resistance Gene by Interferon β-1b. Journal of Interferon and Cytokine Research 35, 186-199 (2014).
368. T. Doyle et al., The interferon-inducible isoform of NCOA7 inhibits endosome-mediated viral entry. Nat Microbiol 3, 1369-1376 (2018).
369. J. T. Nguyen et al., Mammalian EAK-7 activates alternative mTOR signaling to regulate cell proliferation and migration. Science Advances 4, eaao5838 (2018).
370. J. T. Nguyen et al., mEAK-7 Forms an Alternative mTOR Complex with DNA-PKcs in Human Cancer. iScience 17, 190-207 (2019).
371. I. Chang et al., Targeting of lysosomal-bound protein mEAK-7 for cancer therapy.

Front Oncol 14, 1375498 (2024).
372. C. Zucchini et al., TLDc Domain-Containing Genes in Autism Spectrum Disorder: New Players in the Oxidative Stress Response. Int J Mol Sci 24, (2023).
373. M. Merkulova et al., Mapping the H(+) (V)-ATPase interactome: identification of proteins involved in trafficking, folding, assembly and phosphorylation. Sci Rep 5, 14827 (2015).
374. M. M. Khan et al., Oxidative stress protein Oxr1 promotes V-ATPase holoenzyme disassembly in catalytic activity-independent manner. EMBO J 41, e109360 (2022).
375. S. Klössel et al., Yeast TLDc domain proteins regulate assembly state and subcellular localization of the V-ATPase. The EMBO Journal 43, 1870-1897-1897 (2024).
376. L. Wang, D. Wu, C. V. Robinson, T.-M. Fu, Identification of mEAK-7 as a human V-ATPase regulator via cryo-EM data mining. Proceedings of the National Academy of Sciences 119, e2203742119 (2022).
377. R. Wang, Y. Qin, X.-S. Xie, X. Li, Molecular basis of mEAK7-mediated human V-ATPase regulation. Nature Communications 13, 3272 (2022).
378. R. A. Oot, S. Wilkens, Human V-ATPase function is positively and negatively regulated by TLDc proteins. Structure, (2024).
379. F. Chen, R. Kang, J. Liu, D. Tang, The V-ATPases in cancer and cell death. Cancer Gene Therapy 29, 1529-1541 (2022).
380. A. F. Eaton, M. Merkulova, D. Brown, The H(+)-ATPase (V-ATPase): from proton pump to signaling complex in health and disease. Am J Physiol Cell Physiol 320, C392-c414 (2021).
381. J. Wade, D. J. Byrne, C. J. Ballentine, H. Drakesmith, Temporal variation of planetary iron as a driver of evolution. Proceedings of the National Academy of Sciences 118, e2109865118 (2021).
382. M. R. Teh, A. E. Armitage, H. Drakesmith, Why cells need iron: a compendium of iron utilisation. Trends in Endocrinology and Metabolism, (2024).
383. W. M. Gardner et al., Prevalence, years lived with disability, and trends in anaemia burden by severity and cause, 1990–2021: findings from the Global Burden of Disease Study 2021. The Lancet Haematology 10, e713-e734 (2023).
384. S.-R. Pasricha, J. Tye-Din, M. U. Muckenthaler, D. W. Swinkels, Iron deficiency. The Lancet 397, 233-248 (2021).
385. C. C. Winterbourn, Toxicity of iron and hydrogen peroxide: the Fenton reaction. Toxicology Letters 82-83, 969-974 (1995).
386. S. J. Dixon, J. A. Olzmann, The cell biology of ferroptosis. Nature Reviews Molecular Cell Biology 25, 424-442 (2024).
387. H. Drakesmith, A. M. Prentice, Hepcidin and the Iron-Infection Axis. Science 338, 768-772 (2012).

388. B. Galy, M. Conrad, M. Muckenthaler, Mechanisms controlling cellular and systemic iron homeostasis. Nature Reviews Molecular Cell Biology 25, 133-155 (2024).
389. L. C. Montemiglio et al., Cryo-EM structure of the human ferritin-transferrin receptor 1 complex. Nat Commun 10, 1121 (2019).
390. A. Dautry-Varsat, Receptor-mediated endocytosis: The intracellular journey of transferrin and its receptor. Biochimie 68, 375-381 (1986).
391. Y. Yu et al., Hepatic transferrin plays a role in systemic iron homeostasis and liver ferroptosis. Blood 136, 726-739 (2020).
392. R. S. Ohgami et al., Identification of a ferrireductase required for efficient transferrin-dependent iron uptake in erythroid cells. Nat Genet 37, 1264-1269 (2005).
393. C.-Y. Wang et al., ZIP8 Is an Iron and Zinc Transporter Whose Cell-surface Expression Is Up-regulated by Cellular Iron Loading. Journal of Biological Chemistry 287, 34032-34043 (2012).
394. J. P. Liuzzi, F. Aydemir, H. Nam, M. D. Knutson, R. J. Cousins, Zip14 (*Slc39a14*) mediates non-transferrin-bound iron uptake into cells. Proceedings of the National Academy of Sciences 103, 13612-13617 (2006).
395. S. Müller et al., CD44 regulates epigenetic plasticity by mediating iron endocytosis. Nature Chemistry 12, 929-938 (2020).
396. B. Yu et al., Interactions of ferritin with scavenger receptor class A members. J Biol Chem 295, 15727-15741 (2020).
397. J. Jia et al., Ferritin triggers neutrophil extracellular trap-mediated cytokine storm through Msr1 contributing to adult-onset Still's disease pathogenesis. Nat Commun 13, 6804 (2022).
398. H. Zhang et al., Ferritin-mediated neutrophil extracellular traps formation and cytokine storm via macrophage scavenger receptor in sepsis-associated lung injury. Cell Communication and Signaling 22, 97 (2024).
399. S. Janciauskiene, V. Vijayan, S. Immenschuh, TLR4 Signaling by Heme and the Role of Heme-Binding Blood Proteins. Front Immunol 11, 1964 (2020).
400. D. J. Schaer, F. Vinchi, G. Ingoglia, E. Tolosano, P. W. Buehler, Haptoglobin, hemopexin, and related defense pathways—basic science, clinical perspectives, and drug development. Frontiers in Physiology 5, (2014).
401. F. A. Fischbach, J. W. Anderegg, An X-ray scattering study of ferritin and apoferritin. Journal of Molecular Biology 14, 458-IN415 (1965).
402. F. Hoelzgen et al., Structural basis for the intracellular regulation of ferritin degradation. Nature Communications 15, 3802 (2024).
403. Z. Wang, Iron regulation in ferroptosis. Nature Cell Biology 25, 515-515 (2023).
404. L. Vanoaica, D. Darshan, L. Richman, K. Schümann, L. C. Kühn, Intestinal ferritin H is required for an accurate control of iron absorption. Cell Metab 12, 273-282 (2010).

405. M. S. Ryu, D. Zhang, O. Protchenko, M. Shakoury-Elizeh, C. C. Philpott, PCBP1 and NCOA4 regulate erythroid iron storage and heme biosynthesis. J Clin Invest 127, 1786-1797 (2017).
406. Y. Pan et al., Structural basis of ion transport and inhibition in ferroportin. Nat Commun 11, 5686 (2020).
407. I. Yanatori, D. R. Richardson, K. Imada, F. Kishi, Iron Export through the Transporter Ferroportin 1 Is Modulated by the Iron Chaperone PCBP2. J Biol Chem 291, 17303-17318 (2016).
408. Q. Wu et al., Renal control of life-threatening malarial anemia. Cell Reports 42, 112057 (2023).
409. D. L. Zhang et al., Erythrocytic ferroportin reduces intracellular iron accumulation, hemolysis, and malaria risk. Science 359, 1520-1523 (2018).
410. D. L. Zhang, M. C. Ghosh, H. Ollivierre, Y. Li, T. A. Rouault, Ferroportin deficiency in erythroid cells causes serum iron deficiency and promotes hemolysis due to oxidative stress. Blood 132, 2078-2087 (2018).
411. J. M. Muriuki et al., The ferroportin Q248H mutation protects from anemia, but not malaria or bacteremia. Sci Adv 5, eaaw0109 (2019).
412. G. Corna et al., The Repair of Skeletal Muscle Requires Iron Recycling through Macrophage Ferroportin. J Immunol 197, 1914-1925 (2016).
413. C. Cao, M. D. Fleming, Loss of the placental iron exporter ferroportin 1 causes embryonic demise in late-gestation mouse pregnancy. Development 149, (2022).
414. X. Wang et al., Physiological functions of ferroportin in the regulation of renal iron recycling and ischemic acute kidney injury. American Journal of Physiology-Renal Physiology 315, F1042-F1057 (2018).
415. M. Truman-Rosentsvit et al., Ferritin is secreted via 2 distinct nonclassical vesicular pathways. Blood 131, 342-352 (2018).
416. C. W. Brown et al., Prominin2 Drives Ferroptosis Resistance by Stimulating Iron Export. Dev Cell 51, 575-586.e574 (2019).
417. I. Yanatori, D. R. Richardson, H. S. Dhekne, S. Toyokuni, F. Kishi, CD63 is regulated by iron via the IRE-IRP system and is important for ferritin secretion by extracellular vesicles. Blood 138, 1490-1503 (2021).
418. A. Lopez, P. Cacoub, I. C. Macdougall, L. Peyrin-Biroulet, Iron deficiency anaemia. Lancet 387, 907-916 (2016).
419. Z. I. Cabantchik, W. Breuer, G. Zanninelli, P. Cianciulli, LPI-labile plasma iron in iron overload. Best Pract Res Clin Haematol 18, 277-287 (2005).
420. N. Wilkinson, K. Pantopoulos, The IRP/IRE system *in vivo*: insights from mouse models. Front Pharmacol 5, 176 (2014).
421. C. T. Taylor, C. C. Scholz, The effect of HIF on metabolism and immunity. Nature

Reviews Nephrology 18, 573-587 (2022).
422. Y. M. Shah, L. Xie, Hypoxia-Inducible Factors Link Iron Homeostasis and Erythropoiesis. Gastroenterology 146, 630-642 (2014).
423. S. J. Dixon et al., Ferroptosis: an iron-dependent form of nonapoptotic cell death. Cell 149, 1060-1072 (2012).
424. Y. Hirata et al., Lipid peroxidation increases membrane tension, Piezo1 gating, and cation permeability to execute ferroptosis. Curr Biol 33, 1282-1294.e1285 (2023).
425. J. Samarin et al., Low level of antioxidant capacity biomarkers but not target overexpression predicts vulnerability to ROS-inducing drugs. Redox Biol 62, 102639 (2023).
426. M. Conrad, D. A. Pratt, The chemical basis of ferroptosis. Nat Chem Biol 15, 1137-1147 (2019).
427. S. J. Dixon, D. A. Pratt, Ferroptosis: A flexible constellation of related biochemical mechanisms. Mol Cell 83, 1030-1042 (2023).
428. Y. Dondelinger et al., NINJ1 is activated by cell swelling to regulate plasma membrane permeabilization during regulated necrosis. Cell Death Dis 14, 755 (2023).
429. D. R. Green, The Coming Decade of Cell Death Research: Five Riddles. Cell 177, 1094-1107 (2019).
430. L. E. Pope, S. J. Dixon, Regulation of ferroptosis by lipid metabolism. Trends Cell Biol 33, 1077-1087 (2023).
431. Z. Li, M. Lange, S. J. Dixon, J. A. Olzmann, Lipid Quality Control and Ferroptosis: From Concept to Mechanism. Annu Rev Biochem, (2023).
432. Z. Xiang et al., Piezo1 channel exaggerates ferroptosis of nucleus pulposus cells by mediating mechanical stress-induced iron influx. Bone Research 12, 20 (2024).
433. L. Magtanong et al., Context-dependent regulation of ferroptosis sensitivity. Cell Chem Biol 29, 1409-1418.e1406 (2022).
434. A. N. von Krusenstiern et al., Identification of essential sites of lipid peroxidation in ferroptosis. Nature Chemical Biology 19, 719-730 (2023).
435. O. Zilka et al., On the Mechanism of Cytoprotection by Ferrostatin-1 and Liproxstatin-1 and the Role of Lipid Peroxidation in Ferroptotic Cell Death. ACS Cent Sci 3, 232-243 (2017).
436. S. E. Wenzel et al., PEBP1 Wardens Ferroptosis by Enabling Lipoxygenase Generation of Lipid Death Signals. Cell 171, 628-641.e626 (2017).
437. T. S. Anthonymuthu et al., Resolving the paradox of ferroptotic cell death: Ferrostatin-1 binds to 15LOX/PEBP1 complex, suppresses generation of peroxidized ETE-PE, and protects against ferroptosis. Redox Biol 38, 101744 (2021).
438. X. Jiang, B. R. Stockwell, M. Conrad, Ferroptosis: mechanisms, biology and role in disease. Nature Reviews Molecular Cell Biology 22, 266-282 (2021).
439. A. Roveri, M. Maiorino, C. Nisii, F. Ursini, Purification and characterization of phos-

pholipid hydroperoxide glutathione peroxidase from rat testis mitochondrial membranes. Biochim Biophys Acta 1208, 211-221 (1994).
440. J. P. Friedmann Angeli et al., Inactivation of the ferroptosis regulator Gpx4 triggers acute renal failure in mice. Nat Cell Biol 16, 1180-1191 (2014).
441. A. Seiler et al., Glutathione peroxidase 4 senses and translates oxidative stress into 12/15-lipoxygenase dependent- and AIF-mediated cell death. Cell Metab 8, 237-248 (2008).
442. I. Ingold et al., Selenium Utilization by GPX4 Is Required to Prevent Hydroperoxide-Induced Ferroptosis. Cell 172, 409-422.e421 (2018).
443. K. Bersuker et al., The CoQ oxidoreductase FSP1 acts parallel to GPX4 to inhibit ferroptosis. Nature 575, 688-692 (2019).
444. S. Doll et al., FSP1 is a glutathione-independent ferroptosis suppressor. Nature 575, 693-698 (2019).
445. E. Dai, L. Meng, R. Kang, X. Wang, D. Tang, ESCRT-III-dependent membrane repair blocks ferroptosis. Biochem Biophys Res Commun 522, 415-421 (2020).
446. Z. Lin et al., The lipid flippase SLC47A1 blocks metabolic vulnerability to ferroptosis. Nat Commun 13, 7965 (2022).
447. L. Jiang et al., Ferroptosis as a p53-mediated activity during tumour suppression. Nature 520, 57-62 (2015).
448. W. Wang et al., CD8(+) T cells regulate tumour ferroptosis during cancer immunotherapy. Nature 569, 270-274 (2019).
449. M. Jakaria, A. A. Belaidi, A. I. Bush, S. Ayton, Ferroptosis as a mechanism of neurodegeneration in Alzheimer's disease. J Neurochem 159, 804-825 (2021).
450. L. A. Youssef et al., Increased erythrophagocytosis induces ferroptosis in red pulp macrophages in a mouse model of transfusion. Blood 131, 2581-2593 (2018).
451. Y. Chen, X. Li, S. Wang, R. Miao, J. Zhong, Targeting Iron Metabolism and Ferroptosis as Novel Therapeutic Approaches in Cardiovascular Diseases. Nutrients 15, (2023).
452. S. H. Brütsch et al., Expression of inactive glutathione peroxidase 4 leads to embryonic lethality, and inactivation of the Alox15 gene does not rescue such knock-in mice. Antioxid Redox Signal 22, 281-293 (2015).
453. M. Matsushita et al., T cell lipid peroxidation induces ferroptosis and prevents immunity to infection. J Exp Med 212, 555-568 (2015).
454. S. Altamura et al., Glutathione peroxidase 4 and vitamin E control reticulocyte maturation, stress erythropoiesis and iron homeostasis. Haematologica 105, 937-950 (2020).
455. S. Ma et al., A role of PIEZO1 in iron metabolism in mice and humans. Cell 184, 969-982 e913 (2021).
456. H. S. Kain et al., Liver stage malaria infection is controlled by host regulators of lipid peroxidation. Cell Death Differ 27, 44-54 (2020).

457. S. Li et al., Ferroptosis plays an essential role in the antimalarial mechanism of low-dose dihydroartemisinin. Biomed Pharmacother 148, 112742 (2022).
458. S. Lin, Y. Zheng, M. Chen, L. Xu, H. Huang, The interactions between ineffective erythropoiesis and ferroptosis in β-thalassemia. Front Physiol 15, 1346173 (2024).
459. F. Vallelian et al., Heme-stress activated NRF2 skews fate trajectories of bone marrow cells from dendritic cells towards red pulp-like macrophages in hemolytic anemia. Cell Death Differ 29, 1450-1465 (2022).
460. A. Cuadrado et al., Therapeutic targeting of the NRF2 and KEAP1 partnership in chronic diseases. Nat Rev Drug Discov 18, 295-317 (2019).
461. H. Sies, C. Berndt, D. P. Jones, Oxidative Stress. Annu Rev Biochem 86, 715-748 (2017).
462. P. J. Lim et al., Nrf2 controls iron homoeostasis in haemochromatosis and thalassaemia via Bmp6 and hepcidin. Nature Metabolism 1, 519-531 (2019).
463. K. C. Wu, J. Y. Cui, C. D. Klaassen, Beneficial role of Nrf2 in regulating NADPH generation and consumption. Toxicol Sci 123, 590-600 (2011).
464. J. D. Hayes, A. T. Dinkova-Kostova, The Nrf2 regulatory network provides an interface between redox and intermediary metabolism. Trends Biochem Sci 39, 199-218 (2014).
465. M. Tanito, M. P. Agbaga, R. E. Anderson, Upregulation of thioredoxin system via Nrf2-antioxidant responsive element pathway in adaptive-retinal neuroprotection *in vivo* and *in vitro*. Free Radic Biol Med 42, 1838-1850 (2007).
466. S. Kovac et al., Nrf2 regulates ROS production by mitochondria and NADPH oxidase. Biochim Biophys Acta 1850, 794-801 (2015).
467. K. Igarashi, M. Watanabe-Matsui, Wearing Red for Signaling: The Heme-Bach Axis in Heme Metabolism, Oxidative Stress Response and Iron Immunology. The Tohoku Journal of Experimental Medicine 232, 229-253 (2014).
468. T. W. Sedlak et al., Bilirubin and glutathione have complementary antioxidant and cytoprotective roles. Proc Natl Acad Sci U S A 106, 5171-5176 (2009).
469. R. K. Thimmulappa et al., Nrf2 is a critical regulator of the innate immune response and survival during experimental sepsis. J Clin Invest 116, 984-995 (2006).
470. X. Kong et al., Enhancing Nrf2 pathway by disruption of Keap1 in myeloid leukocytes protects against sepsis. Am J Respir Crit Care Med 184, 928-938 (2011).
471. M. Long et al., An Essential Role of NRF2 in Diabetic Wound Healing. Diabetes 65, 780-793 (2016).
472. E. H. Kobayashi et al., Nrf2 suppresses macrophage inflammatory response by blocking proinflammatory cytokine transcription. Nat Commun 7, 11624 (2016).
473. T. Arisawa et al., *Nrf2* gene promoter polymorphism is associated with ulcerative colitis in a Japanese population. Hepatogastroenterology 55, 394-397 (2008).
474. T. Arisawa et al., The relationship between Helicobacter pylori infection and pro-

moter polymorphism of the *Nrf2* gene in chronic gastritis. Int J Mol Med 19, 143-148 (2007).
475. S. A. Rushworth et al., The high Nrf2 expression in human acute myeloid leukemia is driven by NF-κB and underlies its chemo-resistance. Blood 120, 5188-5198 (2012).
476. D. F. Lee et al., KEAP1 E3 ligase-mediated downregulation of NF-kappaB signaling by targeting IKKbeta. Mol Cell 36, 131-140 (2009).
477. D. Olagnier et al., Nrf2 negatively regulates STING indicating a link between antiviral sensing and metabolic reprogramming. Nat Commun 9, 3506 (2018).
478. D. Olagnier et al., Activation of Nrf2 Signaling Augments Vesicular Stomatitis Virus Oncolysis via Autophagy-Driven Suppression of Antiviral Immunity. Mol Ther 25, 1900-1916 (2017).
479. L. Jiang et al., RNF217 regulates iron homeostasis through its E3 ubiquitin ligase activity by modulating ferroportin degradation. Blood 138, 689-705 (2021).
480. E. Nemeth et al., Hepcidin Regulates Cellular Iron Efflux by Binding to Ferroportin and Inducing Its Internalization. Science 306, 2090-2093 (2004).
481. A. Frimpong et al., Profiling the E3 Ubiquitin Ligase Landscape in Normal and Sickle Red Blood Cells. Blood 140, 11096-11096 (2022).
482. S. Aschemeyer et al., Structure-function analysis of ferroportin defines the binding site and an alternative mechanism of action of hepcidin. Blood 131, 899-910 (2018).
483. C. Guida et al., A novel inflammatory pathway mediating rapid hepcidin-independent hypoferremia. Blood 125, 2265-2275 (2015).
484. G. Nicolas et al., Lack of hepcidin gene expression and severe tissue iron overload in upstream stimulatory factor 2 (USF2) knockout mice. Proc Natl Acad Sci U S A 98, 8780-8785 (2001).
485. H. Drakesmith et al., Resistance to hepcidin is conferred by hemochromatosis-associated mutations of ferroportin. Blood 106, 1092-1097 (2005).
486. J. K. Olynyk, G. A. Ramm, Hemochromatosis. N Engl J Med 387, 2159-2170 (2022).
487. R. Gupta, K. M. Musallam, A. T. Taher, S. Rivella, Ineffective Erythropoiesis: Anemia and Iron Overload. Hematology/Oncology Clinics of North America 32, 213-221 (2018).
488. C. Clara, N. Antonella, S. Laura, Iron metabolism and iron disorders revisited in the hepcidin era. Haematologica 105, 260-272 (2020).
489. M. V. Verga Falzacappa et al., STAT3 mediates hepatic hepcidin expression and its inflammatory stimulation. Blood 109, 353-358 (2007).
490. N. K. Shanmugam, K. Chen, B. J. Cherayil, Commensal Bacteria-induced Interleukin 1β (IL-1β) Secreted by Macrophages Up-regulates Hepcidin Expression in Hepatocytes by Activating the Bone Morphogenetic Protein Signaling Pathway. J Biol Chem 290, 30637-30647 (2015).

491. L. Kautz et al., Iron regulates phosphorylation of Smad1/5/8 and gene expression of Bmp6, Smad7, Id1, and Atoh8 in the mouse liver. Blood 112, 1503-1509 (2008).
492. N. Spottiswoode, P. E. Duffy, H. Drakesmith, Iron, anemia and hepcidin in malaria. Front Pharmacol 5, 125 (2014).
493. A. E. Armitage et al., Hepcidin regulation by innate immune and infectious stimuli. Blood 118, 4129-4139 (2011).
494. J. N. Frost et al., Plasma iron controls neutrophil production and function. Science Advances 8, eabq5384 (2022).
495. J. N. Frost et al., Hepcidin-Mediated Hypoferremia Disrupts Immune Responses to Vaccination and Infection. Med 2, 164-179.e112 (2021).
496. A. E. Preston, H. Drakesmith, J. N. Frost, Adaptive immunity and vaccination - iron in the spotlight. Immunother Adv 1, ltab007 (2021).
497. P. Slusarczyk, K. Mleczko-Sanecka, The Multiple Facets of Iron Recycling. Genes (Basel) 12, (2021).
498. M. H. Ahmed, M. S. Ghatge, M. K. Safo, Hemoglobin: Structure, Function and Allostery. Subcell Biochem 94, 345-382 (2020).
499. D. J. Weatherall, The genetic control of protein synthesis: The haemoglobin model. J Clin Pathol Suppl (R Coll Pathol) 8, 1-11 (1974).
500. A. E. Preston et al., Ancient genomic linkage couples metabolism with erythroid development. bioRxiv, (2023).
501. B. J. Ravenhill et al., Quantitative comparative analysis of human erythrocyte surface proteins between individuals from two genetically distinct populations. Communications Biology 2, 350 (2019).
502. A. L. Caulier, V. G. Sankaran, Molecular and cellular mechanisms that regulate human erythropoiesis. Blood 139, 2450-2459 (2022).
503. M. L. Tyan, Age-related increase in erythrocyte oxidant sensitivity. Mechanisms of Ageing and Development 20, 25-32 (1982).
504. H. Li et al., Rate of Progression through a Continuum of Transit-Amplifying Progenitor Cell States Regulates Blood Cell Production. Dev Cell 49, 118-129.e117 (2019).
505. J. Liu et al., Quantitative analysis of murine terminal erythroid differentiation *in vivo*: novel method to study normal and disordered erythropoiesis. Blood 121, e43-e49 (2013).
506. K. Chen et al., Resolving the distinct stages in erythroid differentiation based on dynamic changes in membrane protein expression during erythropoiesis. Proc Natl Acad Sci U S A 106, 17413-17418 (2009).
507. M. M. Rhodes et al., Stress reticulocytes lose transferrin receptors by an extrinsic process involving spleen and macrophages. American Journal of Hematology 91, 875-882 (2016).

508. P. Huang et al., Putative regulators for the continuum of erythroid differentiation revealed by single-cell transcriptome of human BM and UCB cells. Proceedings of the National Academy of Sciences 117, 12868-12876 (2020).
509. H. Yan et al., Comprehensive phenotyping of erythropoiesis in human bone marrow: Evaluation of normal and ineffective erythropoiesis. Am J Hematol 96, 1064-1076 (2021).
510. B. K. Tusi et al., Population snapshots predict early haematopoietic and erythroid hierarchies. Nature 555, 54-60 (2018).
511. A. Lepelley, Y. J. Crow, Erythrocyte-derived mitochondria take to the lupus stage. Cell Metabolism 33, 1723-1725 (2021).
512. S. Caielli et al., Erythroid mitochondrial retention triggers myeloid-dependent type I interferon in human SLE. Cell 184, 4464-4479.e4419 (2021).
513. M. J. Koury, M. C. Bondurant, Erythropoietin retards DNA breakdown and prevents programmed death in erythroid progenitor cells. Science 248, 378-381 (1990).
514. K. R. Reissmann, Studies on the mechanism of erythropoietic stimulation in parabiotic rats during hypoxia. Blood 5, 372-380 (1950).
515. S. V. Bhoopalan, L. J. Huang, M. J. Weiss, Erythropoietin regulation of red blood cell production: from bench to bedside and back. F1000Res 9, (2020).
516. H. Zhang et al., EpoR-tdTomato-Cre mice enable identification of EpoR expression in subsets of tissue macrophages and hematopoietic cells. Blood 138, 1986-1997 (2021).
517. D. Kuhrt, D. M. Wojchowski, Emerging EPO and EPO receptor regulators and signal transducers. Blood 125, 3536-3541 (2015).
518. J. Ratajczak et al., The role of insulin (INS) and insulin-like growth factor-I (IGF-I) in regulating human erythropoiesis. Studies *in vitro* under serum-free conditions–comparison to other cytokines and growth factors. Leukemia 12, 371-381 (1998).
519. T. Umemura, A. al-Khatti, R. E. Donahue, T. Papayannopoulou, G. Stamatoyannopoulos, Effects of interleukin-3 and erythropoietin on *in vivo* erythropoiesis and F-cell formation in primates. Blood 74, 1571-1576 (1989).
520. G. Migliaccio, A. R. Migliaccio, J. W. Adamson, *In vitro* differentiation of human granulocyte/macrophage and erythroid progenitors: comparative analysis of the influence of recombinant human erythropoietin, G-CSF, GM-CSF, and IL-3 in serum-supplemented and serum-deprived cultures. Blood 72, 248-256 (1988).
521. R. N. Suragani et al., Transforming growth factor-β superfamily ligand trap ACE-536 corrects anemia by promoting late-stage erythropoiesis. Nat Med 20, 408-414 (2014).
522. J. Tay et al., Imaging flow cytometry reveals that granulocyte colony-stimulating factor treatment causes loss of erythroblastic islands in the mouse bone marrow. Exp Hematol 82, 33-42 (2020).
523. I. Berman, The ultrastructure of erythroblastic islands and reticular cells in mouse bone marrow. Journal of Ultrastructure Research 17, 291-313 (1967).

524. K. Okreglicka et al., PPARgamma is essential for the development of bone marrow erythroblastic island macrophages and splenic red pulp macrophages. J Exp Med 218, (2021).
525. W. Li et al., Identification and transcriptome analysis of erythroblastic island macrophages. Blood 134, 480-491 (2019).
526. M. J. Leimberg, E. Prus, A. M. Konijn, E. Fibach, Macrophages function as a ferritin iron source for cultured human erythroid precursors. J Cell Biochem 103, 1211-1218 (2008).
527. V. Menon, S. Ghaffari, Erythroid enucleation: a gateway into a "bloody" world. Experimental Hematology 95, 13-22 (2021).
528. F. A. Spring et al., Intercellular adhesion molecule-4 binds $\alpha 4\beta 1$ and αV-family integrins through novel integrin-binding mechanisms: Presented in part as abstracts at the 40th annual meeting of the American Society of Hematology, Miami, FL, December 1998 (Blood 1998;92:589a) and at the annual meeting of the British Blood Transfusion Society, Edinburgh, United Kingdom, September 1999 (Transfus Med 1999;9:[suppl 1]9). Blood 98, 458-466 (2001).
529. M. Kristiansen et al., Identification of the haemoglobin scavenger receptor. Nature 409, 198-201 (2001).
530. B. O. Fabriek et al., The macrophage CD163 surface glycoprotein is an erythroblast adhesion receptor. Blood 109, 5223-5229 (2007).
531. J. A. Chasis, N. Mohandas, Erythroblastic islands: niches for erythropoiesis. Blood 112, 470-478 (2008).
532. L. F. Bennett et al., Inflammation induces stress erythropoiesis through heme-dependent activation of SPI-C. Science Signaling 12, eaap7336 (2019).
533. T. Ulyanova, S. R. Phelps, T. Papayannopoulou, The macrophage contribution to stress erythropoiesis: when less is enough. Blood 128, 1756-1765 (2016).
534. J. P. Levesque et al., Macrophages form erythropoietic niches and regulate iron homeostasis to adapt erythropoiesis in response to infections and inflammation. Exp Hematol 103, 1-14 (2021).
535. J. Zhang et al., Rats provide a superior model of human stress erythropoiesis. Experimental Hematology 78, 21-34.e23 (2019).
536. C. Liao, K. S. Prabhu, R. F. Paulson, Monocyte-derived macrophages expand the murine stress erythropoietic niche during the recovery from anemia. Blood 132, 2580-2593 (2018).
537. H. Hara, M. Ogawa, Erythropoietic precursors in mice under erythropoietic stimulation and suppression. Exp Hematol 5, 141-148 (1977).
538. J. Xiang, D. C. Wu, Y. Chen, R. F. Paulson, *In vitro* culture of stress erythroid progenitors identifies distinct progenitor populations and analogous human progenitors.

Blood 125, 1803-1812 (2015).
539. S. F. Libregts et al., Chronic IFN-γ production in mice induces anemia by reducing erythrocyte life span and inhibiting erythropoiesis through an IRF-1/PU.1 axis. Blood 118, 2578-2588 (2011).
540. L. S. Rusten, S. E. Jacobsen, Tumor necrosis factor (TNF)-alpha directly inhibits human erythropoiesis *in vitro*: role of p55 and p75 TNF receptors. Blood 85, 989-996 (1995).
541. A. C. Gomes et al., IFN-γ-Dependent Reduction of Erythrocyte Life Span Leads to Anemia during Mycobacterial Infection. J Immunol 203, 2485-2496 (2019).
542. J. D. Milner et al., Sustained IL-4 exposure leads to a novel pathway for hemophagocytosis, inflammation, and tissue macrophage accumulation. Blood 116, 2476-2483 (2010).
543. S. Millot et al., Erythropoietin stimulates spleen BMP4-dependent stress erythropoiesis and partially corrects anemia in a mouse model of generalized inflammation. Blood 116, 6072-6081 (2010).
544. Y. Nagai et al., Toll-like receptors on hematopoietic progenitor cells stimulate innate immune system replenishment. Immunity 24, 801-812 (2006).
545. F. C. Lin et al., IFN-γ causes aplastic anemia by altering hematopoietic stem/progenitor cell composition and disrupting lineage differentiation. Blood 124, 3699-3708 (2014).
546. A. Jackson, M. R. Nanton, H. O'Donnell, A. D. Akue, S. J. McSorley, Innate immune activation during Salmonella infection initiates extramedullary erythropoiesis and splenomegaly. J Immunol 185, 6198-6204 (2010).
547. S. Gardenghi et al., Distinct roles for hepcidin and interleukin-6 in the recovery from anemia in mice injected with heat-killed Brucella abortus. Blood 123, 1137-1145 (2014).
548. G. Weiss, T. Ganz, L. T. Goodnough, Anemia of inflammation. Blood 133, 40-50 (2019).
549. R. E. Mebius, G. Kraal, Structure and function of the spleen. Nat Rev Immunol 5, 606-616 (2005).
550. D. Z. de Back, E. B. Kostova, M. van Kraaij, T. K. van den Berg, R. van Bruggen, Of macrophages and red blood cells; a complex love story. Front Physiol 5, 9 (2014).
551. Z. Bian et al., Cd47-Sirpα interaction and IL-10 constrain inflammation-induced macrophage phagocytosis of healthy self-cells. Proc Natl Acad Sci U S A 113, E5434-5443 (2016).
552. P. A. Oldenborg et al., Role of CD47 as a marker of self on red blood cells. Science 288, 2051-2054 (2000).
553. R. Banerjee, S. Khandelwal, Y. Kozakai, B. Sahu, S. Kumar, CD47 regulates the phagocytic clearance and replication of the Plasmodium yoelii malaria parasite. Proc Natl Acad Sci U S A 112, 3062-3067 (2015).
554. S. Khandelwal, N. van Rooijen, R. K. Saxena, Reduced expression of CD47 during

murine red blood cell (RBC) senescence and its role in RBC clearance from the circulation. Transfusion 47, 1725-1732 (2007).
555. M. Olsson, P. A. Oldenborg, CD47 on experimentally senescent murine RBCs inhibits phagocytosis following Fcgamma receptor-mediated but not scavenger receptor-mediated recognition by macrophages. Blood 112, 4259-4267 (2008).
556. N. G. Sosale et al., Cell rigidity and shape override CD47's "self"-signaling in phagocytosis by hyperactivating myosin-II. Blood 125, 542-552 (2015).
557. C. A. Schaer, G. Schoedon, A. Imhof, M. O. Kurrer, D. J. Schaer, Constitutive endocytosis of CD163 mediates hemoglobin-heme uptake and determines the noninflammatory and protective transcriptional response of macrophages to hemoglobin. Circ Res 99, 943-950 (2006).
558. T. R. L. Klei et al., Hemolysis in the spleen drives erythrocyte turnover. Blood 136, 1579-1589 (2020).
559. V. Hvidberg et al., Identification of the receptor scavenging hemopexin-heme complexes. Blood 106, 2572-2579 (2005).
560. C. White et al., HRG1 is essential for heme transport from the phagolysosome of macrophages during erythrophagocytosis. Cell Metab 17, 261-270 (2013).
561. C. Delaby et al., Subcellular localization of iron and heme metabolism related proteins at early stages of erythrophagocytosis. PLoS One 7, e42199 (2012).
562. K. M. O'Callaghan et al., Heme-binding protein HRG-1 is induced by insulin-like growth factor I and associates with the vacuolar H+-ATPase to control endosomal pH and receptor trafficking. J Biol Chem 285, 381-391 (2010).
563. R. H. Pek et al., Hemozoin produced by mammals confers heme tolerance. eLife 8, e49503 (2019).
564. K. D. Poss, S. Tonegawa, Heme oxygenase 1 is required for mammalian iron reutilization. Proceedings of the National Academy of Sciences 94, 10919-10924 (1997).
565. G. Kovtunovych, M. A. Eckhaus, M. C. Ghosh, H. Ollivierre-Wilson, T. A. Rouault, Dysfunction of the heme recycling system in heme oxygenase 1-deficient mice: effects on macrophage viability and tissue iron distribution. Blood 116, 6054-6062 (2010).
566. A. Yachie, Heme Oxygenase-1 Deficiency and Oxidative Stress: A Review of 9 Independent Human Cases and Animal Models. Int J Mol Sci 22, (2021).
567. A. Yachie et al., Oxidative stress causes enhanced endothelial cell injury in human heme oxygenase-1 deficiency. J Clin Invest 103, 129-135 (1999).
568. Y. Nakayama et al., A secretory protein neudesin regulates splenic red pulp macrophages in erythrophagocytosis and iron recycling. Communications Biology 7, 129 (2024).
569. M. Haldar et al., Heme-mediated SPI-C induction promotes monocyte differentiation into iron-recycling macrophages. Cell 156, 1223-1234 (2014).

570. M. Kohyama et al., Role for Spi-C in the development of red pulp macrophages and splenic iron homeostasis. Nature 457, 318-321 (2009).
571. Y. Lu et al., Interleukin-33 Signaling Controls the Development of Iron-Recycling Macrophages. Immunity 52, 782-793.e785 (2020).
572. E. Karsten, B. R. Herbert, The emerging role of red blood cells in cytokine signalling and modulating immune cells. Blood Reviews 41, 100644 (2020).
573. D. Hashimoto et al., Tissue-resident macrophages self-maintain locally throughout adult life with minimal contribution from circulating monocytes. Immunity 38, 792-804 (2013).
574. Yang, W.-p., et al., High-altitude hypoxia exposure inhibits erythrophagocytosis by inducing macrophage ferroptosis in the spleen, Cold Spring Harbor Laboratory. (2023).
575. S. M. Lai et al., Organ-Specific Fate, Recruitment, and Refilling Dynamics of Tissue-Resident Macrophages during Blood-Stage Malaria. Cell Reports 25, 3099-3109.e3093 (2018).
576. M. T. Khairallah et al., SMN deficiency negatively impacts red pulp macrophages and spleen development in mouse models of spinal muscular atrophy. Hum Mol Genet 26, 932-941 (2017).
577. Y. Chen et al., Epo receptor signaling in macrophages alters the splenic niche to promote erythroid differentiation. Blood 136, 235-246 (2020).
578. H. M. Akilesh et al., Chronic TLR7 and TLR9 signaling drives anemia via differentiation of specialized hemophagocytes. Science 363, (2019).
579. P. Slusarczyk et al., Impaired iron recycling from erythrocytes is an early hallmark of aging. Elife 12, (2023).
580. C. C. Kim et al., Splenic red pulp macrophages produce type I interferons as early sentinels of malaria infection but are dispensable for control. PLoS One 7, e48126 (2012).
581. M. Enders et al., Splenic Red Pulp Macrophages Cross-Prime Early Effector CTL That Provide Rapid Defense against Viral Infections. J Immunol 204, 87-100 (2020).
582. D. Kurotaki et al., CSF-1-dependent red pulp macrophages regulate CD4 T cell responses. J Immunol 186, 2229-2237 (2011).
583. Z. Alam et al., Counter Regulation of Spic by NF-/*kappa*B and STAT Signaling Controls Inflammation and Iron Metabolism in Macrophages. Cell Rep 31, 107825 (2020).
584. S. J. Lee, S. Y. Park, M. Y. Jung, S. M. Bae, I. S. Kim, Mechanism for phosphatidylserine-dependent erythrophagocytosis in mouse liver. Blood 117, 5215-5223 (2011).
585. Y. Sonoda, K. Sasaki, Hepatic extramedullary hematopoiesis and macrophages in the adult mouse: histometrical and immunohistochemical studies. Cells Tissues Organs 196, 555-564 (2012).
586. M. Pfefferlé et al., Hemolysis transforms liver macrophages into antiinflammatory

erythrophagocytes. J Clin Invest 130, 5576-5590 (2020).
587. I. Theurl et al., On-demand erythrocyte disposal and iron recycling requires transient macrophages in the liver. Nature Medicine 22, 945-951 (2016).
588. D. J. Schaer et al., CD163 is the macrophage scavenger receptor for native and chemically modified hemoglobins in the absence of haptoglobin. Blood 107, 373-380 (2006).
589. B. O. Fabriek et al., The macrophage scavenger receptor CD163 functions as an innate immune sensor for bacteria. Blood 113, 887-892 (2009).
590. Y.-J. Yap et al., The clinical utility of CD163 in viral diseases. Clinica Chimica Acta 541, 117243 (2023).
591. H. J. Møller, N. A. Peterslund, J. H. Graversen, S. K. Moestrup, Identification of the hemoglobin scavenger receptor/CD163 as a natural soluble protein in plasma. Blood 99, 378-380 (2002).
592. K. A. Hintz et al., Endotoxin induces rapid metalloproteinase-mediated shedding followed by up-regulation of the monocyte hemoglobin scavenger receptor CD163. J Leukoc Biol 72, 711-717 (2002).
593. A. Etzerodt et al., Structural Basis for Inflammation-driven Shedding of CD163 Ectodomain and Tumor Necrosis Factor-α in Macrophages*. Journal of Biological Chemistry 289, 778-788 (2014).
594. H. J. Moller, Soluble CD163. Scand J Clin Lab Invest 72, 1-13 (2012).
595. A. Etzerodt et al., Soluble ectodomain CD163 and extracellular vesicle-associated CD163 are two differently regulated forms of 'soluble CD163' in plasma. Scientific Reports 7, 40286 (2017).
596. K. Subramanian, R. Du, N. S. Tan, B. Ho, J. L. Ding, CD163 and IgG codefend against cytotoxic hemoglobin via autocrine and paracrine mechanisms. J Immunol 190, 5267-5278 (2013).
597. M. K. Skytthe, J. H. Graversen, S. K. Moestrup, Targeting of CD163(+) Macrophages in Inflammatory and Malignant Diseases. Int J Mol Sci 21, (2020).
598. J. Abramson et al., Accurate structure prediction of biomolecular interactions with AlphaFold 3. Nature 630, 493-500 (2024).
599. J. Jumper et al., Highly accurate protein structure prediction with AlphaFold. Nature 596, 583-589 (2021).

Chapter 2

Materials and Methods

All reagents used in this study are listed in Table 6.1.

2.1 Materials

2.1.1 Cells

All cell lines used in this study are listed in Table 2.1.

Cells were cultured at 37°C with 5% CO_2 and were negative for mycoplasma contamination, tested every 3 months. Primary MEFs were cultured in 3% O_2. Adherent cells were lifted with Trypsin-EDTA (0.25%) dissociation reagent (Gibco). Foetal calf serum was obtained from Sigma-Aldrich.

Human embryonic kidney (HEK)293, HEK293T, Huh7.5, A549, HeLa, Vero, HFF-TERT, 3T3, L929 and baby hamster kidney (BHK) cells were maintained in Dulbecco's modified Eagle medium (DMEM) containing 2 mM L-glutamine (Gibco) and 10% (v/v) FCS.

THP1 and RAW cells were maintained in Roswell Park Memorial Institute (RPMI) medium containing 2mM L-glutamine (Gibco) and 10% (v/v) FCS.

Mouse embryonic fibroblasts (MEFs; primary and immortalised) were cultured in DMEM containing 2 mM L-glutamine (Gibco) and 20% (v/v) FCS.

HepB3 cells were cultured on collagen-coated plates (Sigma) in DMEM containing Glutamax (Gibco), 1% non-essential amino acids (ThermoFisher) and 2 mM L-glutamine (Gibco).

Bone marrow-derived macrophages (BMDMs) were derived from differentiating bone marrow in RPMI medium containing 2 mM L-glutamine, 10% (v/v) FCS and 20% supernatant

from L929 cells, which contains M-CSF. Media changes for adherent and non-adherent cells were performed every other day, for a total of eight days.

Madin-Darby canine kidney (MDCK) cells were maintained in DMEM containing 2 mM L-glutamine (Gibco), 1mg/mL geneticin (Gibco) and 10% (v/v) FCS.

2.1.2 Viruses

All viruses were aliquotted and stored at -80°C.

Encephalomyocarditis virus (EMCV)
EMCV was propagated, and titre determined in baby hamster kidney cells (BHKs). Viral stocks were generated by Anne Bridgeman in the Rehwinkel lab. EMCV virus stocks were a gift from Caetano Reis e Sousa (The Francis Crick Institute, UK).

Herpes simplex 1 (HSV-1) KOS strain
HSV-1 was propagated and titre determined in Vero cells. HSV-1 virus inoculum was a gift from Caetano Reis e Sousa (The Francis Crick Institute, UK), originally purchased from ATCC.

Vaccinia virus (VACV)
VACV stocks were produced in HeLa cells and titre determined through plaque assay in Vero cells. VACV western reserve strains were a gift from Persephone Borrow (University of Oxford) and Geoff Smith (University of Oxford). VACV western reserve mutant strains were a gift from Geoff Smith, originating from two studies (2, 3).

VACV-GFP
VACV-GFP stocks were produced in HeLa cells and titre determined through plaque assay in Vero cells. VACV-GFP western reserve was a gift from Geoff Smith.

Adenovirus
Adenovirus (AdV-CRE-GFP) stocks were generated by Anne Bridgeman in the Rehwinkel lab and were originally a gift from Doug Higgs (University of Oxford).

Influenza A/PR8 (H1N1) and Influenza/A/X-31 (H3N2)
A kind gift from Jack (Tiong) Tan (University of Oxford, U.K.).

Sendai
Sendai viral stocks were purchased from ATCC, catalogue number VR-907. It was produced in SPF embryonated chicken eggs.

Zika virus (ZIKV)
ZIKV/*H.sapiens*/Brazil/PE243/2015 was produced in Vero cells and titre determined

Table 2.1: Cell lines used in this study.

Cell Line	Cell type	Origin
HEK293	Human embryonic kidney (HEK) cells (female origin).	Kind gift from Caetano Reis e Sousa (The Francis Crick Institute, UK).
HEK293T	HEK cells transformed with the SV40 large T antigen.	Kind gift from Caetano Reis e Sousa (The Francis Crick Institute, UK).
Huh7.5	Hepatocyte-derived carcinoma cell line taken from a liver tumour in a 57-year-old male.	Kind gift from Jane McKeating (University of Oxford).
A549	Human lung epithelial carcinoma cell line derived from a 58-year-old male.	Kind gift from Georg Kochs (University of Freiburg).
HeLa	Epithelial cell cervical carcinoma cell line named after the patient from which they were isolated, Henrietta Lacks, who was 31 at the time.	ATCC.
Vero	Kidney epithelial cell line originating from African green monkeys.	ATCC.
HFF-TERT	Primary cells, human foreskin fibroblasts.	Kind a gift from Michael Weeks (University of Cambridge).
3T3	Mouse embryonic fibroblast cell line, derived from BALB.C 14–17-day old embryos.	Kind gift from Caetano Reis e Sousa (The Francis Crick Institute, UK).
L929	Mouse cell line derived from normal subcutaneous areolar and adipose tissue of a 100-day-old male C3H/An mouse.	These cells were a gift from Michael Way (The Francis Crick Institute, UK).
BHK	Baby hamster kidney cells.	ATCC.
THP1	Monocytic cell line derived from the peripheral blood of a one-year-old male with acute monocytic leukaemia.	Kind gift from Soren Paludan (Aarhus University, Denmark).
RAW	Murine macrophage cell line derived from BALB.C mice with Abelson murine leukaemia virus-induced tumour.	Kind gift from Vincenzo Cerundolo (University of Oxford).
HepB3	Human hepatocellular carcinoma cell line which originated from a paediatric liver tumour.	Kind gift from Jane McKeating (University of Oxford).
MEF	Mouse embryonic fibroblast.	Generated from 12.5-14.5-day old embryos with head and foetal liver removed.
Immortalised MEF	Immortalised with a retrovirus expressing the large T antigen and a puromycin resistance gene.	Selected via puromycin.
BMDM	Bone marrow derived macrophages.	Bone marrow was differentiated into BMDMs over 7 days with 20% L929 supernatent.
MDCK-SIAT1	Epithelial cell line originating from a cocker spaniel dog.	Kind gift from Tiong (Jack) Tan (University of Oxford).

through plaque assay on A549 cells. RNA for transfection was provided by Alain Kohl, and virus stocks were produced by Mirjam Schilling in the Rehwinkel lab.

Murine leukemia virus (MLV)
A kind gift from Caetano Reis e Sousa (The Francis Crick Institute, UK).

HIV-GFP first generation lentivector
VSV-G-pseudotyped lentivirus encoding GFP, in which GFP expression is driven from the endogenous LTR promotor. Made through the transfection of HEK293T cells with two plasmids: a VSV-G expressing plasmid for pseudotyping (pMD2.G) and a plasmid for the HIV-1 genome containing endoplasmic reticulum (ER)-retained truncated Env-EGFP fusion protein (Table 2.2). Viral supernatant was harvested and purified through centrifugation over a sucrose cushion, and titre determined through flow cytometry (see section 2.2.2).

HIV-GFP second generation lentivector
VSV-G-pseudotyped lentivirus encoding GFP, in which GFP expression is driven from an introduced CMV promotor. Made through the transfection of HEK293T cells with three plasmids: a packaging plasmid (p8.91), VSV-G envelope plasmid (pCMV-VSV-G) and HIV-1-GFP vector plasmid (pCSGW) (see Table 2.2). Viral supernatant was harvested and purified through centrifugation over a sucrose cushion, and titre determined through flow cytometry see section 2.2.2).

2.1.3 Plasmids

All plasmids used in this study are listed in Table 2.2.

Table 2.2: Plasmids used in this study

Name	Description	Origin
pCMV-VSV-G	VSV-G expressing plasmid for lentiviral pseudotyping.	Gift from Bob Weinberg
p8.91	Lentiviral packaging plasmid	Gift from Greg Towers (UCL)
pMD2.G	VSV-G expressing plasmid for kentiviral pseudotyping	Addgene Cat. Number 12259
pNL4-3ΔE-EGFP	HIV-1 genome containing endoplasmic reticulum (ER)-retained truncated Env-EGFP fusion protein	NIBSC Center for AIDS reagents
pCSGW	HIV-1 genome encoding GFP	Gift from Greg Towers (UCL)

Table 2.2: Plasmids used in this study

Name	Description	Origin
pLentiCRISPRv2	Third generation lentiviral backbone encoding Cas9 gene	Addgene Cat. number 52961
pLentiCRISPRv2-HGLibA-64384	Lentiviral backbone containing Cas9 and sgRNA targetting a control sequence (ACGGAGGC-TAAGCGTCGCAANGG)	Gift from Andrew Bassett
pLentiCRISPRv2-IFI44-1	Lentiviral plasmid containing Cas9 and sgRNA targetting human IFI44	Designed by Philp Hublitz Genome Engineering Facility, WIMM), generated by me
pLentiCRISPRv2-IFI44-2	Lentiviral plasmid containing Cas9 and sgRNA targetting human IFI44	Designed by Philp Hublitz Genome Engineering Facility, WIMM), generated by me
pLentiCRISPRv3-IFI44-1	Lentiviral plasmid containing Cas9 and sgRNA targetting human IFI44	Designed by Philp Hublitz Genome Engineering Facility, WIMM), generated by me
pLentiCRISPRv2-IFI44-4	Lentiviral plasmid containing Cas9 and sgRNA targetting human IFI44	Designed by Philp Hublitz Genome Engineering Facility, WIMM), generated by me
pLentiCRISPRv2-IFI44L-1	Lentiviral plasmid containing Cas9 and sgRNA targetting human IFI44	Designed by Philp Hublitz Genome Engineering Facility, WIMM), generated by me
pLentiCRISPRv2-IFI44L-2	Lentiviral plasmid containing Cas9 and sgRNA targetting human IFI44	Designed by Philp Hublitz Genome Engineering Facility, WIMM), generated by me
pLentiCRISPRv2-IFI44L-3	Lentiviral plasmid containing Cas9 and sgRNA targetting human IFI44	Designed by Philp Hublitz Genome Engineering Facility, WIMM), generated by me
pLentiCRISPRv2-IFI44L-4	Lentiviral plasmid containing Cas9 and sgRNA targetting human IFI44	Designed by Philp Hublitz Genome Engineering Facility, WIMM), generated by me
Gateway Entry Vectors		
pCR8/GW/TOPO/huIFI44W9R	Entry clone containing human IFI44 gene, amplified with PCR primers for ”no-stop” and with a GCCGCC kozac sequence.	From THP1 cDNA

Table 2.2: Plasmids used in this study

Name	Description	Origin
pCR8/GW/TOPO/huIFI44LH73RV217IR296C	Entry clone containing human IFI44L gene, amplified with PCR primers for ”no-stop” and with a GCCGCC kozac sequence.	From THP1 cDNA
pCR8/GW/TOPO/moIFI44	Entry clone containing mouse IFI44 gene, amplified with PCR primers for ”no-stop” and with a GCCGCC kozac sequence.	From C57BL/6N cDNA
pCR8/GW/TOPO/moIFI44L	Entry clone containing mouse IFI44L gene, amplified with PCR primers for ”no-stop” and with a GCCGCC kozac sequence.	From RAW cell cDNA
pCR8/GW/TOPO/EV	Entryclonecontainingacontrolvectorthathasa20bprandomsequence (ATCTACCCGCGAGGTCAGAC)intheexpressioncassette.	Cloned by Jonny Hertzog, Rehwinkel lab
pCR8/GW/TOPO/eGFP	Entry clone containing a control vector that contains eGFP	Cloned by Jonny Hertzog, Rehwinkel lab
Gateway Destination Vectors		
pLenti6.3/TO/V5-DEST	Lentiviral mammalian expression vector that confers a C-terminal V5 tag	Invitrogen
pcDNA3.2/FLAG-DEST	Mammalian expression vector that confers a C-terminal FLAG-tag.	Cloned by Jonny Hertzog, Rehwinkel lab
pcDNA3.2/V5-DEST	Mammalian expression vector that confers a C-terminal V5-tag.	Invitrogen

2.1.4 Oligonucleotides

General oligonucleotides can be found in Table 2.3, while TaqMan primer probes can be found in Table 2.4.

Table 2.3: Oligonucleotides used in this study

Name	Purpose	Forward primer	Reverse primer
H-IFI44-Kozak-no-stop	PCR amplification of human IFI44, with a kozak sequence and no stop codon	GCCGCCATGGCA GTGACAACTCGTT TGACA	TTTTTTTCCTTGT GCACAGTTGATA ATT
H-IFI44L-Kozak- no-stop	PCR amplification of human IFI44L, with a kozak sequence and no stop codon	GCCGCCATGGAA GTGACAACAAGA TTGACATGGA	AATGCAGGGCTG AACGCTC
M-IFI44-Kozak-no-stop	PCR amplification of mouse IFI44, with a kozak sequence and no stop codon	GCCGCCATGGCC ATGAGAACTCGTT TGACA	TTTGTTCAAAGGC AAATCCTCCAAGA AT
M-IFI44L-Kozak- no-stop	PCR amplification of mouse IFI44L, with a kozak sequence and no stop codon	GCCGCCATGAAA GTGACAGCCAGA TTGACATGGA	AATGCAGGGCTG TAACGCTC
sgRNA-IFI44-1	sgRNA targetting human IFI44	CACCGGTCTTTCA TCCAGTGAATCT	AAACAGATTCACT GGATGAAAGACC
sgRNA-IFI44-2	sgRNA targetting human IFI44	CACCGGCAAGGG CATGTAACGCATC	AAACGATGCGTT ACATGCCCTTGCC
sgRNA-IFI44-3	sgRNA targetting human IFI44	CACCGGTAACGCA TCAGGCTTTGGT	AAACACCAAAGCC TGATGCGTTACC
sgRNA-IFI44-4	sgRNA targetting human IFI44	CACCGGCTGGGT CCAATTGGAGCT	AAACACCAAAGCC TGATGCGTTACC
sgRNA-IFI44L-1	sgRNA targetting human IFI44L	CACCGGTAACCTA GACGACATAAAG	AAACCTTTATGTC GTCTAGGTTACC
sgRNA-IFI44L-2	sgRNA targetting human IFI44L	CACC GGTGACTG-GCCAAGCCGTAGT	AAACACTACGGCT TGGCCAGTCACC
sgRNA-IFI44L-3	sgRNA targetting human IFI44L	CACCGGTATAGG CCCTATGCAGACT	AAACAGTCTGCAT AGGGCCTATACC
sgRNA-IFI44L-4	sgRNA targetting human IFI44L	CACCGGATCAGAC CCCACTACGGCT	AAACAGCCGTAG TGGGGTCTGATC C
Cyagen-gRNA-3	guide RNA targetting mouse IFI44 exon 1		ACTAGTGTGCATC CCTCCAGAGG

Table 2.3: Oligonucleotides used in this study

Name	Purpose	Forward primer	Reverse primer
Cyagen-gRNA-4	guide RNA targetting mouse IFI44 exon 6	TTTACAGTCAAGA TGCTGTGTGG	
Cyagen-gRNA-5	guide RNA targetting mouse IFI44 exon 8		AAATCCAACAGAA TTGCGATTGG
M-IFI44-KO	Genotyping *Ifi44*$^{-/-}$ mice	CTTCTTTGTGTTT GCTACTCTGGGTC TC	AATCAAGGGATA CATGATGTAGGG GC
M-IFI44-WT/Het	Genotyping *Ifi44*$^{+/+}$ mice	GGTAAATTCAACA AGTTGCTGTAGA TGGAC	GACTTTCTTCTGC TTTGCAGCATCC
M-IFI44	Genotyping C57BL/6 *Ifi44* gene	AAGACAGAAACT TGGGAAAGTGAG AGC	CCTGTGTGGCATT TCTTAGTGATGG
M-IFI44-Seq-F	Sequencing mouse *Ifi44* gene	CACTGCCCTGCAG CACTCTTATTT	
M-IFI44-Seq-F2	Sequencing mouse *Ifi44* gene	GCGACATCCTTCT TGTAGCC	
M-IFI44-Seq-F3	Sequencing mouse *Ifi44* gene	GGATACTCCCCAT CCCTCTC	
M-IFI44L-Seq	Sequencing mouse *Ifi44l* gene	CCATCCATGAGGT CATGAAGCA	TAGGGGAATGCC AGGTTGGT
M-IFI44L-Seq-1	Sequencing mouse *Ifi44l* gene	AGCTATGTCTACA ACCCAGGA	
M-IFI44L-Seq-2	Sequencing mouse *Ifi44l* gene	AAACCATCTTGGC ACATTCCT	
M-IFI44L-Seq-3	Sequencing mouse *Ifi44l* gene	TTGCAAGTGCGT TTGAGGC	
M-IFI44L-Seq-4	Sequencing mouse *Ifi44l* gene	TCCACAGGTTCAG AATGTCC	
M-IFI44L-Seq-5	Sequencing mouse *Ifi44l* gene	GCCTTGTAGTCCC AAAGCTCA	
M-IFI44L-Seq-6	Sequencing mouse *Ifi44l* gene	GAGGGCCTATTT CCCATGATT	

Table 2.3: Oligonucleotides used in this study

Name	Purpose	Forward primer	Reverse primer
pCR8-seq	Sequencing pCR8/TOPO constructs	T7F primer	M13F primer
pLenti-seq	Sequencing pLenti6.2 constructs	CMVF-pcDNA3	V5R
pcDNA-seq	Sequencing pcDNA3.2 constructs	CMVF-pcDNA3	V5R

Table 2.4: TaqMan primer probes used in this study

Gene	Protein	AssayID
Human		
DDX58	RIG-I	Hs01061436_m1
GAPDH	GAPDH	Hs02758991_g1
HPRT1	HPRT	Hs99999909_m1
IFI44	IFI44	Hs00951349_m1
IFI44L	IFI44L	Hs00915292_m1
IFIT1	IFIT1	Hs01911452_s1
ISG15	ISG15	Hs01921425_s1
MAVs	MAVs	HHs00920075_m1
MX1	MX1	Hs00895608_m1
Mouse		
Actb	β-actin	Mm02619580_g1
Adar1	ADAR1	Mm00508001_m1
Cd163	CD163	Mm00474091_m1
Ddit3	DDIT3	Mm01135937_g1
Ddx58	RIG-I	Mm01216853_m1
Flt1	FLT1	Mm00438980_m1
Fth1	FTH1	Mm00850707_g1
Gapdh	GAPDH	Mm99999915_g1
Gclc	GCLC	Mm00802655_m1
Gzmb	GZMB	Mm00442837_m1
Hmox1	HMOX1	Mm00516005_m1
Hprt	HPRT	Mm03024075_m1
Ifi44	IFI44	Mm00505665_m1

Table 2.4: TaqMan primer probes used in this study

Gene	Protein	AssayID
Ifi44l	IFI44L	Mm00518988_m1
Ifit1	IFIT1	Mm00515153_m1
Ifit2	IFIT2	Mm00492606_m1
Ifnb1	IFN-β1	Mm00439552_s1
Ifng	IFN-γ	Mm01168134_m1
Il2	IL2	Mm00434256_m1
Il2ra	IL2RA	Mm01340213_m1
Isg15	ISG15	Mm01705338_s1
Isg20	ISG20	Mm00469585_m1
Mavs	MAVs	Mm00523170_m1
Oas1a	OAS1a	Mm00523170_m1
Oas1l	OAS1L	Mm004550581_m1
Prf1	PRF	Mm00812512_m1
Slc11a2	NRAM2	Mm00435363_m1
Slc39a14	ZIP14	Mm01317439_m1
Slc40a1	FPN	Mm01254822_m1
Sptb	SPTB	Mm01284057_m1
Tnf	TNF	Mm00443258_m1
Urod	UROD	Mm00447681_m1
Uros	UROS	Mm00447685_m1
Zbp1	ZBP1	Mm01247052_m1
Virus		
E9L	VACV WR E9L	Custom primer designed by Baker *et al* (4)
NP	Influenza/A NP	Custom primer based on NC_002019.1

2.1.5 Antibodies

All antibodies used in this study are listed in Table 2.5.

Table 2.5: Antibodies used in this study

Target	Conjugate	Source	Manufacturer	Cat Number	Dilution
Western Blot					
β-actin	HRP	mouse monoclonal	Sigma Aldrich	AC-15	1:10,000
FLAG	HRP	mouse monoclonal	Sigma Aldrich	M2	1:1,000
GFP	-	mouse monoclonal	Roche	11814460001	1:1,000
ICP5/VP5	-	mouse monoclonal	Santa Cruz	sc-56989	1:1,000
IFI44	-	rabbit polyclonal	ThermoFischer	PA565370	1:1,000
IgG	HRP	rabbit monoclonal	Cell signalling technology	7074	1:2,000
IgG	HRP	mouse monoclonal	Cyriva	NA931	1:2,000
PR8 PB2	-	rabbit polyclonal	GeneTex	GTX125925	1:1,000
RIG-I	-	mouse monoclonal	AdipoGen	AG20B0009C100	1:1,000
V5	-	mouse monoclonal	Biolegend	680602	1:1,000
V5	HRP	mouse monoclonal	Invitrogen	R961-25	1:1,000
VACV	HRP	rabbit polyclonal	Abcam	ab87387	1:5,000
ZIKV NS5	-	rabbit polyclonal	Gift from Andres Merit	-	1:500
Flow Cytometry					
B220	APC-Cy7	mouse monoclonal	Biolegend	103223	1:200

Table 2.5: Antibodies used in this study

Target	Conjugate	Source	Manufacturer	Cat Number	Dilution
CD11b	APC-Cy7	mouse monoclonal	Biolegend	101225	1:200
CD11b	PE	mouse monoclonal	Biolegend	117309	1:400
CD16/32	-	mouse monoclonal	eBioscience	14016185	1:100
CD163	BV421	mouse monoclonal	Biolegend	155309	1:400
CD19	BV421	mouse monoclonal	Biolegend	152411	1:200
CD3	APC-Cy7	mouse monoclonal	Biolegend	100221	1:200
CD335	APC-Cy7	mouse monoclonal	Biolegend	137645	1:200
CD44	APC	mouse monoclonal	Biolegend	103011	1:400
CD45	PE-Cy7	mouse monoclonal	Biolegend	103113	1:200
CD45	PE-Cy5	mouse monoclonal	Biolegend	103109	1:200
CD68	FITC	mouse monoclonal	Biolegend	1037005	1:400
CD71	FITC	mouse monoclonal	Biolegend	113805	1:400
CD90.2	FITC	mouse monoclonal	Biolegend	105327	1:200
F4/80	BV605	mouse monoclonal	Biolegend	123133	1:400
Ki67	PE-Cy7	mouse monoclonal	Biolegend	151217	1:200
Ly6C	PE-Cy7	mouse monoclonal	Biolegend	128011	1:200
Ly6G	PE-Cy7	mouse monoclonal	Biolegend	127623	1:200

Table 2.5: Antibodies used in this study

Target	Conjugate	Source	Manufacturer	Cat Number	Dilution
Ly6G	APC-Cy7	mouse monoclonal	Biolegend	127623	1:200
Ly6G	BV421	mouse monoclonal	Biolegend	127627	1:400
Ter119	PE	mouse monoclonal	Biolegend	116207	1:400
Ter119	AF700	mouse monoclonal	Biolegend	116220	1:200
Ter119	PerCP-Cy5.5	mouse monoclonal	Biolegend	116227	1:200
V5	FITC	mouse monoclonal	Invitrogen	R963-25	1:400
VCAM-1	BUV395	mouse monoclonal	BD Biosciences	745672	1:200
Immunofluorescence					
FLAG	AF647	rabbit monoclonal	AbCam	ab245893	10 µg/ml
Tubulin	AF647	mouse monoclonal	ThermoFischer	MA138000A647	10 µg/ml
V5	AF488	mouse monoclonal	ThermoFischer	377500A488	1:100
Immunoprecipitation					
FLAG	-	mouse monoclonal	Sigma Aldrich	M2	-
V5	-	mouse monoclonal	Biolegend	680602	-

2.1.6 Mice

Mice were housed and bred under standard conditions at the University of Oxford Biomedical Services Animal Facilities. All mice used were on the C57BL/6 N background and were 7-16 weeks old, both male and female. This work was performed in accordance with UK Animal (Scientific Procedures) Act 1986 on project licences granted by the UK Home Office: PC041D0AB, PP5102963 and PP1487090. Knock-out lines were crossed to bought-in C57BL/6N wild-type mice after two years of breeding to minimise genetic

drift, and homozygous knock-out animals were subsequently obtained by interbreeding heterozygous animals. Littermate controls were used where indicated to minimise the effect of passenger mutations (4, 5).

Ifi44 knock-out mice

The *Ifi44* knock-out strategy was designed by Jan Rehwinkel, Rachel Rigby and Anne Bridgeman with help from the WIMM Genome Engineering Facility. Guide RNAs (gRNAs) were designed that target exons 1-5 for deletion with no off-target effects predicted (Figure 3.5D). *Ifi44*$^{-/-}$ mice were made by Cyagen. The gRNA and Cas9 mRNA were co-injected into fertilised mouse eggs to generate targeted knockout offspring. F_0 founder animals were identified by PCR followed by sequence analysis, which were bred to wild-type mice to test germline transmission and F_1 animal generation. After shipment of F_1 mice to Oxford, these were bred and validated by Jan Rehwinkel, Rachel Rigby and Anne Bridgeman.

Ifi44 knock-out on an *Adar1*$^{mZa/mZa}$ background

Adar1$^{mZa/mZa}$ mice were described previously (6, 7). We generated *Ifi44*$^{-/-}$; *Adar1*$^{mZa/mZa}$ mice by crossing the two lines to generate double heterozygotes (*Ifi44*$^{+/-}$; *Adar1*$^{+/mZa}$), and subsequently crossing heterozygous mice together (F_2). Mice that were homozygous for either *Ifi44* or *Adar1* were selected as breeders, and mice were subsequently bred until homozygosity on both *Ifi44* and *Adar1* were achieved.

2.2 Methods

2.2.1 Cloning

Generation of entry vectors containing human and mouse IFI44L

Human and mouse IFI44 and IFI44L were cloned into Gateway entry vectors (Table 2.2) through polymerase chain reaction (PCR) gene amplification of a cDNA template and ligation into the vectors.

The cDNA template for human IFI44 and IFI44L was generated by stimulating THP1 cells with 500 U/mL universal type I IFN (IFNa/D; Bio-Techne) for 19 hours, followed by RNA extraction using a QIAshredder (Qiagen) and RNeasy Mini Kit (Qiagen). RNA was converted to cDNA by using Superscript III reverse transcriptase (Invitrogen) and random hexamers (Invitrogen), according to manufacturer's instructions. The cDNA template for mouse IFI44 was derived from C57BL/6 BMDMs, previously generated by Rachel Rigby.

For mouse IFI44L, cDNA was derived from RAW cells in the same way as with human IFI44/L.

Primers for PCR amplification of human and mouse IFI44 and IFI44L sequences were designed based on the Ensembl transcript sequences (ENSG00000137965, ENSG00000137959, ENSMUSG00000028037, MGP-BALBcJ-G0027955). The forward primers included a Kozac sequence (GCCGCC) inserted immediately 5' of the start codon, and the reverse primer excluded the Stop codon to allow for the addition of a C-terminal tag. PCR reactions were performed using Herculase II fusion DNA polymerase (Agilent Technologies) according to manufacturer's instructions. PCR reactions were analysed by agarose gel electrophoresis and amplicons were extracted from the gel using QIAquick Gel Extraction Kit (Qiagen). Next, 3'A overhangs were added to the purified PCR product with GO Taq DNA polymerase (Promega) and dATP (New England Biolabs) to allow ligation into the pCR8/TOPO Gateway entry vector (Invitrogen). After TOPO ligation, plasmids were transformed into E. coli (New England Biolabs), and resulting successful single colonies were amplified in LB broth with 50 mg/mL spectinomycin and plasmids purified through Miniprep or Midiprep kits (Qiagen). The orientation and sequence of the insert was confirmed by Sanger sequencing.

Generation of Gateway® destination vectors

Using a recombinase (LR Clonase II Enzyme Mix (Invitrogen)), inserts were shuttled from entry vectors to destination vectors including pLenti6.3/TO/V5/DEST (Invitrogen), pcDNA3.2/V5-DEST (Invitrogen) or pcDNA3.2/FLAG-DEST (generated by Jonny Hertzog) (see Table 2.2). Resulting plasmids were transformed and propagated in recombination-deficient Stbl3 bacteria (Invitrogen) with 50 mg/mL carbenicillin and purified through Midiprep kits (Qiagen). Constructs were assured through Sanger sequencing.

Generation of LentiCRISPRv2 plasmids

Single guide RNAs (sgRNAs) targeting human IFI44 or IFI44L were designed by Philip Hublitz at the Genome Engineering Facility at the WIMM and inserted into pLentiCRISPRv2 vectors encoding Cas9 transcript. For *IFI44*, three single guides were designed to target exon four. For *IFI44L*, one single guide was designed to target exon three and three single guides were designed to target exon four.

First, the pLentiCRISPRv2 vector was digested and dephosphorylated using FastDigest BsmBI (ThermoFisher) and FastAP Thermosensitive Alkaline Phosphatase (ThermoFisher), and digestion validated via agarose gel electrophoresis. Next, the oligonucleotides encoding the sgRNAs were phosphorylated through incubation with T4 Polynucleotide Kinase (ThermoFisher) and annealed at 95°C. The pLentiCRISPRv2 vector and

sgRNA were then be ligated through incubation with T4 DNA ligase (ThermoFisher), and the resulting plasmid was transformed into Stbl3 bacteria (Invitrogen). Single colonies were propagated in LB broth with 50 mg/mL carbenicillin, and plasmids purified through Miniprep or Midiprep kits (Qiagen). The orientation of the insert was checked through Sanger sequencing.

2.2.2 Lentiviral Particles

HEK293T cells were seeded in 15 cm cell culture dishes at 1.2x10^7 cells/dish in growth medium. The following day, cells were transfected. After 16 hours, supernatant was removed and fresh growth media added. After another 24 hours, supernatant containing lentiviral particles were removed and fresh growth media added. Supernatant containing lentiviral particles were stored at 4°C. After another 24 hours, supernatant containing lentiviral particles were removed again, pooled with the first batch and clarified through centrifugation and filtration through a 0.45 µm filter. Supernatant containing lentiviral particles were aliquoted into cryovials and stored at -80°C.

Lentiviruses for transduction

Cells were transfected with 9 µg lentiviral expression plasmids containing the gene of interest, 9 µg p8.91 plasmid and 3 µg pVSV-G using Lipofectamine 2000 (Invitrogen) (see Table 2.2).

For transduction of adherent cells, lentiviral stocks were added 1:1 with growth media. The same stock of lentiviral particles was used throughout. Cells were incubated for 48 hours, and then the selection reagent blasticidin was added at 10 µg/mL to cells. When 80-100% cell death was seen in the Lipofectamine-2000-only control, selection was complete. Blasticidin at 10 µg/mL was maintained in the growth media for all transduced cell lines for all of their passages.

Lentivirus for *in vivo* infection

Cells were transfected with 2.5 µg pMD2.G, 2.5 µg p8.91 and 3.75 µl pCSGW using Fugene 6 (Promega) (see Table 2.2). Filtered virus supernatant was added to ultracentrifugation tubes, and a sucrose cushion was made through addition of 20% sucrose in PBS (autoclaved and sterile), backfilled into the bottom of the tube. Virus was then centrifuged at 23000rpm for 2.5 hours with no deceleration/brake. After centrifugation, the supernatant was removed, and virus pellets pooled and concentrated into 1.5mL PBS. Virus was stored at -80°C.

Titre was determined for GFP-expressing lentivirus through flow cytometry. HEK293T

cells were seeded in 24-well plates at 8x10^4 cells per well. The following day, 10-fold serial dilutions were made in duplicate. After 48 hours, cells were washed with PBS, stained with LIVE/DEAD™ Fixable NIR cell stain kit (Invitrogen) at 1:1000 in PBS for 20 minutes at 4°C, washed and resuspended in 4% paraformaldehyde. Flow cytometry was performed on an Attune™ NxT Flow Cytometer (Invitrogen).

2.2.3 *In vitro* virus infection

Virus screen in HEK293T cells overexpressing IFI44/L

HEK293T cells stably overexpressing IFI44, IFI44L or GFP via lentiviral transduction were seeded at 1.8x10^5 cells per well in 12-well plates. The following day, cells were infected with two different concentrations of virus as follows:

Virus	MOI low	MOI high
VACV	0.02	0.2
HSV-1	0.01	0.02
AdV-GFP	750	1500
HIV-GFP	1:500	1:250
HIV2-GFP	1:500	1:250
PR8	1	10
Sendai	0.1	1
ZIKV	0.1	1

Table 2.6: MOI of virus used for *in vitro* virus screen

After 48 hours the cells were washed with PBS and processed for RNA or protein collection. For RNA, cells were lysed in in Buffer RLT plus, homogenised through QIAshredder (Qiagen) and stored at -80°C. For protein, cells were lysed in RIPA buffer (65 mM Tris-base, 154 mM NaCl, 1% NP-40, 1% Na-deoxycholate, 5 mM EDTA, 5 mM EGTA, 0.1% SDS, pH 7.4) with 1:100 protease inhibitor cocktail (Cell Signalling Technology) and protein concentrations were determined through Pierce™ BCA Protein Assay Kit (Invitrogen) and stored at -20°C. Samples were then analysed for viral RNA content through RT-qPCR (see section 2.2.8) or for viral protein content through immunoblotting (see section 2.2.5).

Vaccinia virus kinetics and cleavage assays

HEK293T cells were seeded at 1.8x10^5 cells per well in 12-well plates. Cells were either stably overexpressing IFI44, IFI44L or GFP through lentiviral transduction, or after 24 hours, cells were transiently transfected with 1 µg pcDNA3.2/IFI44/V5, 1 µg

pcDNA3.2/IFI44L/FLAG or 0.5 µg of both using Lipofectamine-2000 (Invitrogen). For virus titration, the following day cells were infected in a 3-fold dilution series with VACV WR, from 0.0074 multiplicity of infection (MOI) to 0.2 MOI. After 24 hours, cells were harvested. For virus time-course: cells were infected with VACV WR at 1 MOI, and harvests were performed at 2, 4, 6, 8, 12 and 18 hours. For proteasome inhibition assays: cells were infected with VACV WR at 1 MOI in low medium (500 µl per well). To mediate viral attachment, cells were rocked every 10 minutes for one hour. After three more hours, MG-132 proteasome inhibitor (Sigma-Aldrich) was added to cells at a concentration of 5 µM in DMSO (or DMSO only as a carrier control). After another 2 hours, cells were harvested. Harvests and RNA/protein isolation were processed as in section 2.2.3. Samples were then analysed through RT-qPCR (see section 2.2.8) or through immunoblotting (see section 2.2.5).

Vaccinia virus cleavage of endogenous IFI44

HEK293T cells were seeded at $3x10^5$ cells per well in 6-well plates. The following day, cells were stimulated with 50 U/mL universal type I IFN (IFN a/D; Biotechne). After 19 hours, cells were infected with VACV WR at an MOI of 1. After 6 hours of infection, cells were harvested. Protein was harvested and processed as in section 2.2.3. Samples were then analysed immunoblotting with antibodies detecting endogenous proteins (see section 2.2.5).

VACV-GFP live cell imaging

HEK293T cells were seeded at $1.8x10^5$ cells per well in 12-well plates. After 24 hours, cells were transiently transfected with 1 µg pcDNA3.2/IFI44/V5, 1 µg pcDNA3.2/IFI44L/FLAG or 1 µg pcDNA3.2/EV/V5 using Lipofectamine-2000 (Invitrogen). The following day, cells were infected with 0.0001 MOI of VACV-GFP, and cell plates were placed in the Incucyte Live Cell Imager (Sartorius). Images were taken every 6 hours for a total period of 48 hours. Cell confluence and GFP fluorescence intensity was measured on the Incucyte Software.

Infection of MEFs

Immortalised or primary MEFs were seeded at $1x10^5$ cells per well in 24-well plates. The following day, cells were stimulated with 0 U/mL or 100 U/mL mL universal type I IFN (IFN a/D; Biotechne). After 19 hours, cells were infected with a 10-fold dilution series of EMCV from 0.0001 MOI to 1 MOI, a 10-fold dilution series of HSV-1 from 0.01 MOI to 100 MOI or a 10-fold dilution series of VACV from 0.0003 MOI to 3 MOI. Infectivity was analysed via crystal violet staining or Incucyte Live Cell Imaging (Sartorius).

2.2.4 Plaque assay

HEK293 cells or MEFs were seeded at 5x10^5 cells per well in 6-well plates. After 24 hours, HEK293 cells were transiently transfected with 1 µg pcDNA3.2/IFI44/V5, 1 µg pcDNA3.2/IFI44L/FLAG, 0.5 µg of both or 1 µg pcDNA3.2/GFP/V5, using Lipofectamine-2000 (Invitrogen) while MEFs were stimulated with 0 U/mL or 100 U/mL mL universal type I IFN (IFN a/D; Biotechne). The next day, 25 pfu of HSV-1 was added to HEK293 cells, while 5 pfu of HSV-1 or VACV was added to MEFs. The virus was incubated at 37°C for 1.5 hours and then removed. Cells were washed in growth media and a 0.5% CMC overlay was added. When plaques became visible under the microscope (typically around 55 hours), the overlay was removed and cells were fixed with formaldehyde at a concentration of 1:4 in PBS. After 20 minutes, the fix was removed and 1% crystal violet stain in PBS added for a further 20 mins. Crystal violet stain was rinsed off with distilled water, and cell plates were imaged when fully dry.

2.2.5 Immunoblotting

Protein concentrations were equalised to 5-50 µg through dilution in PBS. Subsequently, 4x NuPAGE LDS Sample Buffer (Invitrogen) was added, and samples were incubated at 95°C for 5 minutes. Samples were run on NuPAGE Novex 4-12% Bis-TRIS gels (Invitrogen) using NuPAGE MOPS-SDS running buffer (Invitrogen) at 100V for 2 hours. Next, proteins were blotted onto PROTRAN Pure nitrocellulose membrane (PerkinElmer) using transfer buffer (25 mM TRIS, 192 mM glycine, 20% MeOH). Gel loading was confirmed with ponceau stain, which was washed off in distilled H_2O and membranes were then blocked in 5% skim milk powder (Sigma-Aldrich) in TBS-T (TBS + 0.2% Tween-20) for one hour at room temperature. After blocking, membranes were incubated with primary antibodies in 5% milk in TBS-T at 4°C overnight, or at room temperature for one hour, depending on the sensitivity of the antibody (see Table 2.5). Subsequently, membranes were washed three times in TBS-T for five minutes each. For antibodies not directly conjugated to horseradish peroxidase (HRP), membranes were incubated with HRP-coupled secondary antibodies in 5% milk in TBS-T for one hour at room temperature. Membranes were washed as before, and proteins detected using Western Lightening Plus-ECL (PerkinElmer) and iBright FL 1000 Imaging System (Thermo Fisher) or the Odyssey M Li-Cor Imaging System (LiCorBio). If needed, HRP was removed from the membranes through quenching in 1% sodium azide for 45 minutes (and subsequent washing 5 times in TBS-T for 5 minutes each), or proteins were stripped from the membrane in stripping buffer (200 mM glycine, 0.1% SDS, 1% Tween-20, pH 2.2) for an hour (and subsequent washing 5 times in TBS-T for 5 minutes each). In the case of stripping, membranes were re-blocked in 5% milk in TBS-T. Subsequently, membranes could be washed, probed and

imaged.

2.2.6 Immunoprecipitation

HEK293T cells stably overexpressing IFI44 or IFI44L via lentiviral transduction were seeded in 15 cm cell culture dishes and grown to confluency. Alternatively, HEK293T cells were seeded in 15 cm cell culture dishes at 1.2x10^7 cells per dish in growth medium, and the following day transiently transfected with 1 µg pcDNA3.2/IFI44/V5, 1 µg pcDNA3.2/IFI44L/FLAG, 0.5 µg of both or 1 µg pcDNA3.2/GFP/V5 using Lipofectamine-2000 (Invitrogen). After 24 hours, cells were lysed in either IP Lysis Buffer (20 mM TRIS-HCl pH 7.4, 100 mM NaCl, 1 mM EDTA, 0.5% NP-40(=IGEPAL CA-630)) or RIPA buffer (see section 2.2.3) with 1:100 protease inhibitor cocktail (Cell Signalling Technology). Lysates were subject to a 'pre-clearing' step whereby they were incubated with 50 µl Dynabeads Protein G (Invitrogen) per sample at 4°C rotating for one hour to minimise unspecific binding. During this time, 50 µl Dynabeads Protein G per sample were coated in 5 µg anti-V5 or 5 µg anti-FLAG antibody (depending on the pull down) for one hour at 4°C, rotating (see Table 2.5). Next, an aliquot of clarified lysate was removed as the 'input' fraction for each sample, and subsequently the clarified lysates were incubated with the antibody-coated beads for one hour at 4°C, rotating. After this, total lysate was removed as the 'unbound fraction', and the beads were washed three times in IP Lysis Buffer. The bound fraction was eluted through incubation with 1 mg/mL V5 synthetic peptide (Stratech Scientific) or 1 mg/mL 3X FLAG elution peptide (Cambridge Bioscience Ltd) at 37°C shaking for 10 minutes, depending upon which antibody the beads were conjugated to. This elution step was performed twice to increase yield from the beads. Input, unbound and bound samples were subject to immunoblotting as in section 2.2.5, or bound fractions were prepared for mass spectrometry (see section 2.2.19).

2.2.7 Immunofluorescence

HEK293T cells or HFFs stably overexpressing IFI44 or IFI44L via lentiviral transduction were seeded in 8-well µslide chambers (Ibidi) at 7x10^4 cells/mL in 300 µl total. Alternatively, HEK293T or HeLa cells were seeded in 8-well µslide chambers at 7x10^4 cells/mL, and the following day were transiently transfected with 0.5 µg pcDNA3.2/IFI44/V5, 0.5 µg pcDNA3.2/IFI44L/FLAG or 0.25 µg of both using Lipofectamine-2000 (Invitrogen). Once the cells had reached 80% confluency (typically 24 hours), they were washed twice with PBS and fixed with 4% paraformaldehyde in PBS for 20 minutes. Cells were washed again in PBS and blocked and permeabilised for 30 minutes at room temperature with 2% BSA or 5% mouse serum and 0.1% Triton-X 100. Cells were washed again, and incubated with the relevant antibody: 5 µg V5-AF488, 2.5 µg/mL Tubulin-AF647 or 2.5 µg/mL

FLAG-AF647 in 0.1% BSA and 0.1% Triton-X 100 overnight at 4°C (see Table 2.5). The next day, cells were washed with PBS and 3 drops mounting medium containing DAPI (Ibidi) were added. Slides were stored at 4°C in the dark until imaging.

2.2.8 RT-qPCR

For cell lines and MEFs, cells were lysed in RLT Plus Buffer and RNA was extracted using RNeasy Plus Mini Kit (Qiagen) as in section 2.2.3. For mouse organs, tissues were stored in RNAlater (Invitrogen) at 4°C overnight, homogenised in TRIzol reagent (Invitrogen) using Precellys homogenising tubes and homogeniser, and RNA extracted as per manufacturer's instructions through phenol-chloroform separation followed by ezDNase treatment (Invitrogen). RNA was quantified on a nanodrop, and 1 µg was annealed to random hexamers (Invitrogen) to prime production of cDNA by SuperScript III Reverse Transcriptase (Invitrogen), as per manufacturer's instructions. Next, cDNA was diluted 1:5 in UltraPure water (Gibco) and 1.5 µl was used as a template for RT-qPCR using TaqMan Fast PCR Master Mix (Applied Biosystems) and Taqman probes. The qPCR reaction was run on a QuantStudio 7 Flex Real-Time PCR System (ThermoFisher) with standard settings. Gene expression was analysed using the Ct method (8) and *GAPDH*, *HPRT* or *ACTB* were used as indicated for normalisation. All TaqMan probes used are documented in Table 2.4.

2.2.9 *In vivo* infection, organ harvesting and downstream processing

Humane endpoints as described in the project licences were: weight loss reaching 15% (or for influenza infection, 20% or remaining greater than 15% for 48 hours) or hunched posture, piloerection or reduced activity that did not self-resolve within 24 hours. At the experimental or humane endpoint, mice were sacrificed through either a rising concentration of CO_2 or exsanguination under terminal anaesthesia. Blood was collected into EDTA-coated microtainers (blood profiling) or amber microtainers (serum) (BD Biosciences). Organs were harvested into RPMI containing 2% FCS for flow cytometry (see section 2.2.13) or RNAlater (Invitrogen) for RT-qPCR (section 2.2.8). Organs in RNAlater were incubated at 4°C for 2 days and then frozen at -80°C until RNA processing (section 2.2.8).

In vivo Influenza/A/X-31 infection

C57BL/6N mice were anesthetised with isoflurane and infected intranasally with 0.04 HAU of influenza/A/X-31 (H3N2 strain) in 50 µl total and baseline weight measurement was obtained. This was done in collaboration with Tiong (Jack) Tan. Mice were weighed at the same time every day until they reached the experimental endpoint. This was either 7-10 days-post infection, or the humane endpoint, and organs were harvested as in 2.2.9.

In vivo Lentiviral infection

Replication-deficient GFP-tagged lentiviral particles were made as described in section 2.2.2. C57BL/6N mice were injected intravenously with $1.6x10^7$ infectious units in 200 µl volume and baseline weight measurement was obtained. Mice were weighed at the same time every day until they reached the experimental endpoint. This was either 5 days-post infection, or the humane endpoint, and organs were harvested as in 2.2.9.

In vivo induction of acute anaemia with phenylhydrazine hydrochloride

On day 0, phenylhydrazine hydrochloride (PHZ) powder was dissolved in PBS to derive a 20 mg/mL stock solution, and the pH was adjusted to 7.4 with 2M NaOH (filter-sterilised). C57BL/6N mice were weighed to obtain baseline weight, and animals were injected intraperitoneally with 0.08 mg PHZ per g of body weight. On day 2, this was repeated, and mice were weighed at the same time every day until the experimental endpoint. This was either 6 days-post treatment, or the humane endpoint. At the endpoint, mice were sacrificed through exsanguination under terminal anaesthesia, and blood collected into EDTA-coated microtainers (BD Biosciences). Organs were harvested as in 2.2.9.

DNA extraction for genotyping

C57BL/6 mouse ears were clipped, and the clippings incubated with PCR lysis buffer (100 mM Tris-HCL, 200 mM NaCl, 5 mM EDTA, 0.3% SDS, 1:200 Proteinase K) at 55°C with shaking for 3.5 hours. Lysate was centrifuged at 17000 *xg* and precipitated in isopropanol, centrifuged to pellet and the pellet washed with 70% ethanol and resuspended in water.

Ifi44 was PCR-amplified with genotyping primers, and genotypes determined by agarose gel electrophoresis. After initial validation, mice were genotyped through the company Transnetyx by custom-designed, proprietary RT-qPCR.

Murine blood processing

For blood profiling, murine blood was collected through exsanguination under terminal anaesthesia into EDTA-coated microtainers (BD Biosciences) and mixed thoroughly to prevent from clotting. As soon as possible after collection, blood was profiled on a Pentra-ES 60 (Horiba).

For serum collection, murine blood was collected post-mortem through cardiac puncture into amber microtainers (BD Biosciences) to encourage clotting. Blood was left to clot at room temperature for 1-4 hours. Tubes were centrifuged at 17000 *xg* for 10 minutes, and serum poured off into eppendorf tubes. Serum was stored at 4°C until further processing.

2.2.10 Microneutralisation assay

Microneutralisation assays were performed in collaboration with Tiong (Jack) Tan. First, infected mouse serum (alongside positive control monoclonal antibodies (mAbs)) was subject to serial dilution in a 96-well plate in virus growth medium (VGM; DMEM, 0.1% BSA, 10 mM HEPES buffer, 5% Pen/Strep and 2 mM L-glutamine). The negative controls included a virus-only control and a cell-only control. Previously titrated recombinant Influenza Virus-GFP or S-Flu (9) was diluted to 2 HAU in VGM, and 50 µl of this was added to relevant wells of the plate. Next, MDCK-SIAT cells were diluted in VGM and $3x10^4$ cells were added to relevant wells. The plates were incubated overnight at 37°C. The following day, supernatant was removed and cells were fixed in 10% Formalin at 4°C for 30 minutes. The wells were washed twice with PBS, and a third wash of PBS placed on. The presence of eGFP was measured using a CLARIOstar Plus Microplate Reader (BMG Labtech).

2.2.11 Pearl's Prussian Blue Staining

C57BL/6N mice aged 10-16 weeks were sacrificed through exsanguination under terminal anaesthesia, and their spleens and livers removed. Organs were washed in PBS and then fixed in 10% Neutral Buffered Formalin (Sigma-Aldrich). Histological processing was performed by the Oxford Centre for Histopathology Research. Organs were placed in a histology cassette and then dehydrated in 70%-100% ethanol, cleared with various % of Xylene before paraffin wax infiltration. Next, the organs were fully embedded in a block of paraffin wax, which was sectioned with a microtome. Spleen sections were 4 µM thick, such that red pulp, splenic cords of billroth and white pulp were visible. Liver sections were also 4 µM thick and sectioned in the axial plane. Pearl's working solution was generating through mixing 2% HCl and 2% Potassium Ferrocyamide, and filtering the resulting solution. Slides were rinsed with distilled water and submerged in Pearl's working solution for 15 minutes. The slides were removed and thoroughly rinsed. 0.5% Neutral red was then filtered onto the slides for two minutes before another washing step. Slides were then dehydrated in 100% ethanol and cleared with Xylene, before scanning at 40X resolution. Digitised slides were quantified by Nasullah Khalid Alham using the Visiopharm Integrator System (VIS) platform version 2023.09. Image analysis protocols are implemented as Analysis Protocol Packages (APP) in VIS. An APP was designed to quantify slides stained with iron. Prior to the image analysis, it is important to outline the Region of Interest (ROI), an auxiliary APP was designed to detect ROIs. The APP runs on the slide using threshold classification that identifies the tissue regions. An APP runs on 40X on the slides using the U-Net network of the VIS AI module that identifies iron positive staining. As a post-processing step; 2 different intensity thresholds (60 and

160) of the H and E Haematoxylin feature were used to classify the detected iron stains into high and low intensity classes. The output variables obtained from the APPs include: total tissue area, iron with high intensity area, iron with low intensity area.

2.2.12 Serum iron quantification

Serum iron was quantified through the iron assay kit (Sigma-Aldrich).

2.2.13 Flow Cytometry

Flow cytometry was performed on either an Attune™ NxT Flow Cytometer (Invitrogen) or an LSR Fortessa™ X50 (BD Biosciences). Compensation was performed using single-stain control Compensation Particles Set (BD Biosciences). Population analysis was performed using FlowJo software. In all cases, fluorescence minus one (FMO) controls were used to determine gate placement.

Analysis of cellular populations in murine spleen and bone marrow

Murine organs were harvested as in section 2.2.9. Spleens were dissociated through mechanical disruption followed by enzymatic digestion with Collagenase type II (Rockland) and DNase I (Sigma-Aldrich) at 37°C for an hour. Cell suspensions were then filtered through 70 µM cell strainers, centrifuged to pellet, and red blood cells removed by resuspending the pellet in Red Blood Cell Lysis Buffer (RBCL; Sigma-Aldrich) for four minutes. RBCL was neutralised with RPMI containing 10% FCS and removed via centrifugation. The RBCL step was omitted when flow cytometry for erythrocytic precursors in the spleen was performed. Bone marrow was flushed out of the hindlegs into RPMI containing 2% FCS and spun to wash. Cells were resuspended in RPMI containing 10% FCS, counted, and one million cells seeded per well in a 96-well V-bottom plate. Cells were seeded every other well to avoid spillover. Cells were washed with PBS and incubated with LIVE/DEAD™ Fixable cell stain kit (Invitrogen) at 1:1000 and blocked with α-CD16/32 at 1:100 in PBS for 20 minutes at 4°C. Tetramer staining using reagents from the NIH tetramer facility (Table 6.1) was carried out at room temperature for 30 minutes in Tetramer buffer (PBS with 2% FCS and 0.04% sodium azide) prior to antibody staining. Cells were washed in PBS, and antibody cocktail along with FMO controls made up in FACS buffer (PBS with 2% FCS) and added to relevant wells. Cells were incubated for 30 minutes at 4°C and then washed in ice-cold FACS buffer three times. If only using surface stain, cells were fixed in Fixation Buffer (BioLegend) at 4°C for 20 minutes and then resuspended in FACS buffer and stored at 4°C. For intracellular staining, cells were fixed and permeabilised using the eBioscience™ Foxp3 / Transcription Factor Staining Buffer Set for 45 minutes at 4°C. Cells were washed in permeabilisation (perm) buffer,

and antibody cocktail along with FMO controls made up in perm buffer and added to relevant wells. Cells were incubated for 30 minutes at 4°C and then washed in perm buffer twice. Cells were resuspended in FACS buffer and stored at 4°C.

Cell cycle flow cytometry

Splenocytes were derived as in section 2.2.13, or HEK293T cells stably overexpressing IFI44, IFI44L or GFP via lentiviral transduction were counted, and one million per condition washed in PBS and pelleted. Cells were then fixed through the drop-wise addition of ice-cold 70% ethanol while vortexing and incubated on ice for two hours. Cells were washed in PBS, and then resuspended in staining buffer, containing 50 µg/mL Propidium Iodide (Sigma-Aldrich) and 100 µg/mL RNase A (Sigma-Aldrich) in PBS.

2.2.14 IL-1β ELISA

BMDMs from C57BL/6N mice were seeded in 24-well plates at 1.6x10^5 cells per well and cultured for two days. The non-canonical inflammasome was activated through stimulating cells with 1 µg/mL LPS for four hours, and then after washing with PBS, cells additionally stimulated with an ATP pulse using 5 mM ATP for 20 minutes. Cells were washed again, growth media added and incubated for a further hour. Supernatant was then harvested and IL-1β was quantified with the Mouse IL-1β Uncoated ELISA Kit with Plates (Invitrogen), and plates read using a CLARIOstar Plus Microplate Reader (BMG Labtech).

2.2.15 Bacterial PAMP Stimulation Assays

Hindlegs from C57BL/6N mice were removed and shipped to the Broz lab in Lausanne, Switzerland. The Broz lab derived BMDMs in DMEM with 10% (v/v) FCS, 10% L929 supernatent, 10 mM HEPES and nonessential amino acids. One day prior to infection, BMDMs were seeded at 5x10^5 in 96-well plates. BMDMs were primed with LPS O111:B4 (InvivoGen) for four hours prior to addition of stimuli. Cell lysis was assessed by quantifying the amount of lactate dehydrogenase (LDH) in the cell supernatent using LDH cytotoxicity kit (Takara) according to manufacturer's instructions. LDH was normalised to untreated controls and 100% lysis. Cytokine release into the supernatent (IL-1β) was measured by ELISA (ThermoFischer Scientific) according to the manufacturer's instructions.

Nigericin

Cells were LPS-primed for four hours and then treated with Nigericin (5 µg/ml; Sigma-Aldrich) for 30 minutes before assaying LDH release and IL-1β production.

Salmonella

Wild-type *Salmonella typhimurium* SL1344 was grown in LB broth at 37°C with aeration.

For assaying NLRC4 activation, *Salmonella* were subcultured for four hours to induce SPI-T3SS expression before infection. Cells were infected with MOI 10 or 20 logarythmic phase *S. typhimurium*. Plates were centrifuged for 15 minutes at 500 *xg* to synchronise the infection and placed at 37°C for one hour before assaying LDH release and IL-1β production.

For assaying caspase-11 activation, bacteria (Δ*OrgA* Δ*FliC/FljB S. typhimurium* SL1344) were diluted in fresh pre-warmed macrophage medium and added to the BMDMs at MOI 100 for one hour. Plates were centrifuged for 15 minutes at 500 *xg* to synchronise the infection and placed at 37°C for one hour. Next, 100 µg/ml gentamycin was added to kill any extracellular bacteria. After one hour incubation, BMDMs were washed once with DMEM and given fresh macrophage medium containing 10 µg/ml gentamycin for the remainder of the infection. Cells were left for 16-18 hours before assaying LDH release and IL-1β production.

Francisella

For infections with *F. novicida* U112, bacteria were grown overnight in BHI or TSB at 37°C with aeration. The bacteria were added to the BMDMs at MOI 100. Plates were centrifuged for 15 minutes at 500 *xg* to ensure compatible adhesion of the bacteria to cells and placed at 37°C for 120 minutes. BMDMs were washed and fresh medium with 10 µg/ml gentamycin (Invitrogen) was added to kill extracellular bacteria. Plates were incubated for 16-18 hour before assaying LDH release and IL-1β production.

dA:dT transfection

AIM2 inflammasome activation was achieved by transfecting 0.4 µg poly(dA:dT) (InvivoGen) per 10^5 cells. In seperate tubes, poly(dA:dT) and linear polyethylenimine (PEI) (1 µg per 105 cells; PolyScience) were mixed with OptiMEM by vortexing and incubated for 3 minutes at room temperature. Next, poly(dA:dT) and PEI were mixed together, vortexed shortly, and incubated for 15 minutes before adding a quater of the total volume on top of the cells. Transfection was facilitated by centrifugation at 300 *xg* for five minutes at 37°C, before assaying LDH release and IL-1β production.

2.2.16 Hemin Stimulation Assay

This experiment was adapted from Sundaram *et al* (10). BMDMs were seeded in 6-well plates at 8x10^5 cells per well. The next day, BMDMs were stimulated with 50 µM hemin (Merck)/well and 500 ng/mL R848 (InvivoGen) in growth medium including 8000x YoYo3 Iodide (Invitrogen). Cell plates were imaged with the Incucyte Live Cell Imager (Sartorius). Images were taken every 6 hours for a total period of 48 hours. Cell confluence and YoYo3 stain intensity were measured on the Incucyte Software.

2.2.17 Cell-titre Glo Assay

MEFs were seeded in 96-well plates at 2.7x10^4 cells per well. The following day, cells were stimulated with 0 U/mL or 500 U/mL IFN a/D (Bio-Techne) for 19 hours. Alternatively, HEK293T cells stably overexpressing IFI44, IFI44L or GFP via lentiviral transduction were seeded in collagen-coated 96-well plates at 4000 cells per well. The next day, oxidative stress was induced with a two-fold dilution series of hydrogen peroxide from 12.5 µM to 200 µM or with sodium arsenite from 0.19 µM to 50 µM. After 20 hours, cell viability was measured with the Cell Titre Glo Kit (Promega) as per manufacturer's instructions.

2.2.18 ROS Glo Assay

MEFs were seeded in 96-well plates at 2.7x10^4 cells per well. The following day, cells were stimulated with 0 U/mL or 500 U/mL IFN a/D (Bio-Techne) for 19 hours. Baseline ROS levels were measured with the ROS Glo Kit (Promega) as per manufacturer's instructions.

2.2.19 Mass Spectrometry

Input fractions generated from immunoprecipitation as in section 2.2.6 were prepared for mass spectroscopy using S-Trap™ (Protifi) in collaboration with Adan Pinto Fernandez. Samples were prepared as per S-Trap™ manufacturer's instructions. Briefly, SDS was added to each sample for a final concentration of 2.5%. Samples were reduced with 5 mM of DTT at 37°C while shaking for 30 minutes. Then, samples were alkylated with 20 mM Iodoacetamide (Promega) for 15 minutes at room temperature, protected from light. Samples were acidified with 12% phosphoric acid, and S-Trap™ binding buffer (90% MeOH, 100 mM TEAB, pH 7.1) added. Each lysate is then added to an S-Trap™ column and centrifuged at 4000 *xg* for 30 seconds. The column is washed with S-Trap™ binding buffer with centrifugation thrice, before the membrane is dried with centrifugation and incubated with 30 µg trypsin overnight at 37°C. The following day, the sample is eluted using three different elution buffers: 50 mM TEAB and centrifugation, 0.2% formic acid

and centrifugation and finally 50% acetonitrile and centrifugation. Eluted peptides are pooled, dried down and resuspended and stored at -80°C.

Subsequently, mass spectroscopy was performed by Iolanda Vendrell, Roman Fischer and Benedikt Kessler at the Target Discovery Institute. Peptide samples were loaded onto Evotips (Evosep) according to the manufacturer's instructions, then chromatographically separated using an Evosep One (Evosep) using the 30 spd standard method. Peptides were eluted onto a TimsTOF Pro mass spectrometer operated in diaPASEF mode using 16 diaPASEF scans per TIMS-MS scan. The ion mobility range was set to 0.6-1.6 Vs/cm^2. Each mass window isolated was 26 m/z wide, ranging from 400-1200 m/z with an ion mobility-dependent collision energy that increased linearly from 20 eV to 59 eV between 0.6-1.6 Vs/cm^2. Data were analysed by Adan Pinto Fernandez. Raw mass spectrometry (.d) files were searched and label-free quantified using DIA-NN (version 1.8) in library-free mode using the Uniprot proteome UP000005640 (2022) as a FASTA file. DIA-NN output data was further processed in Perseus (v1.6.2.3).56 and volcano plots were generated using VolcanosR.

2.2.20 RNA Sequencing

RNA was isolated from spleens and livers of C57BL/6N mice using TriZol, as described in Section 2.2.8. RNA integrity was probed using TapeStation RNA ScreenTape System (Aligent). Poly(A) RNA sequencing was performed by either the Oxford Genomics Centre or Source Biosciences. Subsequently, data was analysed by Rachel Rigby, Tanja Davis and Aleksandr Fedorov.

Reads Processing

Adapters, low-quality base pairs, and poly-A and poly-G tails were trimmed using the fastp program (11). Poly-G clipping was necessary to eliminate known technical artifacts from Illumina's two-colour chemistry, where weak or absent signals at the end of a read are misinterpreted as high-quality G bases.

Alignment and quality control

Further data processing was performed using the community-curated Nextflow "rnaseq" pipeline (12). Briefly, reads were mapped to the GRCh39 assembly from the Ensembl database (13), then sorted using samtools (14), with duplicates marked by Picard. RNA abundance was estimated using Salmon (15) in pseudo-alignment mode. Quality control was conducted with FastQC, DESeq2 (16), and RSeQC (17), with results visualized through MultiQC (18). All trimmed libraries exhibited acceptable quality metrics at both

the sequencing and mapping stages.

Transcriptome analysis

Differential expression was assessed with DESeq2 (16). Gene ontology analysis of differentially expressed genes was conducted using the gprofiler package (19). Gene set enrichment analysis was performed using the fgsea package (20). All P values were adjusted for multiple testing using the Benjamini–Hochberg method, and results with P adjusted ≤ 0.05 were considered significant.

2.3 Data analysis and software

Unless indicated otherwise, data were analysed using Excel for Mac 16.86 (Microsoft) and GraphPad Prism 10.2.3 (GraphPad Software). SnapGene 5.2.1 (GSL Biotech) was used for nucleic acid sequences. Statistical analysis as detailed in the figure legends was performed using GraphPad Prism 10. Graphs and figures were created using GraphPad Prism 10 and Adobe Illustrator 28.5 (Adobe Systems). Flow cytometry data were analysed using FlowJo 10.8.2 (FlowJo, LLC).

References for Chapter 2

1. S. Ahmad et al., Breaching Self-Tolerance to Alu Duplex RNA Underlies MDA5-Mediated Inflammation. Cell 172, 797-810.e713 (2018).
2. G. J. Kotwal, B. Moss, Analysis of a large cluster of nonessential genes deleted from a vaccinia virus terminal transposition mutant. Virology 167, 524-537 (1988).
3. J. A. Symons et al., The vaccinia virus C12L protein inhibits mouse IL-18 and promotes virus virulence in the murine intranasal model. J Gen Virol 83, 2833-2844 (2002).
4. R. Holmdahl, B. Malissen, The need for littermate controls. Eur J Immunol 42, 45-47 (2012).
5. T. Vanden Berghe et al., Passenger Mutations Confound Interpretation of All Genetically Modified Congenic Mice. Immunity 43, 200-209 (2015).
6. Q. Tang et al., Adenosine-to-inosine editing of endogenous Z-form RNA by the deaminase ADAR1 prevents spontaneous MAVS-dependent type I interferon responses. Immunity 54, 1961-1975.e1965 (2021).
7. R. de Reuver et al., ADAR1 prevents autoinflammation by suppressing spontaneous ZBP1 activation. Nature 607, 784-789 (2022).
8. T. D. Schmittgen, K. J. Livak, Analyzing real-time PCR data by the comparative C(T) method. Nat Protoc 3, 1101-1108 (2008).
9. T. J. Powell et al., A single cycle influenza virus coated in H7 haemagglutinin generates neutralizing antibody responses to haemagglutinin and neuraminidase glycoproteins and protection from heterotypic challenge. J Gen Virol 100, 431-445 (2019).
10. B. Sundaram et al., NLRP12-PANoptosome activates PANoptosis and pathology in response to heme and PAMPs. Cell 186, 2783-2801.e2720 (2023).
11. S. Chen, Y. Zhou, Y. Chen, J. Gu, fastp: an ultra-fast all-in-one FASTQ preprocessor. Bioinformatics 34, i884-i890 (2018).
12. P. Di Tommaso et al., Nextflow enables reproducible computational workflows. Nat Biotechnol 35, 316-319 (2017).
13. F. J. Martin et al., Ensembl 2023. Nucleic Acids Res 51, D933-d941 (2023).
14. P. Danecek et al., Twelve years of SAMtools and BCFtools. Gigascience 10, (2021).
15. R. Patro, G. Duggal, M. I. Love, R. A. Irizarry, C. Kingsford, Salmon provides fast and bias-aware quantification of transcript expression. Nat Methods 14, 417-419 (2017).
16. M. I. Love, W. Huber, S. Anders, Moderated estimation of fold change and dispersion for RNA-seq data with DESeq2. Genome Biol 15, 550 (2014).
17. L. Wang, S. Wang, W. Li, RSeQC: quality control of RNA-seq experiments. Bioinformatics 28, 2184-2185 (2012).
18. P. Ewels, M. Magnusson, S. Lundin, M. Käller, MultiQC: summarize analysis results for multiple tools and samples in a single report. Bioinformatics 32, 3047-3048 (2016).

19. L. Kolberg et al., g:Profiler—interoperable web service for functional enrichment analysis and gene identifier mapping (2023 update). Nucleic Acids Research 51, W207-W212 (2023).
20. A. A. Sergushichev, An algorithm for fast preranked gene set enrichment analysis using cumulative statistic calculation. bioRxiv, 060012 (2016).

Chapter 3

IFI44 and IFI44L are Prototypical Interferon-Stimulated Genes

The category 'ISG' is diverse, broadly encompassing any gene that responds to IFN treatment. These genes may be expressed ubiquitously, but have their expression altered by IFN, or they may rely on IFN for expression. A 'prototypical ISG', then, refers to a gene which has little or no expression in the absence of IFN, and expression is hugely upregulated by IFN treatment across all, or many, cell types.

IFI44 and *IFI44L* are ISGs of unknown molecular function, however current published data suggest that they are important players in the type I IFN-mediated antiviral response (1-28). Indeed, *IFI44* and *IFI44L* expression has been linked with COVID-19 disease severity (15, 18, 29-32). Data mining the Immunological Proteomic Resource (ImmPRes) (33) displayed that IFI44 expression is associated with moderate, severe and critically severe COVID-19 on day one, moderate and severe COVID-19 at day seven, a lack of recovery at day 29 and seems to be specifically associated with COVID-19 as opposed to lower respiratory tract infections (LRTIs) (Figure S1 A-D). Interestingly, IFI44L expression in these settings does not mirror that of IFI44. Instead, there is much more IFI44L expression in healthy controls than IFI44, and as such IFI44L expression does not seem to be correlated with a lack of recovery at day 29 (Figure S1 E-H). However, IFI44L expression is associated with moderate and severe COVID-19 on day one, and this is a specific association with COVID-19 as opposed to LRTIs (Figure S1 E-H). Further, recent work from our lab posted on Biorxiv has identified *IFI44L* as a 'core' ISG that is upregulated *ex vivo* by almost every cell within most white blood cell types in response to all subtypes of type I IFN (34) (Figure 3.1A, B; Figure S2; Figure S3). The expression of *IFI44* is similar and is amongst the top 50 most highly upregulated ISGs in response to type I IFN stimulation in PBMCs (Figure 3.1B; Figure S3). The main difference seen

in this setting between *IFI44* and *IFI44L* expression is that *IFI44* is not expressed by every cell within a cell type, while *IFI44L* largely is (Figure 3.1A, B; Figure S2; Figure S3) (34). The expression data of *IFI44* and *IFI44L* leads one to hypothesise that *IFI44* and *IFI44L* have evolved highly responsive ISREs, such that their expression is rapidly and highly upregulated in response to IFN, and therefore they can mediate and/or exert antiviral effects, aiding in host innate defence. As this dataset only includes one concentration of IFN and one time point, it would be prudent to fully examine the expression kinetics of *IFI44* and *IFI44L* at the transcript and protein level, alongside titrating the IFN dose to discover the lowest dose that can upregulate the two proteins. Further, baseline expression of IFI44 and IFI44L is undetectable in PBMCs (Figure 3.1A, B; Figure S2; Figure S3). Whether this is true in mammalian organs is a relevant question that requires addressing.

Both *IFI44* and *IFI44L* are conserved as far down as shellfish (26, 35, 36). Indeed, presence of *IFI44* protects scallops against bacterial infection in culture (26). Intriguingly, invertebrates lack genes homologous to IFNs or their main effectors, and whether crustaceans employ type I IFN or an analogous system remains an open question (37-39). Thus, *IFI44* and *IFI44L* seemingly evolved prior to the IFN system itself. These proteins likely mediate their molecular functionality through their two highly conserved protein domains, discussed in section 1.3. While both domains are highly conserved, how either may act has not been addressed – especially since the P loop NTPase domain has not been confirmed to bind to or hydrolyse GTP, and the TLDc domain is the most evolutionarily distinct of the TLDc-domain containing family (Figure 1.9).

The cellular localisation of IFI44 and IFI44L may additionally provide clues as to their molecular functionality. The localisation of IFI44 is disputed, with conflicting evidence for cytosolic or nuclear localisation at baseline and after IFN induction/infection (1, 19, 25). In addition, as IFI44 was first discovered as microtubule-associated aggregates in hepatocytes of HCV infected chimpanzees (40), it is possible that IFI44 exists as aggregates. However, this has not been experimentally demonstrated.

Lastly, there is some evidence suggesting that IFI44 is antiproliferative (1, 23). Whether this can be reproduced, and whether IFI44L exhibits this same effect, remains open. It is noteworthy that both proteins have been implicated in various cancers (3, 16, 21, 24, 41-45).

Thusly, the question of IFI44/L's expression kinetics, protein domain functionality, cellular localisation and antiproliferative effects remain unanswered. This led us to test these experimentally, to gain further insights into how IFI44/L may be acting on a molecular level.

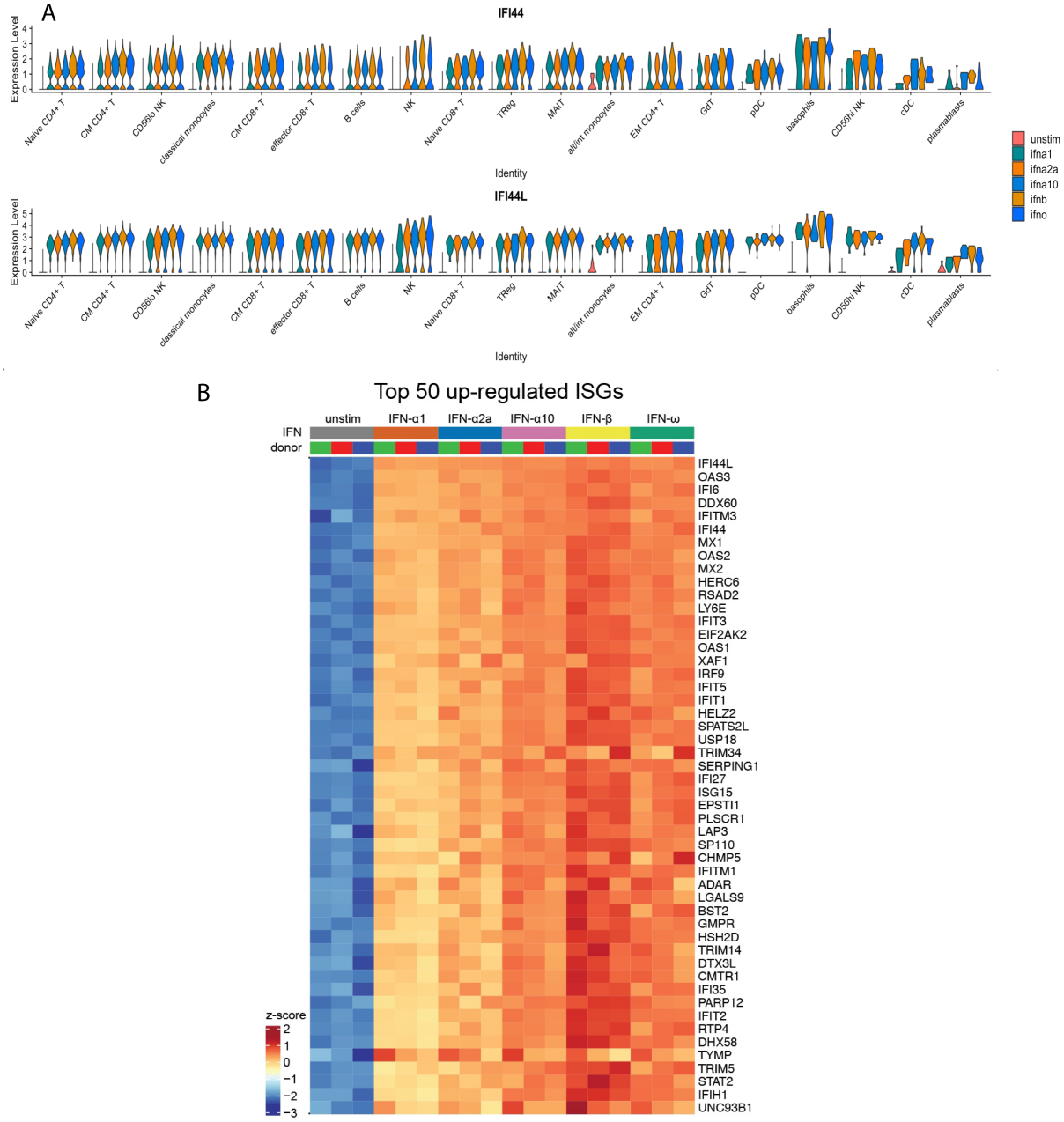


Figure 3.1: *IFI44* and *IFI44L* are 'core' ISGs expressed in response to all subtypes of type I IFN, in most cell types in PBMCs.

A. Violin plot depicting the expression of *IFI44* and *IFI44L* in different cell types. Single-cell RNA sequencing data in PBMCs after 24-hours of stimulation with 250U/mL of recombinant type I IFN. Dataset available via the IFN Resource Database. **B.** Bulk RNA sequencing depicting the top 50 upregulated ISGs after 24-hours of stimulation with 250U/mL of recombinant type I IFN across three donors. Data included in Rigby et al, 2023 (34). Figures generated by Rachel Rigby.

3.1 The expression kinetics of IFI44 and IFI44L

I confirmed that *IFI44* and *IFI44L* are prototypical ISGs, expressed at mRNA and protein levels after recombinant universal type I IFN (IFN a/D) treatment in all human cell lines tested (Figure 3.2A-C) (with the exception of Huh7.5 cells, data not shown). At the protein level, IFI44 is not expressed without IFN, except in THP-1 cells treated with PMA (Figure 3.2A) and *IFI44* transcript follows a similar pattern (Figure 3.2B). I was unable to obtain protein level data for IFI44L due to lack of availability of a specific antibody, but *IFI44L* transcript is expressed at low levels in unstimulated cells and upregulated by IFN a/D in a dose-dependent manner (Figure 3.2C). For comparison with another prototypical ISG, *DDX58* and the encoded RIG-I protein were tested, which displayed very similar expression patterns to IFI44 and *IFI44L* (Figure 3.2A, D).

To determine the expression kinetics of *IFI44* and *IFI44L*, I stimulated HEK293T cells with 500 U/mL of IFN a/D and performed a time-course from 0 hours to 72 hours. At the mRNA level, *IFI44* and *IFI44L* can be considered late ISGs, with no expression at 0 hours, low expression from 8 hours and a peak in expression at 72 hours (Figure 3.3 A, B). This is in contrast with *DDX58*, an early ISG, the expression of which was highly upregulated at 8 hours post-stimulation (Figure 3.3C; Figure S4A-C). At the protein level, IFI44 showed no expression at 0 hours and 8 hours post-stimulation, but was lowly expressed at 16 hours, with expression increasing thereafter (Figure 3.3D; S4A-C). This follows the expression pattern of the *IFI44* transcript, demonstrating that there was no significant delay from mRNA expression to protein expression, meaning there does not appear to be a second signal driving protein expression. IFI44 was upregulated at the protein level by just 50 U/mL of IFN a/D, and expression increases in a dose-dependent manner (Figure 3.3E). Strikingly, for all three ISGs tested, expression remains 'on' and stable for up to 72 hours. I hypothesised that this was due to the fact that IFN a/D is stable in culture. Confirming this, when IFN a/D was washed off the cells after 24 hours (Figure 3.4A), expression of *IFI44*, *IFI44L* and *DDX58* decreased – with IFI44 and IFI44L decreasing gradually, and *DDX58* displaying an 'on-off' switch-type expression pattern (Figure 3.4B-E).

3.2 Generation of *Ifi44*$^{-/-}$ mice

In human cell lines grown in standard two-dimensional (2D) cultures, there is no IFI44 expression in the absence of IFN stimulation (Figure 3.3A, D, E). Within organs, there may be tonic IFN signalling present at baseline, for example due to the volume of extracellular fluid being much less than that in 2D cultures, resulting in low-level expression of highly responsive ISGs (46, 47). This may be true of *Ifi44* in mice – I detected low-level expres-

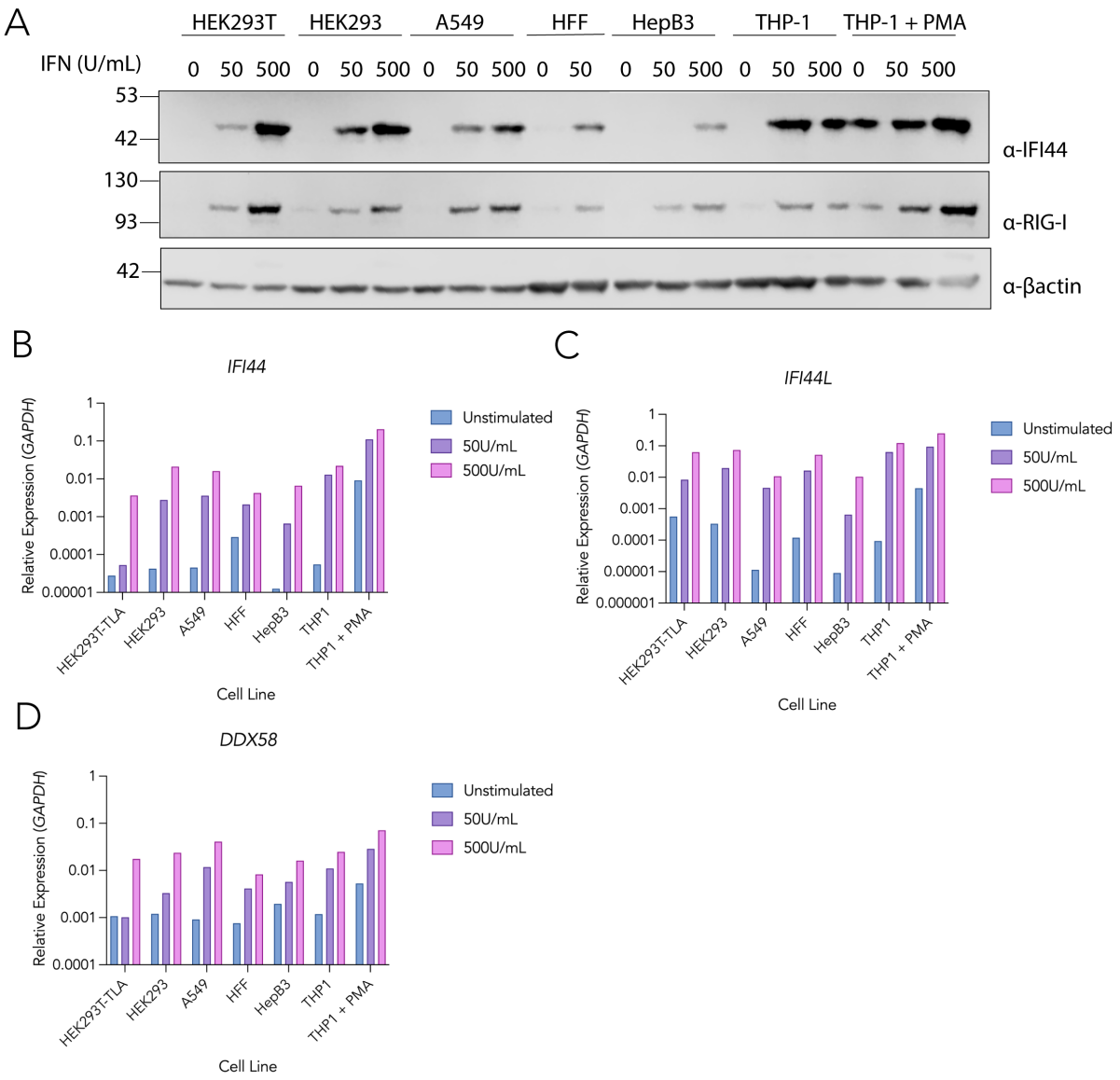


Figure 3.2: *IFI44* and *IFI44L* are expressed after IFN stimulation across a variety of human cell lines, and at baseline in PMA treated THP-1 cells.

A-D. HEK293T, HEK293, A549, HFF, HepB3, THP-1 or THP-1 cells treated with 20ng/mL PMA for 24 hours were stimulated with 0 U/mL, 50 U/mL or 500 U/mL of recombinant universal type I IFN (IFN a/D). After 19 hours, cells were lysed in RIPA buffer or buffer RLT, and protein and transcript expression of IFI44 and RIG-I was detected by western blot using antibodies detecting endogenous proteins and by RT-qPCR. (A) Results for HEK293T, HEK293, A549, THP-1 and THP-1 +PMA are representative data of three separate biological repeats. Results for HepB3 and HFF have one biological replicate. (B-D) Results for HEK293T, HEK293, A549, HepB3 THP-1 and THP-1 +PMA are representative data of two separate biological repeats. Results for HFF have one biological replicate.

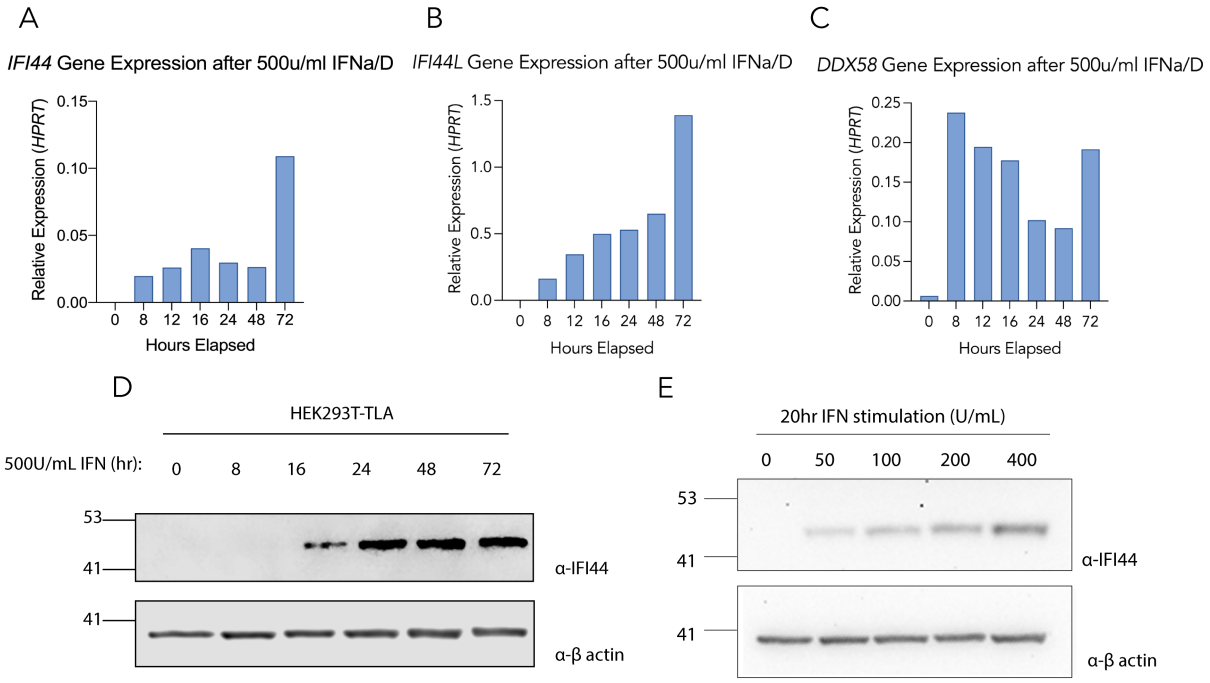


Figure 3.3: *IFI44* and *IFI44L* are late ISGs.

A-D. HEK293T cells were stimulated as before and lysed in buffer RLT or RIPA buffer at 0 hr, 8 hr, 16 hr, 24 hr, 48 hr and 72 hr. (A-C) RNA was extracted and RT-qPCR was performed for the indicated genes, or (D) protein expression determined through western blot using an endogenous α-IFI44 antibody. **E.** HEK293T cells were stimulated with 0 U/mL, 50 U/mL, 100 U/mL, 200 U/mL or 400 U/mL IFN a/D for 20 hours. Cells were lysed in RIPA buffer, and expression of IFI44 was detected through western blot using an endogenous α-IFI44 antibody. (A-D) Results shown are representative of three separate biological repeats, with results in A-C being the average of technical duplicates. (E) Results shown are representative of two separate biological repeats.

sion of *Ifi44* in the absence of IFN stimulation or infection (Figure 3.5A), potentially due to tonic IFN signalling. To identify cell types expressing IFI44 protein at baseline, I took high-resolution mass spectrometry data of C57BL/6J mouse haematopoietic populations from the ImmPRes database and searched for IFI44 (33). Here, IFI44 protein expression was only seen in M-CSF differentiated BMDMs, and not in any other immune cell type tested (Figure 3.5B).

C57BL/6 mice naturally lack *Ifi44l*, likely due to inbreeding. As such, *Ifi44l* is a pseudogene in C57BL/6 mice, with the loss of IFI44L being stable, heritable and with no known negative effects. Indeed, the NCBI Reference Sequence Database (RefSeq) states that in C57BL/6 mice, the 5' region of this gene, including the translational start codon and the first 293 amino acids, is absent from the genome, and this has been experimentally confirmed (23, 48). However, other inbred mouse strains, such as BALB mice, retain *Ifi44l*.

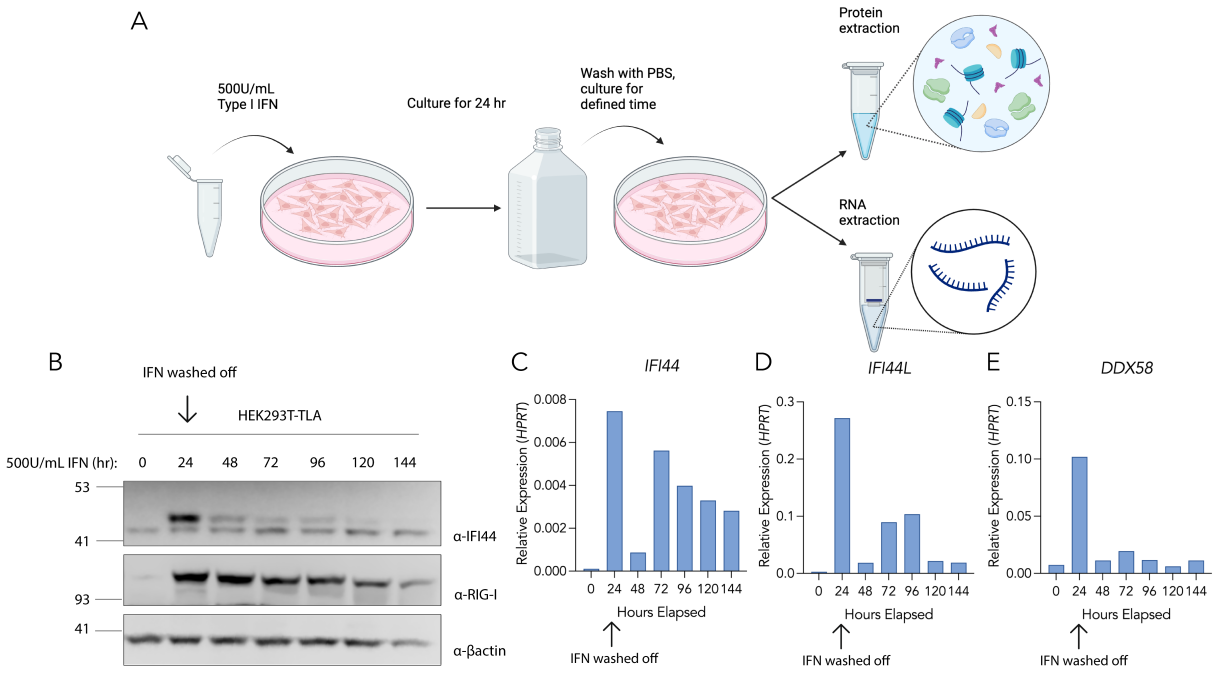


Figure 3.4: *IFI44* and *IFI44L* expression gradually decreases after interferon stimulation is removed.

A. Schematic of experimental procedure. **B.** HEK293T cells were stimulated with 500U/mL of IFN a/D. At 24 hr, media containing IFN was removed, cells were washed with PBS and fresh media added. Cells were then cultured for a further 24 hr, 48 hr, 72 hr, 96 hr or 120 hr, after which cells were lysed. Protein expression of IFI44 and RIG-I was detected through western blot using antibodies detecting endogenous proteins. **C-E.** Cells were lysed in buffer RLT and RNA extracted with the RNeasy QIAgen kit. RT-qPCR was performed for the indicated genes. Results shown are representative of three separate biological repeats, and results in C-E are the average of technical duplicates.

I confirmed these findings through PCR amplification of murine *Ifi44l*: the gene was not amplified from C57BL/6N mice nor CD1 outbred mice, but was amplified from BALB.C mice (Figure 3.5C). Interestingly, in BALB.B mice with a functional *Ifi44l* gene, the protein is the precursor to HA-28 minor histocompatibility antigen and immunising C57BL/6 mice with BALB.B splenocytes elicits a cytotoxic T cell response, which is attributed to the HA-28 antigen (48).

To discover the phenotypic effect of a total loss of the *Ifi44(l)* genes in a mammal, a knock-out mouse model on a C57BL/6N background was designed and validated by Jan Rehwinkel, Anne Bridgeman and Rachel Rigby and created by the company Cyagen, using CRISPR-Cas9 genome editing. As C57BL/6N mice naturally lack *Ifi44l*, there will not be any redundancy effects between the two proteins. In the knock-out model, exons one to five were removed, consisting of a total of 10372 base pairs (Figure 3.5D, E). *Ifi44*$^{-/-}$ mice were born, fertile and bred at expected Mendelian ratios (Figure 3.5F). They displayed no

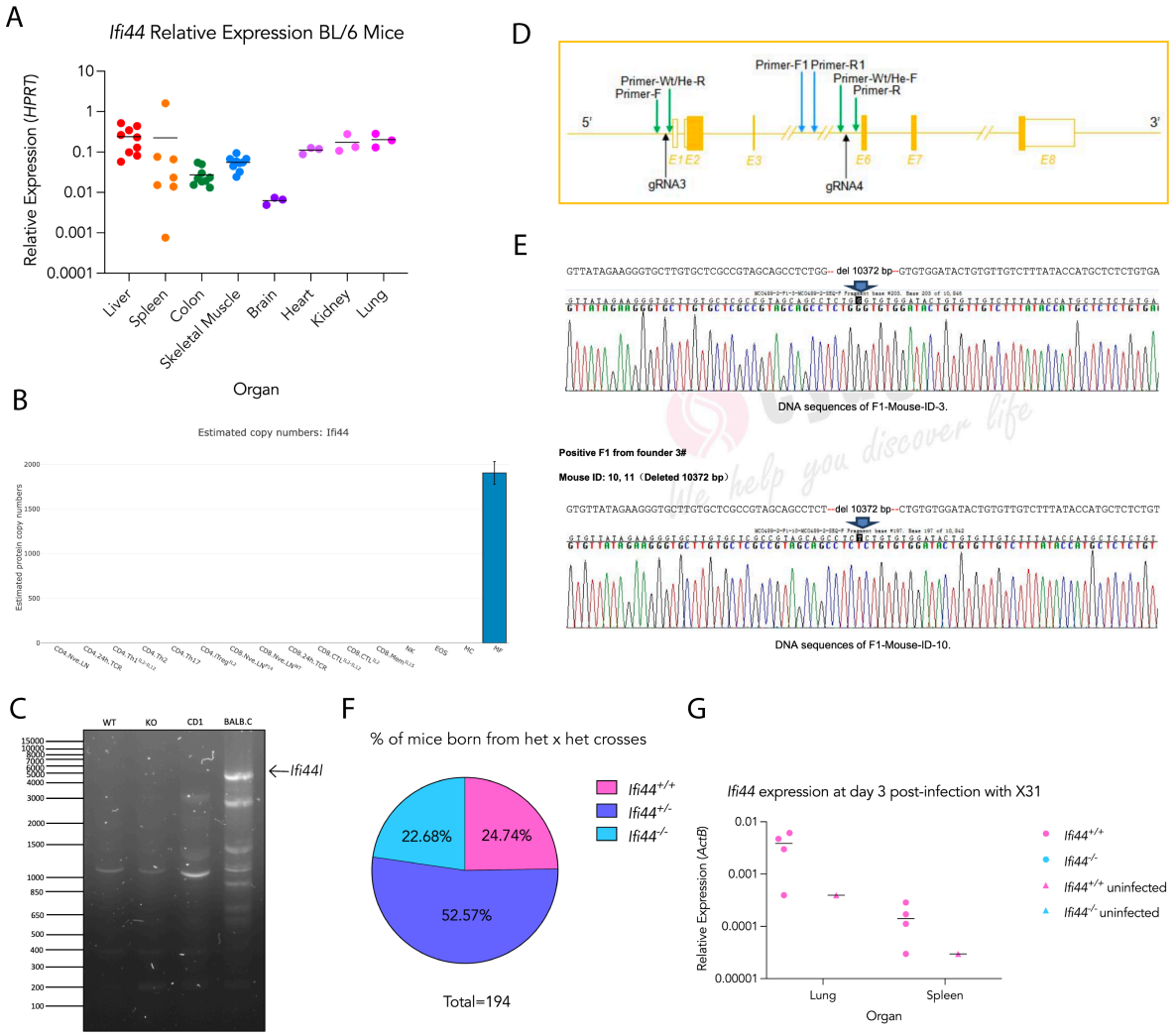


Figure 3.5: Generation of an *Ifi44*$^{-/-}$ mouse on a C57BL/6N background, which naturally lack *Ifi44l*.

Organs were harvested from C57BL/6N mice, homogenised in TRIzol reagent, RNA extracted through phenol-chloroform seperation and RT-qPCR performed for murine *Ifi44*. **B.** IFI44 protein expression across different cell types in a C57BL/6J mouse from the ImmPRes database (33). **C.** Genomic DNA was extracted from murine ear clips, and *Ifi44l* amplified using PCR. The resulting PCR product was approximately 5,000 base pairs. **D.** CRISPR-Cas9 targeting technique of murine *Ifi44*. **E.** Confirmed knock-out of *Ifi44*$^{-/-}$ founder mice through DNA sequencing, provided by Cyagen. **F.** Genotype outcomes from *Ifi44*$^{+/-}$ x *Ifi44*$^{+/-}$ breedings; percentages indicated from 194 mice. **G.** Mice were infected intranasally with 0.04 HAU Influenza A/H3N2 virus (or PBS) and sacrificed on day 3. Organs were homogenised in TRIzol reagent, RNA extracted and RT-qPCR performed for murine *Ifi44*. (A and G) each data point represents one biological replicate and is the average of two technical replicates. Unmarked datapoints were undetectable. (C) data is indicative of two repeats.

obvious outward phenotype – being indistinguishable from *Ifi44*$^{+/+}$ mice during standard husbandry and natural breeding. I confirmed the knock-out of *Ifi44* through RT-qPCR using lung and spleen samples from uninfected mice and mice infected with 0.04 HAU of influenza A/X-31 (H3N2) virus. While *Ifi44*$^{+/+}$ mice expressed *Ifi44* both at baseline, and induced *Ifi44* to higher levels upon infection, *Ifi44*$^{-/-}$ mice did not express *Ifi44* in either setting, in fact, transcript level *Ifi44* was undetectable (Figure 3.5G).

3.3 IFI44 does not have antiproliferative activity *in vitro*, *in vivo* or *ex vivo*

The antiproliferative activity of type I IFN is well documented (49, 50). In addition, some papers have demonstrated that IFI44 displays direct antiproliferative activity (1, 23). RNA sequencing on bulk splenic RNA from I*fi44*$^{+/+}$ and *Ifi44*$^{-/-}$ mice revealed that a subset of genes in the cell cycle gene ontology category (GO:0007049) were significantly downregulated in *Ifi44*$^{-/-}$ spleens (Figure 3.6A). Further, while this gene ontology category was not shared in genes downregulated in *Ifi44*$^{-/-}$ livers, there were a subset genes downregulated in both the liver and the spleen involved in cell cycle control (Figure S6). Thus, this phenotype may not be restricted to murine spleens. This led me to hypothesise that *Ifi44* plays a role in the cell cycle. As such, I went on to determine cellular proliferation rates between *Ifi44*$^{+/+}$ and *Ifi44*$^{-/-}$ mouse embryonic fibroblasts (MEFs); however no difference was seen between the two genotypes (Figure 3.6B). As the RNA sequencing phenotype came from bulk splenic RNA, MEFs might not have been the most appropriate model to study cellular proliferation. As such, I isolated murine splenocytes in order to determine more nuanced differences in cell cycle phasing using flow cytometry. However, no differences in cell cycle phasing was observed between *Ifi44*$^{+/+}$ and *Ifi44*$^{-/-}$ splenocytes (Figure 3.6C). Therefore, the transcript level differences in cell cycle-related genes in *Ifi44*$^{-/-}$ splenocytes did not translate to differences in cell cycle phasing in splenocytes, nor cellular proliferation differences in MEFs. It is possible that the transcriptional reduction in cell cycle-related genes in *Ifi44*$^{-/-}$ splenocytes arose from a small splenic subpopulation of cells. As such, gating on specific splenic cellular populations in turn might allow for the detection of cell cycle differences using flow cytometry. In sum, whether these transcriptional differences exert a biological effect remains to be seen.

To uncover whether IFI44 or IFI44L exert antiproliferative activity in human cells, I first cloned human *IFI44* and *IFI44L* into pCR®8/GW/TOPO® entry vectors, and then into pLenti6.3 destination vectors with a V5 tag on the C-terminus, using the Gateway® Cloning system (Figure 3.6D). From these, I created lentiviral stocks, and used these to stably overexpress IFI44 or IFI44L in HEK293T cells. Overexpression of IFI44 or IFI44L

through lentiviral transduction in HEK293T cells remained stable over the course of six passages (Figure 3.6E). In addition, there was no difference in cell cycle phasing between HEK293T cells transduced with green fluorescent protein (GFP), IFI44 or IFI44L, while parental HEK293T cells had slightly more cells in G1 phase, and slightly less cells in S and G2 phase, indicating that lentiviral transduction affects cell cycle phasing (Figure 3.6F). Therefore, in HEK293T cells, overexpression of IFI44 or IFI44L did not affect cellular proliferation rates, and while IFI44 has had documented antiproliferative activity elsewhere, I did not confirm this experimentally.

3.4 Localisation of IFI44 and IFI44L

The localisation of IFI44 is disputed, with conflicting evidence for cytosolic or nuclear localisation at baseline and after IFN induction/infection (1, 19, 25). In addition, as IFI44 was first discovered as microtubule-associated aggregates in hepatocytes of HCV infected chimpanzees (40), it is possible that IFI44 exists as aggregates; however this has not been experimentally confirmed. The localisation of IFI44L is listed on the UniProt web server as 'cytosolic', and this is cited by some papers; again, there does not seem to be experimental evidence confirming this.

One study used α-IFI44 rabbit serum in immunofluorescence experiments with human melanoma cell lines and found that IFI44 localises in the nuclei of unstimulated cells, but moves to the cytoplasm after IFN-α treatment (1). However, this could not be confirmed by the same authors through cellular fractionation. Indeed, there was no evidence that a control was used to confirm that the antibody used in immunofluorescence was specific. When these authors overexpressed IFI44 in human melanoma cell lines, they documented a diffuse cytoplasmic fluorescence, which differed from a typical microtubule staining pattern. A separate study reported the opposite, namely that IFI44 exists in the cytoplasm at baseline, but localises to nuclei of cells during HIV-1 infection of HEK293T cells stably overexpressing IFI44-HA (19). This was confirmed through cellular fractionation, immunostaining and IFI44 binding the HIV-1 LTR in the nucleus (tested with ChIP-PCR). Confirming both cytosolic and nuclear presence of IFI44, another study used A549 cells transiently transfected with IFI44-HA and concluded that poly(I:C), IFN-α and IAV treatment have no effect on the cellular localisation of IFI44 (25).

Given these inconsistencies, I sought to analyse where IFI44 and IFI44L are localised in HEK293T cells stably overexpressing IFI44-V5 through lentiviral transduction, and whether this was affected by IFN treatment or infection. I opted to use an overexpression system with V5 tagged proteins as the IFI44 antibody detecting endogenous protein displayed a strong cross-reactivity with a protein running at ca. 90 KDa in western blot,

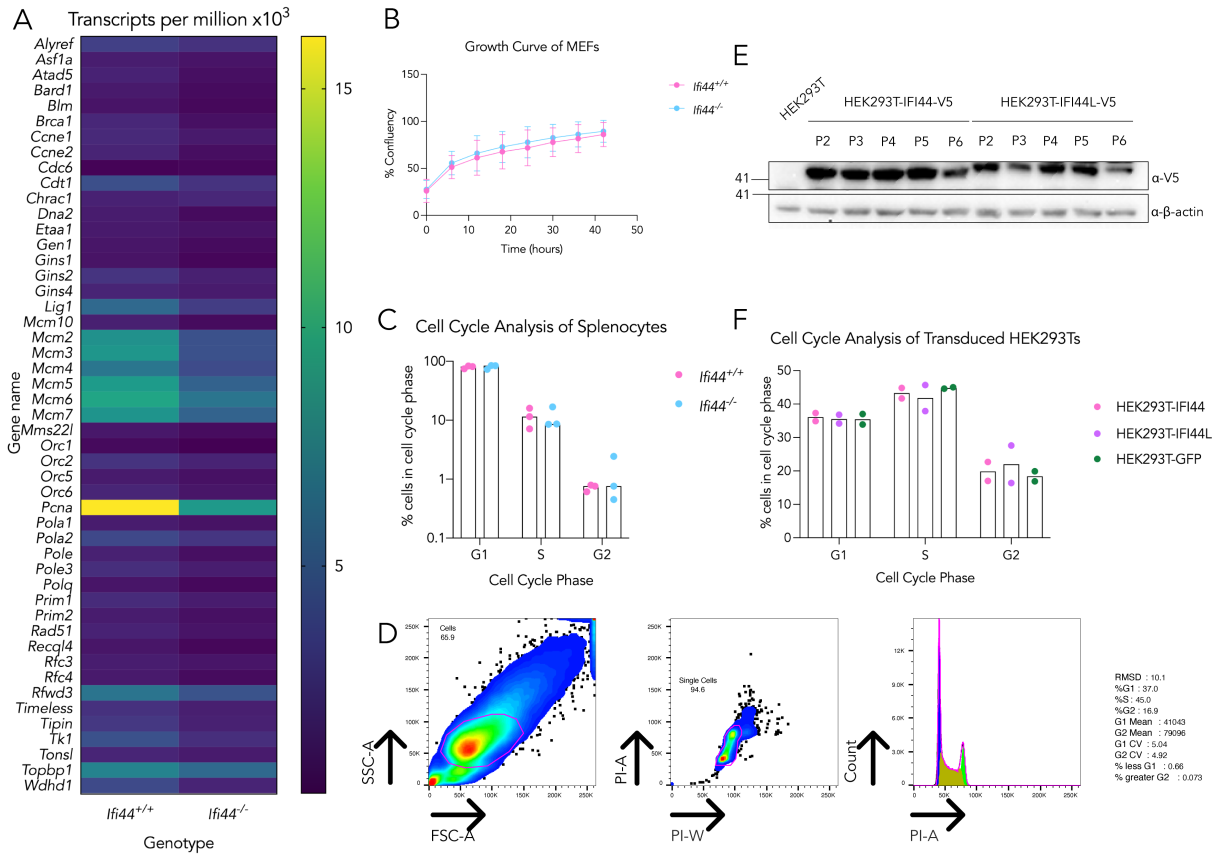


Figure 3.6: IFI44 and IFI44L are not antiproliferative in mouse splenocytes or HEK293T cells. **A.** TPM-normalized expression of genes differentially expressed in *Ifi44*$^{-/-}$ spleens in the GO category 'cell cycle' (GO:0007049)(adj. p-value < 0.05). Differential gene expression was assessed with DESeq2 (70). Analysis performed by Rachel Rigby. **B.** Growth curve of mouse embryonic fibroblasts (MEFs) from 0 hours to 48 hours determined with an Incucyte live cell imager. **C.** Murine splenocytes (derived from enzymatic digestion) or **F.** stably transduced and selected HEK293T cells were fixed with ice-cold ethanol and stained with propidium iodide. Cell cycle flow cytometry was performed on an Attune flow cytometer. **D.** Gating strategy for cell cycle flow cytometry. **E.** Stably transduced HEK293T cells were selected with blasticidin and cultured for 6 passages. Sample were collected at each passage and lysed in RIPA buffer. Protein expression of IFI44 and IFI44L were detected through western blot using α-V5 antibody. (A) Data shown is the average of four biological replicates. (B) Representative data of three independent repeats. (C) Each data point represents one biological replicate. (E) Data shown is one independent repeat, however during the course of my PhD, many western blots were performed using cells transduced with this same lentiviral stock at various passages, and strong signal was consistently seen. (F) Each data point is one biological replicate from independent repeats.

and therefore is likely inappropriate for use in immunofluorescence (Figure 3.7A). Moreover, I found commercially available α-IFI44L antibodies to be non-specific in western blot (data not shown). Stable overexpression of IFI44-V5 and IFI44L-V5 was confirmed

by western blot (Figure 3.7B) and confocal imaging with an AF488-tagged V5 antibody revealed that IFI44-V5 and IFI44L-V5 are localised in both the nuclei and cytoplasm of cells (Figure 3.7C). However, this is not conclusive data as there was some background V5 antibody staining in the non-transduced control, and although this was much weaker, it cannot be ruled out as contributing to the staining seen in the overexpressing cell lines. Tubulin was also stained for to show the distribution of cytoskeletal elements, and to determine whether these co-localised with IFI44/L. As IFI44/L and Tubulin all showed diffuse staining, it cannot be said whether IFI44/L are specifically co-localising to microtubule elements in this setting. As such, I was unable to conclusively determine the subcellular localisation of IFI44 and IFI44L.

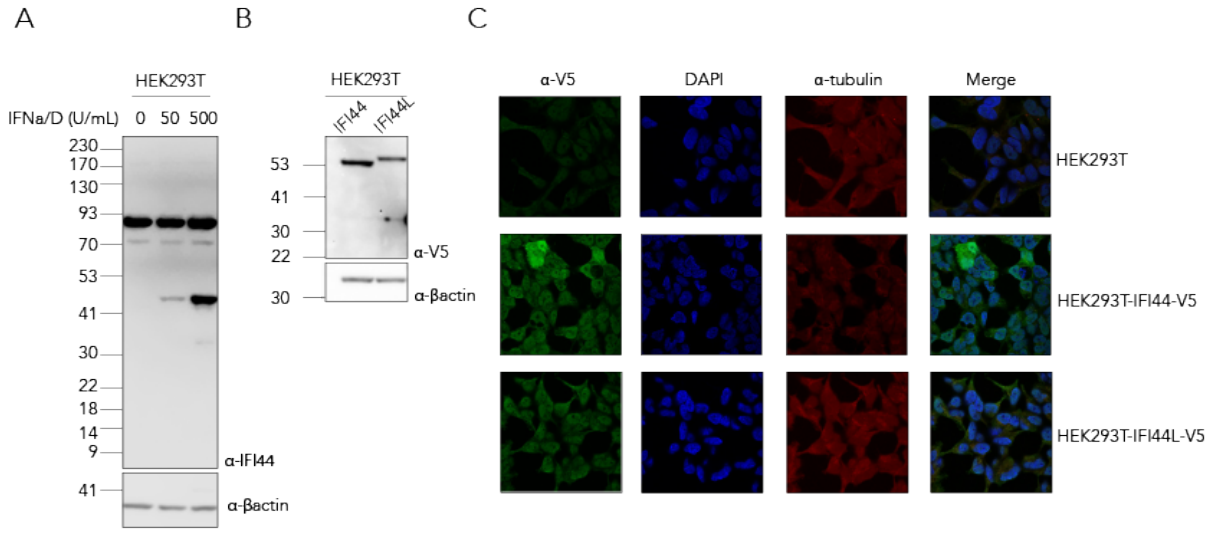


Figure 3.7: The sub-cellular localisation of IFI44 and IFI44L is non-conclusive.

A. HEK293T cells were stimulated with 0 U/mL, 50 U/mL or 500 U/mL of recombinant universal type I IFN (IFN a/D) for 24 hours or **B.** Stably transduced and selected HEK293T cells expressing either V5 tagged IFI44 or V5 tagged IFI44L. Cells were lysed in RIPA buffer and protein expression of IFI44 was detected by western blot using (A) an antibody detecting endogenous protein - the specific band for IFI44 was at 50KDa, whereas nonspecific staining was detected around 90KDa - or (B) V5 antibody. **C.** Cells were cultured in Ibidi imaging chambers, fixed and stained with anti-V5 AF488 conjugated antibody and anti-tubulin AF647 conjugated antibody. Mounting media containing DAPI was used. Images were taken on a Zeiss LSM 780 inverted confocal microscope. (A) Representative data from three biological repeats. (B,C) Representative data from two independent repeats.

3.5 Functionality of the TLDc Domain in IFI44 and IFI44L

IFI44 and IFI44L both contain a TLDc domain, and while this is phylogenetically distant from other TLDc family members at the amino acid sequence level, there is structural

conservation of TLDc domains within the family (Figure 1.9). The functionality of the TLDc domain present in IFI44 and IFI44L has never been experimentally tested. As presence of the TLDc domain in other proteins provides protection against oxidative stress (51, 52), I sought to test whether IFI44/L were protective against oxidative-stress induced cell death. Oxidative stress was induced in *Ifi44*$^{+/+}$ and *Ifi44*$^{-/-}$ MEFs or HEK293T cells transiently transfected with IFI44 or IFI44L through addition of increasing concentrations of hydrogen peroxide (H_2O_2), and cell viability was measured with the Cell-Titre Glo assay that detects ATP as a surrogate of cell viability. Neither knock-out of *Ifi44* in MEFs (with or without IFN stimulation) nor overexpression of IFI44/L in HEK293T cells provided any protection from H_2O_2-induced cell death (Figure 3.8A, B). One could hypothesise that no difference was seen due to cell death as an experimental endpoint not being an appropriate read-out, and perhaps another read-out should be used. However, one study demonstrated that TLDc-domain containing proteins were protective against oxidative stress-induced cell death in neuronal cells, through using microscopy to count the number of cells with pyknotic nuclei as a measurement of cell death (53). In this setting, oxidative stress was induced with sodium arsenite ($NaAsO_2$). As such, I repeated the experiment using $NaAsO_2$ to induce oxidative stress and cell death. Interestingly, IFN stimulation of *Ifi44*$^{+/+}$ MEFs provided resistance to $NaAsO_2$-induced cell death when compared to baseline, and *Ifi44*$^{-/-}$ MEFs were protected both with and without IFN stimulation (Figure 3.8C). Despite this, there was no difference in cell death resulting from $NaAsO_2$ in human cells overexpressing IFI44/L (Figure 3.8D). The protection observed in *Ifi44*$^{-/-}$ MEFs could be attributed to the fact that *Ifi44*$^{-/-}$ MEFs have a slight IFN signature, as discussed in section 4.1. While this is an exciting finding, one cannot attribute this phenotype to *Ifi44* alone, as any number of ISGs could be responsible for the protection seen, and human cells overexpressing IFI44 did not reproduce this phenotype.

To take a different approach, I tested whether ROS levels in *Ifi44*$^{+/+}$ and *Ifi44*$^{-/-}$ MEFs at baseline were different, to discover whether *Ifi44* mediates a basal protective effect against ROS. To answer this, I performed a ROS-Glo assay after pretreatment with IFN a/D, however no difference was seen in basal ROS levels between IFN-treated or untreated primary or immortalised MEFs (Figure 3.8E).

TLDc domain-containing proteins have also been shown to be a family of V-ATPase interactors, which is likely one mechanism whereby they mediate their molecular functions (54-59). The V-ATPase is a multisubunit complex that contains two domains: an ATP hydrolysis domain (V_1) and a transmembrane proton-pumping pore domain (V_0). In mammals, the V_1 domain is composed of eight subunits (A-H), while the V_0 domain is composed of six different subunits. The V-ATPase B2 subunit is ubiquitously expressed, with cells of the monocyte lineage expressing it in intracellular compartments and on

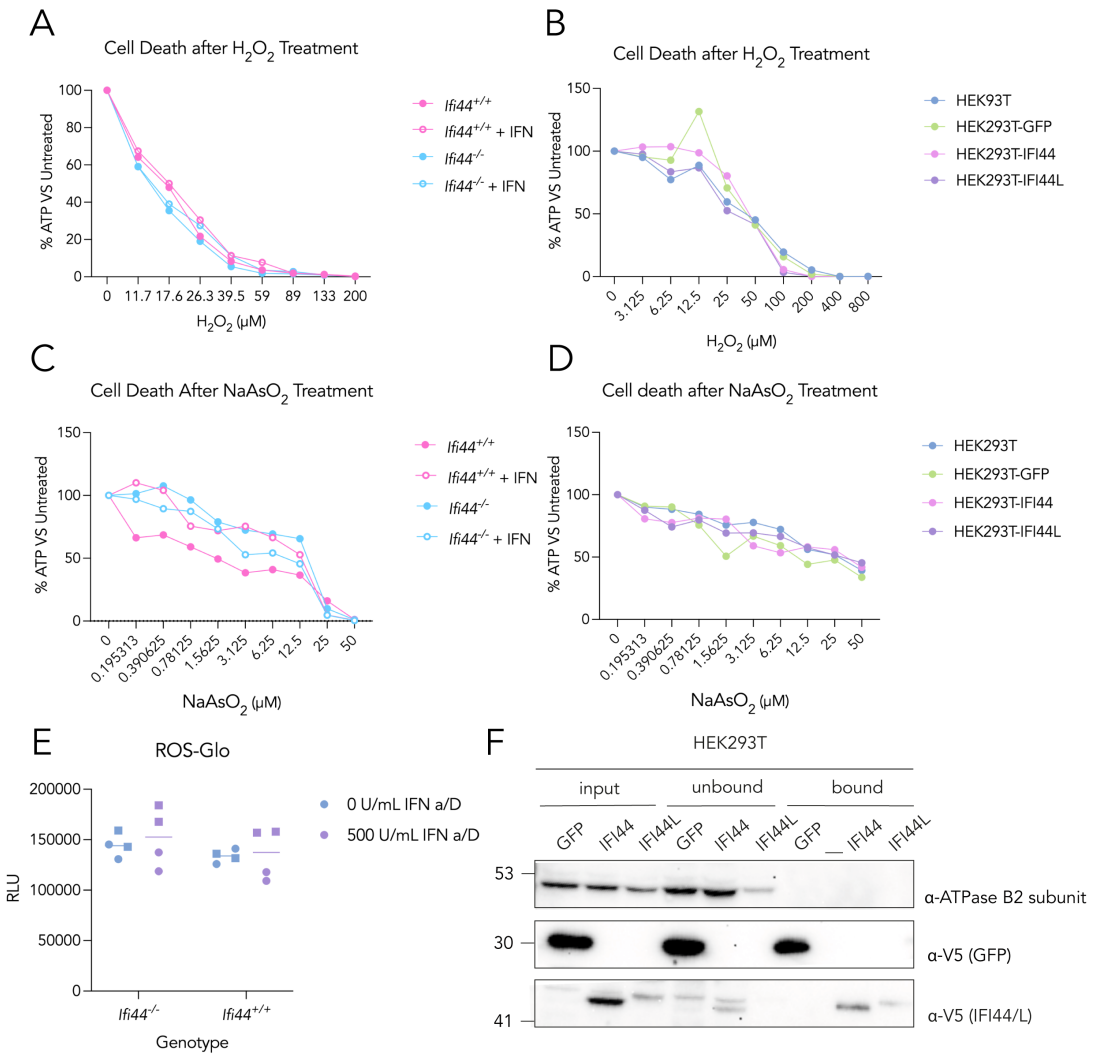


Figure 3.8: The TLDc domain of IFI44 and IFI44L does not protect against hydrogen peroxide- or arsenic- induced cell death, nor does it bind to any tested V-ATPase subunit.

A. *Ifi44*$^{+/+}$ and *Ifi44*$^{-/-}$ immortalised or **C.** primary MEFs were pre-treated with 0 U/mL or 500 U/mL IFN a/D for 24 hours or **B, D** HEK293T cells stably overexpressing GFP, IFI44 or IFI44L were treated with the indicated concentrations of hydrogen peroxide (A, B) or sodium arsenite (C, D). Cell viability was measured using the Cell Titre Glo kit - percentage of ATP as a proxy for cell viability when compared with the untreated control. **E.** *Ifi44*$^{+/+}$ and *Ifi44*$^{-/-}$ MEFs were pre-treated with 0 U/mL or 500 U/mL IFN a/D for 24 hours, and baseline ROS levels measured through a ROS-Glo kit. **F.** Stably overexpressing HEK293T cells were lysed with RIPA buffer and binding partners isolated through V5 pull-down. Immunoblotting was performed with an α-ATPase B2 subunit antibody. (A, E) Each data point is one biological replicate and the average of three technical replicates. Data shown is representative of three independent repeats. (B, C) Representative data of two or (D) three independent repeats. Each data point is the average of three technical replicates. (F) Data indicative of one repeat.

plasma membranes (60). To test whether the TLDc domain of IFI44/L can interact with the cellular V-ATPase, I performed an immunoprecipitation (IP) assay using lysates from HEK293T cells stably overexpressing GFP-V5, IFI44-V5 or IFI44L-V5. I used V5-conjugated magnetic beads to isolate these V5-tagged proteins along with their binding partners. I then immunoblotted for the V-ATPase B2 subunit, as it is ubiquitously expressed, and because other TLDc domain-containing proteins have been shown to bind to it (54). However, while the V-ATPase B2 subunit was clearly detected in the input and unbound fractions, no signal was detectable in the bound fraction, suggesting it does not interact with IFI44/L in this setting – although this experiment has only been performed once (Figure 3.8F). I went on to test whether IFI44/L interact with the lysosomal V-ATPase subunit, however the data were inconclusive as there was no specific band detected in western blot with this antibody (data not shown). Therefore, I cannot rule out that IFI44/L interact with the cellular V-ATPase as there are many different subunits that remain to be tested, and under other conditions. For example, perhaps the V5 tag on the C-terminus of IFI44 disrupted the true interaction of these proteins with the V-ATPase (although the TLDc domain of IFI44/L is closer to the N-terminus), or perhaps IFI44/L specifically interact with the lysosomal subunit of the V-ATPase. In sum, in these settings and under the conditions I used, I could not demonstrate a function of the TLDc domain of IFI44/L.

3.6 Binding Partners of IFI44 and IFI44L

Uncovering the binding partners of IFI44 and IFI44L may provide insight into the molecular pathways IFI44/L are acting in and generate novel hypotheses relating to their molecular functionality. As such, I aimed to isolate interacting partners of IFI44 or IFI44L through IP. For this, I utilised HEK293T cells transiently transfected with IFI44-V5, IFI44L-V5 or GFP-V5 (as a negative control) and performed an IP assay with V5-conjugated Dynabeads (Figure 3.9A). IP fractions were analysed by immunoblotting and silver nitrate staining. Initially, I used a gentle lysis buffer containing 20 mM TRIS-HCl, 100 mM NaCl, 1 mM EDTA and 0.5% NP-40, such that weak bonds between proteins remain intact. In addition, as IFI44 and IFI44L are ISGs, it is possible that their binding partners are also ISGs. As such, I pretreated some cells with 500 U/mL IFN a/D for 19 hours before lysis. The results demonstrated that IFI44 and IFI44L were successfully enriched in the bound fractions (although were not detectable in the input samples) (Figure 3.9B), and many proteins co-precipitated with both IFI44 and IFI44L in the presence and absence of IFN, but not with GFP (Figure 3.9C; Figure S7A). However, these bands were not consistently detected in all repeats (Figure S7B) and the bands that were detected differed between repeats (Figure 3.9C; Figure S7A). I hypothesised that the gentle lysis

buffer was resulting in the co-precipitation of proteins that may weakly or transiently interact with IFI44/L, and not strong, stable binding partners. In addition, this lysis buffer only allows the isolation of cytosolic binding partners (as nuclei remain intact and are spun out), but as there is some evidence that IFI44 localises to the nucleus (1, 19, 25), important binding partners may be present here. As such, I repeated the IP using RIPA buffer. The results showed that again IFI44 and IFI44L were successfully enriched in the bound fraction, and the binding partners that coprecipitated remained consistent over three independent experimental repeats (Figure 3.9D, E). I prepared samples from the RIPA-lysis bound fraction of IFI44-V5, IFI44L-V5 and GFP-V5 (all with and without IFN pretreatment) for mass spectrometry in collaboration with Adan Pinto Fernandez. Mass spectrometry was subsequently carried out by Iolanda Vendrell, Roman Fischer and Benedikt Kessler at the Target Discovery Institute. The data were analysed by Adan Pinto Fernandez. The data for IFI44L was very 'noisy', such that no hits were present above the stringent confidence limit threshold. As such, we continued only with IFI44, with and without IFN pretreatment (Figure 3.10A). GFP IP samples were used as a comparison to remove nonspecific interactors, and a number of hits were identified as specific interactors with IFI44: some were detected only after IFN treatment, some only in the absence of IFN treatment, and some hits were found in both conditions (Figure 3.10B, C, D).

We found some interesting interactors with IFI44, which I carefully analysed (Figure 3.10B). SET interacts with IFI44 with and without IFN treatment. SET is a protein involved in apoptosis and nucleosome assembly: in the course of cytotoxic T-lymphocyte-induced apoptosis, granzyme-A cleaves SET, disrupting its binding to NME1 and releasing NME1 inhibition (61). Interestingly, *Gzma* was found to be significantly downregulated in *Ifi44*$^{-/-}$ mice (data not shown). Drebrin was also found to interact with IFI44 with and without IFN and is an actin cytoskeleton-organising protein with roles at immunological synapses (62). This is interesting, given that IFI44 was first discovered as microtubule-associated aggregates and is thought to be involved in anti-viral immunity (23, 40). ADP/ATP translocase 2 (SLC25A5; ANT2) was found to interact with IFI44 in the presence of IFN and is a gated pore which translocates ADP/ATP between the cytoplasm and the mitochondria (63), implicated in macrophage activation and adipocyte hypoxia during obesity (64-66). It has recently been identified as the only known transporter of RNAs across the mitochondrial membrane (67). HSP70 (heat shock protein family A) also interacted with IFI44 in the presence of IFN, a molecular chaperone which is expressed in response to stress (68). While all these findings are very interesting, there are no significant gene ontology between these top hits, and moreover, no obvious molecular pathway in which they are all acting. Aside from Drebrin, there are no obvious links to what is currently known about IFI44, and the data for IFI44 being a cytoskeletal protein is likely

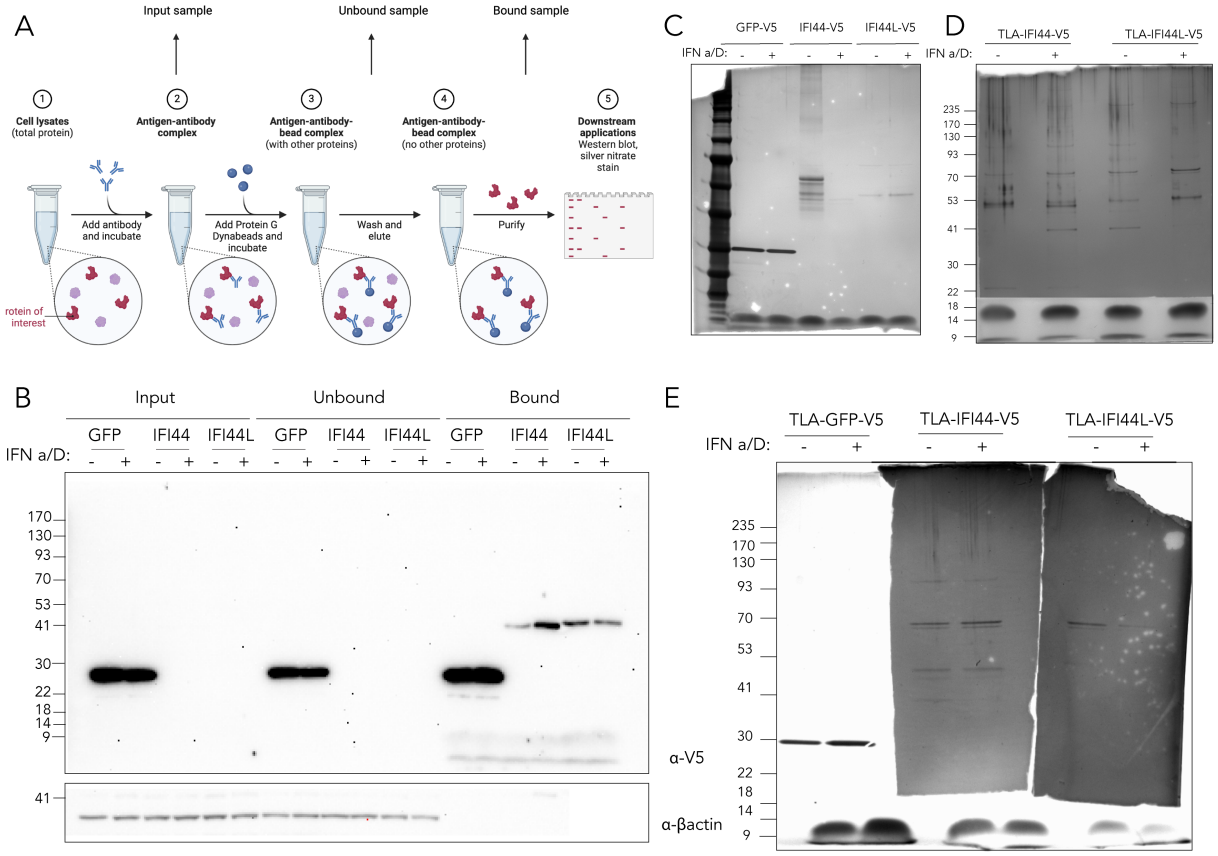


Figure 3.9: Immunoprecipitation of IFI44 and IFI44L and silver nitrate staining reveals multiple binding partners.

A. Schematic of experimental procedure. HEK293T cells transiently transfected with IFI44, IFI44L or GFP were stimulated with 500 U/mL IFN a/D or not for 19 hours and then lysed and incubated with protein G Dynabeads conjugated to V5 antibody. Input, unbound and bound fractions were collected for downstream processing. **B.** Representative western blot validating the IP. For each silver nitrate gel stain, a western blot was performed in parallel, validating the IP. **C.** Silver nitrate staining in IPs from cells lysed with a gentle NP40 lysis buffer. **D.** and **E.** Silver nitrate staining in two separate repeats in which cells were lysed with RIPA buffer. (C) One blot shown from three independent repeats. Other blots can be seen in Figure S4. (D, E) two representative blots from three total independent repeats.

circumstantial (40). As such, validation of these hits and follow-up experiments were deprioritised in favour of focusing on the novel haematological phenotype I discovered for IFI44 (see Chapter 5).

I was curious as to whether IFI44 and IFI44L were able to interact with each other, as even though IFI44L did not appear as a mass spectrometry hit for IFI44, this could be due to the stringent filtering and threshold application. In addition, we wondered whether endogenous IFI44 interacted with V5-tagged IFI44, as the silver nitrate stain showed protein bands at the correct size marker for IFI44 in the presence of IFN (Figure 3.9D, E). To

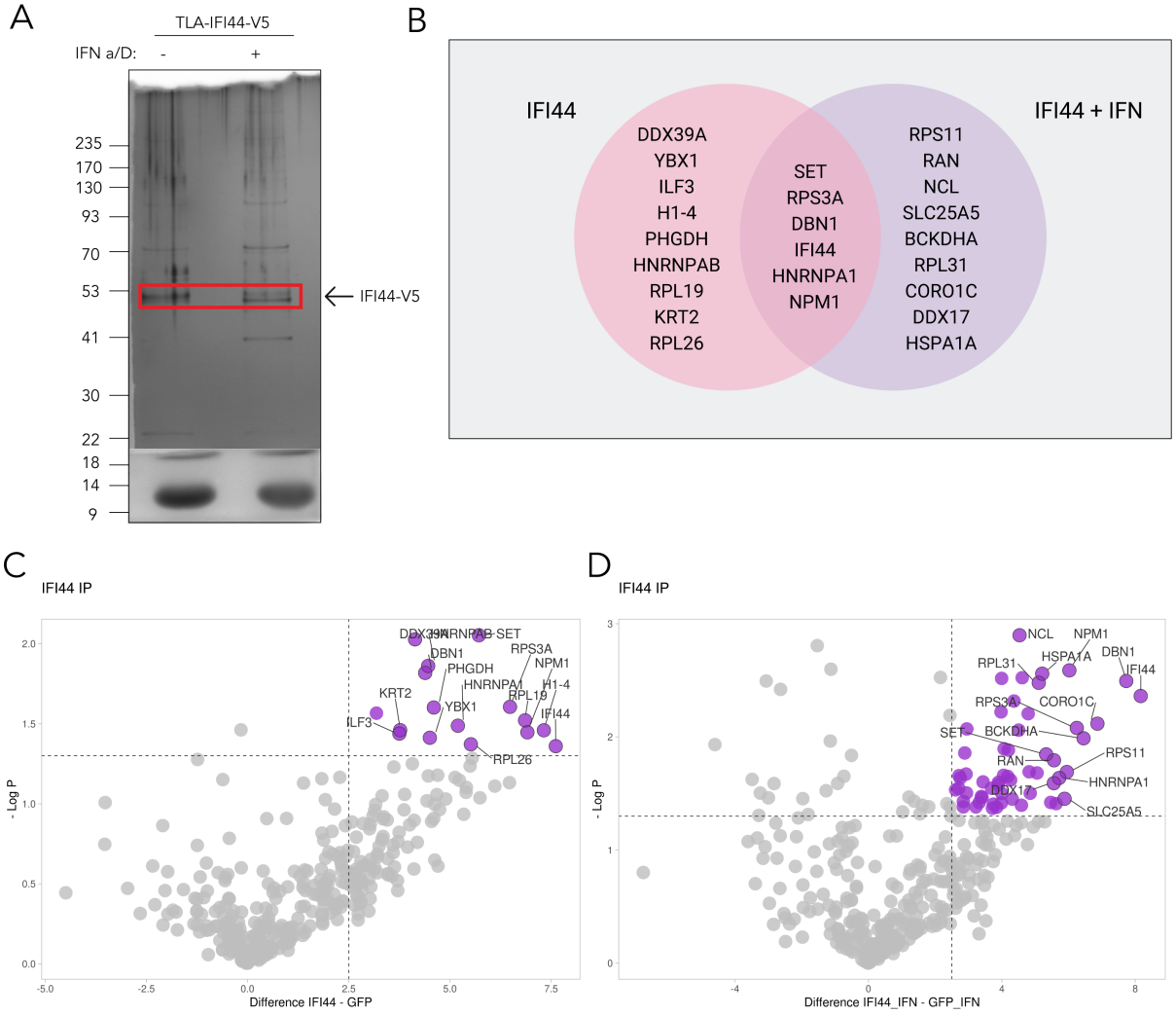


Figure 3.10: Binding partners of IFI44.

A. HEK293T cells transiently transfected with IFI44 were stimulated with 500 U/mL IFN a/D or not for 19 hours and then lysed and incubated with protein G Dynabeads conjugated to V5 antibody. Half of the bound fraction was run on a gel and stained with silver nitrate to visualise the interaction partners, while the other half of the sample was used in mass spectrometry. **B.** Binding partners of IFI44 in HEK293T cells with or without IFN treatment as determined by mass spectrometry. **C.** Mass spectrometry hits of unstimulated HEK293T-IFI44 cells, compared with HEK293T-GFP cells. **D.** Mass spectrometry hits of IFN-stimulated HEK293T cells overexpressing IFI44, compared with IFN-stimulated HEK293T cells overexpressing GFP. (A) is representative of three independent repeats, all of which were used in mass spectrometry in (B), (C) and (D).

test whether IFI44 and IFI44L interact *in cellulo*, and whether IFI44 interacts with itself, a master's student under my supervision, Isobel Davis, generated pcDNA3.2 constructs with either V5- or FLAG- tagged IFI44 or IFI44L using the Gateway cloning system and my entry vectors. In the first instance, Isobel tested the interaction of IFI44 with itself

by transfecting IFI44-V5 and IFI44-FLAG into HEK293T cells, performing an IP using anti-V5-antibody conjugated Dynabeads and immunoblotting for both V5 and FLAG. A clear V5 signal was enriched in the bound fraction, and FLAG signal was detected in both the input and unbound fractions; however no FLAG signal was seen in the bound fraction, indicating IFI44 did not interact detectably with itself in this setting (Figure 3.11A). Isobel also tested whether IFI44L could interact with itself, however these experiments were inconclusive as the V5 antibody did not provide any signal in western blot in two independent repeats (data not shown). To determine whether IFI44 and IFI44L interact, I took a similar approach: I transfected FLAG-tagged IFI44L and V5-tagged IFI44 into HEK293T cells, performed an IP using anti-FLAG-antibody conjugated Dynabeads and immunoblotted for FLAG and IFI44. As expected, FLAG signal was detected in the input, depleted in the unbound and enriched in the bound fractions (Figure 3.11B). IFI44 signal was detected in the input and unbound fractions, and a weak signal was also detected in the doubly transfected condition (Figure 3.11B). This indicated that IFI44 and IFI44L interact, and I confirmed this in three independent repeats. Further, Isobel performed the same experiment but used anti-V5-antibody conjugated Dynabeads as opposed to anti-FLAG-conjugated Dynabeads. These data also suggest in three independent repeats that IFI44 and IFI44L interact (data not shown). Confirming this, I used AlphaFold 3 (69) to model IFI44-IFI44L interaction *in silico*. The predicted structure showed a perfect interaction surface between the two proteins (Figure 3.11C, D). As such, I conclude that IFI44 and IFI44L interact with each other; however, IFI44 does not interact with itself and whether IFI44L can interact with itself remains to be seen. This may be important for their function – one can postulate that IFI44 and IFI44L require heterodimerisation or heteromultimerisation in order to perform their molecular functions. Indeed, the size of the complex they form is another unknown.

3.7 Summary for Chapter 3

In this chapter, I confirmed and substantiated that *IFI44* and *IFI44L* are prototypical ISGs, expression of which are highly upregulated by IFN. Human IFI44 and IFI44L proteins interacted with each other, a discovery which could be of importance to their functionality. Interestingly, a total loss of the *Ifi44(l)* genes in C57BL/6 mice did not confer an overt phenotype in animal breeding, gene inheritance or normal activity. It is worth noting that since C57BL/6 mice naturally lack *Ifi44l*, the wild-type control can be considered *Ifi44l*$^{-/-}$, and as such discoveries in this model can only be attributed to *Ifi44*. IFI44/L have two conserved protein domains, a TLDc domain and a P Loop NTPase domain with predicted affinity for GTP. In other proteins, the TLDc domain confers protection against oxidative stress. However, I did not identify a role for the TLDc do-

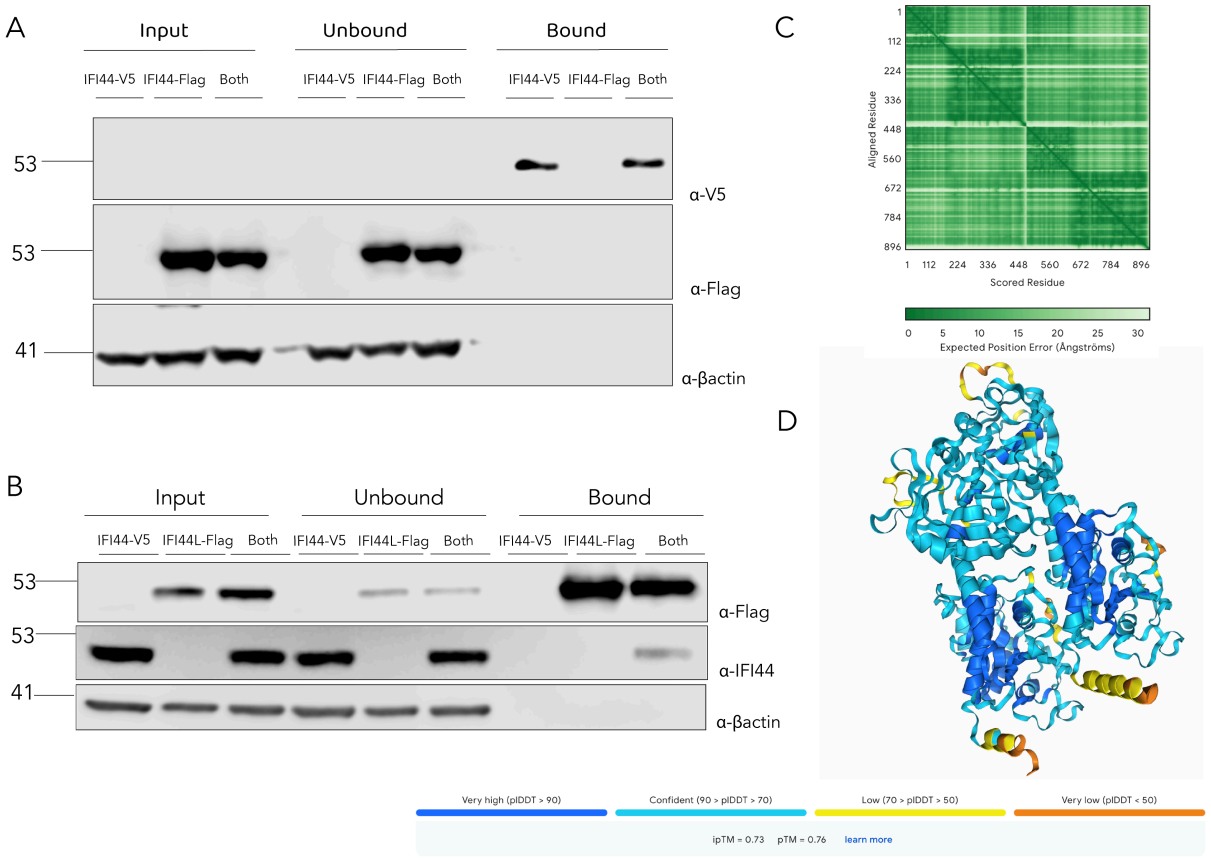


Figure 3.11: IFI44 and IFI44L interact.

A. HEK293T cells were transiently transfected with IFI44-V5, IFI44-FLAG or both and then lysed with RIPA buffer and incubated with protein G Dynabeads conjugated to V5 antibody. Input, unbound and bound fractions were collected, and analysed by immunoblotting with α-V5 and α-FLAG antibodies. **B.** HEK293T cells were transiently transfected with IFI44-V5, IFI44L-FLAG or both and then lysed with RIPA buffer and incubated with protein G Dynabeads conjugated to FLAG antibody. Input, unbound and bound fractions were collected, and analysed by immunoblotting with α-IFI44 and α-FLAG antibodies. **C.** Interaction matrix of IFI44 and IFI44L, as determined by AlphaFold 3 (69). **D.** Interaction schematic of IFI44 and IFI44L, as determined by AlphaFold 3 (69). (A) Representative blot of three independent repeats, although one of the repeats showed no V5 staining. (B) Representative blot of three independent repeats.

main of IFI44 protecting against oxidative stress in human cells overexpressing IFI44, nor enhanced susceptibility in *Ifi44*$^{-/-}$ MEFs. Further, I did not observe the TLDc domain of IFI44/L binding to the V-ATPase. In both of these settings, IFI44/L were singly expressed; perhaps overexpression of both in conjunction is necessary to observe functionality in these settings, since they interact. Binding partners of IFI44 were identified by mass spectrometry but did not provide many 'clues' as to the pathways in which this protein may be acting. In the following chapters, I explore other hypotheses as to the

cellular and molecular function of IFI44 and IFI44L.

References for Chapter 3

1. L. C. Hallen et al., Antiproliferative activity of the human IFN-alpha-inducible protein IFI44. J Interferon Cytokine Res 27, 675-680 (2007).
2. B. Feenstra et al., Common variants associated with general and MMR vaccine-related febrile seizures. Nat Genet 46, 1274-1282 (2014).
3. Y. Zeng et al., Comprehensive Analysis of Immune Implication and Prognostic Value of IFI44L in Non-Small Cell Lung Cancer. Frontiers in Oncology 11, (2022).
4. M. Salesi, M. H. Dehabadi, R. Salehi, A. Salehi, B. Pakzad, Differentially methylation of IFI44L gene promoter in Iranian patients with systemic lupus erythematosus and rheumatoid arthritis. Mol Biol Rep 49, 3065-3072 (2022).
5. S. Luo, R. Wu, Q. Li, G. Zhang, Epigenetic Regulation of IFI44L Expression in Monocytes Affects the Functions of Monocyte-Derived Dendritic Cells in Systemic Lupus Erythematosus. J Immunol Res 2022, 4053038 (2022).
6. S. Tian et al., *FAM89A* and *IFI44L* for distinguishing between viral and bacterial infections in children with febrile illness. Pediatr Investig 5, 195-202 (2021).
7. P. K. Yadalam et al., Gene Interaction Network Analysis Reveals IFI44L as a Drug Target in Rheumatoid Arthritis and Periodontitis. Molecules 27, (2022).
8. I. H. Haralambieva et al., Genome-wide associations of *CD46* and *IFI44L* genetic variants with neutralizing antibody response to measles vaccine. Human Genetics 136, 421-435 (2017).
9. Y. Wang et al., Identification and Clinical Correlation Analysis of *IFI44* in Systemic Lupus Erythematosus Combined with Bioinformatics and Immune Infiltration Analysis. J Inflamm Res 16, 3219-3231 (2023).
10. L. Shen et al., Identification and Validation of *IFI44* as Key Biomarker in Lupus Nephritis. Front Med (Lausanne) 8, 762848 (2021).
11. S. Liu, W. Ren, J. Yu, C. Li, S. Tang, Identification of Hub Genes Associated with Diabetes Mellitus and Tuberculosis Using Bioinformatic Analysis. Int J Gen Med 14, 4061-4072 (2021).
12. Y. Wang et al., Identification of *IFI44L* as a new candidate molecular marker for systemic lupus erythematosus. Clin Exp Rheumatol, (2022).
13. X. Zhao et al., Identification of key biomarkers and immune infiltration in systemic lupus erythematosus by integrated bioinformatics analysis. J Transl Med 19, 35 (2021).
14. M. Shen et al., Identification of key interferon-stimulated genes for indicating the condition of patients with systemic lupus erythematosus. Front Immunol 13, 962393 (2022).
15. Z. Dong, Q. Yan, W. Cao, Z. Liu, X. Wang, Identification of key molecules in COVID-19 patients significantly correlated with clinical outcomes by analyzing transcriptomic data. Front Immunol 13, 930866 (2022).

16. A. Reyimu et al., Identification of latent biomarkers in connection with progression and prognosis in oral cancer by comprehensive bioinformatics analysis. World J Surg Oncol 19, 240 (2021).
17. L. Li, Y. A. Ni, Z. Song, Z. Yi, F. Wang, Identification of pathogenic genes and transcription factors in respiratory syncytial virus. BMC Pediatr 21, 27 (2021).
18. Q. Zheng, D. Wang, R. Lin, Q. Lv, W. Wang, *IFI44* is an immune evasion biomarker for SARS-CoV-2 and *Staphylococcus aureus* infection in patients with RA. Front Immunol 13, 1013322 (2022).
19. D. Power et al., IFI44 suppresses HIV-1 LTR promoter activity and facilitates its latency. Virology 481, 142-150 (2015).
20. Y. Li et al., IFI44L expression is regulated by IRF-1 and HIV-1. FEBS Open Bio 11, 105-113 (2021).
21. W.-C. Huang, S.-L. Tung, Y.-L. Chen, P.-M. Chen, P.-Y. Chu, IFI44L is a novel tumor suppressor in human hepatocellular carcinoma affecting cancer stemness, metastasis, and drug resistance via regulating met/Src signaling pathway. BMC Cancer 18, 609-609 (2018).
22. M. Zhao et al., *IFI44L* promoter methylation as a blood biomarker for systemic lupus erythematosus. Ann Rheum Dis 75, 1998-2006 (2016).
23. D. C. Busse et al., Interferon-Induced Protein 44 and Interferon-Induced Protein 44-Like Restrict Replication of Respiratory Syncytial Virus. J Virol 94, (2020).
24. H. Pan et al., Interferon-Induced Protein 44 Correlated With Immune Infiltration Serves as a Potential Prognostic Indicator in Head and Neck Squamous Cell Carcinoma. Front Oncol 10, 557157 (2020).
25. M. L. DeDiego, A. Nogales, L. Martinez-Sobrido, D. J. Topham, Interferon-Induced Protein 44 Interacts with Cellular FK506-Binding Protein 5, Negatively Regulates Host Antiviral Responses, and Supports Virus Replication. mBio 10, (2019).
26. X. Qu et al., Potential roles of IFI44 genes in high resistance to Vibrio in hybrids of Argopecten scallops. Fish Shellfish Immunol, 108702 (2023).
27. H. Xu, J. Chen, Y. Wang, Y. Wu, Y. Liang, SELL and IFI44 as potential biomarkers of Sjögren's syndrome and their correlation with immune cell infiltration. Genes Genet Syst, (2021).
28. J. Wang et al., DNA methylation of *IFI44L* as a potential blood biomarker for childhood-onset systemic lupus erythematosus. Pediatric Research, (2024).
29. S.-D. Cho, H. Shin, S. Kim, H. J. Kim, Insights on interferon-independent induction of interferon-stimulated genes shaping the lung's response in early SARS-CoV-2 infection. Heliyon 9, e22997 (2023).
30. Z. Zhang et al., Bioinformatics and system biology approach to identify the influences among COVID-19, influenza, and HIV on the regulation of gene expression. Front Im-

munol 15, 1369311 (2024).
31. H. Luo, X. Zhou, Bioinformatics analysis of potential common pathogenic mechanisms for COVID-19 infection and primary Sjogren's syndrome. Front Immunol 13, 938837 (2022).
32. Z. Lin et al., Type I Interferon Pathway-Related Hub Genes as a Potential Therapeutic Target for SARS-CoV-2 Omicron Variant-Induced Symptoms. Microorganisms 11, (2023).
33. A. J. Brenes, A. I. Lamond, D. A. Cantrell, The Immunological Proteome Resource. Nature Immunology 24, 731-731 (2023).
34. R. E. Rigby, K. Rue-Albrecht, D. Sims, J. Rehwinkel, Single-cell analysis of signalling and transcriptional responses to type I interferons. bioRxiv, 2023.2007.2003.547491 (2023).
35. X. Qiao et al., The involvement of an interferon-induced protein 44-like (CgIFI44L) in the antiviral immune response of Crassostrea gigas. Fish Shellfish Immunol 129, 96-105 (2022).
36. M. Rey-Campos, A. Saco, B. Novoa, A. Figueras, Transcriptomic and functional analysis of the antiviral response of mussels after a poly I:C stimulation. Fish Shellfish Immunol, 109867 (2024).
37. H. Liu, K. Söderhäll, P. Jiravanichpaisal, Antiviral immunity in crustaceans. Fish Shellfish Immunol 27, 79-88 (2009).
38. K. Buchmann, Evolution of Innate Immunity: Clues from Invertebrates via Fish to Mammals. Front Immunol 5, 459 (2014).
39. J. Robalino et al., Induction of antiviral immunity by double-stranded RNA in a marine invertebrate. J Virol 78, 10442-10448 (2004).
40. Y. Honda et al., Isolation and purification of a non-A, non-B hepatitis-associated microtubular aggregates protein. J Gen Virol 71 (Pt 9), 1999-2004 (1990).
41. D. Rupa et al., ACSL4 upregulates *IFI44* and *IFI44L* expression and promotes the proliferation and invasiveness of head and neck squamous cell carcinoma cells. Cancer Sci, (2024).
42. E. Boccardo et al., Expression of human papillomavirus type 16 E7 oncoprotein alters keratinocytes expression profile in response to tumor necrosis factor-alpha. Carcinogenesis 31, 521-531 (2010).
43. H. Wang et al., Long Noncoding RNA LINC01116 Contributes to Gefitinib Resistance in Non-small Cell Lung Cancer through Regulating IFI44. Mol Ther Nucleic Acids 19, 218-227 (2020).
44. Y. Wang, Y. Chen, B. Zhu, L. Ma, Q. Xing, A Novel Nine Apoptosis-Related Genes Signature Predicting Overall Survival for Kidney Renal Clear Cell Carcinoma and its Associations with Immune Infiltration. Front Mol Biosci 8, 567730 (2021).

45. D. Ou, Y. Wu, The prognostic and clinical significance of IFI44L aberrant downregulation in patients with oral squamous cell carcinoma. BMC Cancer 21, 1327 (2021).
46. X. Tu et al., Interruption of post-Golgi STING trafficking activates tonic interferon signaling. Nature Communications 13, 6977 (2022).
47. I. J. Marié et al., Tonic interferon restricts pathogenic IL-17-driven inflammatory disease via balancing the microbiome. Elife 10, (2021).
48. S. Malarkannan et al., Differences that matter: major cytotoxic T cell-stimulating minor histocompatibility antigens. Immunity 13, 333-344 (2000).
49. T. Dierckx et al., IFN-β induces greater antiproliferative and proapoptotic effects and increased p53 signaling compared with IFN-α in PBMCs of Adult T-cell Leukemia/Lymphoma patients. Blood Cancer Journal 7, e519-e519 (2017).
50. J. Bragazzi Cunha et al., Type I interferon signaling induces a delayed antiproliferative response in respiratory epithelial cells during SARS-CoV-2 infection. J Virol 97, e0127623 (2023).
51. M. J. Finelli, L. Sanchez-Pulido, K. X. Liu, K. E. Davies, P. L. Oliver, The Evolutionarily Conserved Tre2/Bub2/Cdc16 (TBC), Lysin Motif (LysM), Domain Catalytic (TLDc) Domain Is Neuroprotective against Oxidative Stress. The Journal of biological chemistry 291, 2751-2763 (2016).
52. M. J. Finelli, P. L. Oliver, TLDc proteins: new players in the oxidative stress response and neurological disease. Mammalian Genome 28, 395-406 (2017).
53. M. J. Finelli, L. Sanchez-Pulido, K. X. Liu, K. E. Davies, P. L. Oliver, The Evolutionarily Conserved Tre2/Bub2/Cdc16 (TBC), Lysin Motif (LysM), Domain Catalytic (TLDc) Domain Is Neuroprotective against Oxidative Stress. J Biol Chem 291, 2751-2763 (2016).
54. A. F. Eaton, D. Brown, M. Merkulova, The evolutionary conserved TLDc domain defines a new class of (H(+))V-ATPase interacting proteins. Sci Rep 11, 22654 (2021).
55. R. A. Oot, S. Wilkens, Human V-ATPase function is positively and negatively regulated by TLDc proteins. Structure, (2024).
56. R. Wang, Y. Qin, X.-S. Xie, X. Li, Molecular basis of mEAK7-mediated human V-ATPase regulation. Nature Communications 13, 3272 (2022).
57. E. Castroflorio et al., The *Ncoa7* locus regulates V-ATPase formation and function, neurodevelopment and behaviour. Cell Mol Life Sci 78, 3503-3524 (2021).
58. M. M. Khan et al., Oxidative stress protein Oxr1 promotes V-ATPase holoenzyme disassembly in catalytic activity-independent manner. EMBO J 41, e109360 (2022).
59. S. Klössel et al., Yeast TLDc domain proteins regulate assembly state and subcellular localization of the V-ATPase. The EMBO Journal 43, 1870-1897-1897 (2024).
60. N. Nelson, Structural conservation and functional diversity of V-ATPases. Journal of Bioenergetics and Biomembranes 24, 407-414 (1992).

61. Z. Fan, P. J. Beresford, D. Y. Oh, D. Zhang, J. Lieberman, Tumor suppressor NM23-H1 is a granzyme A-activated DNase during CTL-mediated apoptosis, and the nucleosome assembly protein SET is its inhibitor. Cell 112, 659-672 (2003).
62. M. Pérez-Martínez et al., F-actin-binding protein drebrin regulates CXCR4 recruitment to the immune synapse. J Cell Sci 123, 1160-1170 (2010).
63. B. Clémençon, M. Babot, V. Trézéguet, The mitochondrial ADP/ATP carrier (SLC25 family): pathological implications of its dysfunction. Mol Aspects Med 34, 485-493 (2013).
64. J. S. Moon et al., ANT2 drives proinflammatory macrophage activation in obesity. JCI Insight 6, (2021).
65. I. Leake, ANT2 mediates hypoxia and inflammation in obesity. Nat Rev Endocrinol 15, 64 (2019).
66. J. B. Seo et al., Knockdown of *Ant2* Reduces Adipocyte Hypoxia And Improves Insulin Resistance in Obesity. Nat Metab 1, 86-97 (2019).
67. P. Wang et al., ANT2 functions as a translocon for mitochondrial cross-membrane translocation of RNAs. Cell Research 34, 504-521 (2024).
68. C. G. Evans, L. Chang, J. E. Gestwicki, Heat shock protein 70 (hsp70) as an emerging drug target. J Med Chem 53, 4585-4602 (2010).
69. J. Abramson et al., Accurate structure prediction of biomolecular interactions with AlphaFold 3. Nature 630, 493-500 (2024).
70. M. I. Love, W. Huber, S. Anders, Moderated estimation of fold change and dispersion for RNA-seq data with DESeq2. Genome Biol 15, 550 (2014).//

Chapter 4

The role of IFI44 in the Immune Response

The expression kinetics of IFI44 (Figure 3.1C), along with its various implications in infection (1-8), autoimmune disease (9-12) and cancer (13-15) led me to hypothesise that IFI44 plays an important role in the innate immune response to infection. Indeed, IFI44 has described roles during infection in different models, although some of these are conflicting, and the molecular functionality of the protein has not been elucidated.

Overexpression of IFI44 in human cell lines has been shown to inhibit RSV (1), Bunyamwera virus (3), HIV-1 (4) and Porcine Epidemic Diarrhoea virus (5). In the case of RSV, overexpression of IFI44 in A549 cells results in a small reduction in infectivity of GFP-RSV from 10.7% to 6.33%, as determined by flow cytometry (1). Confirming this, *IFI44* knock-out through CRISPR-Cas9 in A549 cells results in increased RSV titre in cell supernatants (1). In addition, *Ifi44*$^{-/-}$ C57BL/6 mice loose more weight over the course of RSV infection than wild-type mice (1). Further, children with confirmed RSV in paediatric intensive care have lower *IFI44* expression than those in the general ward (1). Since *IFI44* is a highly inducible ISG, this finding may be attributed to children in intensive care having a weaker *overall* IFN response, and therefore their reduced ability to clear RSV may not necessarily be due to reduced *IFI44* expression. *IFI44* was also identified alongside other ISGs in a microarray dataset to discover antiviral effectors of RSV, although since this study relied upon expression data alone, causality of any individual gene in clearance of RSV cannot be implied (2). IFI44 may exert anti-viral activity in other viral infections too, as IFI44 overexpression in HEK293T cells restricts Bunyamwera virus 10-fold (3), overexpression in MARC-145 cells reduces Porcine Epidemic Diarrhoea virus genome and titre (5) and MAGI-HeLa cells expressing IFI44 significantly decrease HIV-IIIB infection rate in the presence or absence of IFN-α (4). Interestingly, IFI44 depletion

specifically affects the replication of LTR-driven lentiviral vectors and wild-type HIV-1 viruses, and HEK293 cells overexpressing IFI44 show a reduction in LTR-driven luciferase expression (4). This is likely a direct effect of IFI44, as IFI44 localises to the nuclei of HIV-1 infected cells and binds to the LTR, which was shown through immunostaining, cellular fractionation and ChIP-PCR (4).

Conversely, another study suggests that IFI44 exerts proviral activities, as siRNA-induced knock-down of *IFI44* in A549 cells decreases IAV/PR8 and CMV titres (6). However, this study lacked confirmation that there were no off-target effects, and a different paper silencing *IFI44* through siRNA found this did produce unwanted off-target effects (1). To address this, the authors used CRISPR-generated *IFI44*$^{-/-}$ HAP-1 cells, which show a 100-fold decrease in rVSV-GFP titres compared to wild-type cells after IFN-α treatment. Complimenting this, overexpression of IFI44 results in an increase of rVSV-GFP titres. The authors did not test infection with IAV or CMV, as in the knock-down model, so whether these findings repeat in an overexpression setting is unknown (6). This study also indicates that *IFI44* knock-down results in a decrease in *IFIT2* expression after Lymphocytic choriomeningitis virus (LCMV), VSV, Sendai virus (SeV) and IAV infection and also after Poly(I:C) and IFN-α treatment, while IFI44 overexpression induced *IFIT2* in response to IAV infection (6). In agreement that IFI44 may have proviral activities, another study identified IFI44 as a key protein in immune evasion and escape in RA patients with SARS-CoV-2 or *S. aureus* infections, and specifically linked expression of *IFI44* with activated DCs (7). This was performed through bioinformatic analysis of pre-existing datasets, and so correlation may not indicate causality, with *IFI44* instead being a proxy for IFN (7).

Due to the conflicting nature of the existing work, I sought to discover the precise role of IFI44 in the innate immune response after infection with a wide range of viruses or stimulation with bacterial PAMPs *in vitro*, *ex vivo* and *in vivo*. I also aimed to address whether IFI44 is regulated through post-translational modifications, and whether IFI44 itself can regulate the expression of other ISGs. In addition, the role of IFI44 in the adaptive immune response has not been elucidated, and as such I aimed to discover whether IFI44 plays a role in T- or B-cell immunity.

4.1 IFI44 is not a regulator of the interferon response

As IFI44 has implicated roles in a vast range of immunopathologies, I initially sought to discover whether IFI44 is a regulator of the IFN response. I performed RT-qPCR on RNA extracted from *Ifi44*$^{+/+}$ and *Ifi44*$^{-/-}$ MEFs to determine expression levels of ISGs as a proxy for IFN signalling. *Ifi44*$^{-/-}$ MEFs showed a slight IFN signature, with ISG expression levels

having a trend to be elevated above those from *Ifi44*$^{+/+}$ MEFs, and with *Ddx58* and *Adar1* reaching statistical significance (Figure 4.1A). To determine whether this ISG signature was present in mouse organs, I performed RT-qPCR on RNA isolated from multiple different organs from *Ifi44*$^{+/+}$ and *Ifi44*$^{-/-}$ mice. In this setting, the ISG signature observed in MEFs did not reproduce in any organ tested (Figure 4.1B; Figure S8). It should be noted that the spread of datapoints in these data were high, which may indicate that the RNA had undergone degradation prior to cDNA conversion, impacting the results. Due to the conflicting nature of these findings, I then stimulated HEK293T cells stably overexpressing IFI44 and IFI44L with IFN a/D and assessed ISG expression through RT-qPCR. There was no difference in baseline or induced levels of any ISG tested (Figure 4.1C). Therefore, neither knock-out nor overexpression of *IFI44* consistently impacted ISG expression, and therefore the IFN response more generally. However, I cannot rule out the possibility that expression of specific ISGs might be controlled by IFI44 in some types of cells, potentially including *Adar1* and *Ddx58* in fibroblasts or embryonic cells (Figure 4.1A).

4.2 IFI44 is ISGylated

ISGylation is a post-translational modification in which the IFN-induced protein ISG15 is covalently conjugated to other proteins, in a process similar to ubiquitination (16, 17). This process is reversable by the protein USP18 (18, 19), which in turn has an independent role in negatively regulating IFNAR (19, 20). As ISG15 is an ISG, this process occurs predominantly in response to IFN signalling and can act to regulate and/or mediate the IFN response. ISGylation can mark proteins for degradation, antagonise protein degradation, affect protein localisation, prevent the formation of complexes and free ISG15 can exert anti-viral effects (16-18, 21-25).

Our collaborator Adan Pinto Fernandez found that IFI44 is ISGylated through a mass spectrometry screen in *USP18*$^{-/-}$ cells at residue K199 (18) (Figure 4.2A). I confirmed this finding using *USP18*$^{-/-}$ cells provided by Adan and showed that IFI44 was ISGylated 24 hours after IFN stimulation (Figure 4.2B; Figure S9A-C). However, only a small proportion of total IFI44 (≈50kDa) was ISGylated, and the IFI44-ISG15 band is only visible in *USP18*$^{-/-}$ cells. The effect of ISGylation on IFI44 protein function remains unknown.

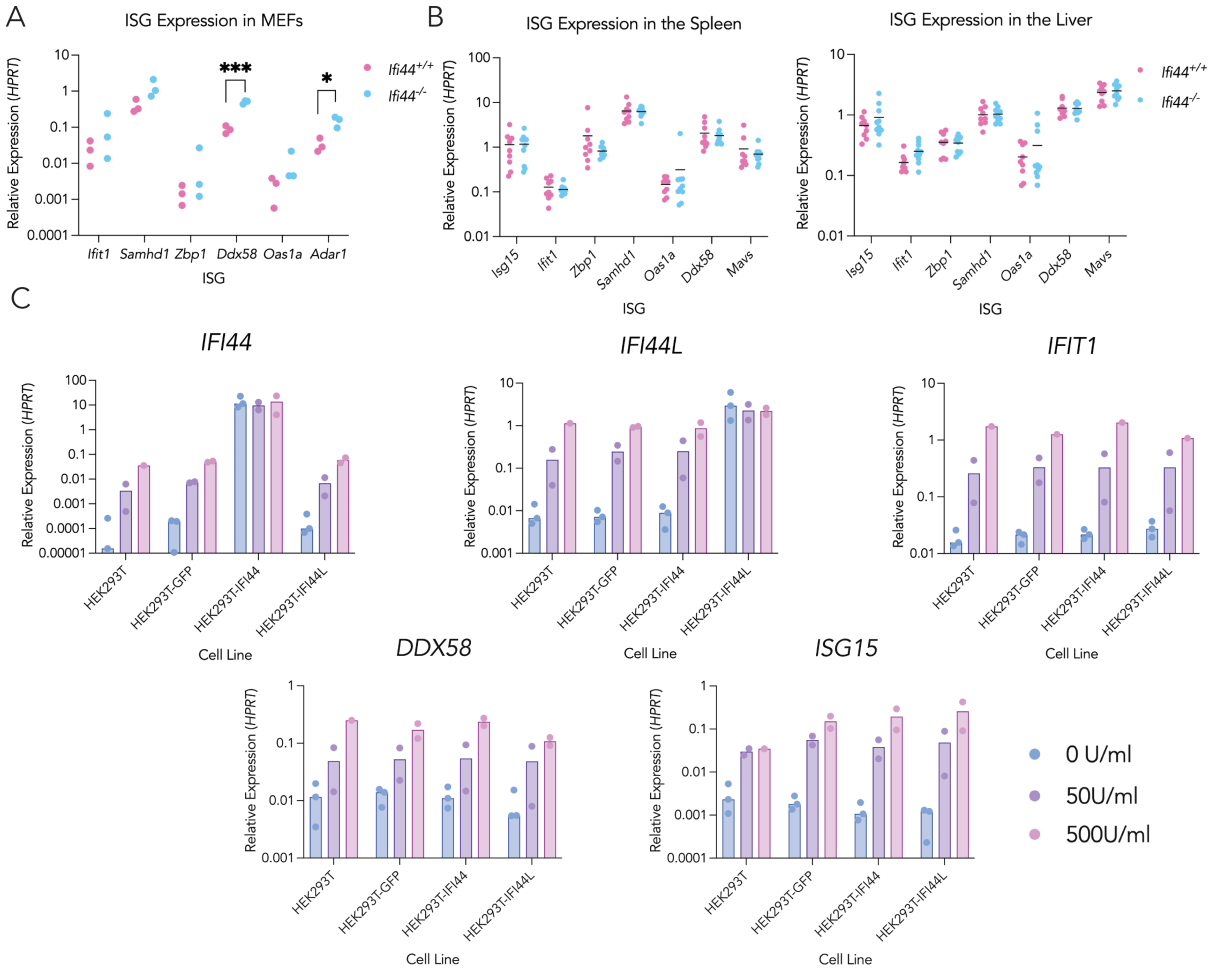


Figure 4.1: IFI44 is not a regulator of the interferon response.

A, B. RNA was isolated from (A) *Ifi44*$^{+/+}$ and *Ifi44*$^{-/-}$ immortalised MEFs or (B) mouse organs and RT-qPCR performed for the indicated genes. **C.** HEK293T cells stably overexpressing IFI44, IFI44L or GFP through lentiviral transduction were stimulated with 0 U/mL, 50 U/mL or 500 U/mL IFN a/D for 19 hours, and RNA isolated. RT-qPCR was performed for the indicated genes. (A-C) Each data point represents an individual biological replicate and is the average of two technical replicates. (C) There were three biological replicates for the 0 U/mL condition, two biological replicates for the 50 U/mL condition and two biological replicates for the 500 U/mL condition except for HEK293T parental cells, for which there was only one. This was due to prioritisation of conditions and cell lines during repeat experiments. (A, B) Statistical analyses were performed using unpaired T-tests. *=p≤0.05, **=p≤0.01, ***=p≤0.001, ****=p≤0.0001. Unmarked lanes are not significant.

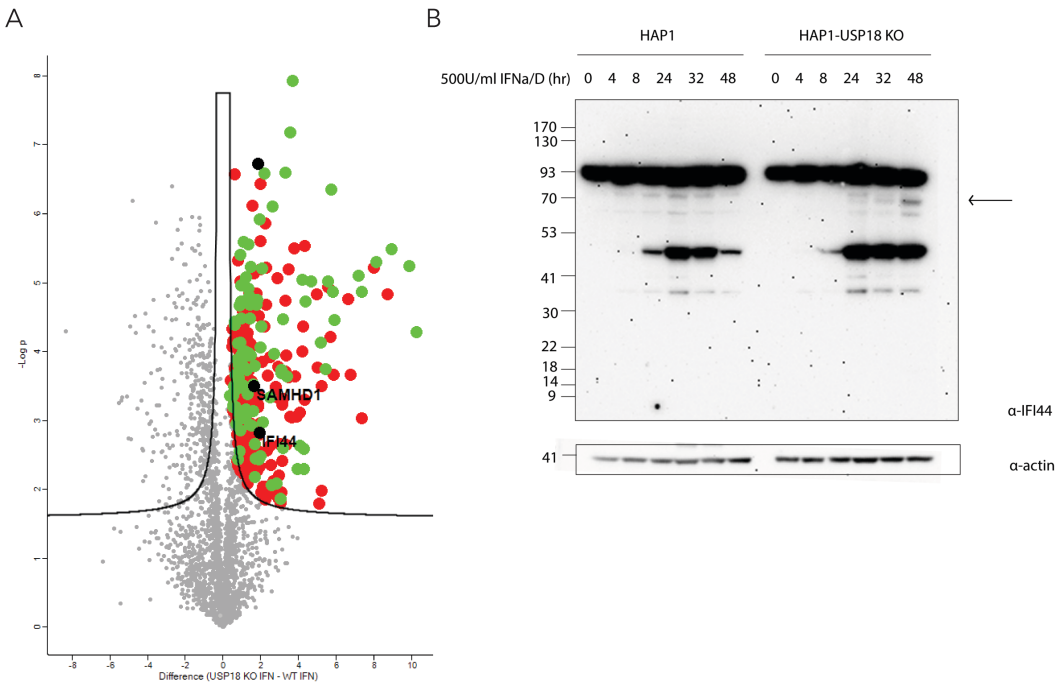


Figure 4.2: IFI44 is ISGylated.

A. Mass spectrometry screen of proteins conjugated to ISG15 in *USP18*$^{-/-}$ cells (18). **B.** HAP1 WT and *USP18*$^{-/-}$ HAP1 cells were stimulated with 500 U/mL IFNa/D for 0, 4, 8, 24, 32 or 48 hours. Cells were lysed in RIPA buffer, and IFI44 detected by immunoblot using an antibody detecting endogenous protein. Arrow indicates the IFI44-ISG15 band. (B). Representative data of three independent experimental repeats.

4.3 IFI44/L overexpression does not affect virus infectivity *in vitro*

As IFI44 is a highly IFN-responsive gene, in the first instance I infected wild-type and *Ifi44*$^{-/-}$ MEFs with viruses that are sensitive to IFN treatment, namely encephalomyocarditis virus (EMCV), vaccinia virus (VACV) and herpes simplex virus-1 (HSV-1) and assessed viral replicative ability through crystal violet stain or plaque assay. In the case of VACV, *Ifi44*$^{-/-}$ MEFs pre-treated with IFN exhibited increased cytopathic effects compared with wild-type cells (Figure 4.3A, B). Although this was only one experimental replicate, I confirmed this finding through a plaque assay, reproducing the phenotype (Figure 4.3C). For HSV-1, there was no difference in cytopathic effects observed (Figure 4.3D, E), however *Ifi44*$^{-/-}$ MEFs contained more plaques than the wild-type (Figure 4.3F). I only performed one experiment of this type, and additional experiments need to be completed to confirm this finding. These experiments were deprioritised due to time restraints during these studies and availability of MEFs. Given this data, I sought to determine whether human cells overexpressing IFI44 are more resistant to VACV infec-

tion through infecting HEK293T cells transiently transfected with pcDNA3.2 plasmids containing either IFI44 or no insert (empty vector, EV) with VACV-GFP (Figure 4.3G). Infectivity was measured by quantification of GFP-positive cells with Incucyte live cell imaging. In this setting, there was no difference in infectivity between the two conditions. To study HSV-1 infectivity in human cells overexpressing IFI44, HEK293T cells transiently transfected with pcDNA3.2 plasmids containing either IFI44 or GFP inserts were infected with HSV-1, and infectivity assessed through a plaque assay (Figure 4.3H). In this setting, there was no difference in plaque number between the two conditions. For these experiments, there is no paired western blot confirming IFI44/L overexpression, however I consistently saw good expression of IFI44/L when using the same stocks of pcDNA3.2 plasmids in other experiments throughout my DPhil, for example in Figure 3.11, Figure 4.5 and Figure 4.6. No phenotype was observed when infecting MEFs with EMCV, as this experimental readout did not produce reproducible results – with some experimental replicates showing that *Ifi44*$^{-/-}$ MEFs were more susceptible, and some showing that they were protected (Figure S10). These MEFs were genotyped each time to ensure that they were correct.

Given the inconclusiveness of the above results, I performed an overexpression-based virus screen in HEK293T cells to discover whether IFI44 or IFI44L affect viral protein expression for a panel of different viruses, using immunoblotting as the read-out. I utilised HSV-1, an alpha herpesvirus with a dsDNA genome; PR8, a mouse-adapted strain of H1N1 influenza A virus (IAV), which has a segmented negative-sense ssRNA genome; VACV, a poxvirus with a linear dsDNA genome, which replicates entirely in the cytoplasm of a cell; VSV-pseudotyped replication-deficient GFP-expressing lentiviruses, which contain two copies of a positive-sense ssRNA genome within a capsid; Zika Virus (ZIKV), a flavivirus with a positive-sense ssRNA genome and Adenovirus, a non-enveloped virus with a dsDNA genome. I selected this virus panel to utilise a breadth of viruses with differing genomes, envelopes and replication cycles. There was no detectable role for IFI44 or IFI44L in amplifying or reducing viral protein expression for any of the viruses used in this setting (Figure 4.4A-H). Initially, I observed a phenotype for HSV-1 and IAV: viral protein expression appeared to be reduced in HEK293T cells stably overexpressing IFI44 or IFI44L at the lower MOIs (Figure S11A, B; Figure S12A, B). However, in repeat experiments I noticed that this reduction in viral protein expression was likely due to the transduction of the cell, as overexpression of GFP also had this effect (Figure 4.4A, B). While there was no difference in VACV protein expression, a reproducible degradation of both IFI44 and IFI44L was observed (Figure 4.4C and S13A-D). Degradation at the protein level preceded the reduction in *IFI44* and *IFI44L* mRNAs that likely resulted from host cell shut off (26, 27), as seen in paired experiments with protein and mRNA data (Figure S13D, E). This indicated that degradation of IFI44/L by VACV is specific,

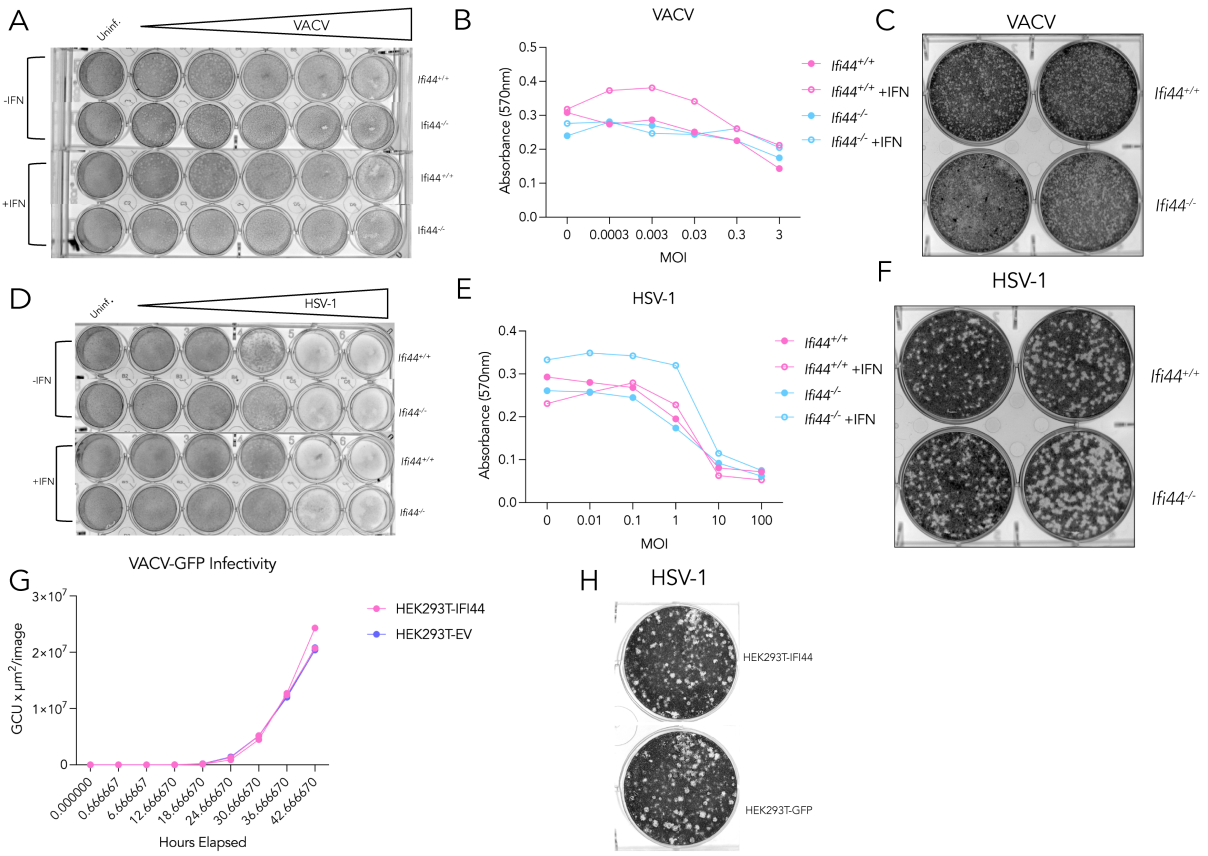


Figure 4.3: HSV-1 and VACV infection of *Ifi44*$^{-/-}$MEFs and IFI44-V5 overexpressing HEK293T cells.

A, D. *Ifi44*$^{+/+}$ and *Ifi44*$^{-/-}$ immortalised MEFs were pre-treated with 0 U/mL or 100 U/mL of recombinant universal type I IFN (IFN a/D) for 24 hours and then infected with a 10-fold dilution series of VACV WR from 0.0003 MOI to 3 MOI, or HSV-1 from 0.01 MOI to 100 MOI, or media. After 24 hours, cells were fixed with 1:4 formaldehyde and stained with 0.05% crystal violet (CV). Plates were washed, dried and imaged. **B, E.** CV stain from (A) was dissolved in 100% methanol, and absorbance at 570nm determined on a CLARIOstar microplate reader. **C, F, H.** *Ifi44*$^{+/+}$ and *Ifi44*$^{-/-}$ immortalised MEFs or HEK293 cells overexpressing IFI44 or GFP were infected with 25 pfu of HSV-1 or 2 pfu of VACV WR. After 1.5 hours, virus was removed and a 1% CMC overlay in DMEM added. Plaques from HSV-1 were developed after 72 hours, and VACV after 48 hours. To develop, cells were fixed with 1:4 formaldehyde, and stained with 1% CV. Plates were washed, dried and imaged. **G.** HEK293T cells transiently transfected with IFI44 or empty vector (EV) were infected with 0.00015 MOI of GFP-VACV and plates were placed in an Incucyte Live Cell Imager for 48 hours, with photos taken every 6 hours. (A-C, E-G) Data is one independent experiment. (D, H) Representative data of two independent experiments.

perhaps pointing to a mechanism whereby VACV specifically degrades these two ISGs, possibly in an effort to evade the immune response. There was no detectable phenotype for VSV-pseudotyped replication-deficient HIV-1 lentiviruses with GFP expression driven from an introduced CMV promotor (second generation; HIV-1-GFP-CMV) (Figure 4.4D; Figure S14) or from the endogenous LTR promotor (first generation; HIV-1-GFP-LTR) (Figure 4.4E). This was surprising, given that one study suggested that IFI44 binds to the HIV-1 LTR and inhibits its activity (4). However, the authors of this study did not observe a difference in infectivity using second generation lentiviruses, and, due to time constraints, I only performed one experiment with HIV-1-GFP-LTR. As no phenotype was observed with HIV-2-GFP-CMV (Figure 4.4F), ZIKV (Figure 4.4G) or Adenovirus (Figure 4.4H), these experiments were deprioritised and have only one replicate.

While the data suggest that IFI44/L overexpression do not impact viral protein expression, one cannot conclude that there is no role for the two proteins in antiviral immunity. For example, the results may be due to an artefact of the lentiviral-induced overexpression system, or the use of HEK293T cells. HEK293T cells are known to lack many innate immune pathways, for example the cGAS-STING pathway, and have in some settings defective IFN responses as a result (28). In addition, in Section 3.6 I discovered that IFI44 and IFI44L interact. Therefore, I hypothesised that overexpression of both proteins may be required to elicit a phenotype. To test whether overexpression of both IFI44 and IFI44L affects virus infectivity, HEK293 cells were transiently transfected with pcDNA3.2 plasmids containing IFI44 and IFI44L or GFP inserts and were then infected with HSV-1, and a plaque assay performed (Figure 4.5A). I did not observe a difference in infectivity in this setting. In addition, HEK293 cells transiently transfected with IFI44 and IFI44L or GFP were infected with VACV, and viral protein expression measured by immunoblotting (Figure 4.5B) and viral RNA expression quantified by RT-qPCR (Figure 4.5C) (29). There was a small but reproducible reduction in *E9L* transcript and viral protein expression in cells overexpressing IFI44, IFI44L or IFI44 + IFI44L, but these data did not reach statistical significance. Degradation of IFI44 by VACV as seen in Figure 4.4C was reproduced, but co-expression with IFI44L stabilised IFI44, and no degradation was seen in the doubly transfected condition (Figure 4.5B). Interestingly, VACV infection resulted in the cleavage of IFI44L into three smaller fragments (Figure 4.5B). These observations led us to hypothesise that VACV specifically cleaves IFI44L and degrades IFI44, in order to circumvent innate immune responses. Indeed, no difference in infectivity was observed in earlier experiments when infecting human cells with VACV (Figure 4.3D; Figure S13), but there did appear to be an increase in virus replication in *Ifi44*$^{-/-}$ MEFs (Figure 4.3A-C). One could speculate that since C57BL/6 mice lack *Ifi44l*, IFI44L protein is not present to exert any anti-viral effects, leading to these observations. In addition, human and mouse IFI44 share 53% amino acid identity, and as such VACV may not be able to cause the

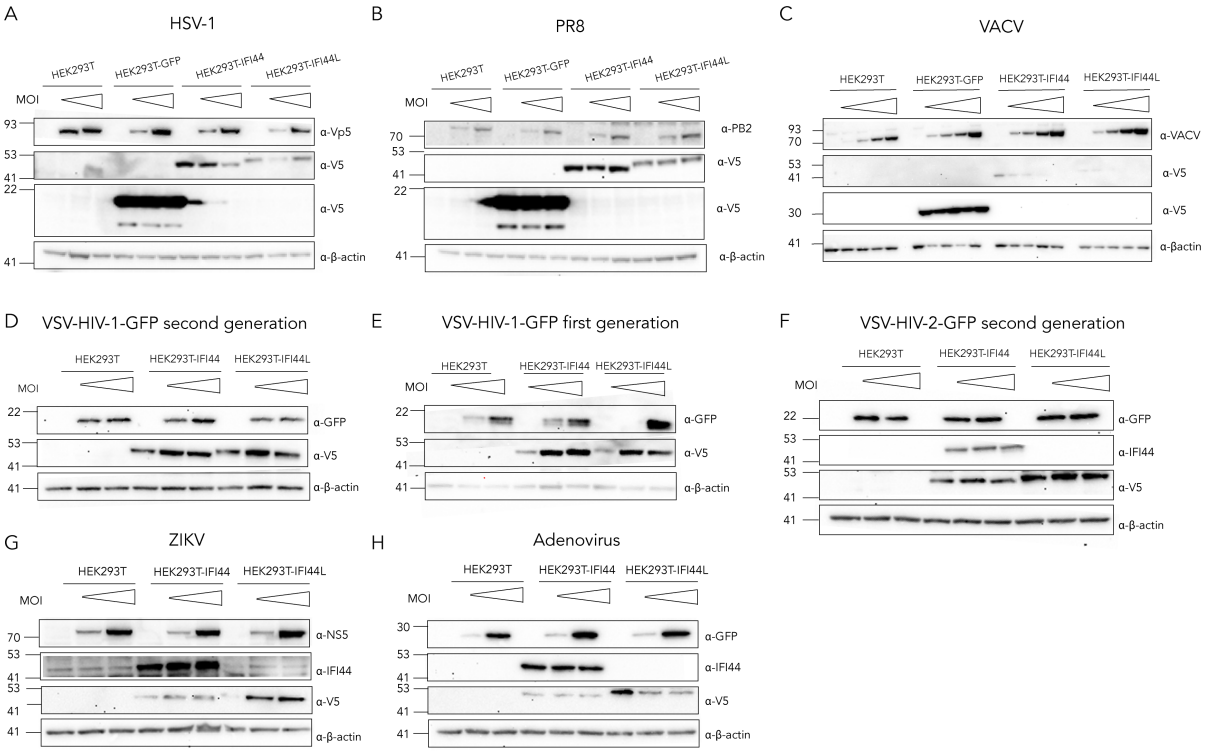


Figure 4.4: Neither IFI44 nor IFI44L confer protection or susceptibility to a panel of different viruses.

A-H. HEK293T cells stably overexpressing IFI44, IFI44L or GFP following lentiviral transduction and blasticidin selection were infected with either: HSV-1 (MOI 0.01 and 0.02), PR8 (MOI 1 and 10), VACV (MOI 0.02 and 0.2), VSV-pseudotyped replication-deficient HIV-1-GFP second generation vectors (1:500 or 1:250), VSV-pseudotyped replication-deficient HIV-1-GFP first generation vectors (1:500 or 1:250), VSV-pseudotyped replication-deficient HIV-2-GFP second generation vectors (1:500 or 1:250), ZIKV (MOI 0.1 or 1) or Adenovirus (MOI 750 or 1,500). Control uninfected cells underwent a media change. After 48 hours, cells were lysed in RIPA buffer and protein expression of viral proteins was detected by western blot using antibodies detecting endogenous proteins. (A-C) Results are representative data of four independent biological repeats. (D) Results are representative data of three independent biological repeats. (E-H) Data are one experiment.

degradation of mouse IFI44.

4.4 VACV cleaves IFI44 and IFI44L

To determine when during its lifecycle VACV cleaves IFI44L, and to thereby aid the identification the likely viral gene(s) responsible, I performed a time-course from 0-18 hours post-infection and analysed IFI44/L cleavage by immunoblotting (Figure 4.6A). I observed that IFI44L was cleaved by VACV from 4 hours post-infection, and IFI44 was

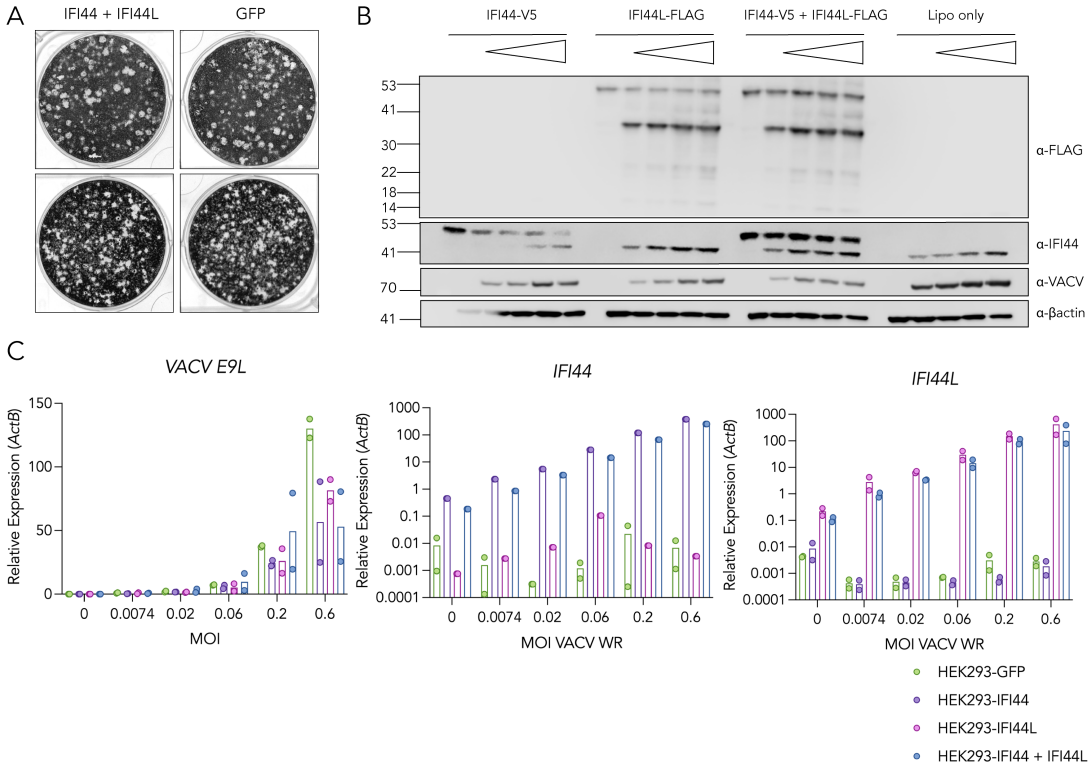


Figure 4.5: Overexpression of IFI44 and IFI44L does not confer protection or susceptibility to HSV-1 or VACV.

A. HEK293 cells transiently transfected with IFI44 + IFI44L or GFP were infected with HSV-1 at 25 pfu/well. After 1.5 hours, virus was removed and a 1% CMC overlay in DMEM added. After 72 hours, cells were fixed with 1:4 formaldehyde, and stained with 1% CV. Plates were washed, dried and imaged. **B, C.** HEK293 cells transiently transfected with IFI44 + IFI44L or GFP were infected with VACV WR in a 3-fold dilution series from 0.2 MOI to 0.0074 MOI. After 24 hours, cells were lysed in RIPA buffer (B) or buffer RLT (C) and protein expression of viral proteins and IFI44 were detected by western blot using antibodies detecting endogenous proteins, while IFI44L was detected with an anti-FLAG antibody (B), or RNA was extracted and RT-qPCR performed for the indicated genes (C). (A) Two independent biological replicates are shown here. (B) Representative data of three biological replicates. (C) Each datapoint is one biological replicate, representing the average of two technical replicates.

also cleaved by VACV from 6 hours post-infection. Next, I interrogated whether the proteasome was involved in this cleavage. To do this, I infected HEK293T cells overexpressing IFI44, IFI44L or GFP with VACV and after four hours, inhibited the proteasome with MG132 (or DMSO as a carrier control). Cells were incubated for a further two hours, and then cleavage analysed by western blot. The addition of the proteasome inhibitor did not affect the ability of VACV to cleave either IFI44 or IFI44L (Figure 4.6B). Additionally, I confirmed published data that VACV enhances global ubiquitination (30, 31) (Figure 4.6B). Since VACV cleaved IFI44-V5 overexpressed in HEK293T cells, I hypothesised that

VACV also cleaves endogenous IFI44. To test this, IFI44 was upregulated in HEK293T cells by pre-treatment with 50 U/mL or 500 U/mL IFN overnight, and cells were infected with VACV. I assessed cleavage by immunoblot with an antibody detecting endogenous IFI44. In this setting, there was no cleavage detectable (Figure 4.6C). However, IFN treatment at 500 U/mL resulted in a downregulation in VACV protein expression, and yet IFI44 was not upregulated to high enough levels to observe the much fainter cleavage products. Therefore, using a different cell line, which induces more IFI44 such as THP-1, and a higher MOI of VACV may be necessary to detect cleavage of endogenous IFI44.

Next, I made and titred stocks of VACV deletion mutants, which were a kind gift from Geoff Smith, to interrogate whether mutant viruses with certain genes deleted could still cleave IFI44/L. These mutant viruses have stretches of genes missing from either end of the genome and have been previously described (32, 33). These viruses are ready to be used in planned future experiments.

4.5 IFI44 does not affect lentiviral infectivity *in vivo*

One study suggested that IFI44 binds to the HIV-1 LTR and inhibits its activity (4). While we did not observe a phenotype when infecting human cells overexpressing IFI44/L with VSV-pseudotyped replication-deficient HIV, I decided to pursue an *in vivo* lentiviral challenge in order to determine whether IFI44 affects lentiviral infection, or virus infection more generally, in a mammal with a complete and functioning immune response. This may highlight phenotypes not visible in cell lines due to importance of soluble factors such as complement, presence of an adaptive immune response, and the heterogenicity of cells and their interactions more generally. I generated HIV-1-GFP-CMV and purified it through centrifugation over a sucrose cushion and titrated the virus on HEK293T cells. Mice were infected with HIV-1-GFP-CMV, and after six days mice were sacrificed, and viral titre in the spleen determined through flow cytometry (Figure 4.7A). There was no difference in infectivity (measured by enumerating GFP-positive splenocytes) in two independent experiments (Figure 4.7B, C). This could be because GFP expression was driven from an introduced CMV promotor, and it is thought that IFI44 specifically interacts with the HIV-1 LTR to mediate its effect (4). However, there was also no effect of IFI44 overexpression on HIV-1-GFP-LTR *in vitro* (Figure 4.4E). As such, I conclude that there it is unlikely that IFI44 controls HIV-1-GFP-CMV infection.

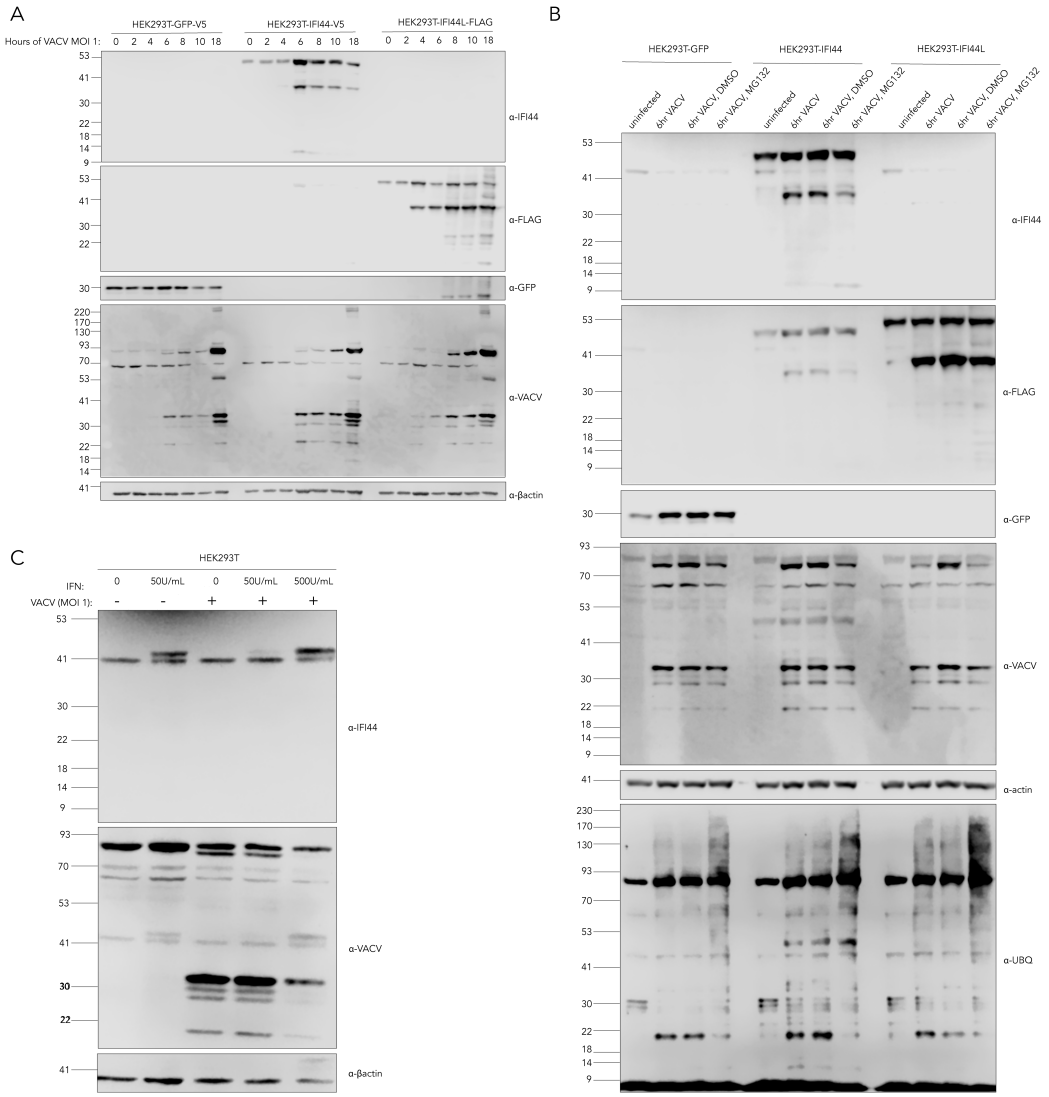


Figure 4.6: IFI44 and IFI44L are cleaved by VACV, in a proteasome-independent manner.

A. HEK293T cells transiently transfected with IFI44, IFI44L or GFP were infected with VACV WR at MOI 1 for a time-course of 0, 2, 4, 6, 8, 10 and 18 hours. **B.** HEK293T cells transiently transfected with IFI44, IFI44L or GFP were infected with VACV WR at MOI 1. After 4 hours, 5 µM MG132 (or media or DMSO as a control) were added to the relevant wells and incubated for another 2 hours. **C.** HEK293T cells were stimulated with 0, 50 or 500 U/mL of IFN a/D overnight, and then infected with VACV WR at MOI 1 for 6 hours. In all cases, cells were lysed in RIPA buffer and protein expression of viral proteins, ubiquitin and IFI44 were detected by western blot using antibodies detecting endogenous proteins, while IFI44L was detected with an anti-FLAG antibody. (A-C) Representative data of three independent biological repeats.

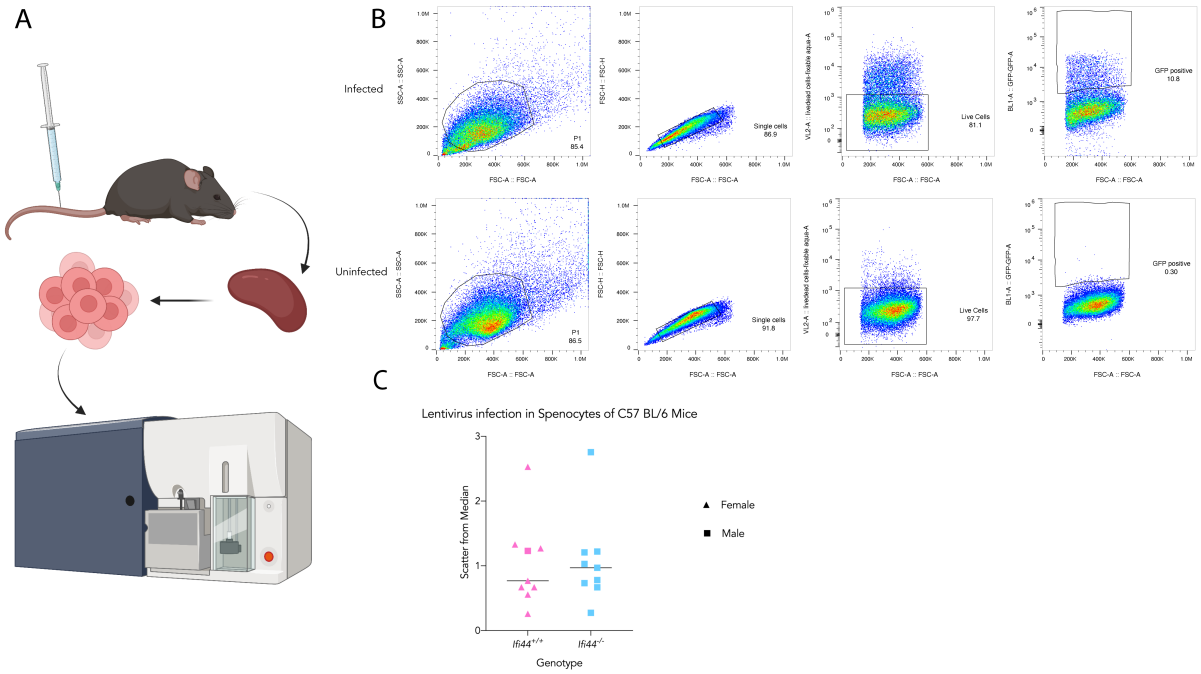


Figure 4.7: There is no difference in lentiviral infectivity in *Ifi44*$^{-/-}$ mice.

A. Schematic of experiment. Mice were injected intravenously with 6.5x10^7 infectious units of VSV-pseudotyped replication-deficient HIV-GFP virus. After 6 days, mice were sacrificed and their spleens removed. Splenocyte suspensions were prepared, and GFP was quantified on an Attune flow cytometer. **B.** Gating strategy. **C.** For each dataset, the median of the dataset for each genotype was set to 1, and each data point divided by this value to generate a plot of scatter about the median. (C) Each datapoint is one biological replicate, and data from two independent experiments are pooled.

4.6 IFI44 does not affect IAV infectivity *in vivo*

Thus far, I had not tested the *in vivo* role of *Ifi44* during infection with a replication-competent virus. In addition, some ISGs stimulate the adaptive immune response, aiding infection clearance at later time points (34) and contribute towards tumour clearance (35-37). Further, some patients with SLE, a well-studied type I interferonopathy, have a wide spectrum of autoantibodies and auto-reactive T cells, which suggests that IFN signalling and resulting ISGs contribute towards the breakdown of tolerance and stimulation of adaptive immunity (38, 39). Whether IFI44 plays a role in stimulating the adaptive immune response had not been addressed, although there is some literature to suggest that *IFI44* expression correlates with immune cell infiltration (7, 10-12, 14, 15, 40), which in turn would stimulate adaptive immunity.

I aimed to discover the role of *Ifi44* during infection with a replication-competent virus, and to determine whether *Ifi44* impacts the adaptive immune response. To do this, I infected *Ifi44*$^{+/+}$ and *Ifi44*$^{-/-}$ mice intranasally with IAV/X-31, a mouse-adapted influenza

H3N2, using a sub-lethal dose. This was performed in collaboration with Dr. Tiong (Jack) Tan. One cohort of mice were sacrificed at day three of infection, when virus titres and ISG expression levels peak, and a different cohort were sacrificed at day 10 of infection, when there is detectable neutralising antibody and specific cytotoxic T cell presence. At day three of infection, there was no difference in viral titre between the genotypes in the lung (primary infection site) or the spleen, as determined by RT-qPCR for viral *NP* (Figure 4.8A). In addition, there was no difference in overt inflammation of the lung or the spleen between the two genotypes, as determined through organ index (Figure 4.8B). In the lung, expression of ISGs in infected mice were elevated compared to uninfected mice, but there was no difference in ISG expression between the two genotypes (Figure 4.8C) and the same was true in the spleen (Figure 4.8D). Given this, *Ifi44* did not appear to be impacting the early stages of infection in either virus replication or the strength of the IFN response. The other cohort of mice were sacrificed 10 days post-infection (Figure 4.9A), during which time the animals lost weight, with maximal weight loss occurring at day 7, and then recovery back to baseline weight by day 10. $Ifi44^{-/-}$ mice lost weight at the same rate as $Ifi44^{+/+}$ mice, however $Ifi44^{-/-}$ mice recovered their weight more slowly, with some not recovering to baseline weight at day 10 (Figure 4.9B). Therefore, there was evidence that *Ifi44* might play a role in the later stages of infection. Despite this observation, there was no difference in overt organ inflammation at day 10 of infection between the genotypes (Figure 4.9C). To evaluate whether *Ifi44* affects the T cell response to infection, lungs and spleens were harvested 10 days post-X-31 infection and T cell population abundances studied through flow cytometry. There was no difference in the total number of live T cells, $CD8^+$ T cells, nor X-31-specific $CD8^+$ T cells between $Ifi44^{-/-}$ and $Ifi44^{+/+}$ mice (Figure 4.9D, E, Figure S15). Confirming this, there was no difference in expression of cytotoxic T cell-related genes between the two genotypes (Figure 4.9F, Figure S16A, B). Further, $Ifi44^{-/-}$ mice showed no difference in $CD4^+$ T cells in infected lungs (Figure S16C, D). To determine whether *Ifi44* affected the generation of neutralising antibodies to IAV, a microneutralisation assay was performed on mouse sera from day 10 of infection by Dr. Tiong (Jack) Tan. There was no difference in neutralising antibody titres in $Ifi44^{-/-}$ mice compared to $Ifi44^{+/+}$ control mice (Figure 4.9E). Therefore, worsened recovery of $Ifi44^{-/-}$ mice after IAV/X-31 infection cannot be attributed to differences in T cell infiltration or neutralising antibody titres. As such, it is possible that the delayed/reduced weight gain during days 7-10 in $Ifi44^{-/-}$ mice was due to some defect in tissue repair, metabolism, or some other aspect of pathology that was not measured.

Given this data, I hypothesised that the weight loss phenotype would be present earlier in infection if $Ifi44^{-/-}$ mice had ISGs upregulated at baseline prior to infection. As such, I crossed $Ifi44^{-/-}$ mice with $Adar1^{mZa/mZa}$ mice, a previously described mouse model with a baseline IFN signature due to a mutation in the Zα domain of ADAR1 (41, 42). The ISG

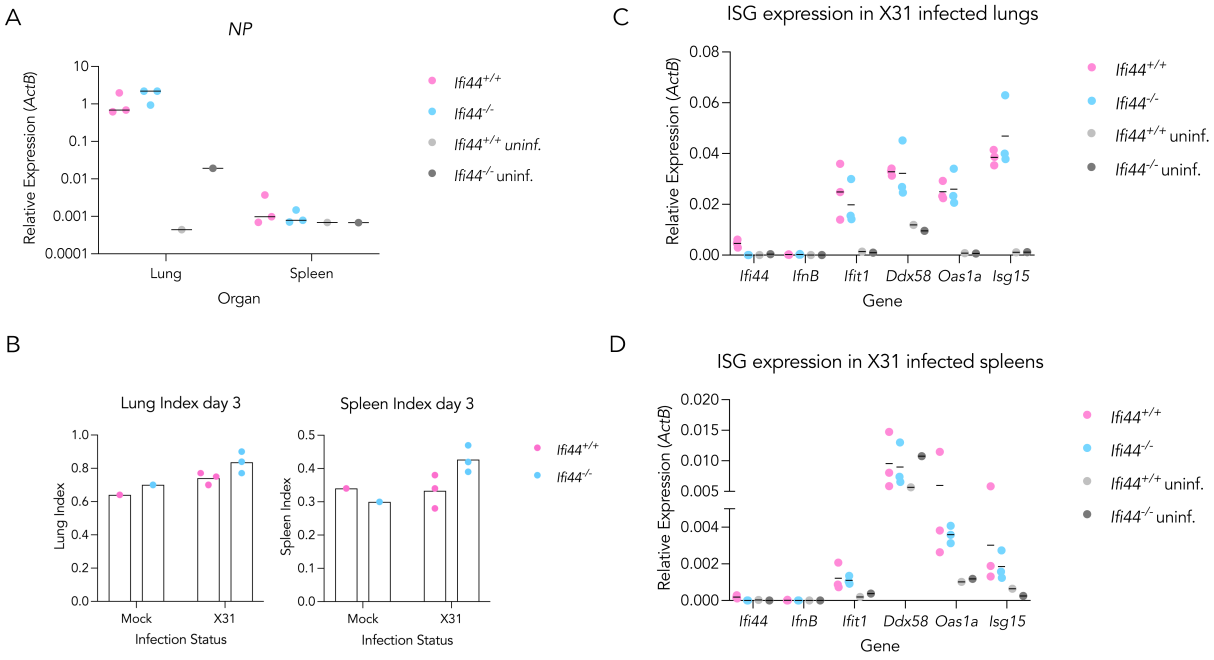


Figure 4.8: There is no difference in IAV infectivity in *Ifi44*$^{-/-}$ mice.

Mice were infected intranasally with 0.04 HAU IAV/X-31 or PBS and sacrificed at day 3 post infection. **A.** IAV titres in the lung were assessed through RNA extraction and RT-qPCR using an *NP* TaqMan probe. **B.** Lung and spleen index were calculated by dividing the organ weight by the total body weight. **C, D.** ISG expression was determined through RNA extraction and RT-qPCR for the indicated genes. (A-D) Each data point represents one biological replicate, and data points not shown were undetectable by qPCR. (A,C,D) Each data point is the average of two technical replicates.

signature was confirmed in *Adar1*$^{mZa/mZa}$ and double mutant mice through RT-qPCR and RNA sequencing of murine spleens (Figure 4.10A, B). These mice were infected with X-31 as before, and a weight curve obtained. *Adar1*$^{mZa/mZa}$ mice were protected from weight loss until day six, confirming a prior study (Figure 4.10C)(41). At day seven, there was a non-significant trend for the double mutant mice to have increased weight loss compared to *Adar1*$^{mZa/mZa}$ mice (Figure 4.10C). This experiment would benefit from extending the timepoint to day 10 as before, however time constraints and mutant mouse availability caused repeats to be deprioritised.

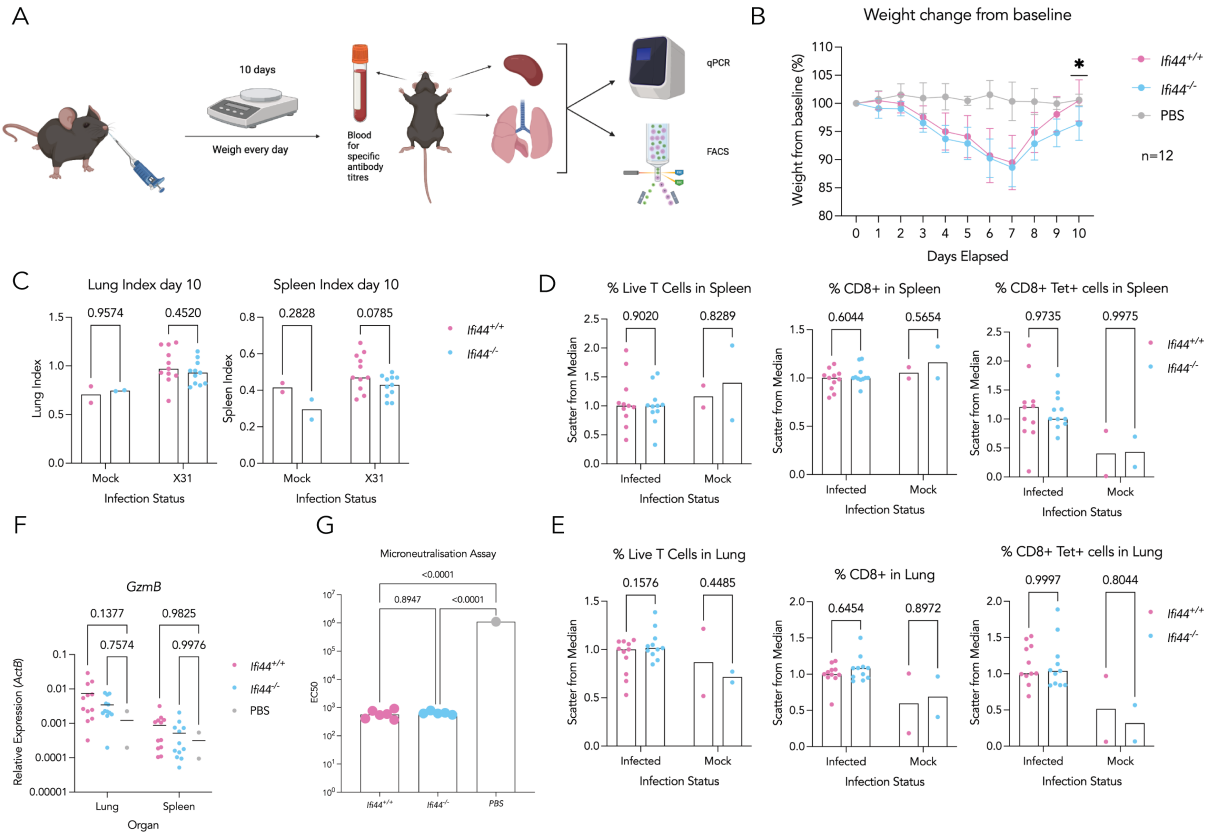


Figure 4.9: There is no difference in the adaptive immune response to IAV in *Ifi44*$^{-/-}$ mice.

A. Schematic of experiment. Mice were infected intranasally with 0.04 HAU IAV/X-31 or PBS and sacrificed at day 10 post-infection. **B.** Weight % change from baseline. **C.** Lung and spleen index were calculated by dividing the organ weight by the total body weight. **D, E.** Spleens and lungs were enzymatically digested and resulting cell suspensions were stained with relevant antibodies and fixed. T cell populations were analysed on an Attune Flow Cytometer. Tetramer peptide targetting IAV NP (ASNENMETM) was restricted by H-2D(b) (C57BL/6). In each instance, the median of the dataset for each genotype was set to 1, and each data point divided by this value to generate a plot of scatter about the median. **F.** RNA was isolated from indicated organs, and RT-qPCR performed for *GzmB*. **G.** Serum was collected, heat inactivated and used to neutralise previously titrated recombinant Influenza Virus-GFP. GFP was measured using a CLARIOstar Plus Microplate Reader, and EC50 determined. (B) each data point is the average of 12 biological replicates. (C, D, E) Each data point is one biological replicate. (F) Each data point is one biological replicate and the average of two technical replicates. (B-F) Data are pooled from two independent experiments. Statistical analyses were performed using (B) Mixed-effect analysis with Sidak's multiple comparisons tests or (C, D, F) two-way ANOVA with Sidak's multiple comparisons test or (G) One-way ANOVA with Turkey's multiple comparisons test. P value displayed, or *=p≤0.05, **=p≤0.01, ***=p≤0.001, ****=p≤0.0001. Unmarked lanes are not significant.

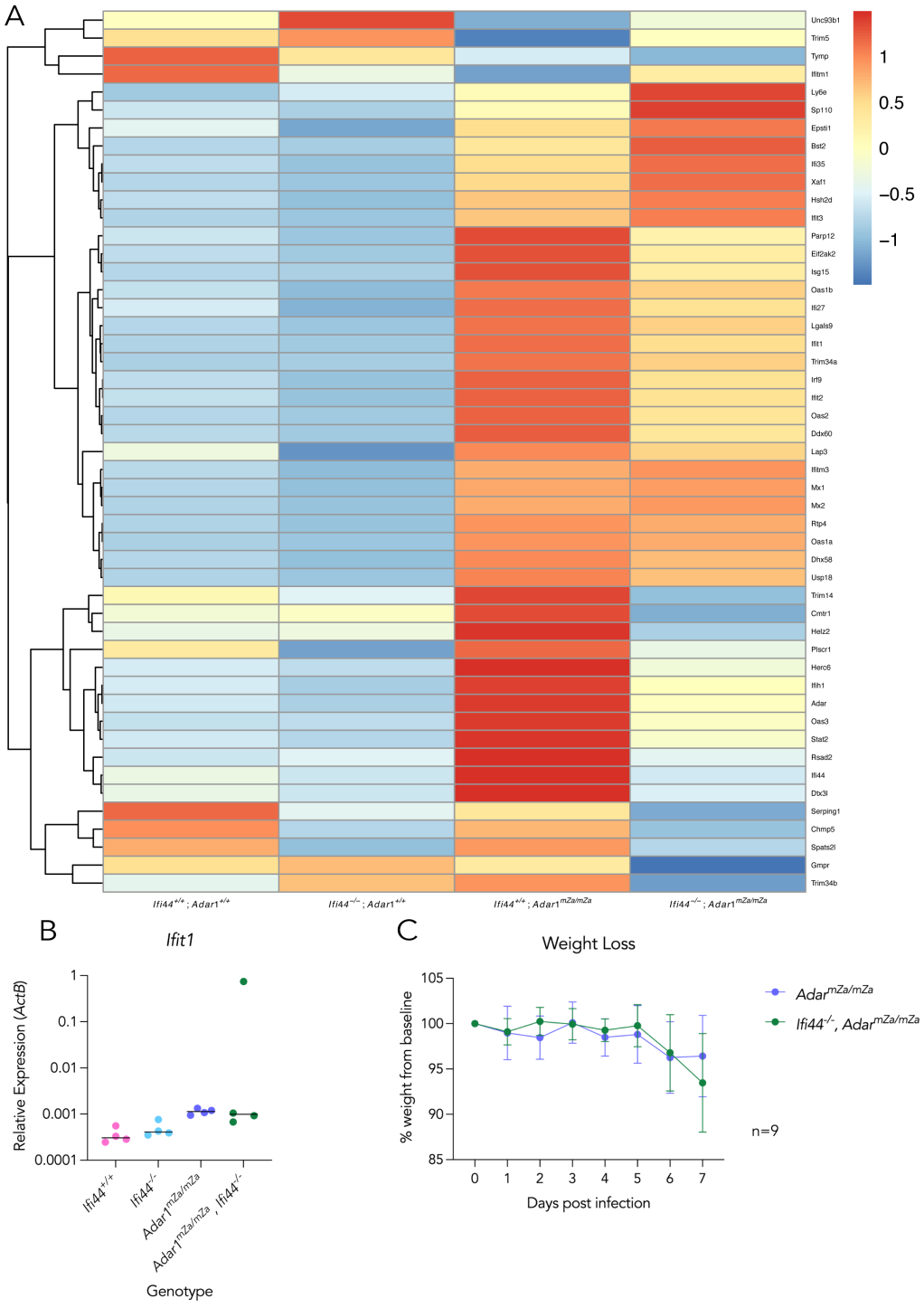


Figure 4.10: *Ifi44*$^{-/-}$; *Adar1*$^{mZa/mZa}$ mice display an interferon signature.

A. TPM-normalized expression in the spleen for a panel of ISGs in WT, *Ifi44*$^{-/-}$, *Adar1*$^{mZa/mZa}$ and *Ifi44*$^{-/-}$;*Adar1*$^{mZa/mZa}$ mice. Differential gene expression was assessed with DESeq2 (2). Analysis was performed by Tanja Davis and Aleksander Fedorov. **B.** RNA was isolated from spleen samples, and RT-qPCR performed for *Ifit1*. **C.** Mice were infected intranasally with 0.04 HAU IAV/X-31 or PBS and sacrificed at day 7 post infection. Weight % change from baseline depicted. (A) Averages from 4 mice per group, except *Ifi44*$^{-/-}$; *Adar1*$^{mZa/mZa}$ is one mouse. (B) Each data point is a biological replicate. (C) Data points represent the average of 9 mice.

4.7 There are no overt differences in the myeloid compartment in the spleen of *Ifi44*$^{-/-}$ mice

As IFI44 has been implicated in immune cell infiltration (7, 10-12, 14, 15, 40), I sought to discover whether there were any differences in the myeloid compartment of *Ifi44*$^{-/-}$ mice. To do this, mice were sacrificed, spleens removed and the myeloid compartment analysed through flow cytometry, using a gating strategy adapted from Rose et al 2012 (43) (Figure 4.11A). Flow cytometry revealed that there were no differences in the abundance of CD45^{+} cells, eosinophils, neutrophils, DCs, monocytes nor macrophages in the spleen at baseline in *Ifi44*$^{-/-}$ mice (Figure 4.11B).

4.8 IFI44 does not play a role in bacterial infection *ex vivo*

I next sought to address whether IFI44 is involved in anti-bacterial immunity, like some other aspects of the IFN pathway (44). For example, GBP proteins are IFN-induced GTPases which mediate protection against intracellular pathogens through direct binding and subsequent activation of the inflammasome (45-49). Additionally, *Ifi44l* clusters with GBP proteins when mapped using the co-essentially tool, possibly due to the shared P Loop NTPase domain (50). To evaluate whether *Ifi44* affects inflammasome activation, I stimulated BMDMs with LPS and subjected them to an ATP-pulse, and then measured IL-1β levels by ELISA in culture supernatants. There was no difference in IL-1β concentration in supernatants from *Ifi44*$^{-/-}$ BMDMs, indicating that *Ifi44* does not affect inflammasome activation in this setting (Figure 4.12A). However, since we used only LPS and the only read-out was secreted IL-1β, we decided to further test bacterial agonists and subsequent IL-1β concentration and cell death via LDH release. We sent BMDMs to Petr Broz in Switzerland, who kindly ran these assays for us. There was no difference in LDH release nor IL-1β secretion between *Ifi44*$^{+/+}$ and *Ifi44*$^{-/-}$ BMDMs in response to an NLRP3 agonist, an NLRC4 agonist, an AIM2 agonist or in response to stationary phase *Salmonella typhimurium*Δ*OrgA*Δ*FliC/FliB* or *Francisella* (Figure 4.12B, C). In all cases, cells were primed with LPS for four hours prior to infection or stimulation. Of note, while four hours of LPS stimulation is enough to upregulate early ISGs such as *Gbps*, *Ifi44* is a late ISG and may require longer priming with LPS to be upregulated in wild-type BMDMs. Thus, in this context, we did not discover a role for *Ifi44* in bacterial infection, however perhaps pre-treatment with IFN to upregulate *Ifi44* prior to stimulation with agonists or bacterial infection would be more informative. This experiment was not completed due to time constraints.

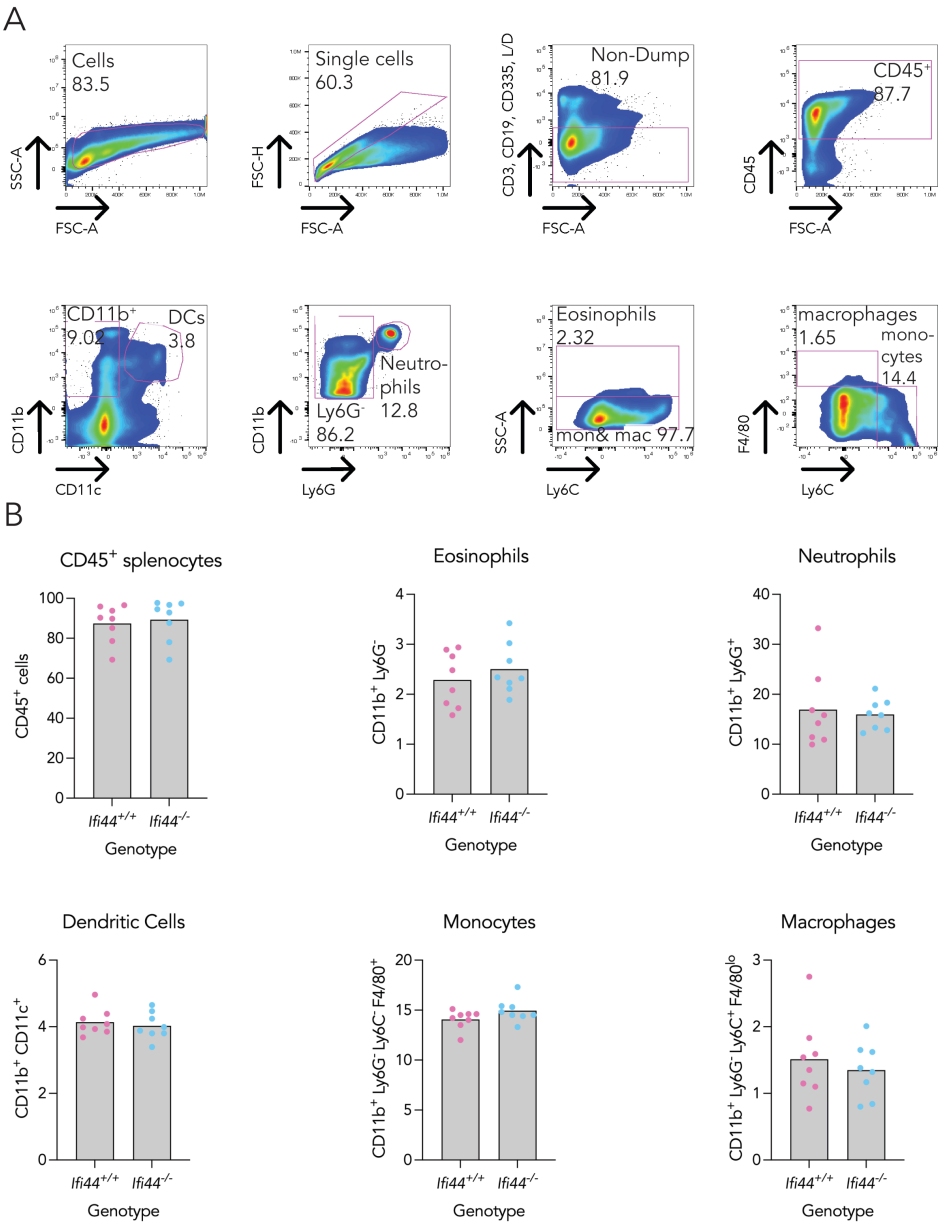


Figure 4.11: There are no overt differences in the myeloid compartment in the spleen of *Ifi44*$^{-/-}$ mice.

A. Splenic myeloid immunophenotyping gating strategy. **B.** Mice were sacrificed, and spleens and lungs were enzymatically digested and resulting cell suspensions were stained with relevant antibodies and fixed, then cell populations were analysed on LSR Fortessa X50 (Symphony A5) flow cytometer. (B) each data point represents one biological replicate. WT and *Ifi44*$^{-/-}$ mice were littermates.

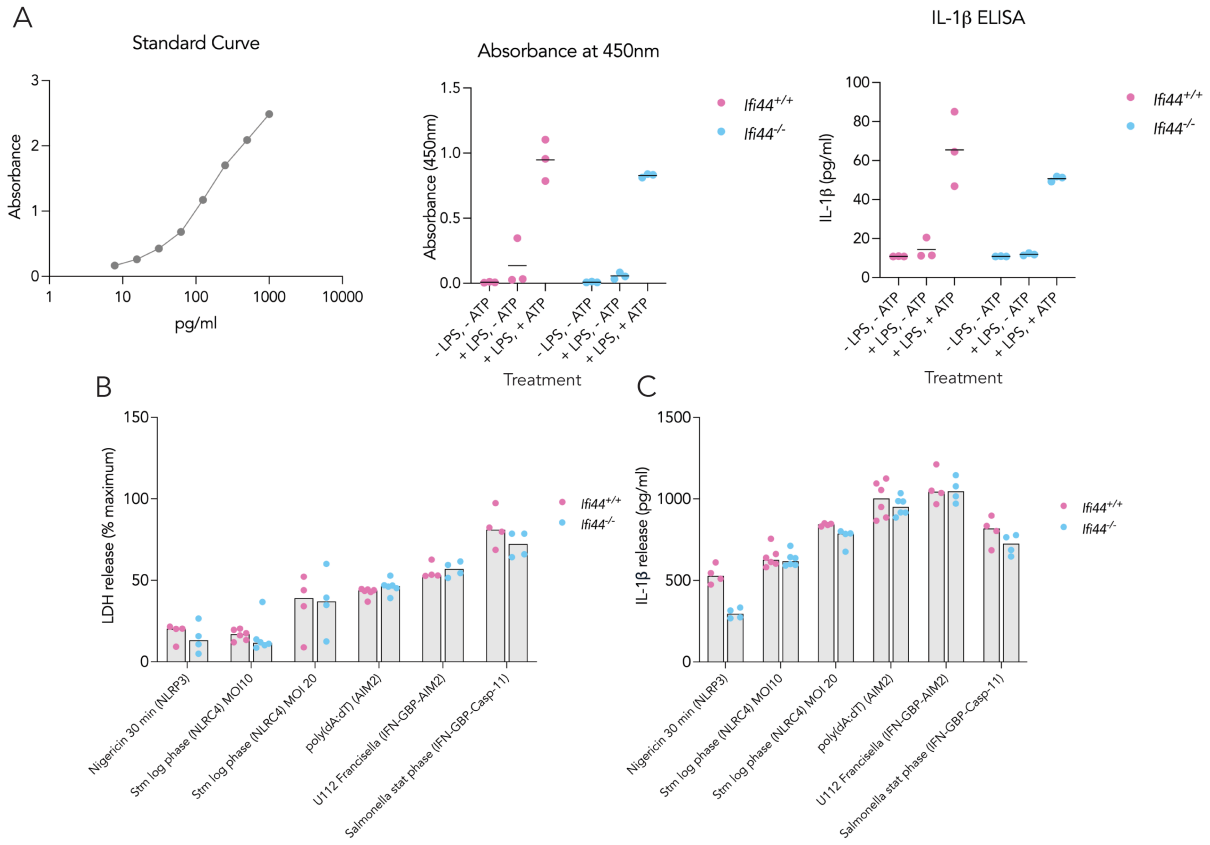


Figure 4.12: *Ifi44* is not involved in the response to bacterial infection.

A. BMDMs were stimulated with LPS and an ATP pulse, resulting supernatant harvested and IL-1β concentration determined through an ELISA. **B, C.** Hindlegs from C57BL/6N mice were removed and shipped to the Broz lab in Lausanne, Switzerland. The Broz lab derived BMDMs and primed these with LPS for four hours prior to addition of stimuli. To activate the AIM2 inflammasome, BMDMs were stimulated with *Francisella novicida* U112 (MOI 100) or stationary phase S*almonella typhimurium deltaOrgA deltaFliC/FljB* (MOI 100) for 18 hours. To activate the NLRP3 and NLRP4 inflammasomes, BMDMs were stimulated with Nigericin (5 µg/ml), log-phase wild-type *Salmonella* (MOI 10 or 20) or 0.2 µg poly(dAdT) transfection for one hour. In all cases, LDH and IL-1β release were measured through ELISAs.

4.9 Summary for Chapter 4

In this chapter, I found no evidence that IFI44 regulates the IFN response, nor that overexpression of IFI44, IFI44L or both results in differences in viral infectivity *in cellulo*. In addition, *Ifi44*$^{-/-}$ BMDMs responded in an analogous way to wild-type BMDMs when challenged with a range of bacterial stimuli. Despite this, *Ifi44*$^{-/-}$ mice displayed a delayed recovery post-IAV/X-31 infection at day 10, indicating that *Ifi44* might be important at the later stages of infection or in immunopathology. Interestingly, this was not attributed to differences in neutralising antibody titres nor specific cytotoxic T cells. However, the

observed delayed weight recovery in *Ifi44*$^{-/-}$ mice could due to a pathology not measured in this study, such as metabolism. Indeed, this could be attributed to iron metabolism, as discussed next in Chapter 5.

References for Chapter 4

1. D. C. Busse et al., Interferon-Induced Protein 44 and Interferon-Induced Protein 44-Like Restrict Replication of Respiratory Syncytial Virus. J Virol 94, (2020).
2. L. Li, Y. A. Ni, Z. Song, Z. Yi, F. Wang, Identification of pathogenic genes and transcription factors in respiratory syncytial virus. BMC Pediatr 21, 27 (2021).
3. C. Carlton-Smith, R. M. Elliott, Viperin, MTAP44, and Protein Kinase R Contribute to the Interferon-Induced Inhibition of Bunyamwera Orthobunyavirus Replication. Journal of Virology 86, 11548-11557 (2012).
4. D. Power et al., IFI44 suppresses HIV-1 LTR promoter activity and facilitates its latency. Virology 481, 142-150 (2015).
5. M. Sun et al., Screening Host Antiviral Proteins under the Enhanced Immune Responses Induced by a Variant Strain of Porcine Epidemic Diarrhea Virus. Microbiol Spectr 10, e0066122 (2022).
6. M. L. DeDiego, A. Nogales, L. Martinez-Sobrido, D. J. Topham, Interferon-Induced Protein 44 Interacts with Cellular FK506-Binding Protein 5, Negatively Regulates Host Antiviral Responses, and Supports Virus Replication. mBio 10, (2019).
7. Q. Zheng, D. Wang, R. Lin, Q. Lv, W. Wang, *IFI44* is an immune evasion biomarker for SARS-CoV-2 and *Staphylococcus aureus* infection in patients with RA. Front Immunol 13, 1013322 (2022).
8. B. Kaczkowski et al., Integrative analyses reveal novel strategies in HPV11,-16 and -45 early infection. Sci Rep 2, 515 (2012).
9. L. Shen et al., Identification and Validation of *IFI44* as Key Biomarker in Lupus Nephritis. Front Med (Lausanne) 8, 762848 (2021).
10. H. Xu, J. Chen, Y. Wang, Y. Wu, Y. Liang, *SELL* and *IFI44* as potential biomarkers of Sjögren's syndrome and their correlation with immune cell infiltration. Genes Genet Syst, (2021).
11. Y. Wang et al., Identification and Clinical Correlation Analysis of IFI44 in Systemic Lupus Erythematosus Combined with Bioinformatics and Immune Infiltration Analysis. J Inflamm Res 16, 3219-3231 (2023).
12. X. Zhao et al., Identification of key biomarkers and immune infiltration in systemic lupus erythematosus by integrated bioinformatics analysis. J Transl Med 19, 35 (2021).
13. D. Rupa et al., ACSL4 upregulates IFI44 and IFI44L expression and promotes the proliferation and invasiveness of head and neck squamous cell carcinoma cells. Cancer Sci, (2024).
14. X. Wu et al., Identification of a Novel Signature and Construction of a Nomogram Predicting Overall Survival in Clear Cell Renal Cell Carcinoma. Front Genet 11, 1017 (2020).

15. H. Pan et al., Interferon-Induced Protein 44 Correlated With Immune Infiltration Serves as a Potential Prognostic Indicator in Head and Neck Squamous Cell Carcinoma. Front Oncol 10, 557157 (2020).
16. O. Mirzalieva, M. Juncker, J. Schwartzenburg, S. Desai, ISG15 and ISGylation in Human Diseases. Cells 11, (2022).
17. Y. C. Perng, D. J. Lenschow, ISG15 in antiviral immunity and beyond. Nat Rev Microbiol 16, 423-439 (2018).
18. A. Pinto-Fernandez et al., Deletion of the deISGylating enzyme USP18 enhances tumour cell antigenicity and radiosensitivity. Br J Cancer 124, 817-830 (2021).
19. V. Jové et al., Type I interferon regulation by USP18 is a key vulnerability in cancer. iScience 27, 109593 (2024).
20. V. François-Newton et al., USP18-based negative feedback control is induced by type I and type III interferons and specifically inactivates interferon α response. PLoS One 6, e22200 (2011).
21. G. Liu et al., ISG15-dependent activation of the sensor MDA5 is antagonized by the SARS-CoV-2 papain-like protease to evade host innate immunity. Nat Microbiol 6, 467-478 (2021).
22. M. Albert, M. Becares, M. Falqui, C. Fernandez-Lozano, S. Guerra, ISG15, a Small Molecule with Huge Implications: Regulation of Mitochondrial Homeostasis. Viruses 10, (2018).
23. M. Zhang et al., ISGylation in Innate Antiviral Immunity and Pathogen Defense Responses: A Review. Front Cell Dev Biol 9, 788410 (2021).
24. Z. Sandy, I. C. da Costa, C. K. Schmidt, More than Meets the ISG15: Emerging Roles in the DNA Damage Response and Beyond. Biomolecules 10, (2020).
25. G. Vere et al., Targeting the Ubiquitylation and ISGylation Machinery for the Treatment of COVID-19. Biomolecules 12, (2022).
26. P. Dhungel, F. M. Cantu, J. A. Molina, Z. Yang, Vaccinia Virus as a Master of Host Shutoff Induction: Targeting Processes of the Central Dogma and Beyond. Pathogens 9, (2020).
27. J. A. Molina, Z. Yang, Rapid and quantitative evaluation of vaccinia virus-induced host shutoff using newly generated cell lines stably expressing secreted Gaussia luciferase. J Med Virol 94, 3811-3819 (2022).
28. J. B. Reus, G. S. Trivino-Soto, L. I. Wu, K. Kokott, E. S. Lim, SV40 Large T Antigen Is Not Responsible for the Loss of STING in 293T Cells but Can Inhibit cGAS-STING Interferon Induction. Viruses 12, (2020).
29. J. L. Baker, B. M. Ward, Development and comparison of a quantitative TaqMan-MGB real-time PCR assay to three other methods of quantifying vaccinia virions. J Virol Methods 196, 126-132 (2014).

30. K. Mottet, B. Bareiss, C. D. Milne, M. Barry, The poxvirus encoded ubiquitin ligase, p28, is regulated by proteasomal degradation and autoubiquitination. Virology 468-470, 363-378 (2014).
31. B. T. Nerenberg et al., The poxviral RING protein p28 is a ubiquitin ligase that targets ubiquitin to viral replication factories. J Virol 79, 597-601 (2005).
32. G. J. Kotwal, B. Moss, Analysis of a large cluster of nonessential genes deleted from a vaccinia virus terminal transposition mutant. Virology 167, 524-537 (1988).
33. J. A. Symons et al., The vaccinia virus C12L protein inhibits mouse IL-18 and promotes virus virulence in the murine intranasal model. J Gen Virol 83, 2833-2844 (2002).
34. J. W. Schoggins, Interferon-Stimulated Genes: What Do They All Do? Annu Rev Virol 6, 567-584 (2019).
35. E. Duong et al., Type I interferon activates MHC class I-dressed CD11b(+) conventional dendritic cells to promote protective anti-tumor CD8(+) T cell immunity. Immunity 55, 308-323.e309 (2022).
36. M. T. Villanueva, Unmasking cancer cell character. Nature Reviews Cancer 19, 130-130 (2019). 37. J. J. Ishizuka et al., Loss of ADAR1 in tumours overcomes resistance to immune checkpoint blockade. Nature 565, 43-48 (2019).
38. H. Lou, G. S. Ling, X. Cao, Autoantibodies in systemic lupus erythematosus: From immunopathology to therapeutic target. Journal of Autoimmunity 132, 102861 (2022).
39. A. A. Herrada et al., Innate Immune Cells' Contribution to Systemic Lupus Erythematosus. Front Immunol 10, 772 (2019).
40. Y. Wang, Y. Chen, B. Zhu, L. Ma, Q. Xing, A Novel Nine Apoptosis-Related Genes Signature Predicting Overall Survival for Kidney Renal Clear Cell Carcinoma and its Associations with Immune Infiltration. Front Mol Biosci 8, 567730 (2021).
41. Q. Tang et al., Adenosine-to-inosine editing of endogenous Z-form RNA by the deaminase ADAR1 prevents spontaneous MAVS-dependent type I interferon responses. Immunity 54, 1961-1975.e1965 (2021).
42. R. de Reuver, J. Maelfait, Novel insights into double-stranded RNA-mediated immunopathology. Nat Rev Immunol 24, 235-249 (2024).
43. S. Rose, A. Misharin, H. Perlman, A novel Ly6C/Ly6G-based strategy to analyze the mouse splenic myeloid compartment. Cytometry A 81, 343-350 (2012).
44. G. M. Boxx, G. Cheng, The Roles of Type I Interferon in Bacterial Infection. Cell Host Microbe 19, 760-769 (2016).
45. K. Tretina, E. S. Park, A. Maminska, J. D. MacMicking, Interferon-induced guanylate-binding proteins: Guardians of host defense in health and disease. J Exp Med 216, 482-500 (2019).
46. J. C. Santos et al., Human GBP1 binds LPS to initiate assembly of a caspase-4 activating platform on cytosolic bacteria. Nat Commun 11, 3276 (2020).

47. D. M. Cerqueira et al., Guanylate-binding protein 5 licenses caspase-11 for Gasdermin-D mediated host resistance to *Brucella abortus* infection. PLoS Pathog 14, e1007519 (2018).
48. M. P. Wandel et al., Guanylate-binding proteins convert cytosolic bacteria into caspase-4 signaling platforms. Nat Immunol 21, 880-891 (2020).
49. M. P. Wandel et al., GBPs Inhibit Motility of *Shigella flexneri* but Are Targeted for Degradation by the Bacterial Ubiquitin Ligase IpaH9.8. Cell Host Microbe 22, 507-518.e505 (2017).
50. M. Wainberg et al., A genome-wide atlas of co-essential modules assigns function to uncharacterized genes. Nature Genetics 53, 638-649 (2021).

Chapter 5

IFI44 and Erythrocyte Homeostasis

While *IFI44* is a prototypical ISG, highly expressed after infection and in type I interferonopathies, I had not uncovered a role for IFI44 during infection with viruses or bacteria - although it is possible that VACV cleaves/degrades IFI44 to circumvent yet to be defined anti-viral activity. As such, I decided to undertake a non-biased, hypothesis-generating approach to provide novel insights into the molecular pathways in which IFI44 acts and provide new experimental avenues. I performed transcriptomic analysis of spleens and livers from unstimulated and uninfected *Ifi44*$^{+/+}$ and *Ifi44*$^{-/-}$ mice using RNA sequencing. I chose two different organs to increase the likelihood of uncovering a molecular phenotype: spleen, as it is an important organ in the immune system, and liver as IFI44 was first discovered in hepatocytes of chimpanzees (1). In *Ifi44*$^{-/-}$ mice, 19,299 genes were found to be differentially expressed in the spleen and 17,466 in the liver (Figure 5.1 A-C; analysis performed by Rachel Rigby).

5.1 Genes associated with iron recycling are significantly downregulated in *Ifi44*$^{-/-}$ spleens

To determine the biological processes that these differentially expressed genes were involved in, gene ontology analysis was performed by Rachel Rigby. For the liver, *Ifi44*$^{-/-}$ mice displayed down-regulation of genes involved in neutrophil activation, complement activation, myeloid cell differentiation and the innate immune response (Figure S17). However, at most, these genes made up only 5-10% of the total GO category, with very few total genes differentially expressed for each category. In addition, since I had already performed multiple infection studies and observed no significant differences (see sections 4.5, 4.6, 4.7 and 4.8), I decided not to follow up on this finding. Further, this phenotype was not found in the spleen (Figure S19) and myeloid immunophenotyping in the spleens

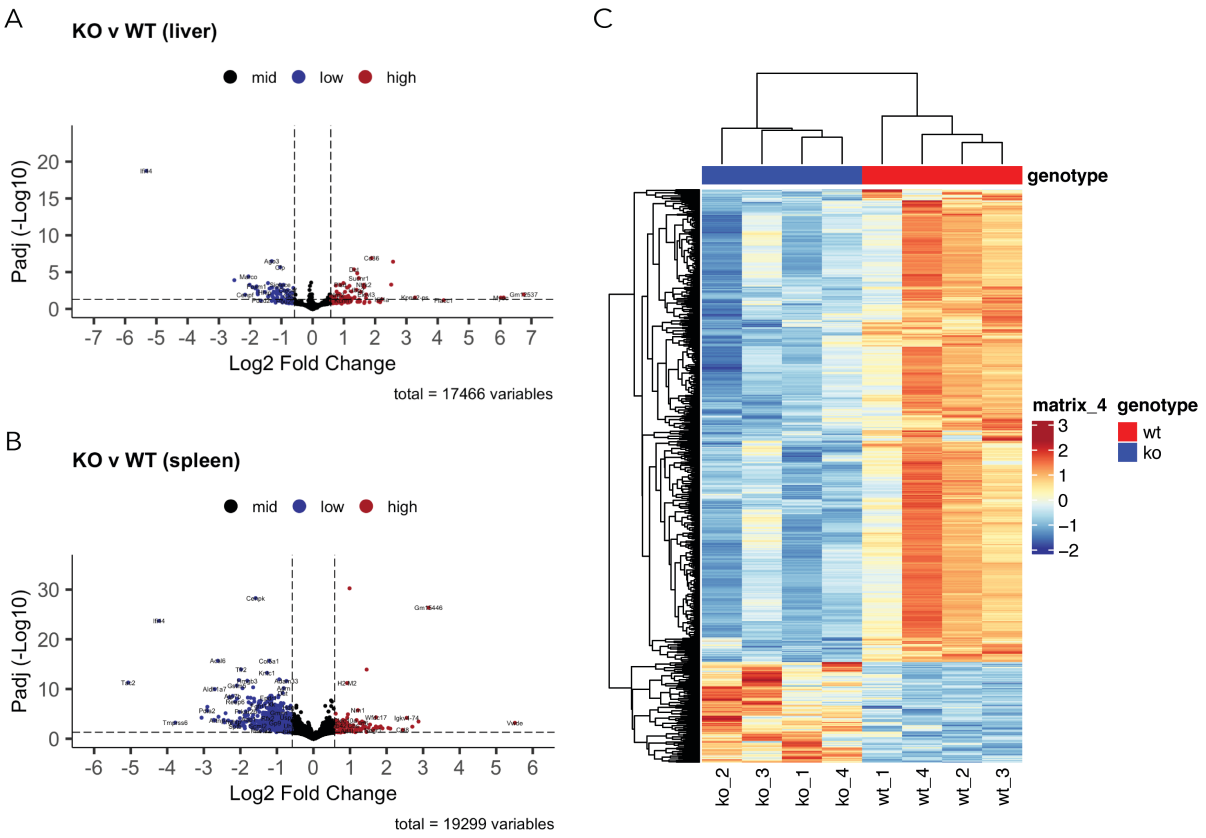


Figure 5.1: Differentially expressed genes in spleens and livers from *Ifi44*$^{-/-}$ mice.

A, B. Poly(A) RNA sequencing of *Ifi44*$^{+/+}$ and *Ifi44*$^{-/-}$ liver (A) and splenic (B) RNA. Differential gene expression was assessed with DESeq2 (2). All P values were adjusted for multiple testing using the Benjamini–Hochberg method, and results with P adjusted ≥ 0.05 were considered significant. **C.** Heatmap of differentially regulated genes in *Ifi44*$^{-/-}$ spleens. (A, B) Data is the average of four biological repeats. (C) Each column represents an individual biological replicate. RNA sequencing analysis was performed by Rachel Rigby, Tanja Davis and Aleksandr Fedorov.

of *Ifi44*$^{-/-}$ mice showed no differences in myeloid populations (Figure 4.11). Similarly, we did not find strong phenotypes in up-regulated genes in the liver and did not follow up on these findings either (Figure S18), choosing instead to focus on the spleen. In the spleen, many genes in the GO categories for haem biosynthesis (GO:0006783) and erythrocyte homeostasis (GO:0034101) were significantly downregulated in *Ifi44*$^{-/-}$ mice (Figure 5.2A; Figure S19) – indicating an exciting, unprecedented role for IFI44, or more widely for an ISG, in iron homeostasis. Almost every gene in the haem biosynthetic pathway was downregulated, for example, *Urod*, *Uros* and *Sptb* – all of which are enzymes directly involved in the synthesis of haem (Figure 5.2B). Further, genes involved in the recycling of erythrocytes, for example *Cd163* (a haem scavenging receptor), *Slc40a1* (ferroportin; the only known cellular iron exporter) and *Hmox1* (an enzyme converting haem to iron)

were also downregulated (Figure 5.2B). Genes involved in iron storage (e.g. ferritin genes *Ftl1* and *Fth1* (3)), iron transport (e.g. *Slc11a2* (4) and *Zip14* (5)) and iron redox activity (e.g. *Gclc* (6) and *Ddit3* (7)) were not significantly downregulated in the RNA sequencing dataset (data not shown), nor in an RT-qPCR using RNA from *Ifi44*$^{+/+}$ and *Ifi44*$^{-/-}$ spleens (Figure 5.2C). As such, the downregulation of genes in *Ifi44*$^{-/-}$ spleens was restricted to erythrocyte homeostasis and haem biosynthesis, and was not more widely shared with genes involved in iron storage or redox regulation. I hypothesised that the downregulation of haem biosynthetic genes in *Ifi44*$^{-/-}$ spleens would be exacerbated in an infection setting, since *Ifi44* is an ISG and *Ifi44* induction was observed in *Ifi44*$^{+/+}$ mice at day three of infection (Figure 3.5). Interestingly, the downregulation of haem biosynthetic genes observed in infected naïve mice was reduced in this context (Figure 5.2D). This could be due relative sensitivity of qPCR vs RNA sequencing at detecting small fold-changes. Equally, there is much complexity during an infection, with many other factors at play that could exhibit an effect on this observed phenotype.

Genes upregulated in *Ifi44*$^{-/-}$ spleens were involved in many B cell related pathways (Figure S20A). This could be indicative of differences in B cell populations between the two genotypes: perhaps *Ifi44*$^{-/-}$ mice have more splenic B cells. However, flow cytometric analysis of the spleen determined that while there was a non-significant increase in bulk B220^{+} cells in *Ifi44*$^{-/-}$ mice at day three of IAV/X-31 infection, baseline levels between the two genotypes were very similar (Figure S20B). However, it should be noted that I only used one biological replicate for the uninfected control in this instance, and more replicates would be necessary to draw conclusions. In addition, in the lung (the primary infection site for IAV/X-31), the opposite was true (Figure S20B). As such, I did not follow up this finding further.

5.2 *Ifi44*$^{-/-}$ mice have microcytic RBCs

As genes associated with iron recycling and erythrocyte homeostasis were significantly downregulated in *Ifi44*$^{-/-}$ mice (Figure 5.2A, B), I aimed to discover whether these mice were anaemic, as anaemia is one of the most common presentations of iron deficiency (8). To do this, cardiac punctures were performed on *Ifi44*$^{-/-}$ and *Ifi44*$^{+/+}$ mice and their blood was analysed using an automated haemocytometer. RBCs from *Ifi44*$^{-/-}$ mice had a significantly lower mean corpuscular volume (MCV) and a non-significant trend to have a lower mean corpuscular haemoglobin (MCH) accompanied by a slightly yet non-significant higher RBC count (Figure 5.3A). The lower MCH observed in *Ifi44*$^{-/-}$ mice could be indicative of the smaller MCV, as less haemoglobin can be loaded per RBC. Agreeing with this, the ratio of haem:RBC relative to size (MCHC) is the same between

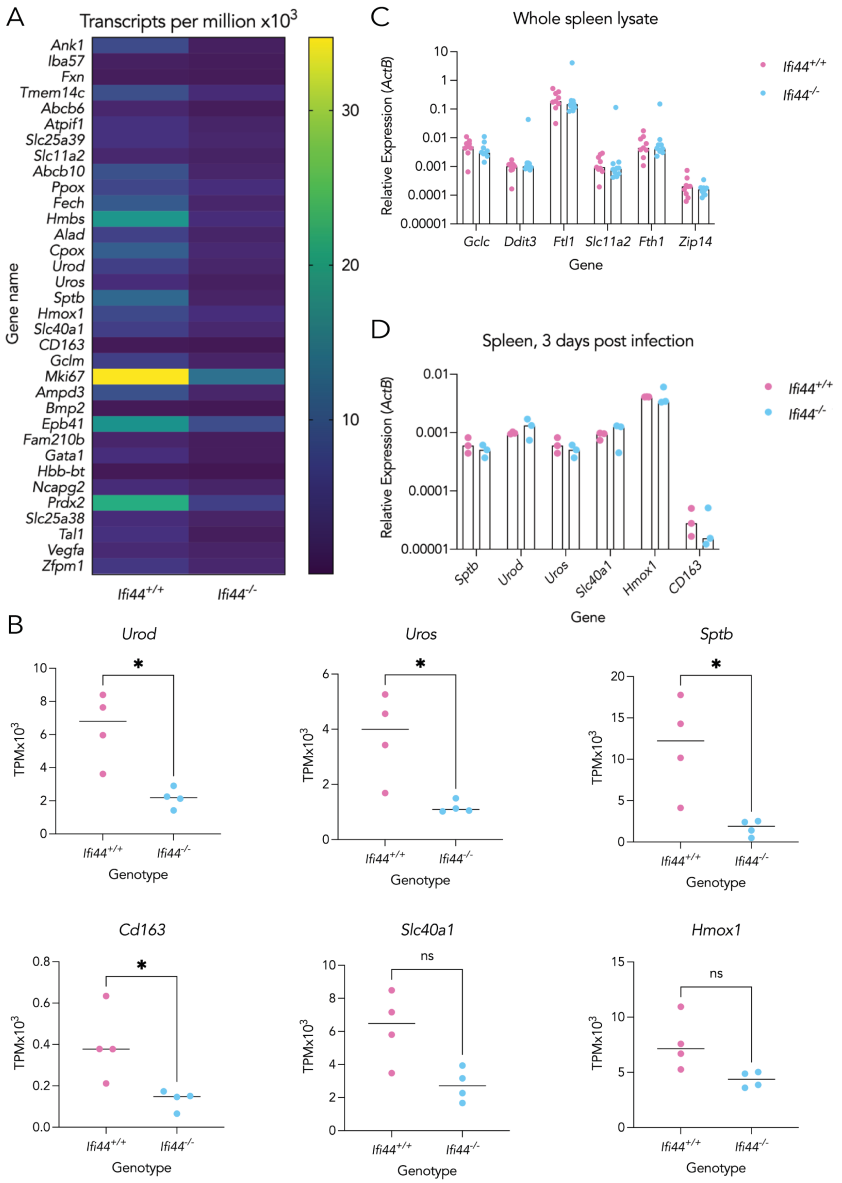


Figure 5.2: Genes involved in erythrocyte homeostasis are downregulated in *Ifi44*$^{-/-}$ mice.
A, B. TPM-normalized expression of genes differentially expressed in *Ifi44*$^{-/-}$ spleens in the GO categories 'erythrocyte homeostasis' and 'haem biosynthesis' (adj. p-value < 0.05). Differential gene expression was assessed with DESeq2 (2). Gene ontology analysis was conducted using the gprofiler package (56). Analysis performed by Rachel Rigby, Tanja Davis and Aleksander Fedorov. **C, D.** RNA was isolated from murine spleens (C) at baseline or (D) day 3 post-infection with 0.04 HAU IAV/X-31 and RT-qPCR performed for the indicated genes. (A) Each column is the average of four biological repeats. (B) Each data point is one biological replicate. (C, D) Each data point is one biological replicate and is the average of two technical replicates. Statistical analysis was performed using unpaired T-test. *=p<0.05, ns=not significant.

the two genotypes, while the proportion of RBCs in the blood (HCT) is slightly higher in *Ifi44*$^{-/-}$ (Figure S21A). The observed increase in RBC count may explain why the mice were phenotypically healthy and displayed no ill effects. There was no difference observed in total haemoglobin count, likely because there are slightly more RBCs circulating, which compensates for the lower MCH (Figure 5.3A; Figure S21A). Interestingly, genes encoding different haemoglobin subunits are significantly downregulated in *Ifi44*$^{-/-}$ spleens (Figure S21B-E). In the future, I plan to analyse haemoglobin transcript levels in the bone marrow - where haemoglobinisation of erythroid cells occurs.

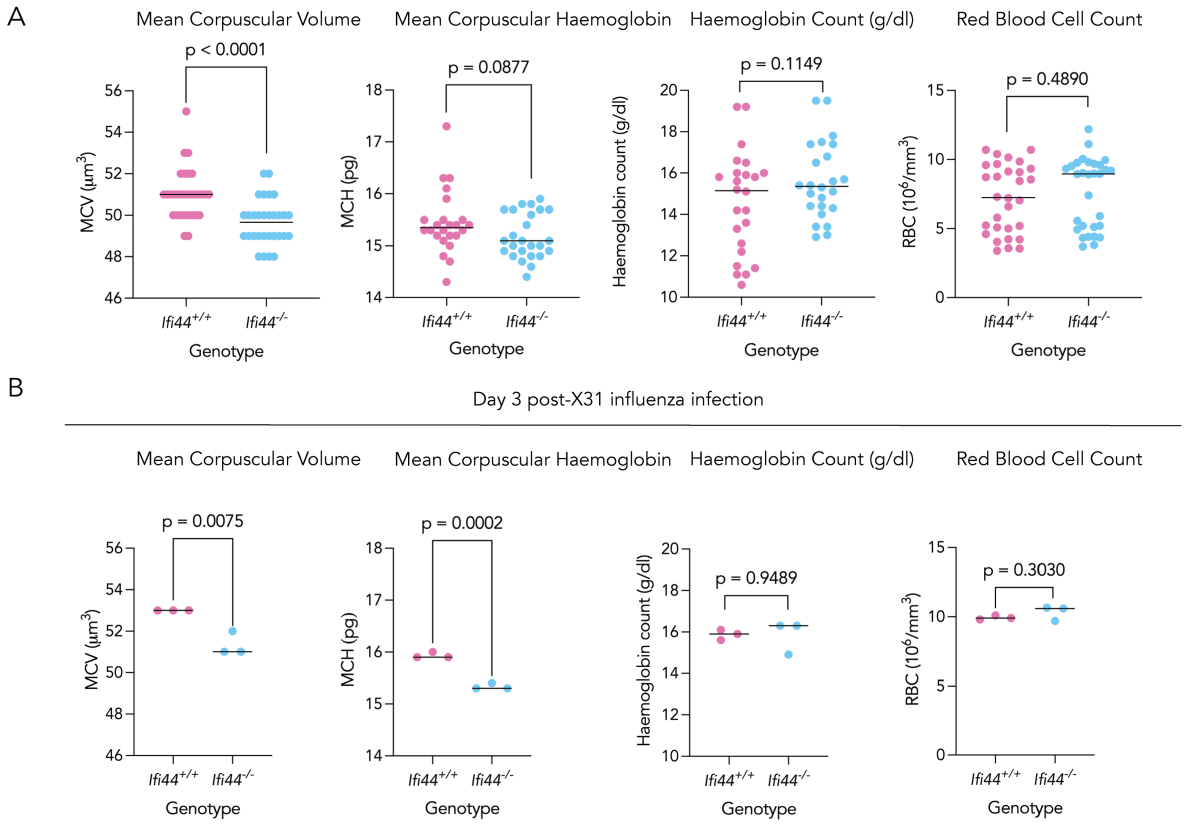


Figure 5.3: *Ifi44*$^{-/-}$ mice display a mild, microcytic anaemia, which is unchanged in IAV/X-31 infection.

A. *Ifi44*$^{+/+}$ and *Ifi44*$^{-/-}$ mice were sacrificed through exsanguination under terminal anaesthesia, and blood collected into EDTA-coated microtainers to prevent clotting. Blood was then analysed using a Pentra ES-60 machine. **B.** *Ifi44*$^{+/+}$ and *Ifi44*$^{-/-}$ mice were infected intranasally with 0.04 HAU IAV/X-31 and sacrificed 3 days post-infection, followed by analysis as in (A). (A) Each data point represents one biological replicate. Data from six independent experiments have been pooled. (B). Each data point represents one biological replicate from one independent experiment. Statistical analysis was performed using unpaired T-test, p value indicated. *Ifi44*$^{+/+}$ and *Ifi44*$^{-/-}$ mice were littermates.

To determine whether observed abnormal blood parameters were exacerbated or rescued

during infection, *Ifi44*$^{+/+}$ and *Ifi44*$^{-/-}$ mice infected with IAV/X-31 were sacrificed at day 3 of infection through cardiac puncture, and blood assayed as before. There was no change to the phenotype in this setting (Figure 5.3B). However, as RBCs circulate for 40 days in mice before renewal, perhaps a long-term chronic infection model would have been more appropriate to determine the effect of inflammation or infection on this phenotype.

Supporting our data, the International Mouse Phenotyping Consortium made an *Ifi44*$^{-/-}$ mouse on a C57BL/6 background (9, 10). These mice show a (non-significant) reduction in MCH, an increased RBC count and similar total haemoglobin levels, just as we observed (Figure S22A-F). They observe no difference in MCV, however as only 7 mice were tested, this might not be powered enough to observe the subtle difference that we determined (Figure S22F). Interestingly, their mice show a significantly increased basophil and eosinophil count accompanying this (Figure S22A).

Anaemia can be subcategorised into microcytic, normocytic or macrocytic, based on MCV values. As *Ifi44*$^{-/-}$ mice had smaller MCV than the wild-type, they can be considered to have microcytes. In humans, iron deficiency anaemia is the most common presentation of microcytic anaemia (11-14), along with anaemia of inflammation (AoI) (12). In addition, erythropoiesis can directly affect MCV, as a reduced number of erythroblastic precursors can result in mature RBCs with smaller MCVs (15) and iron-limited erythropoiesis can also result in smaller MCV (16, 17). In mice, *TfR1* haploinsufficiency or dysfunctions in components of TfR1 endocytosis results in microcytic anaemia (14, 18). In addition, IRP proteins post-translationally regulate the expression of TfR1, ferritin and other iron metabolism proteins, and *Irp2*$^{-/-}$ mice show a mild microcytic anaemia, likely as a result of iron-limited erythropoiesis (16).

Microcytes in *Ifi44*$^{-/-}$ mice cannot be attributed to iron deficiency anaemia, as these mice did not display a decrease in total haemoglobin levels (although there is reduced expression of transcript level haemoglobin). AoI also does not appear to be contributing to microcytic anaemia, as there was no difference in transcript level *Hamp* (Hepcidin mRNA) in the liver between the two genotypes (Figure 5.4A). Further, there was no difference in transcript level *Il6* in the spleen at baseline as determined through RNA-sequencing, and only a very low level was expressed (data not shown). To induce *Il6* expression, mice were infected intranasally with IAV/X-31 virus and sacrificed 10-days post infection. There was no transcript level difference in *Il6* in the spleen between the two genotypes under these conditions (Figure 5.4B). However, it should be noted that serum protein levels for hepcidin or IL6 were not tested due to time constraints. Interestingly, splenic transcript levels of *TfR1* were significantly downregulated in *Ifi44*$^{-/-}$, accompanied by a non-significant decrease in total *Trf* (transferrin) (Figure 5.4C). These differences in *TfR1* may contribute towards the microcytic anaemia observed in *Ifi44*$^{-/-}$ (14, 18). However,

there was no decrease observed in TfR1 (aka CD71) expression on Ter119$^+$ cells in the bone marrow of *Ifi44*$^{-/-}$ mice (Figure 5.4D) or Ter119$^+$ cells in the spleen of *Ifi44*$^{-/-}$ mice (Figure 5.4E). As RNA sequencing was performed on bulk splenic RNA, I additionally analysed the total expression level of CD71 in total splenic cells, however there was no difference between the two genotypes (Figure 5.4F). Therefore, AoI does not appear to be contributing towards the microcytic phenotype observed in *Ifi44*$^{-/-}$ mice.

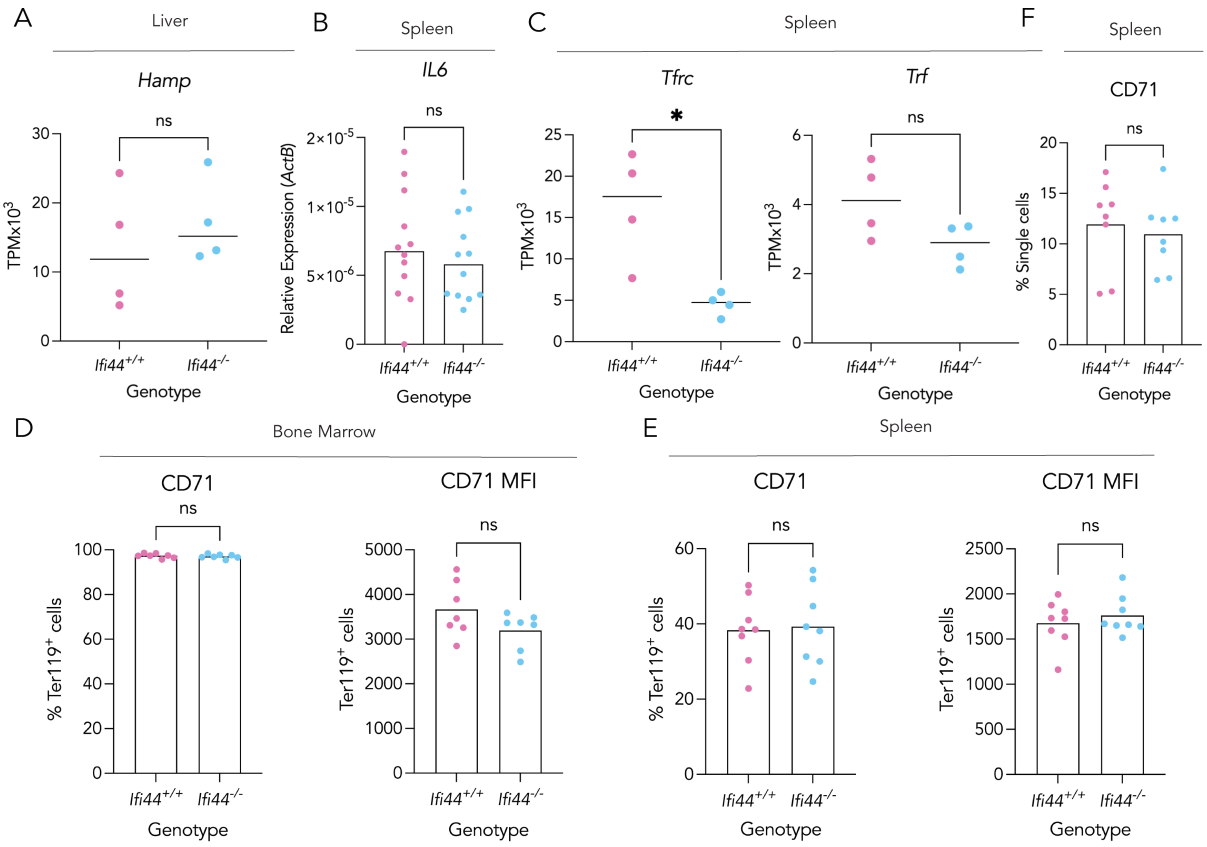


Figure 5.4: *Ifi44*$^{-/-}$ mice do not show signs of AI.

A, C. Differential gene expression of indicated genes. Analysis performed as in Figure 5.2. **B.** *Ifi44*$^{+/+}$ and *Ifi44*$^{-/-}$ mice were infected intranasally with 0.04 HAU IAV/X-31 or PBS and sacrificed 10 days post-infection. RNA was isolated from spleens using TriZol reagent, and RT-qPCR performed for *Il6*. **D.** Hindlegs were harvested from *Ifi44*$^{+/+}$ and *Ifi44*$^{-/-}$ mice, and CD71 expression in Ter119$^+$ cells in the bone marrow was analysed on an Attune NxT Flow Cytometer. **E, F.** Spleens were harvested from *Ifi44*$^{+/+}$ and *Ifi44*$^{-/-}$ mice and enzymatically digested. CD71 expression was analysed on an Attune NxT Flow Cytometer. (A-F) Each data point represents one biological replicate. (B, D) Data is pooled from two independent experiments. Statistical analysis was performed using unpaired T-test. *=p<0.05, **=p<0.01, ***=p<0.001, ****=p<0.0001, ns = not significant.

5.3 Erythroid progenitor populations in the bone marrow and spleen from *Ifi44*$^{-/-}$ mice are indistinguishable from those in wild-type mice

Dysfunctional erythropoiesis can result in microcytes (15, 19-21). To study whether erythropoiesis differed in *Ifi44*$^{-/-}$ mice, flow cytometry was performed on murine bone marrow, and erythrocytic precursors identified through CD44 staining (22) (Figure 5.5A, B). There were no detectable differences in erythrocytic precursor populations between *Ifi44*$^{-/-}$ and *Ifi44*$^{+/+}$ (Figure 5.5C), indicating that defective erythropoiesis was not responsible for the microcytic phenotype observed in *Ifi44*$^{-/-}$ mice.

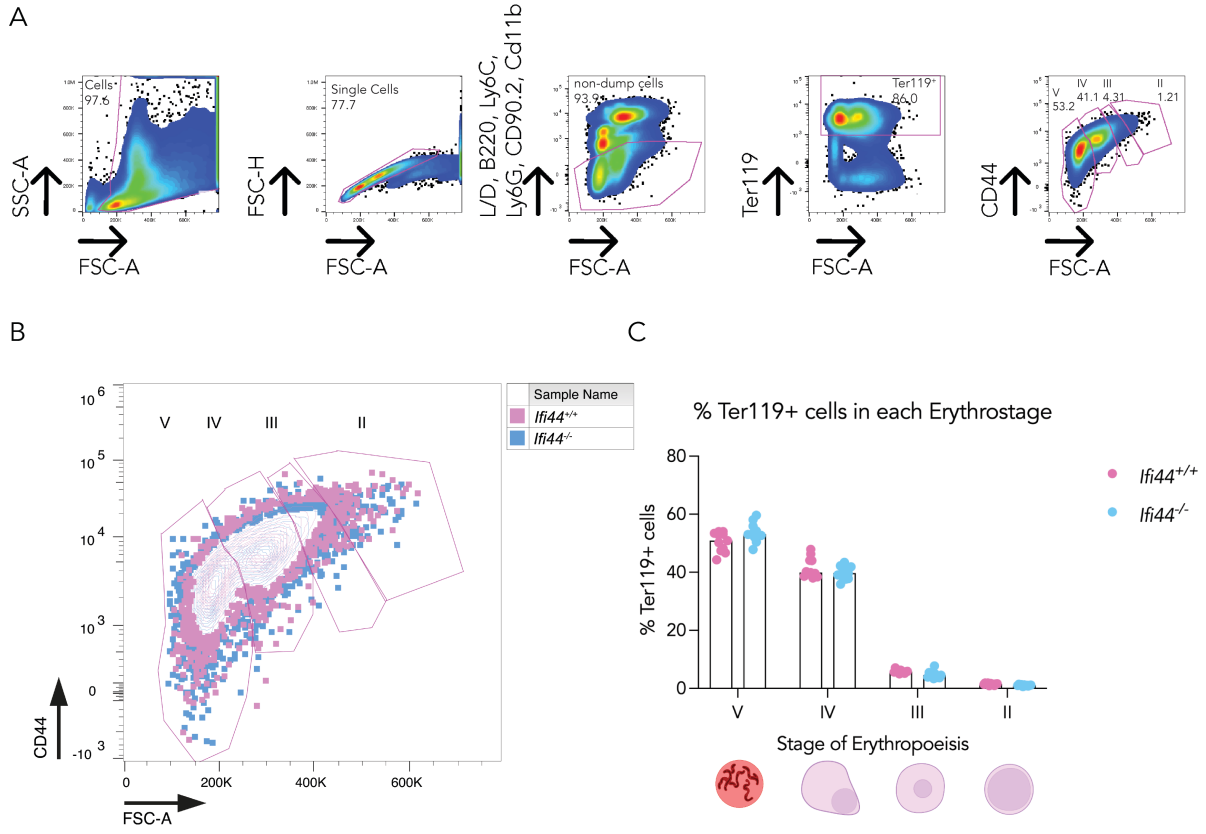


Figure 5.5: Erythroid progenitor populations are indistinguishable in the bone marrow of *Ifi44*$^{-/-}$ and *Ifi44*$^{+/+}$ mice.

Ifi44$^{-/-}$ and *Ifi44*$^{+/+}$ mice were sacrificed, and their bone marrow harvested from hindlegs. Bone marrow was stained and fixed for flow cytometry, and cell populations determined on an Attune NxT Flow Cytometer. **A.** Gating strategy. **B.** Comparison of the different erythrostages, distinguished by size and CD44 expression, in *Ifi44*$^{-/-}$ and *Ifi44*$^{+/+}$ mice. **C.** Pooled from two independent experiments. Each data point represents one biological replicate. *Ifi44*$^{-/-}$ and *Ifi44*$^{+/+}$ mice were littermates.

In mice, stress erythropoiesis occurs in the spleen when homeostatic erythropoiesis cannot keep up with the erythrocytic demand (19, 23-25). To determine whether non-medullary erythropoiesis was occurring at baseline in *Ifi44*$^{-/-}$ mice, resulting in microcytes, flow cytometry for erythrocytic precursors was performed on splenocytes (Figure 5.6A). There were no differences observed in splenic erythrocytic precursors between the two genotypes, indicating that there was no stress erythropoiesis occurring in *Ifi44*$^{-/-}$ mice at baseline (Figure 6 B). As such, erythropoiesis in both the bone marrow and the spleen was indistinguishable between *Ifi44*$^{-/-}$ and *Ifi44*$^{+/+}$ mice, and was thus unlikely to be the cause of the microcytic phenotype or the differentially expressed genes observed in the spleen.

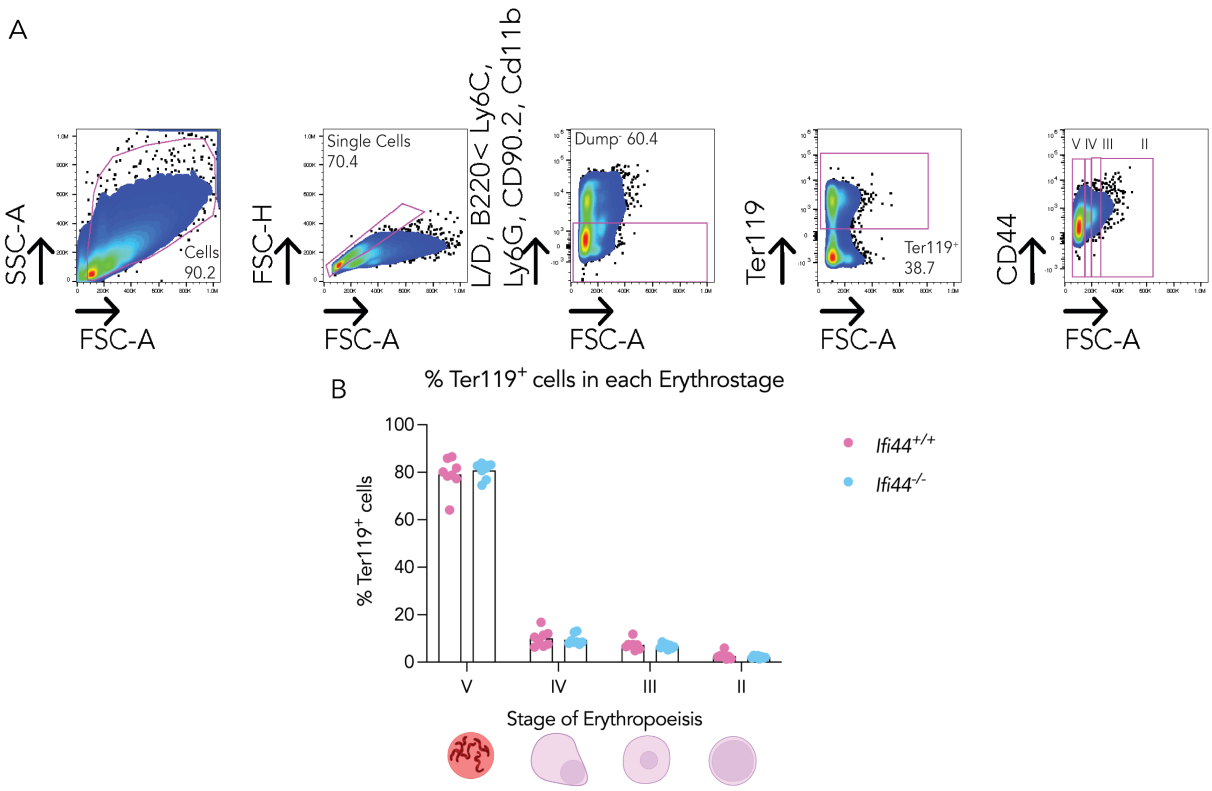


Figure 5.6: Erythroid progenitor populations are indistinguishable in the spleen of *Ifi44*$^{-/-}$ and *Ifi44*$^{+/+}$ mice.

Spleens from *Ifi44*$^{-/-}$ and *Ifi44*$^{+/+}$ mice were enzymatically digested, stained and fixed for flow cytometry. Cell populations were determined on an Attune NxT Flow Cytometer. **A.** Gating strategy. **B.** Each data point represents one biological replicate. *Ifi44*$^{-/-}$ and *Ifi44*$^{+/+}$ mice were littermates.

5.4 *Ifi44*$^{-/-}$ spleens contain fewer tissue-resident RPMs due to increased ferroptosis

After ≈120 days of circulation, RBCs are recycled by splenic RPMs, and the recovered iron is transported back to the bone marrow for further erythropoiesis. As erythropoiesis was not found to be responsible for the splenic transcript level reduction in haem biosynthetic genes and microcytes observed in *Ifi44*$^{-/-}$ mice, I hypothesised that perhaps iron recycling is disrupted in *Ifi44*$^{-/-}$ mice. Consistent with this idea, microcytes are more readily phagocytosed, with the resulting increase in erythrophagocytosis leading to iron accumulation in macrophages, iron deposition in tissues, and RPM apoptosis/ferroptosis (15, 26, 27). As such, I quantified the presence of specialised RPMs in the spleens of *Ifi44*$^{-/-}$ and *Ifi44*$^{+/+}$ mice using flow cytometry (Figure S23). *Ifi44*$^{-/-}$ spleens contained fewer RPMs compared to paired wild-type samples (Figure 5.7A, B), and *Ifi44*$^{-/-}$ RPMs expressed less CD163 (Figure 5.7C, D). This observation is consistent with our RNA sequencing dataset, wherein *Cd163* transcript was significantly downregulated in *Ifi44*$^{-/-}$ mice (Figure 5.2B). As discussed in Section 1.4.3, CD163 is a transmembrane haem scavenger receptor, and is highly expressed on iron-recycling macrophages. Indeed, it is a marker of a specialised erythrophagocyte, capable of internalising haemoglobin-haptoglobin complexes and free haemoglobin resulting from haemolysis (28, 29). This indicated that the RPMs present in *Ifi44*$^{-/-}$ mice were less specialised to recycle erythrocytes and had a reduced capacity to recycle free or complexed haemoglobin.

Less iron recycling capacity in *Ifi44*$^{-/-}$ spleens due to a reduced RPM population and lower CD163 expression should in turn result in increased tissue iron loading, as iron that is not recycled by RPMs forms insoluble deposits in the tissue (26, 27). To test this hypothesis, spleens from *Ifi44*$^{-/-}$ and *Ifi44*$^{+/+}$ mice were fixed, sectioned and stained with Pearl's Prussian Blue stain by the Oxford Centre for Histopathological Research (OCHRe). *Ifi44*$^{-/-}$ spleens contained more insoluble iron deposits than wild-type spleens (Figure 5.8A, B). In addition, serum iron was quantified using an Iron Assay Kit. Surprisingly, there were no differences in serum iron concentration between the genotypes (Figure 5.8C). This kit measured total iron, both Fe^{2+} and Fe^{3+}. Perhaps an improved measurement would be transferrin saturation, as opposed to total serum iron, as an indicator for the bioavailability of iron. Nevertheless, the histological data indicated that *Ifi44*$^{-/-}$ mice had increased iron loading localised in the spleen – likely as a result of inefficient iron recycling due to reduced numbers of RPMs that additionally expressed less CD163.

RPMs are yolk-sac seeded tissue-resident macrophages with self-renewal capacity and are maintained in adulthood by a haem-responsive transcription factor, SPI-C (Figure 5.9A). Indeed, mice lacking *Spic* do not develop RPMs, but other myeloid compartments are

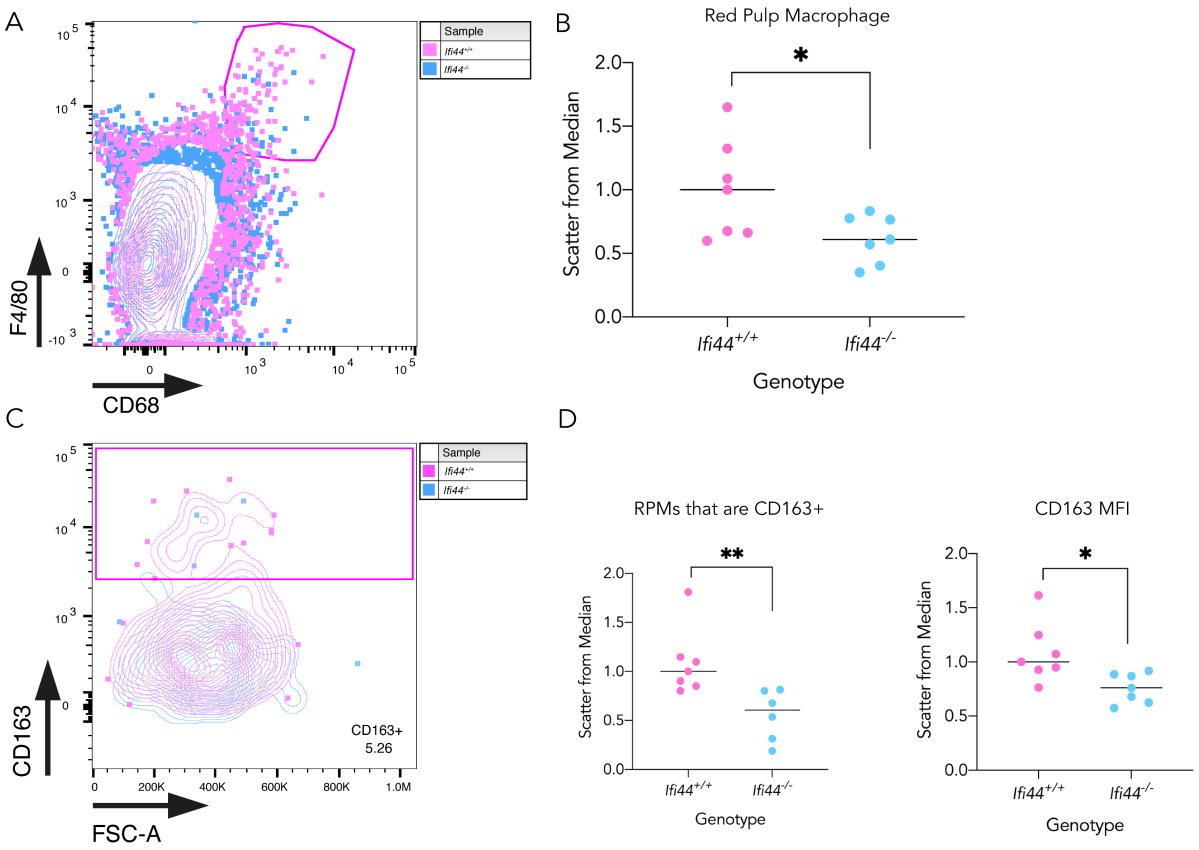


Figure 5.7: *Ifi44*$^{-/-}$ spleens have fewer RPMs displaying reduced expression of the haem-scavenging receptor CD163.

Ifi44$^{+/+}$ and *Ifi44*$^{-/-}$ mice were sacrificed, spleens harvested and enzymatically digested. Resulting splenocytes were stained and fixed for flow cytometry, and cell populations determined on an Attune NxT Flow Cytometer. **A,C.** Comparison of RPMs (A) and of CD163^{+} RPMs (C) in *Ifi44*$^{+/+}$ and *Ifi44*$^{-/-}$ mice. **B,D.** Pooled data from two independent experiments; each data point represents one biological replicate. Scatter from the median was calculated through normalising each data point to the median of each group (i.e. calculating the median value for each of the genotypes in each individual experiment, and dividing each value by the corresponding median value). *Ifi44*$^{+/+}$ and *Ifi44*$^{-/-}$ mice were littermates. Statistical analysis was performed using unpaired T-test. *=p<0.05, **=p<0.01, ***=p<0.001, ****=p<0.0001, ns=not significant.

normal (30, 31). To determine whether the observed reduction in RPMs in *Ifi44*$^{-/-}$ mice was due to a reduction in *Spic*, I determined *Spic* transcript levels in *Ifi44*$^{+/+}$ and *Ifi44*$^{-/-}$ spleens by mining the RNA sequencing dataset. There was no difference in *Spic* expression between the genotypes (Figure 5.9B). As such, the reduction in RPMs in *Ifi44*$^{-/-}$ mice could not be attributed to a reduction in SPI-C. However, increased erythrophagocytic activity from engulfing microcytes could result in iron accumulation in macrophages, iron tissue deposition and eventual ferroptosis of RPMs (26, 27, 32, 33). Ferroptosis is

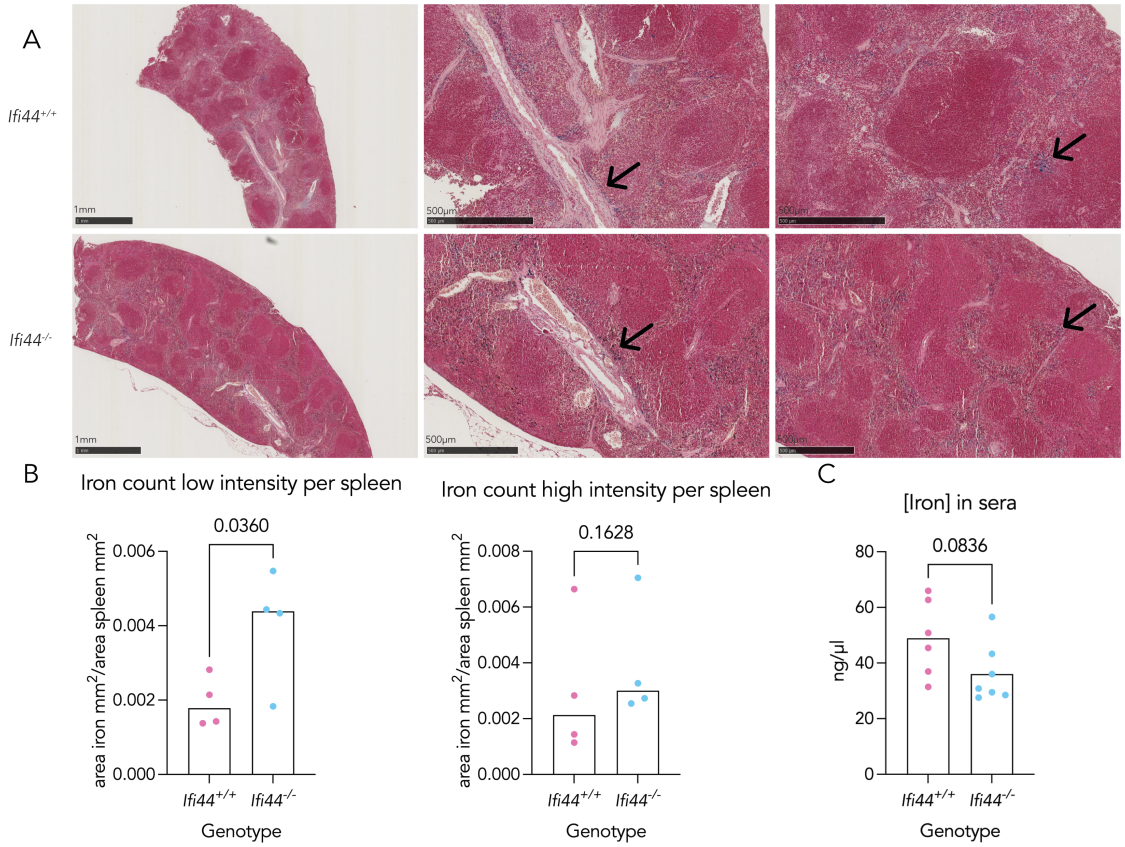


Figure 5.8: *Ifi44*$^{-/-}$ mice have more tissue iron loading in their splenic compartments.
A. *Ifi44*$^{+/+}$ and *Ifi44*$^{-/-}$ mice were sacrificed, and spleens fixed in neutral buffered formalin. Wax embedding, tissue sectioning at 4 µM thickness and Pearl's Prussian blue staining was performed by the Oxford Centre for Histopathological Research. Arrows indicate iron deposits around blood vessels and pulp zones. **B.** Quantification of Pearl's Prussian Blue stain was performed in the AI module of Visiopharm version 2023.9 x64 by Nasullah Khalid Alham. As a post-processing step, two different intensity thresholds (60 and 160) of the H and E Haematoxylin feature were used to classify the detected iron stains into high and low intensity classes. **C.** Iron levels in the serum from *Ifi44*$^{+/+}$ and *Ifi44*$^{-/-}$ mice was analysed using an Iron Assay Kit (Merck). (B, C) Each data point represents one biological replicate. *Ifi44*$^{+/+}$ and *Ifi44*$^{-/-}$ mice were littermates. Statistical analysis was performed using unpaired T-test. P value is displayed.

inhibited by an array of detoxifying enzymes, the most important of which for erythrocytes is peroxiredoxin 2 (PRDX2), in which it constitutes the third most abundant protein (34). Mice deficient in *Prdx2* develop severe haemolytic anaemia, splenomegaly and Heinz bodies (oxidatively denatured haemoglobin) (35). In humans, PRDX2 imbalance is also linked to a variety of diseases (36). *Prdx2* expression was significantly downregulated in spleens from *Ifi44*$^{-/-}$ mice, suggesting that there was less antioxidant capacity, which could result in increased ferroptosis (Figure 5.9B). To determine whether macrophages from

Ifi44$^{-/-}$ mice were more sensitive to ferroptosis induced by haem stimulation, BMDMs from *Ifi44*$^{+/+}$ and *Ifi44*$^{-/-}$ mice were stimulated with Hemin (a haem derivative) and R848 (a PAMP to induce *Ifi44*), and cell death was quantified through live cell imaging (37). *Ifi44*$^{+/+}$ and *Ifi44*$^{-/-}$ BMDMs both exhibited cell death in response to Hemin, however *Ifi44*$^{-/-}$ BMDMs showed significantly increased cell death at later timepoints (Figure 5.9D). This was not due to a difference in cell confluency, as the confluency remained the same throughout the experiment between the genotypes (Figure 5.9E). This experiment has been completed once with three biological repeats, and I aim to repeat this experiment at the next available opportunity to confirm these findings. In total, these data describe a role for *Ifi44* in protecting against oxidative cell death by reducing tissue iron loading and haem stress.

5.5 *Ifi44*$^{-/-}$;*Adar1*$^{mZa/mZa}$ mice phenocopy *Ifi44*$^{-/-}$ mice in their blood profile, erythroid progenitor populations and RPM population

I used an *Ifi44*$^{-/-}$ mouse harbouring an additional mutation in *Adar1*, resulting in increased baseline ISG expression (*Ifi44*$^{-/-}$;*Adar1*$^{mZa/mZa}$; Figure 4.10) to determine whether a sterile ISG response affects the observed differences in *Ifi44*$^{-/-}$ mice at baseline. I observed that these mice phenocopied *Ifi44*$^{-/-}$ mice in their blood profile (Figure 5.10A), their erythroid progenitor populations (Figure 5.10B), and their RPM population (Figure 5.10C). This indicated that increased ISG expression had no effect on the haematopoietic abnormalities observed in *Ifi44*$^{-/-}$ mice, signifying that these were unaffected by ISG expression. This indicated that the role of *Ifi44* in mediating erythrocyte recycling was a baseline role. This is a surprising finding for an ISG, the expression of which is largely induced by IFN during inflammatory states. However, RPMs do express type I IFN at baseline, and are IFN-responsive cells (38, 39). Therefore, one could hypothesise that *Ifi44* is expressed to high levels in RPMs at baseline and does not require induction by a systemic IFN response in this setting.

5.6 *Ifi44*$^{-/-}$ exhibit a delayed recovery in response to acute haemolytic anaemia

RPMs are essential for maintaining erythrocyte homeostasis by recycling aged RBCs, thereby providing haem for the generation of new RBCs. Excess haemolysis during acute anaemia (27) or malaria (40) results in RPM stress and cell death.

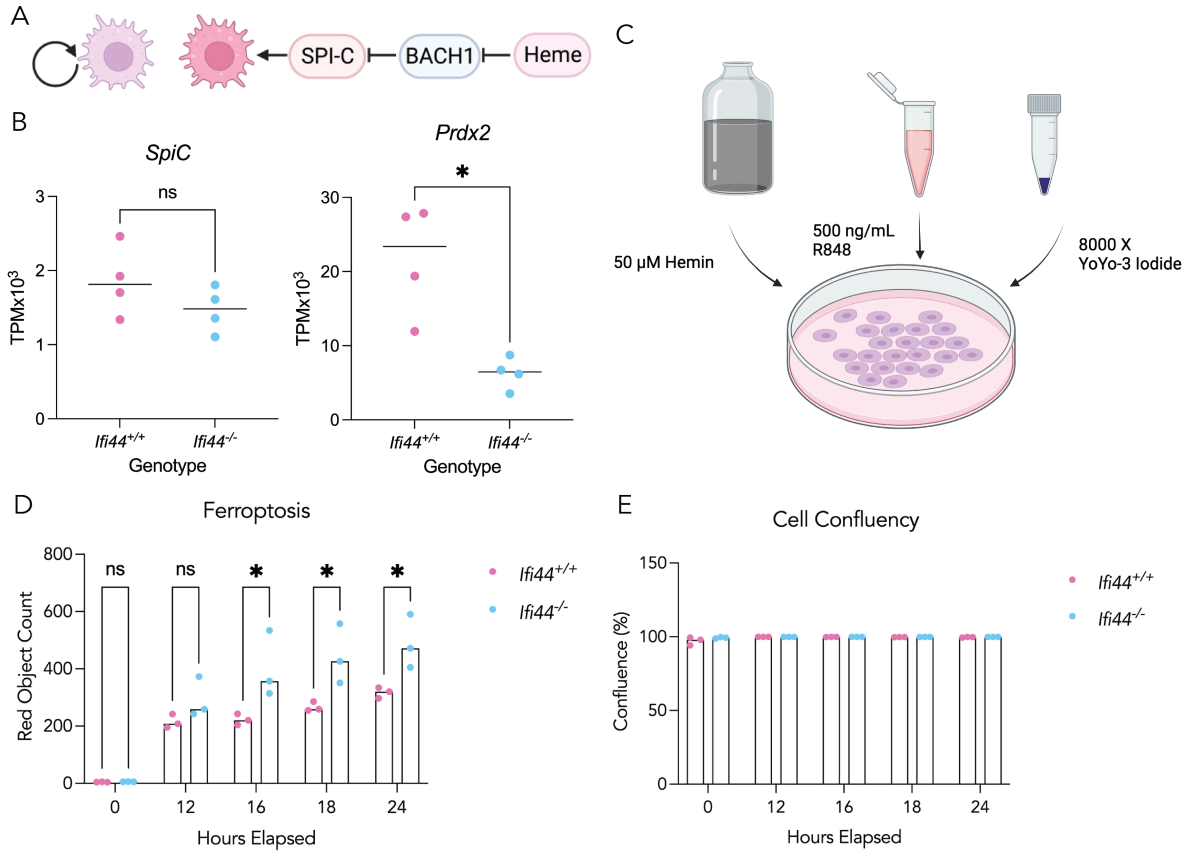


Figure 5.9: The reduced number of splenic RPMs in *Ifi44*$^{-/-}$ mice may be due to increased ferroptosis.

A. In adulthood, yolk-sac seeded RPMs have self-renewal capacity. RPM survival is governed by a haem-responsive transcription factor, SPI-C. **B.** RNA sequencing data from Figure 5.1B are shown for the indicated genes. **C.** Schematic of experiment, adapted from Sundaram *et al* 2023 (36). **D.** *Ifi44*$^{+/+}$ and *Ifi44*$^{-/-}$ BMDMs were stimulated with Hemin and R848, and cell plates were placed in an Incucyte Live Cell Imager. Dead cells were detected through the addition of YoYo-3 iodide. Red Object Count (reflecting the number of dead cells) was determined with the Incucyte software. **E.** Cell confluency was determined using the Incucyte software. (B, D, E) Each data point represents one biological replicate. Statistical analysis was performed using (B) T-test or (D) two-way ANOVA with Sidak's multiple comparisons test. *=p<0.05, **=p<0.01, ***=p<0.001, ****=p<0.0001, ns=not significant.

I have previously observed that *Ifi44*$^{-/-}$ mice and *Ifi44*$^{-/-}$;*Adar1*$^{mZa/mZa}$ mice have fewer tissue-resident RPMs at baseline, with these expressing less of the haem scavenger CD163. I hypothesised that *Ifi44*$^{-/-}$ mice would therefore be slower to recover in a model of induced acute anaemia. Acute haemolytic anaemia was induced in *Ifi44*$^{-/-}$ and *Ifi44*$^{+/+}$ mice with phenylhydrazine hydrochloride (PHZ) (41-43) (Figure 5.11A). Mice were treated with PHZ on day zero and day two, and mice were sacrificed on day six (44-47). Weight was measured every day to monitor the animals' overall health and blood, spleen and bone

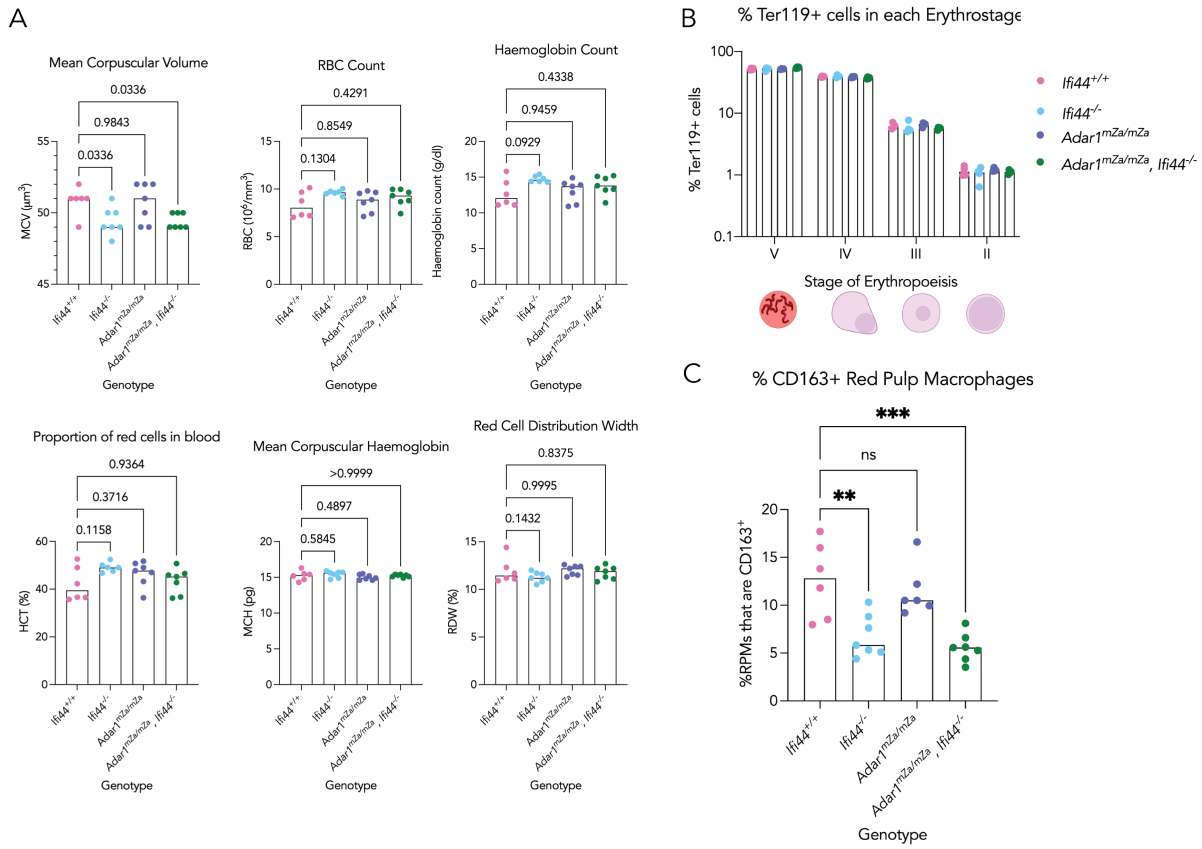


Figure 5.10: *Ifi44*$^{-/-}$;*Adar1*$^{mZa/mZa}$ mice phenocopy *Ifi44*$^{-/-}$ mice.

A. Blood from *Ifi44*$^{+/+}$, *Ifi44*$^{-/-}$, *Adar1*$^{mZa/mZa}$ and *Ifi44*$^{-/-}$;*Adar1*$^{mZa/mZa}$ mice was obtained and analysed as in Figure 5.3. **B, C.** *Ifi44*$^{+/+}$, *Ifi44*$^{-/-}$, *Adar1*$^{mZa/mZa}$ and *Ifi44*$^{-/-}$;*Adar1*$^{mZa/mZa}$ mice were sacrificed, hindlegs and spleens harvested and bone marrow and splenocytes were stained and fixed for flow cytometry. Cell populations were determined on an Attune NxT Flow Cytometer. (A-C) Each data point represents one biological replicate. (A, C) Data are pooled from two independent experiments. Statistical analysis was performed using two-way ANOVA with Dunnett's multiple comparisons test. *=p<0.05, **=p<0.01, ***=p<0.001, ****=p<0.0001, ns=not significant.

marrow were harvested on day six. *Ifi44*$^{-/-}$ mice displayed delayed weight recovery on day six, with most mice in the group not regaining baseline weight, unlike *Ifi44*$^{+/+}$ mice (Figure 5.11B). This indicated that *Ifi44*$^{-/-}$ mice had worse recovery to acute haemolytic stress. Both *Ifi44*$^{-/-}$ and *Ifi44*$^{+/+}$ mice had larger MCV, less RBCs and less haemoglobin compared to *Ifi44*$^{+/-}$ control mice that only received PBS (Figure 5.11C). However, there were no differences in blood parameters when comparing PHZ treated *Ifi44*$^{-/-}$ and *Ifi44*$^{+/+}$ mice (Figure 5.11C). This could be due to the fact that the stress response may have been saturated, and taking a reading at a different day or using a lower concentration of PHZ might in turn allow differences between the genotypes to be observed. Both *Ifi44*$^{-/-}$ and *Ifi44*$^{+/+}$ PHZ-treated mice presented with splenomegaly (Figure 5.12A). Further,

PHZ-treated *Ifi44*$^{-/-}$ mice had a non-significant trend to have slightly larger spleens than *Ifi44*$^{+/+}$ mice (Figure 5.12A). Cell suspension from spleens from PHZ-treated mice had generally more dead cells and debris than PBS-control mice, and many of these cells were CD45^{+} and CD3^{+}, CD19^{+} and CD335^{+} (Figure 5.12B, C). *Ifi44*$^{+/+}$ PHZ-treated mice exhibited an expansion of monocytes and RPMs compared to PBS control mice, however *Ifi44*$^{-/-}$ PHZ-treated mice did not show this same expansion, with an apparent reduction in monocytes and the same percentage of RPMs as untreated control mice (Figure 5.12C). This could in part explain the delayed recovery exhibited by these mice, as there were less erythrophagocytic cells to clear the haemolysed RBCs.

Further to this, I examined the expression of CD163 on these monocytes and RPMs, signifying specialised erythrophagocytic cells. There was very low CD163 expression in monocytes in every condition, however the CD163^{+} RPM expression was undetectable in *Ifi44*$^{-/-}$ PHZ-treated mice and was markedly reduced in *Ifi44*$^{+/+}$ PHZ-treated mice (Figure 5.13A, B). This was likely due to receptor endocytosis (29) or shedding (48-50).

During haemolytic stress, Ly6C^{hi} monocytes infiltrate the spleen from the bone marrow and differentiate into RPM-like cells to increase the erythrophagocytic and erythropoietic capacity (24, 40). During a mouse model of malaria, the majority of embryonically seeded RPMs are replaced by bone marrow-derived progenitors, which differentiate into F4/80^{hi}CD11b^{lo} RPMs (40). These monocytes differentiate from monocyte-like cells (Ly6C^{hi}F4/80^{lo}CD11b^{hi}), to pre-RPMs (Ly6C^{lo}F4/80^{lo}CD11b^{hi}) and finally to RPMs, albeit with a few notable differences to tissue-resident RPMs (24). I therefore determined the expression levels of Ly6C on monocytes and RPMs from PHZ-treated *Ifi44*$^{-/-}$ and *Ifi44*$^{+/+}$ mice, and PBS control mice, to determine how many infiltrating monocytes were present in the spleen. While the percentage of Ly6C expressing monocytes remained similar between all conditions, there was a marked increase in the percentage of Ly6C expressing RPMs in PHZ-treated mice, indicating that a majority of RPMs present had originated from the bone marrow, and were not tissue-resident cells (Figure 5.13A, B). However, there was no difference in Ly6C^{+} RPMs between *Ifi44*$^{-/-}$ and *Ifi44*$^{+/+}$ PHZ-treated mice (Figure 5.13B).

VCAM-1 is an erythrocytic adhesion molecule, and high expression results in enhanced erythrophagocytosis (51, 52). I determined the expression of VCAM-1 on monocytes and RPMs, as a proxy for adhesion to RBCs. PHZ-treated mice upregulate VCAM-1 on monocytes, but downregulated VCAM-1 on RPMs (Figure 13 A, B). This is likely due to RPM stress and exhaustion, and indicative of monocytes differentiating into erythrophagocytic cells.

Lastly, I evaluated the erythrophagocytic capacity of these monocytes and macrophages

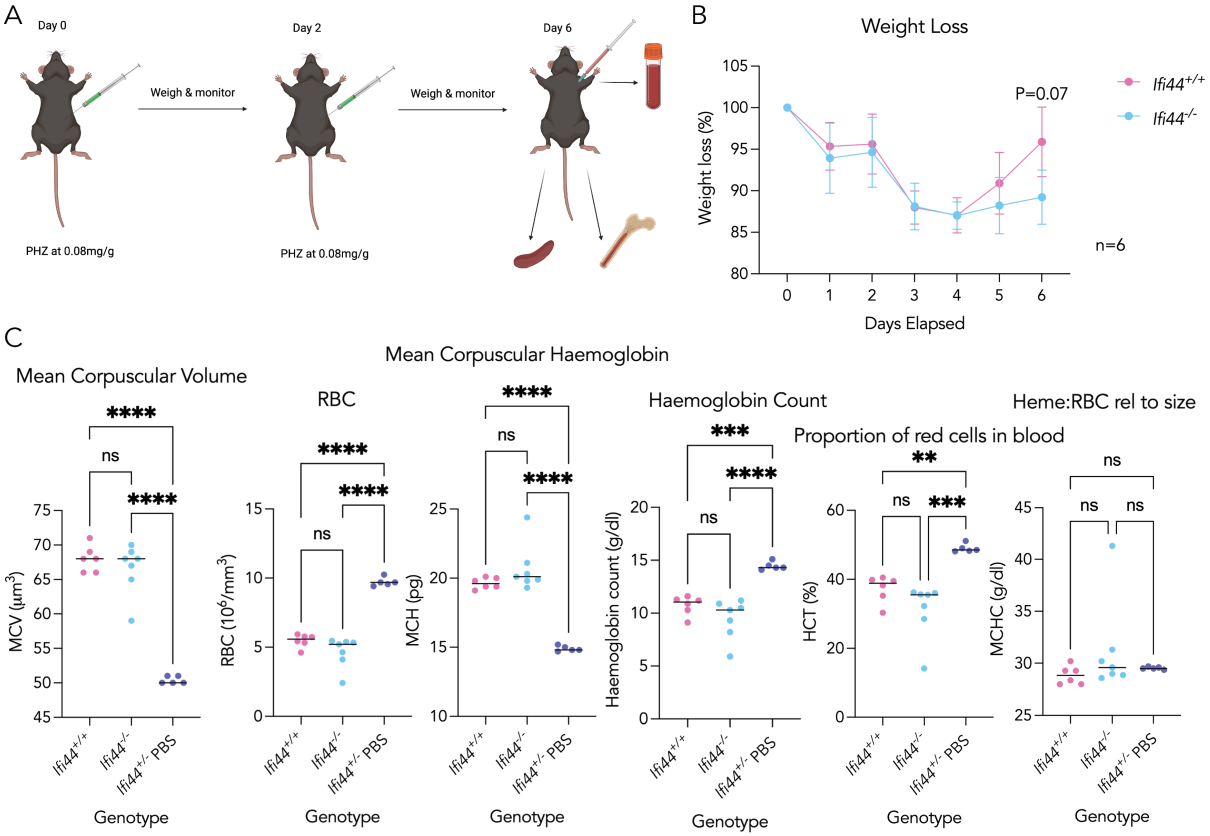


Figure 5.11: *Ifi44*$^{-/-}$ mice display delayed recovery after induced acute haemolytic anaemia.
A. Schematic of the experiment. **B.** *Ifi44*$^{+/+}$ and *Ifi44*$^{-/-}$ mice were injected intraperitoneally with 0.08 mg/ g body weight phenylhydrazine hydrochloride (PHZ) on day 0 and day 2. Weight was measured every day as an indicator of stress induction and recovery. **C.** *Ifi44*$^{+/+}$ and *Ifi44*$^{-/-}$ mice were sacrificed through exsanguination under terminal anaesthesia, and blood collected into EDTA-coated microtainers to prevent clotting. Blood was analysed using a Pentra ES-60 machine. (B) Data points are the average of six biological replicates at day 6. Prior to day 6, data points are the average of six-ten biological replicates, as mice from each genotype reached the humane endpoint prior to the experimental endpoint. Statistical analysis was performed using Mixed-Effects Analysis and Sidak's multiple comparisons test. (C) Each data point represents one biological replicate. (B, C) Data are pooled from two independent experiments. *Ifi44*$^{+/+}$ and *Ifi44*$^{-/-}$ mice were littermates. Statistical analysis was performed using (B) two-way ANOVA with Sidak's multiple comparisons test or (C) one-way ANOVA with Turkey's multiple comparisons test. *=p<0.05, **=p<0.01, ***=p<0.001, ****=p<0.0001, ns=not significant.

through an intracellular Ter119^{+} stain to quantify internalised RBCs. PHZ-treated mice showed enhanced intracellular Ter119 in both monocytes and RPMs, although there were no differences between the genotypes.

Acute haemolytic anaemia causes splenic stress erythropoiesis, as there is a sudden requirement for new red blood cells, and as such an increase in erythrocytic precursors (22,

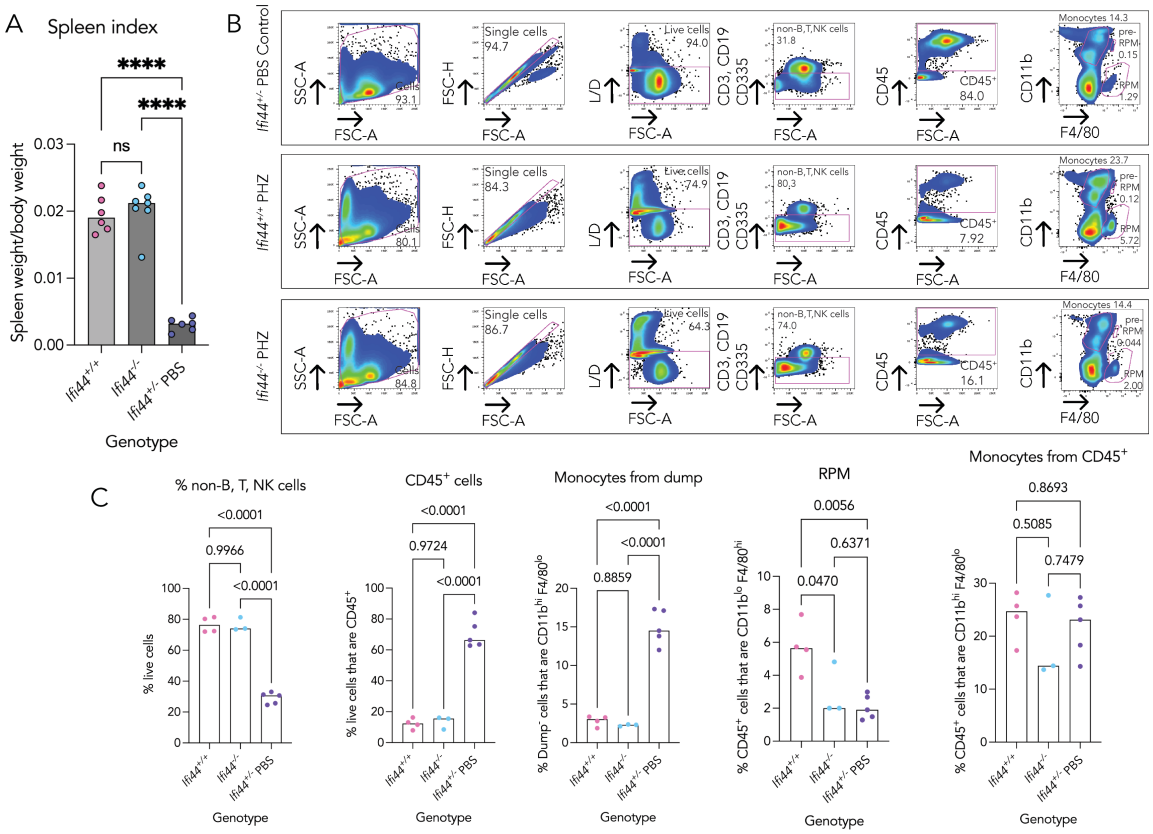


Figure 5.12: *Ifi44*$^{-/-}$ mice do not expand their RPM compartment during acute haemolytic stress.

A. Spleen index of mice from Figure 5.11 was calculated through determining spleen weight / total body weight. **B, C.** *Ifi44*$^{+/+}$ and *Ifi44*$^{-/-}$ spleens were enzymatically digested and cell populations determined using an LSR Fortessa X50 flow cytometer. (B) Gating strategy. (C) Pooled data from two independent experiments. Each data point represents one biological replicate. *Ifi44*$^{+/+}$ and *Ifi44*$^{-/-}$ mice were littermates. (A, C) Statistical analysis was performed using one-way ANOVA with (A) Sidak's or (C) Turkey's multiple comparisons test. *=p<0.05, **=p<0.01, ***=p<0.001, ****=p<0.0001, ns=not significant.

23, 25, 44-46, 53, 54). Mice at day six of PHZ treatment displayed an increase in Ter119 and CD17 positive cells in their spleens and bone marrow, although there was no difference between *Ifi44*$^{-/-}$ and *Ifi44*$^{+/+}$ mice (Figure 5.14A, B; Figure S24A-C). PHZ-treated mice also showed a reduction in late-stage (V) erythrocytic precursors and an increase in early-stage erythrocytic precursors (II-IV), indicating that there is an increase in erythropoiesis – but this was the same in both *Ifi44*$^{-/-}$ and *Ifi44*$^{+/+}$ mice (Figure 5.14A, B; Figure S24A-C).

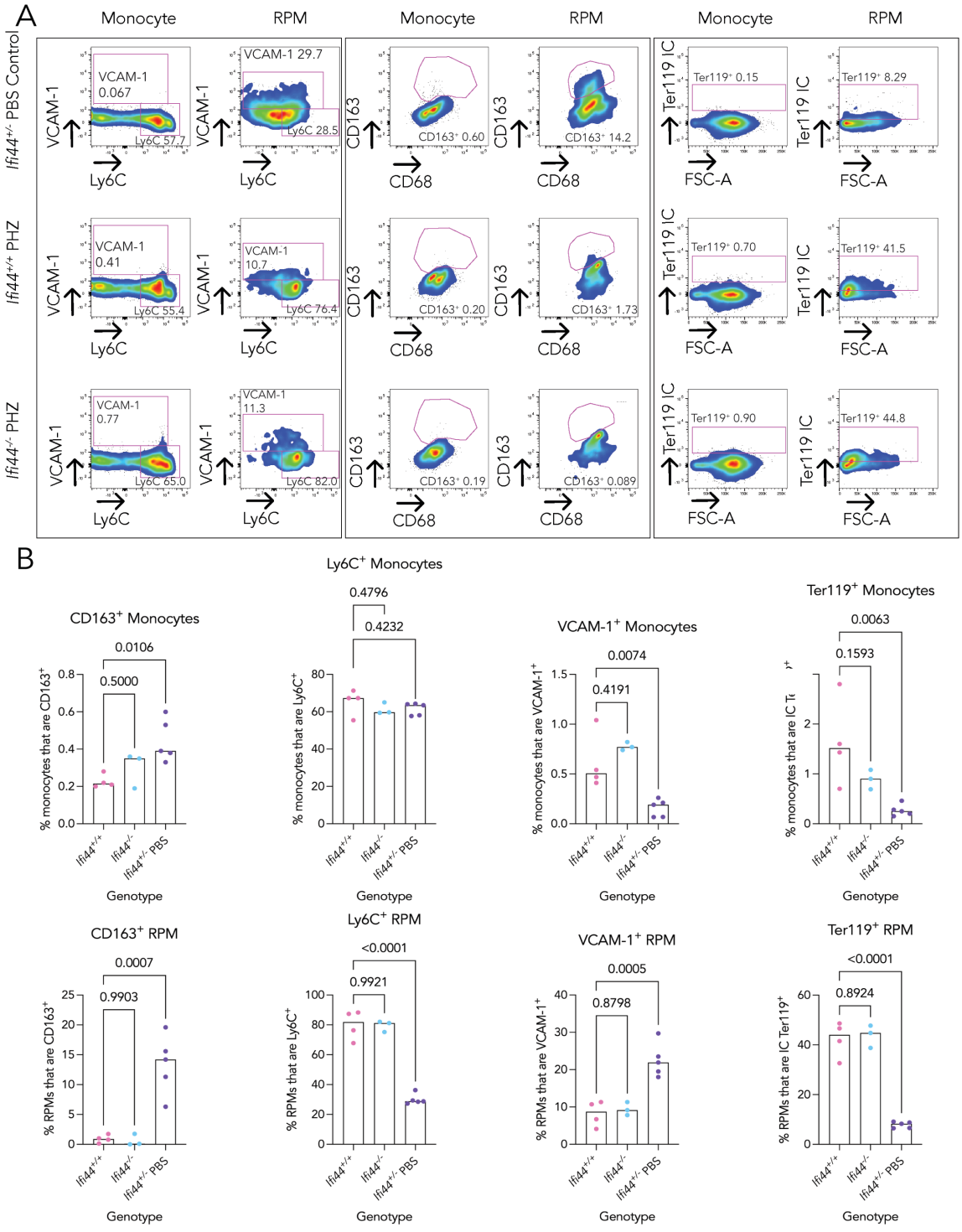


Figure 5.13: PHZ treatment increases erythrophagocytosis in C57BL/6 mice.

A. Gating strategy. These gates follow on from those in Figure 5.12B. **B.** Flow cytometry continued from Figure 5.12. (B) Each data point represents one biological replicate. *Ifi44*$^{+/+}$ and *Ifi44*$^{-/-}$ mice were littermates. Statistical analysis was performed using one-way ANOVA with Dunnett's multiple comparisons test. P values are indicated.

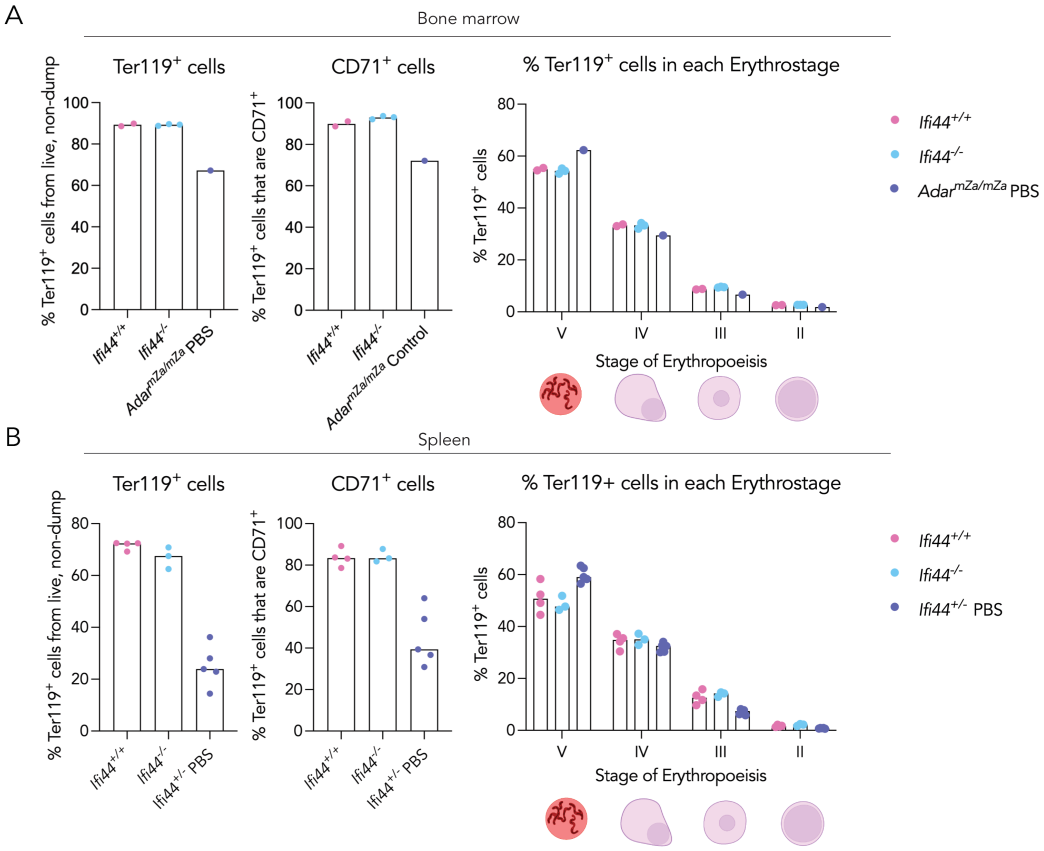


Figure 5.14: Erythroid progenitor populations in the bone marrow and spleen are indistinguishable in *Ifi44*$^{-/-}$ and *Ifi44*$^{+/+}$ mice during acute haemolytic anaemia.

A. Hindlegs from mice in Figure 5.11 were harvested and erythrocytic precursors were determined using an LSR Fortessa X50 flow cytometer. **B.** *Ifi44*$^{-/-}$, *Ifi44*$^{+/+}$ and *Ifi44*$^{+/-}$ spleens were enzymatically digested and cell populations determined using an LSR Fortessa X50 flow cytometer. (A, B) Each data point represents one biological replicate. *Ifi44*$^{-/-}$, *Ifi44*$^{+/+}$ and *Ifi44*$^{+/-}$ mice were littermates. Statistical analysis was performed using one-way ANOVA with Dunnett's comparisons test, p value indicated.

5.7 Summary for Chapter 5

Combined, these data feed into my working hypothesis (Figure 5.15): in *Ifi44*$^{-/-}$ mice, there is a reduction in the RPM population, and as a result, a reduction in splenic RBC recycling. This likely results in increased intravascular haemolysis. Due to this, there is then an increase in splenic iron deposition, which is likely responsible for the observed transcriptional reduction in genes involved in the haem biosynthetic pathway. Further, *Ifi44*$^{-/-}$ macrophages were more susceptible to cell death following haem stimulation, and as such, increased splenic iron loading likely results in increased ferroptosis of RPMs. In turn, this reduces the RPM population and feeds into the reduction in RBC recycling. Under conditions of haemolytic stress, there was likely an increase in RPM cell death and

subsequent iron loading, leading to worsened recovery of *Ifi44*$^{-/-}$ mice. Some questions remain unanswered, such as which one of these observations commences the cycle (Figure 5.15). In addition, it is unclear how microcytes feed into this, especially given that erythropoiesis was not affected at baseline or under anaemic stress. Despite this, it is documented that microcytes are more readily phagocytosed (15, 26, 27), which could lead to increased RPM cell death. Exactly how IFI44 might be mediating erythrocyte homeostasis on a molecular level remains unknown, however, I favour the idea that the TLDc domain confers resistance to oxidative stress in RPMs, leading to ferroptotic resistance.

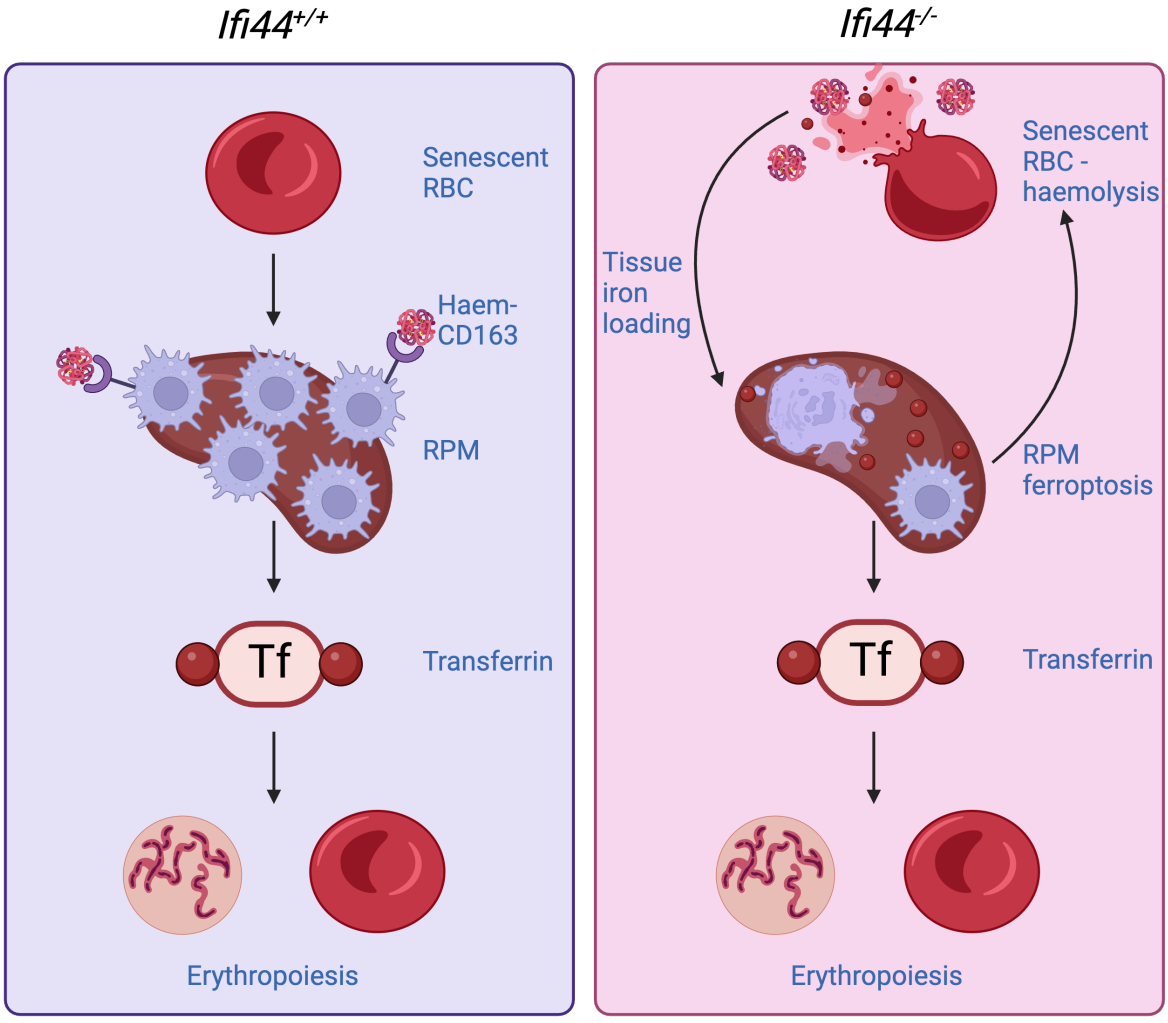


Figure 5.15: *Ifi44* maintains erythrocyte homeostasis.

Splenic RPMs recycle senescent RBCs to derive iron for erythropoiesis. *Ifi44*$^{-/-}$ mice have a reduction in RPM population, therefore more RBC lysis and an increase in splenic iron loading.

References for Chapter 5

1. Y. Honda et al., Isolation and purification of a non-A, non-B hepatitis-associated microtubular aggregates protein. J Gen Virol 71 (Pt 9), 1999-2004 (1990).
2. M. I. Love, W. Huber, S. Anders, Moderated estimation of fold change and dispersion for RNA-seq data with DESeq2. Genome Biol 15, 550 (2014).
3. N. Wilkinson, K. Pantopoulos, The IRP/IRE system *in vivo*: insights from mouse models. Front Pharmacol 5, 176 (2014).
4. A. Dautry-Varsat, Receptor-mediated endocytosis: The intracellular journey of transferrin and its receptor. Biochimie 68, 375-381 (1986).
5. J. P. Liuzzi, F. Aydemir, H. Nam, M. D. Knutson, R. J. Cousins, Zip14 (*Slc39a14*) mediates non-transferrin-bound iron uptake into cells. Proceedings of the National Academy of Sciences 103, 13612-13617 (2006).
6. C. Liu et al., H1N1 influenza virus infection through NRF2-KEAP1-GCLC pathway induces ferroptosis in nasal mucosal epithelial cells. Free Radic Biol Med 204, 226-242 (2023).
7. M. Li et al., DDIT3 Directs a Dual Mechanism to Balance Glycolysis and Oxidative Phosphorylation during Glutamine Deprivation. Adv Sci (Weinh) 8, e2003732 (2021).
8. W. M. Gardner et al., Prevalence, years lived with disability, and trends in anaemia burden by severity and cause, 1990–2021: findings from the Global Burden of Disease Study 2021. The Lancet Haematology 10, e713-e734 (2023).
9. M. E. Dickinson et al., High-throughput discovery of novel developmental phenotypes. Nature 537, 508-514 (2016).
10. T. Groza et al., The International Mouse Phenotyping Consortium: comprehensive knockout phenotyping underpinning the study of human disease. Nucleic Acids Research 51, D1038-D1045 (2023).
11. O. M. P. Jolobe, Prevalence of hypochromia (without microcytosis) vs microcytosis (without hypochromia) in iron deficiency. Clinical and Laboratory Haematology 22, 79-80 (2000).
12. A. C. Massey, Microcytic anemia. Differential diagnosis and management of iron deficiency anemia. Med Clin North Am 76, 549-566 (1992).
13. K. Rampon, Anemia: Microcytic Anemia. FP Essent 530, 12-16 (2023).
14. M. W. Hentze, M. U. Muckenthaler, B. Galy, C. Camaschella, Two to Tango: Regulation of Mammalian Iron Metabolism. Cell 142, 24-38 (2010).
15. J. Giroud-Gerbetant et al., Erythropoietin supplementation ameliorates the immunological and hematological deficiencies of lysinuric protein intolerance in mice. bioRxiv, 2021.2008.2015.456393 (2022).
16. S. S. Cooperman et al., Microcytic anemia, erythropoietic protoporphyria, and neu-

rodegeneration in mice with targeted deletion of iron-regulatory protein 2. Blood 106, 1084-1091 (2005).
17. O. Castro, W. N. Poillon, H. Finke, E. Massac, Improvement of sickle cell anemia by iron-limited erythropoiesis. Am J Hematol 47, 74-81 (1994).
18. A. Iolascon, L. De Falco, C. Beaumont, Molecular basis of inherited microcytic anemia due to defects in iron acquisition or heme synthesis. Haematologica 94, 395-408 (2009).
19. H. Hara, M. Ogawa, Erythropoietic precursors in mice under erythropoietic stimulation and suppression. Exp Hematol 5, 141-148 (1977).
20. S. V. Bhoopalan, L. J. Huang, M. J. Weiss, Erythropoietin regulation of red blood cell production: from bench to bedside and back. F1000Res 9, (2020).
21. B. M. Zhu et al., Hematopoietic-specific *Stat5*-null mice display microcytic hypochromic anemia associated with reduced transferrin receptor gene expression. Blood 112, 2071-2080 (2008).
22. K. Chen et al., Resolving the distinct stages in erythroid differentiation based on dynamic changes in membrane protein expression during erythropoiesis. Proc Natl Acad Sci U S A 106, 17413-17418 (2009).
23. J. Zhang et al., Rats provide a superior model of human stress erythropoiesis. Experimental Hematology 78, 21-34.e23 (2019).
24. C. Liao, K. S. Prabhu, R. F. Paulson, Monocyte-derived macrophages expand the murine stress erythropoietic niche during the recovery from anemia. Blood 132, 2580-2593 (2018).
25. J. Xiang, D. C. Wu, Y. Chen, R. F. Paulson, *In vitro* culture of stress erythroid progenitors identifies distinct progenitor populations and analogous human progenitors. Blood 125, 1803-1812 (2015).
26. P. Slusarczyk et al., Impaired iron recycling from erythrocytes is an early hallmark of aging. Elife 12, (2023).
27. L. A. Youssef et al., Increased erythrophagocytosis induces ferroptosis in red pulp macrophages in a mouse model of transfusion. Blood 131, 2581-2593 (2018).
28. D. J. Schaer et al., CD163 is the macrophage scavenger receptor for native and chemically modified hemoglobins in the absence of haptoglobin. Blood 107, 373-380 (2006).
29. C. A. Schaer, G. Schoedon, A. Imhof, M. O. Kurrer, D. J. Schaer, Constitutive endocytosis of CD163 mediates hemoglobin-heme uptake and determines the noninflammatory and protective transcriptional response of macrophages to hemoglobin. Circ Res 99, 943-950 (2006).
30. M. Haldar et al., Heme-mediated SPI-C induction promotes monocyte differentiation into iron-recycling macrophages. Cell 156, 1223-1234 (2014).
31. M. Kohyama et al., Role for Spi-C in the development of red pulp macrophages and splenic iron homeostasis. Nature 457, 318-321 (2009).

32. S. Altamura et al., Glutathione peroxidase 4 and vitamin E control reticulocyte maturation, stress erythropoiesis and iron homeostasis. Haematologica 105, 937-950 (2020).
33. S. Lin, Y. Zheng, M. Chen, L. Xu, H. Huang, The interactions between ineffective erythropoiesis and ferroptosis in -thalassemia. Front Physiol 15, 1346173 (2024).
34. F. M. Low, M. B. Hampton, C. C. Winterbourn, Peroxiredoxin 2 and peroxide metabolism in the erythrocyte. Antioxid Redox Signal 10, 1621-1630 (2008).
35. T. H. Lee et al., Peroxiredoxin II is essential for sustaining life span of erythrocytes in mice. Blood 101, 5033-5038 (2003).
36. P. Balasubramanian et al., Implications and progression of peroxiredoxin 2 (PRDX2) in various human diseases. Pathol Res Pract 254, 155080 (2024).
37. B. Sundaram et al., NLRP12-PANoptosome activates PANoptosis and pathology in response to heme and PAMPs. Cell 186, 2783-2801.e2720 (2023).
38. M. Enders et al., Splenic Red Pulp Macrophages Cross-Prime Early Effector CTL That Provide Rapid Defense against Viral Infections. J Immunol 204, 87-100 (2020).
39. C. C. Kim et al., Splenic red pulp macrophages produce type I interferons as early sentinels of malaria infection but are dispensable for control. PLoS One 7, e48126 (2012).
40. S. M. Lai et al., Organ-Specific Fate, Recruitment, and Refilling Dynamics of Tissue-Resident Macrophages during Blood-Stage Malaria. Cell Reports 25, 3099-3109.e3093 (2018).
41. M. D. Shetlar, H. A. Hill, Reactions of hemoglobin with phenylhydrazine: a review of selected aspects. Environ Health Perspect 64, 265-281 (1985).
42. N. S. Merle et al., Characterization of Renal Injury and Inflammation in an Experimental Model of Intravascular Hemolysis. Front Immunol 9, 179 (2018).
43. E. Tolosano et al., Defective recovery and severe renal damage after acute hemolysis in hemopexin-deficient mice. Blood 94, 3906-3914 (1999).
44. O. Angulo, O. Gandrillon, F. Crauste, Investigating the role of the experimental protocol in phenylhydrazine-induced anemia on mice recovery. Journal of Theoretical Biology 437, 286-298 (2018).
45. X. Jiang et al., EPO-dependent induction of erythroferrone drives hepcidin suppression and systematic iron absorption under phenylhydrazine-induced hemolytic anemia. Blood Cells, Molecules, and Diseases 58, 45-51 (2016).
46. Z. A. Knight, S. F. Schmidt, K. Birsoy, K. Tan, J. M. Friedman, A critical role for mTORC1 in erythropoiesis and anemia. eLife 3, e01913 (2014).
47. A. E. Preston, PhD Thesis, University of Oxford, University of Oxford (2022).
48. K. A. Hintz et al., Endotoxin induces rapid metalloproteinase-mediated shedding followed by up-regulation of the monocyte hemoglobin scavenger receptor CD163. J Leukoc Biol 72, 711-717 (2002).
49. A. Etzerodt et al., Structural Basis for Inflammation-driven Shedding of CD163

Ectodomain and Tumor Necrosis Factor-α in Macrophages*. Journal of Biological Chemistry 289, 778-788 (2014).
50. A. Etzerodt et al., Soluble ectodomain CD163 and extracellular vesicle-associated CD163 are two differently regulated forms of 'soluble CD163' in plasma. Scientific Reports 7, 40286 (2017).
51. B. E. Gee, O. S. Platt, Sickle reticulocytes adhere to VCAM-1. Blood 85, 268-274 (1995). 52. T. R. Klei, S. M. Meinderts, T. K. van den Berg, R. van Bruggen, From the Cradle to the Grave: The Role of Macrophages in Erythropoiesis and Erythrophagocytosis. Front Immunol 8, 73 (2017).
53. H. Li et al., Rate of Progression through a Continuum of Transit-Amplifying Progenitor Cell States Regulates Blood Cell Production. Dev Cell 49, 118-129.e117 (2019).
54. J. Liu et al., Quantitative analysis of murine terminal erythroid differentiation *in vivo*: novel method to study normal and disordered erythropoiesis. Blood 121, e43-e49 (2013).

Chapter 6

Discussion

This study aimed to characterise the molecular function of a prototypical ISG, *IFI44*. Surprisingly, we discovered an exciting role for *Ifi44* in mediating erythrocyte homeostasis. I describe a link between the IFN response and iron homeostasis, which provides future avenues of research on how IFN, and consequently ISGs, might broadly influence the systemic iron homeostatic landscape. Such a link may be of evolutionary consequence and importance, since some pathogens scavenge iron, some pathogens mediate haemolysis, and some pathogens infect erythrocytes – thus, iron homeostasis and infection are intrinsically interlinked.

6.1 IFI44 and virus infection

I first demonstrated that *IFI44* and *IFI44L* are prototypical, late ISGs; with most human cell lines expressing the two proteins around 8-12 hours after IFN stimulation. Many other ISGs are directly involved in anti-pathogen defence (1-4), and there are studies suggesting that IFI44 is among them (5-9) (see Chapter 4). Directly contrasting this, other studies indicate that IFI44 exerts proviral activities during IAV and r-VSV infection (10, 11). I did not uncover a role for IFI44 exerting antiviral or proviral effects *in vitro*, with viral infectivity measured through a range of read-outs: western blot for viral proteins, plaque assay and RT-qPCR. I utilised several different viruses, including both enveloped and non-enveloped viruses and DNA and RNA viruses. However, I did not test the role of IFI44 in VSV or RSV infection, during which IFI44 had been suggested to exert pro- and anti-viral effects, respectively (5, 10). As such, it is possible that IFI44 exhibits virus-specific effects. I did, however, test the role of IFI44 during *in vitro* and *in vivo* IAV infection, and I could not reproduce the published finding that IFI44 exerts proviral effects (10). It is possible this is due to differences in cell lines used – DeDiego et al. (10) utilised A549

and HAP-1 cells, whereas I used HEK293T cells (10). IFI44 overexpression was suggested to result in a reduction of IRF3 phosphorylation by IKKϵ, which leads to decreased IFN responses, reduced induction of ISGs and thusly proviral effects (10). It was further proposed that this is mediated through the interaction of IFI44 and FK506 binding protein 51 (FKBP5), evidenced by mass spectrometry and immunoprecipitation in HEK293T cells (10). FKBP5 is a negative regulator of the glucocorticoid receptor, and mutations in humans are linked to psychiatric, metabolic, and immune disorders (12). Biochemical data has identified FKBP5 as a binding partner of IKK proteins, and silencing FKBP5 reduces NF-κB nuclear translocation (13). Alongside not observing proviral activities for IFI44 in any viral infection setting, I also did not reproduce the finding of IFI44 binding to FKBP5 in a mass spectrometry experiment using IFI44-V5 pulldown in HEK293T cells in the presence or absence of IFN. I observed that *Ifi44*$^{-/-}$ MEFs show a slight IFN signature, which would fit in with the authors' findings that IFI44 reduces IFN signalling (10). However, this was not recapitulated in different murine organs from *Ifi44*$^{-/-}$ mice, nor in HEK293T cells overexpressing IFI44 – which was the same setting used by the authors. It is possible that as MEFs are embryonic in origin, there are different signalling mechanisms and different roles for ISGs than in adult mice. Additionally, only *Ddx58* and *Adar1* mRNA reached statistical significance, so it is possible that IFI44 regulates these mRNAs by an unknown mechanism independent of IFN signalling. As such, I concluded that neither IFI44 presence nor absence affected the IFN response in adult mice.

My conclusion that human IFI44 does not exert pro- or anti-viral effects *in vitro* was solely based on experiments utilising artificial overexpression of tagged protein. I cloned and generated lentiviruses encoding sgRNAs targeting IFI44, and an undergraduate student I supervised, Sarah, validated these. However, I encountered technical difficulties performing infection experiments in knock-down cell lines. This is because IFN pretreatment was required to induce *Ifi44* expression in wild-type cells, leading to experimental difficulties in balancing the requirement for IFN with productive viral infection. The same was true for *Ifi44*$^{-/-}$ MEF experiments. It is possible that artificial overexpression of IFI44-V5 through lentiviral transduction in HEK293T cells prevents detection of endogenous protein function – especially in an infection context, since a lentivirus was used. However, lentiviral-mediated overexpression systems were used successfully for IFI44 in some studies (5-8, 10), and are a common method in molecular biology. Furthermore, IFI44-V5 overexpression by transient transfection of HEK293 cells resulted in no difference in VACV or HSV-1 infectivity. In addition, I determined that IFI44 and IFI44L interact and hypothesised that perhaps co-expression is required to detect protein functionality. However, co-expression using transient transfection in HEK293 cells did not restrict VACV infection at the protein or RNA level. Due to this finding, I did not employ other virus models to test this hypothesis. Indeed, I discovered that VACV cleaves IFI44 and IFI44L

during infection. In addition, full-length IFI44 is degraded by VACV, and this degradation is less pronounced in the presence of IFI44L. Since I discovered that these two proteins interact, I speculate that binding is important for protein stability during an infection. However, VACV could still cleave both proteins when they were overexpressed together. VACV is a poxvirus, which have a unique viral lifecycle occurring entirely in the cytosol (14). As such, poxviruses are very large viruses encoding a plethora of genes to enable this lifecycle, including many host innate immune antagonists (15-22). This is essential, as replicating a 195 kb DNA genome in the cytosol would not otherwise go unnoticed by the immune response (23). It therefore follows to hypothesise that VACV is capable of antagonising anti-viral ISGs and perhaps IFI44/L is one of these targets, with cleavage preventing their notional anti-viral activity (Figure 6.1).

I demonstrated that the proteasome was not required for VACV-mediated cleavage of IFI44/L, indicating that this cleavage could be mediated by a viral protease. VACV encodes two proteases, I7 and G1 (24). I7 is a cysteine protease expressed late in infection, which is essential for the maturation of core viral proteins (25-27). G1 is a late gene encoding a metalloproteinase, with a HXXEH zinc-binding motif and a downstream ENE metal-binding site, the absence of which results in a lack of mature virions (25, 28, 29). I7 targets an AG*X cleavage motif (30, 31), with a preference for X being a small residue, like A, S or T (32). I7 has a distant homology to ubiquitin-like proteases, sharing substrate specificity, overall 3D folding patterns and identical catalytic core motifs (32). As such, it is plausible that this protease could act on a host protein, especially given its promiscuous peptide cleavage specificity. IFI44 contains two potential AG*X motifs; A^{197}GK and A^{337}GV, both of which are present in the P-Loop NTPase domain. IFI44L contains just one putative site, A^{272}GL, also in the P-Loop NTPase domain. However, since K and L are large amino acids, and V is medium size, whether IFI44/L can be cleaved by I7 is unknown. On the other hand, metalloprotease G1 cleaves preferentially at AG*S/T/L (28, 29) – and IFI44L does contain an A^{272}GL motif. Notably, the cleavage band of IFI44L was much stronger than that of IFI44. The resulting fragments from cleavage at this site are predicted to be 30 kDa and 20 kDa respectively, which does not fit in with the ≈40 kDa fragment seen in the western blot. As such, whether cleavage of these proteins is performed by a viral or host protease, and at which site, remain unknown.

While I hypothesise that VACV-mediated cleavage of IFI44/L results in direct antagonism of putative anti-viral effects, it should be noted that this may not be the case. Indeed, I did not characterise any anti-viral activity for IFI44/L in any context tested. It is plausible that IFI44/L cleavage is merely a bystander effect of infection: IFI44/L may simply contain a recognition site for an introduced or activated protease and are cleaved pleiotropically. Nonetheless, with our knowledge that these are two highly upregulated

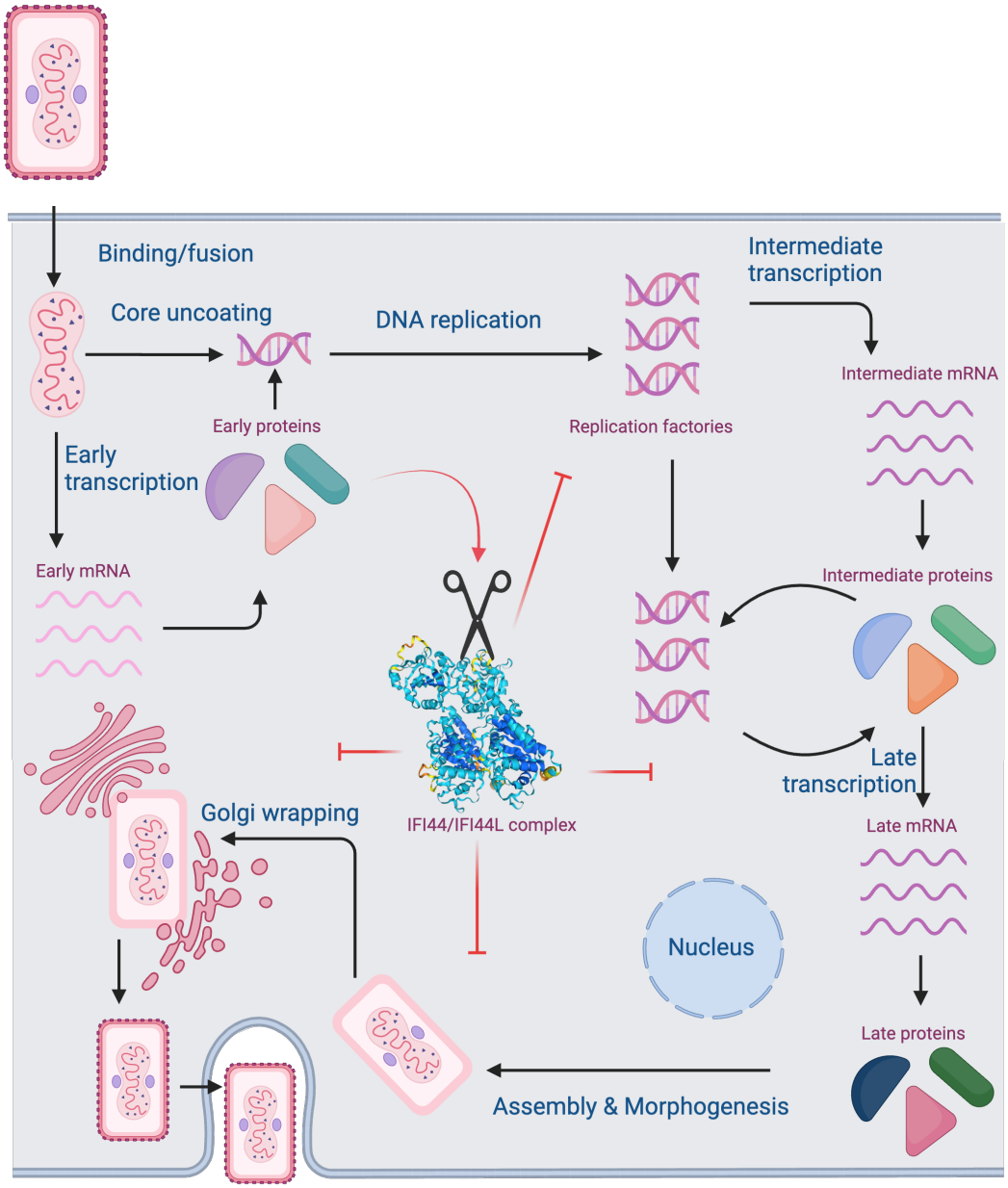


Figure 6.1: IFI44/L are cleaved by VACV.

VACV replicates entirely in the nucleus. Black arrows indicate the VACV lifecycle. Red arrows indicate my hypothesis that the IFI44/L oligomer is cleaved by VACV in order to antagonise notional anti-viral activity.

ISGs during infection, and that VACV employs an arsenal of host innate antagonists, in my view this is unlikely to be a coincidence. Careful co-evolution of humans and viruses tends to disallow such pleiotropic effects, and many aspects of viral infection have specific purpose. An example of this is defective viral particles: initially considered to be an unintentional byproduct of infection, recent studies indicate that these do have

pathological purpose (33). Indeed, given that viral genome size is limiting, all viral-employed proteins should have specific targets and functions in order to enable productive infection and replication.

We have only observed this cleavage when overexpressing tagged proteins in HEK293T cells and did not observe cleavage of endogenous IFI44 (induced by IFN pretreatment). This is likely due to experimental restrictions, as VACV cannot effectively infect an IFN-pretreated cell, and IFI44 needs to be expressed to high levels to detect the relatively small cleavage band. IFI44L has a much more prevalent and strong cleavage band, however we do not have a specific antibody detecting endogenous IFI44L at our disposal, currently preventing further investigation.

I am planning a set of future experiments to determine whether VACV deletion mutants, which have stretches of genes missing from either end of the genome, can still cause the cleavage of IFI44/L (34, 35). This would provide information on which genes may be responsible for this cleavage event seen. Further, this finding has given rise to a project being taken on by a new D.Phil student joining the lab, who aims to characterise where the cleavage site is, whether blocking this cleavage results in attenuated virus infection, and the mechanism of action of putative anti-viral activity. Identifying the mechanism by which a novel anti-viral ISG attenuates VACV infection, and how VACV might mitigate this through cleavage, is of clinical importance, for instance in the use of vaccine vectors, and treatment of infection of other pox viruses, such as MPOX.

6.1.1 IFI44 and *in vivo* infection

HEK293T cells are known to lack many innate immune sensors, for example cGAS, most TLRs and inflammasomes and in some settings have defective IFN and cytokine responses as a result (36). To circumvent this, we could have tested viral infectivity in cell types naturally infected, for example lung cells in the case of IAV. However, we decided that the *Ifi44*$^{-/-}$ mouse model would be more informative, as the immune response to infection in a mammal has many more layers of complexity than that of a 2D cell culture. This includes soluble factors such as complement, limiting factors such as iron, and a complete and intact adaptive immune response. Previously, *Ifi44*$^{-/-}$ mice on a C57BL/6 background have been reported to display heightened susceptibility to RSV infection, with greater weight loss at days five to seven after infection (5). This was attributed to higher levels of RSV RNA in the lung at day four of infection. However, the authors of this study found no differences in levels of any cytokines tested, nor of *Ifn*β or *Ifn*γ expression (5). We infected *Ifi44*$^{-/-}$ mice with IAV/X-31, which like RSV, is a negative-sense RNA virus administered intranasally. However, we chose a recovery instead of an acute infection model. In our setting, we observed no difference in viral RNA titres in the lung at day 3 of infection,

nor any differences in weight loss in the early stage of infection. However, we observed that *Ifi44*$^{-/-}$ mice had a delayed weight recovery at day 10 of infection. We additionally detected no differences in IFN signalling (by assessing ISG expression), similar to the published data during RSV infection (5). Reasons for differences in observations could be due to the viruses used: while these two viruses are both negative-sense RNA viruses, they are from different families. In addition, the type of infection employed was different: we infected with a non-lethal dose and studied recovery, whereas the RSV model was a lethal dose without recovery. Interestingly, we could not attribute the delayed weight recovery of *Ifi44*$^{-/-}$ mice at day 10 to differences in IFN signalling or adaptive immunity; measured by ISG expression, antigen-specific CD8^{+} T cell abundance and neutralising antibody titres. It is possible that there were differences in infiltrating immune cell populations, and we did not perform a total leukocyte immunophenotyping to address this, although the lung and spleen index showed no difference at days 3 and 10 post-infection. We have therefore not identified what could be causing the lack of recovery observed in *Ifi44*$^{-/-}$ mice at 10 days post IAV/X-31 infection. Potential hypotheses for this include a difference in motility or a difference in metabolism and appetite.

It is well documented that the haemagglutinin molecule on the surface of influenza viruses can agglutinate RBCs (37). Indeed, this property is the premise behind the haemagglutination inhibition assay used by influenza virologists for antigenic characterisation (38-41). Influenza infection and vaccination in humans can trigger autoimmune haemolytic anaemia (42-44). One could postulate that *Ifi44*$^{-/-}$ mice are more prone to developing haemolytic disease post infection, and this is the cause of the reduced weight recovery at day 10 post-infection. However, it has been shown that limiting iron results in a weaker neutralising antibody response (45), which we did not observe. Whether haemolysis is contributing to disease pathology in IAV infection of *Ifi44*$^{-/-}$ mice remains to be seen.

6.2 *Ifi44* and cell cycle control

I observed that *Ifi44*$^{-/-}$ murine spleens downregulated genes involved in the cell cycle, which is complimented by various studies documenting anti-proliferative activity for IFI44 (5, 46). Functionally, this may provide an anti-cancer defence, and both IFI44 and IFI44L have been implicated in various cancers (47-55). However, flow cytometric analysis on bulk splenic tissue could not discern any differences in cell cycle phasing. This could be explained through bulk effects: RNA-sequencing is sensitive enough to determine gene downregulation by a small subset of genes in the spleen, however, flow cytometric analysis may not be. Therefore, a future experiment could gate on different cell types in the spleen, and then perform cell cycle analysis on each population. Additionally, single-cell RNA

sequencing would allow for the identification of cellular populations responsible for this downregulation. While there was no gene ontology for cell cycle control in downregulated genes in *Ifi44*$^{-/-}$ livers, there were some shared genes downregulated in the liver and the spleen involved in cell cycle control: *Cenpf*, *Stmn1*, *Mki67*, *Aspm*, *Kif15* and *Ckap2*. As such, this phenotype may be generalised across organs of *Ifi44*$^{-/-}$ mice. However, there was no difference in the cellular proliferation of *Ifi44*$^{-/-}$ and *Ifi44*$^{+/+}$ MEFs, nor human cell lines overexpressing IFI44/L. Further research is needed to determine the cell types responsible for the transcriptional differences in cell cycle control observed in *Ifi44*$^{-/-}$ spleens and livers, and how these translate to phenotypic differences in cells.

6.3 *Ifi44* and erythrocyte homeostasis

I discovered that *Ifi44*$^{-/-}$ mice had a transcriptional reduction in genes involved in haem biosynthesis. Upon examination of the erythrocytic recycling pathway, I observed that *Ifi44*$^{-/-}$ mice had a reduced RPM population, which was not accompanied by overall differences in their splenic myeloid compartment. Further, *Ifi44*$^{-/-}$ RPMs expressed less CD163, indicating that they were less able to scavenge haem. This did not seem to be solely due to CD163 cleavage into its soluble form (56-59), as transcript levels of *Cd163* mRNA were also significantly reduced. At steady-state, systemic iron homeostasis is maintained through the recycling of senescent RBCs by splenic RPMs (60), which use haem oxygenase 1 to degrade haem, liberating iron (61), and ferroportin to deliver iron to the plasma, supporting bone marrow erythropoiesis (62). Clinically, a reduction in RPMs is associated with malaria (63-65), presumably as a result of intravascular haemolysis (66). Agreeing with this, mouse models of anaemia (67, 68) and malaria (69) show a reduction in the RPM compartment. Alongside this reduction in RPMs, *Ifi44*$^{-/-}$ mice presented with microcytic RBCs, increased splenic insoluble iron deposits and a delayed recovery following experimental acute haemolytic anaemia. This suggests that *Ifi44*$^{-/-}$ mice had increased intravascular haemolysis; however, whether this is the cause of the reduction in RPMs, or a result of the reduction in RPMs, is unknown. Studies into IFI44 localisation and binding partners are likely to shed additional light on its cellular and molecular functions if performed in relevant cell types such RPMs. *Ifi44*$^{-/-}$;*Adar1*$^{mZa/mZa}$ mice phenocopied *Ifi44*$^{-/-}$ mice in their red blood cell parameters and RPM abundance, suggesting that maintaining erythrocytic homeostasis is a baseline role for *Ifi44*, unchanged by upregulated ISGs. In future work it would be interesting to confirm this through a chronic infection model, such as MCMV. Interestingly, *Ifi44*$^{-/-}$ mice showed no defect in bone marrow or splenic erythropoiesis, both in homeostasis and after erythroid-stress, despite the reduction in splenic RPM populations. Splenic and bone marrow RPMs play an important role during erythropoiesis, as they act as the EBI macrophage, which facili-

tates the process through providing iron and taking up extruded nuclei, amongst other key roles (70-72). During erythroid stress, this EBI macrophage can be recruited from monocyte-derived macrophages (67, 73), meaning that while *Ifi44*$^{-/-}$ mice had a reduction in tissue-resident RPMs, perhaps monocyte-derived macrophages could compensate for this loss during erythropoiesis. Further, erythropoiesis is sensitive to reductions in iron availability (74-76), and total haemoglobin levels in the blood of *Ifi44*$^{-/-}$ mice remained the same as those of *Ifi44*$^{+/+}$ mice, indicating that there may not be a functional reduction in iron availability. Agreeing with this, total serum iron concentrations did not differ between the genotypes. However, serum transferrin saturation may be a better determinant of iron bioavailability, something that should be tested in future work. Total systemic iron homeostasis may be maintained by liver KCs under certain circumstances to increase iron recycling (77, 78), enabling erythropoietic functionality. The KC population of *Ifi44*$^{-/-}$ mice could not be addressed due to time constraints, although models of murine haemolytic anaemia indicate that KCs are able to compensate for a loss in RPMs (78). In a mouse model of malaria, infiltrating monocytes are also important to provide disease control (64), along with renal epithelial cells (69). The extent to which these populations might be different in *Ifi44*$^{-/-}$ mice at baseline has not been addressed, although the increased splenic iron loading observed would indicate that there may be a defect in splenic erythrocyte recycling. When acute haemolytic anaemia was induced in *Ifi44*$^{-/-}$ mice with PHZ, I observed a trend towards a decrease in total numbers of infiltrating monocytes. Although this was statistically non-significant, it may perhaps indicate there was less capacity in *Ifi44*$^{-/-}$ mice for monocyte-derived macrophages to rescue the phenotype. In addition, PHZ-treated *Ifi44*$^{-/-}$ mice were not able to expand their RPM compartment – which may result in the delayed weight recovery observed at day 10, due to a slower recovery from acute anaemic stress and heightened lethargy. Interestingly, monocytes and RPMs from PHZ-treated mice of both genotypes displayed similar Ly6C, VCAM-1 and CD163 expression patterns – confirming previous findings that these markers are dysregulated after PHZ treatment (79). Additionally, blood parameters of PHZ-treated mice of both genotypes were similar, and PHZ-treated macrophages and monocytes from both genotypes showed equal erythrophagocytic capacity, as determined by intracellular Ter119 staining. I hypothesise that these findings were due to saturation effects, and a lower dose of PHZ may allow for differences to arise between the genotypes – in blood profile, erythrophagocytic capacity and cell surface markers. Future work should include erythrophagocytosis assays, which would determine whether RPMs from *Ifi44*$^{-/-}$ mice have different erythrophagocytic capabilities or whether microcytic RBCs from *Ifi44*$^{-/-}$ mice are more readily engulfed. In addition, it would be interesting to repeat the histological experiments after induced haemolytic anaemia, to determine whether an increase in splenic iron loading in *Ifi44*$^{-/-}$ mice is partly responsible for the reduced recovery observed at day

10.

While no differences in erythropoietic staging were detected in the bone marrow, the ratio of reticulocytes to mature RBCs in the blood was not tested. It is possible that *Ifi44*$^{-/-}$ mice have reticulocytosis, which would explain the microcytic phenotype of the RBCs. Moreover, reticulocytosis in patients is often the result of haemolytic anaemia (80, 81), meaning this would go together with an increased intravascular haemolysis phenotype.

Functionally, I observed that *Ifi44*$^{-/-}$ spleens express significantly less *Prdx2*, knock-out of which is linked with severe haemolytic anaemia in mice (82). Further, *Ifi44*$^{-/-}$ BMDMs were more sensitive to cell death induced by haem. Since the haem-responsive RPM-specific transcription factor, SPI-C, was expressed at similar levels in *Ifi44*$^{-/-}$ and *Ifi44*$^{+/+}$ mice, it is possible that the reduction in the RPM population seen in *Ifi44*$^{-/-}$ mice is due to oxidative cell death - which could be both a cause and a consequence of intravascular haemolysis. Iron-induced cell death typically manifests as ferroptosis (83), but it should be noted that haemolysis can also result in inflammasome activation and induction of other forms of regulated cell death (84). Currently there have not been any major discoveries on the interplay between ferroptosis and erythrocyte homeostasis, however increased uptake of senescent erythrocytes by splenic macrophages induces ferroptosis in mice (85) and ferroptosis provides protection against severe disease in a mouse model of malaria (86, 87). As such, I hypothesise that ferroptosis and erythrocyte homeostasis are intrinsically interlinked, with IFI44 as a putative key player. IFI44 contains a highly conserved TLDc domain, with presence of this domain alone (from other proteins) being protective against oxidative stress, albeit involving unknown mechanisms (88, 89). This domain is conserved from *E. coli* (90) to almost all eukaryotes (89, 91). As such, I predicted that the TLDc domain of IFI44 could protect against oxidative stress-induced cell death in RPMs.

6.3.1 The role of the TLDc domain of IFI44/L in ferroptosis and endosome acidification

While all the other human TLDc domain-containing proteins have oxidative-stress resistance related functions *in vitro* (88, 89), I could not reproduce this finding in HEK293T cells overexpressing IFI44, nor in *Ifi44*$^{-/-}$ MEFs. While I used the same cell-death inducing agent (sodium arsenite) as a prior study, the cell line used differed – Finelli *et al.* overexpressed TLDc-domain containing proteins in N2a cells, a mouse neuroblast cell line (89). This is because other TLDc-domain containing proteins exert neuroprotective effects in mice and humans (89, 92-95). Whether IFI44/L are neuroprotective remains to be seen, although there are no recorded human SNPs providing evidence to this, and *Ifi44*$^{-/-}$ mice do not show outward signs of neurodegeneration. Still, it is possible that

lentivirus-mediated overexpression of tagged protein in HEK293T cells was not an appropriate model for studying oxidative stress resistance. Planned future experiments include the induction of ferroptosis using GPX4 inhibitors in the presence and absence of IFI44. If a protective role for IFI44 can be detected in this setting, mutant protein could be generated without the TLDc domain, to determine whether this rescues the phenotype. In addition, haem-induced ferroptosis can be induced and measured in *Ifi44*$^{-/-}$ and *Ifi44*$^{+/+}$ RPMs *ex vivo*. Lipid peroxidation and ROS levels in RPMs could be determined by flow cytometry, along with commercially available assay kits. This would provide context as to whether *Ifi44* expression levels correlate with lipid peroxidation.

Interestingly, other human TLDc-domain containing proteins bind the V-ATPase, a conserved function that is shared with the TLDc domain of yeast proteins (91, 96, 97). The short isoform of NCOA7 arising from an alternative start site, NCOA7-AS, uses this ability to exert antiviral effects. NCOA7-AS interacts with the V-ATPase and promotes the acidification of virus containing endosomes, which prevents viral membrane fusion (98). Immunoprecipitation of tagged IFI44 overexpressed in HEK293T cells did not detectably co-precipitate the V-ATPase using two detection methods: mass spectrometry and western blot. I also mined a published V-ATPase interactome dataset from mouse kidneys, which identified TLDc-domain containing proteins as V-ATPase interactors (97, 99). This study did not identify IFI44 as a V-ATPase interactor (99). The authors specifically studied the kidney V-ATPase and used antibodies to the highly tissue-specific B1 subunit of the V-ATPase. As such, if IFI44 does not interact with the kidney isoform of the V-ATPase (100), it would not have been found in this study. In addition, other known B1 interactors were also not identified by the study (see figure S5 in ref (99)), and one TLDc domain containing protein, TBC1D24, was detected but did not reach their stringent threshold (99). However, since this is a function conserved down to yeast (91), I predict that if IFI44 contained a functional TLDc domain it would bind to the V-ATPase. Perhaps the settings in which best to investigate this interaction require optimisation, e.g. by testing different cell models (for example, RPMs) and different V-ATPase subunits. The consequence of any interaction of IFI44 with the V-ATPase is unknown, but could be important in the endocytosis of transferrin bound iron (101, 102) and haem (103-105), both of which are processes requiring endosomal acidification by the V-ATPase.

6.3.2 IFI44 and parasitic infection

Likely a consequence of the reduction in RPMs, iron loading and haem sensitivity, *Ifi44*$^{-/-}$ mice show a delayed recovery to PHZ-induced acute haemolytic anaemia. I therefore hypothesise that *Ifi44* is important in diseases resulting in acute haemolysis – for example, parasitic infection. Excitingly, *Ifi44* expression has previously been identified as a

correlate of protection in a bioinformatic analysis of *Babesia microti* – a RBC-infecting parasite - infected murine spleens, along with *TfR1* (106). However, this study relied solely on gene expression data, and since type I IFN is a correlate of protection during liver-stage parasitaemia (but with conflicting roles in blood-stage), increased *Ifi44* gene expression could be indicative of IFN levels (107, 108). Thus, parasitic challenges of *Ifi44*$^{-/-}$ mice would be a better model to determine the role of *Ifi44* during infection and represents important future work for the project. Working with a collaborator, I plan to infect *Ifi44*$^{-/-}$ and *Ifi44*$^{+/+}$ mice intravenously with a recently mosquito-transmitted rodent malaria strain, *P. chabaudi* which constitutively expresses GFP (109). Read-outs would entail weight loss over a 20-day period, parasitaemia, infected and total RBC count, haemoglobin levels and liver and serum iron concentrations, alongside flow cytometry to assess the splenic myeloid compartment, particularly RPMs. I hypothesise that *Ifi44*$^{-/-}$ mice will show reduced recovery from parasitic-induced haemolysis, and fail to expand their RPM compartment alongside displaying increased serum and tissue iron concentrations. The extent of parasitaemia in *Ifi44*$^{-/-}$ mice will be interesting to address; as parasites show a preference for replicating in reticulocytes, and I hypothesise that *Ifi44*$^{-/-}$ mice have reticulocytosis, which would explain their microcytic phenotype (110). In addition, IFI44 itself may directly confer inherent protection against parasitic infection, which would affect parasitaemia and infected RBC count. On the other hand, the microcytes observed in *Ifi44*$^{-/-}$ mice may be less amenable to parasitic infection (110). Iron supplementation is a risk factor in human children for malaria infection (111), and *Ifi44*$^{-/-}$ mice show no difference in total serum iron concentrations at steady-state, meaning that iron bioavailability is likely analogous in *Ifi44*$^{-/-}$ and *Ifi44*$^{+/+}$ mice. However, transferrin saturation has not been determined, nor whether this changes during acute haemolytic anaemia. As such, it will be interesting to uncover any differences in parasitaemia between the genotypes and determine their cause.

6.4 IFI44: the interface of IFN signalling and iron homeostasis

I demonstrated that IFI44 is an ISG, which may have a role in regulating erythroid homeostasis – speculatively through regulating macrophage iron or haem uptake and/or oxidative cell death, thereby controlling intravascular haemolysis. Why is it that mammals would evolve to utilise an innate immune protein to act in this pathway? The answer plausibly lies in iron homeostasis and innate immunity being interlinked. Iron is a scarce but important molecule, coveted by many life forms. Humans have evolved to both recycle iron, and guard it from pathogens. For example, labile haem results in

trained immunity, which confers long term regulation of lineage specific haematopoietic stem cells and priming towards myelopoiesis (112). Innate immune dysfunction also has links to anaemia. Defective reticulocyte maturation and mitochondrial retention is the causative pathology in some SLE patients (113). In addition, 50% of SLE patients experience anaemia, with this predominantly manifesting as AoI (114). In children with SLE, autoimmune haemolytic anaemia can be the initial presentation of disease (115). The evolutionary driving force behind these observations lie in host-pathogen interaction and so-called nutritional immunity (116). This is the process by which a host sequesters trace metals in order to limit pathogen replication. In turn, pathogens have evolved strategies to survive metal depletion and scavenge metal ions from the host (117). Sometimes the interplay between the two can lead to disease tolerance, in which host homeostasis is sustained without interfering with the invading microbes (118).

This led us to determine whether knock-out of *Ifi44* would render cells more susceptible to bacterial infection, hypothesising that IFI44 is important for iron homeostasis. In *Ifi44*$^{-/-}$ BMDMs, there was no difference in IL-1β or LDH release in response to stationary phase *Salmonella typhimurium*Δ*OrgA*Δ*FliC/FliB* or *Francisella*, nor challenge with NLRP3, NLRC4 or AIM2 agonists. However, it is possible that in the wild-type BMDMs, *Ifi44* was not induced to high enough levels prior to these challenges, and that therefore there was only a small difference in *Ifi44* expression levels between wild-type and knockout cells. It is plausible that the role for IFI44 in defending against bacterial infection could be in the context of viral-bacterial co-infection. Co-infection of *Streptococcus pneumoniae* after IAV infection can lead to fatal pneumonia (119, 120) and in a mouse model, IAV predisposes towards *S. pneumoniae* co-infection (121). It is possible that IAV infection would result in *Ifi44* upregulation, which may regulate iron homeostasis and defend against bacterial co-infection. In the future, utilising a mouse co-infection challenge model (121) might determine whether this hypothesis has merit.

Pathogens can directly infect RBCs. It is plausible that a protein at the interface of innate immunity and iron homeostasis could defend against parasitic RBC infection, and the resulting haemolytic anaemia – and I have observed that *Ifi44*$^{-/-}$ mice showed a delayed recovery after induction of acute haemolytic anaemia with PHZ, indicating that perhaps *Ifi44* is of importance in parasitic RBC infection.

It is worth noting with these mouse studies that C57BL/6 mice naturally lack *Ifi44l*. Therefore, while we have eliminated redundancy in the system, the "wild-type" mouse does not have *Ifi44l*. As such, if these two proteins do work together in anti-viral immunity or otherwise, we might not be capturing the full effects with this model. It would be interesting to discover whether the iron-related observations and influenza infection in the *Ifi44*$^{-/-}$ mouse would be more pronounced when knocking-in *Ifi44l* to the wild-type

C57BL/6, or using an *Ifi44*$^{-/-}$;*Ifi44l*$^{-/-}$ mouse on a BALB background.

It is curious how an ISG, the expression of which is strongly upregulated by IFN in almost every cell type, would carry out a basal role in a small splenic cellular population: RPMs. It's therefore possible that IFI44 has evolved to play two separate roles; one at baseline in RPMs, which do have high baseline IFN signalling, and one in all other cell types after IFNAR engagement. RIG-I is an ISG with two predicted roles: after IFN signalling, RIG-I can sense cytosolic RNA, but at baseline, RIG-I has been implicated in digestive organ homeostasis through commensal engagement (122-124). Another possibility is that *IFI44* has evolved a very sensitive ISRE, which allows the protein to be induced in response to small amounts of IFN, as in RPMs. It is here, at baseline, where IFI44 maintains iron homeostasis. Upon infection and subsequent IFN signalling, most other cells upregulate IFI44, and RPMs also upregulate IFI44 to higher levels. This provides all cells with the capacity to utilise IFI44 in defending against oxidative stress as a consequence of haemolysis, which is caused by many pathogens. Meanwhile, IFI44 is able to maintain key erythrophagocytic populations. An example of a different ISG that applies its baseline function to anti-pathogenic capacity is SAMHD1. At baseline, SAMHD1 is responsible for maintaining the cellular dNTP pool, however after retroviral infection, SAMHD1 is upregulated and can deplete available dNTPs to prevent retroviral replication (125). Therefore, it is possible that a prototypical ISG expressed by almost all cell types has a specialised role at baseline, and can adopt additional function during an infection.

I have shown, using a mouse model with a genetic ablation of *Ifi44*, that *Ifi44* deficiency results in microcytic RBCs and a reduction in RPMs resulting in reduced iron-recycling capacity (Figure 6.2). In turn, this results in splenic iron loading and is likely the driving force behind the transcriptional reduction in genes involved in haem biosynthesis. I also observed that *Ifi44*$^{-/-}$ BMDMs are more sensitive to haem-induced cell death, and *Ifi44*$^{-/-}$ mice show a delayed recovery to induced acute anaemia. I hypothesise that IFI44 is protective against oxidative cell death in RPMs, likely attributed to its TLDc domain. As such, a loss of *Ifi44* results in susceptibility to oxidative stress, a reduced RPM population, and iron homeostatic dysregulation. Future work should aim to determine on a molecular level the mechanism of action of IFI44: how the protein functions in RPMs, and the relative contribution of each protein domain. In addition, to determine whether tissue iron loading contributes towards pathological consequence in *Ifi44*$^{-/-}$ mice, one could limit iron bioavailability using mini-hepcidin (45) and determine whether this provides a rescue to the phenotype.

In conclusion, the work presented in this thesis presents IFI44 as a novel link between the IFN response and erythrocyte homeostasis. This could pave the way for future interdisci-

plinary research on the importance of type I IFN in iron homeostasis, and the importance of IFI44 in controlling clinically relevant diseases such as autoimmune haemolytic anaemia and malaria.

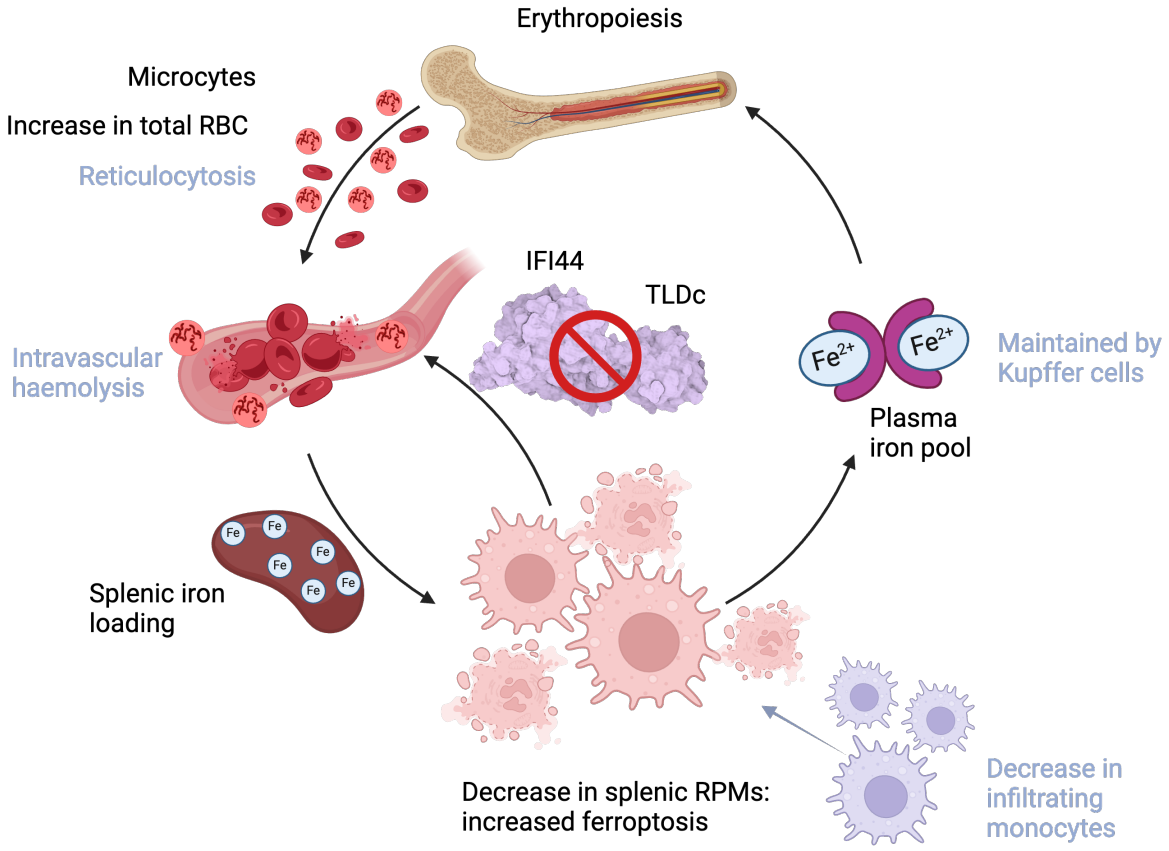


Figure 6.2: The working hypothesis model.

Mice with a genetic ablation of *Ifi44* have a decreased RPM population. As such, there is a reduced capacity to recycle senescent RBCs, and likely more intravascular haemolysis. In turn, this results in increased splenic iron loading, which feeds into the reduction in RPM population. Black text represents findings outlined in this thesis; blue text represents hypotheses.

References for Chapter 6

1. J. W. Schoggins et al., A diverse range of gene products are effectors of the type I interferon antiviral response. Nature 472, 481-485 (2011).
2. J. W. Schoggins, C. M. Rice, Interferon-stimulated genes and their antiviral effector functions. Curr Opin Virol 1, 519-525 (2011).
3. J. W. Schoggins, Interferon-Stimulated Genes: What Do They All Do? Annual Review of Virology 6, 567-584 (2019).
4. J. W. Schoggins et al., Pan-viral specificity of IFN-induced genes reveals new roles for cGAS in innate immunity. Nature 505, 691-695 (2014).
5. D. C. Busse et al., Interferon-Induced Protein 44 and Interferon-Induced Protein 44-Like Restrict Replication of Respiratory Syncytial Virus. J Virol 94, (2020).
6. C. Carlton-Smith, R. M. Elliott, Viperin, MTAP44, and Protein Kinase R Contribute to the Interferon-Induced Inhibition of Bunyamwera Orthobunyavirus Replication. Journal of Virology 86, 11548-11557 (2012).
7. D. Power et al., IFI44 suppresses HIV-1 LTR promoter activity and facilitates its latency. Virology 481, 142-150 (2015).
8. M. Sun et al., Screening Host Antiviral Proteins under the Enhanced Immune Responses Induced by a Variant Strain of Porcine Epidemic Diarrhea Virus. Microbiol Spectr 10, e0066122 (2022).
9. X. Qu et al., Potential roles of IFI44 genes in high resistance to Vibrio in hybrids of Argopecten scallops. Fish Shellfish Immunol, 108702 (2023).
10. M. L. DeDiego, A. Nogales, L. Martinez-Sobrido, D. J. Topham, Interferon-Induced Protein 44 Interacts with Cellular FK506-Binding Protein 5, Negatively Regulates Host Antiviral Responses, and Supports Virus Replication. mBio 10, (2019).
11. Q. Zheng, D. Wang, R. Lin, Q. Lv, W. Wang, *IFI44* is an immune evasion biomarker for SARS-CoV-2 and *Staphylococcus aureus* infection in patients with RA. Front Immunol 13, 1013322 (2022).
12. A. S. Häusl et al., The co-chaperone *Fkbp5* shapes the acute stress response in the paraventricular nucleus of the hypothalamus of male mice. Molecular Psychiatry 26, 3060-3076 (2021).
13. M. Kästle et al., FKBP51 modulates steroid sensitivity and NFB signalling: A novel anti-inflammatory drug target. Eur J Immunol 48, 1904-1914 (2018).
14. M. D. Greseth, P. Traktman, The Life Cycle of the Vaccinia Virus Genome. Annu Rev Virol 9, 239-259 (2022).
15. M. W. Bahar et al., How vaccinia virus has evolved to subvert the host immune response. J Struct Biol 175, 127-134 (2011).
16. B. Hernáez et al., A virus-encoded type I interferon decoy receptor enables evasion of

host immunity through cell-surface binding. Nature Communications 9, 5440 (2018).
17. D. L. Veyer, G. Carrara, C. Maluquer de Motes, G. L. Smith, Vaccinia virus evasion of regulated cell death. Immunol Lett 186, 68-80 (2017).
18. C. Talbot-Cooper et al., Poxviruses and paramyxoviruses use a conserved mechanism of STAT1 antagonism to inhibit interferon signaling. Cell Host Microbe 30, 357-372.e311 (2022).
19. G. L. Smith, Vaccinia virus immune evasion. Immunol Lett 65, 55-62 (1999).
20. G. L. Smith, Vaccinia Virus Protein C6: A Multifunctional Interferon Antagonist. Adv Exp Med Biol 1052, 1-7 (2018).
21. B. Hernaez, A. Alcamí, Poxvirus Immune Evasion. Annual Review of Immunology 42, 551-584 (2024).
22. N. Meade et al., The poxvirus F17 protein counteracts mitochondrially orchestrated antiviral responses. Nature Communications 14, 7889 (2023).
23. M. El-Jesr, M. Teir, C. Maluquer de Motes, Vaccinia Virus Activation and Antagonism of Cytosolic DNA Sensing. Front Immunol 11, 568412 (2020).
24. C. M. Byrd, D. E. Hruby, Vaccinia virus proteolysis–a review. Rev Med Virol 16, 187-202 (2006).
25. C. M. Byrd, T. C. Bolken, D. E. Hruby, The vaccinia virus I7L gene product is the core protein proteinase. J Virol 76, 8973-8976 (2002).
26. J. S. Chen et al., Cleavage of Dicer protein by I7 protease during vaccinia virus infection. PLoS One 10, e0120390 (2015).
27. C. Ansarah-Sobrinho, B. Moss, Role of the I7 protein in proteolytic processing of vaccinia virus membrane and core components. J Virol 78, 6335-6343 (2004).
28. C. Ansarah-Sobrinho, B. Moss, Vaccinia virus G1 protein, a predicted metalloprotease, is essential for morphogenesis of infectious virions but not for cleavage of major core proteins. J Virol 78, 6855-6863 (2004).
29. M. Hedengren-Olcott, C. M. Byrd, J. Watson, D. E. Hruby, The vaccinia virus G1L putative metalloproteinase is essential for viral replication *in vivo*. J Virol 78, 9947-9953 (2004).
30. S. S. Whitehead, N. A. Bersani, D. E. Hruby, Physical and molecular genetic analysis of the multistep proteolytic maturation pathway utilized by vaccinia virus P4a protein. J Gen Virol 76 (Pt 3), 717-721 (1995).
31. E. M. Kane, S. Shuman, Vaccinia virus morphogenesis is blocked by a temperature-sensitive mutation in the I7 gene that encodes a virion component. J Virol 67, 2689-2698 (1993).
32. V. Katritch et al., Discovery of small molecule inhibitors of ubiquitin-like poxvirus proteinase I7L using homology modeling and covalent docking approaches. J Comput Aided Mol Des 21, 549-558 (2007).

33. M. Vignuzzi, C. B. López, Defective viral genomes are key drivers of the virus–host interaction. Nature Microbiology 4, 1075-1087 (2019).
34. G. J. Kotwal, B. Moss, Analysis of a large cluster of nonessential genes deleted from a vaccinia virus terminal transposition mutant. Virology 167, 524-537 (1988).
35. J. A. Symons et al., The vaccinia virus C12L protein inhibits mouse IL-18 and promotes virus virulence in the murine intranasal model. J Gen Virol 83, 2833-2844 (2002).
36. J. B. Reus, G. S. Trivino-Soto, L. I. Wu, K. Kokott, E. S. Lim, SV40 Large T Antigen Is Not Responsible for the Loss of STING in 293T Cells but Can Inhibit cGAS-STING Interferon Induction. Viruses 12, (2020).
37. R. T. C. Huang, R. Rott, H.-D. Klenk, Influenza viruses cause hemolysis and fusion of cells. Virology 110, 243-247 (1981).
38. A. Reber, J. Katz, Immunological assessment of influenza vaccines and immune correlates of protection. Expert Rev Vaccines 12, 519-536 (2013).
39. M. Zacour et al., Standardization of Hemagglutination Inhibition Assay for Influenza Serology Allows for High Reproducibility between Laboratories. Clinical and Vaccine Immunology 23, 236-242 (2016).
40. S. Sawant et al., H3N2 influenza hemagglutination inhibition method qualification with data driven statistical methods for human clinical trials. Front Immunol 14, 1155880 (2023).
41. M. L. Killian, Hemagglutination assay for influenza virus. Methods Mol Biol 1161, 3-9 (2014).
42. S. Montagnani et al., Autoimmune hemolytic anemia following MF59-adjuvanted influenza vaccine administration: a report of two cases. Ann Pharmacother 45, e8 (2011).
43. Y. Schoindre, G. Bollée, M. D. Dumont, P. Lesavre, A. Servais, Cold agglutinin syndrome associated with a 2009 influenza A H1N1 infection. Am J Med 124, e1-2 (2011).
44. V. Silecchia et al., Influenza-associated hemolytic uremic syndrome: The pathogenic role of the virus. Clin Nephrol Case Stud 9, 45-48 (2021).
45. J. N. Frost et al., Hepcidin-Mediated Hypoferremia Disrupts Immune Responses to Vaccination and Infection. Med 2, 164-179.e112 (2021).
46. L. C. Hallen et al., Antiproliferative activity of the human IFN-alpha-inducible protein IFI44. J Interferon Cytokine Res 27, 675-680 (2007).
47. D. Rupa et al., ACSL4 upregulates IFI44 and IFI44L expression and promotes the proliferation and invasiveness of head and neck squamous cell carcinoma cells. Cancer Sci, (2024).
48. Y. Zeng et al., Comprehensive Analysis of Immune Implication and Prognostic Value of IFI44L in Non-Small Cell Lung Cancer. Frontiers in Oncology 11, (2022).
49. E. Boccardo et al., Expression of human papillomavirus type 16 E7 oncoprotein alters keratinocytes expression profile in response to tumor necrosis factor-alpha. Carcinogene-

sis 31, 521-531 (2010).
50. A. Reyimu et al., Identification of latent biomarkers in connection with progression and prognosis in oral cancer by comprehensive bioinformatics analysis. World J Surg Oncol 19, 240 (2021).
51. W.-C. Huang, S.-L. Tung, Y.-L. Chen, P.-M. Chen, P.-Y. Chu, IFI44L is a novel tumor suppressor in human hepatocellular carcinoma affecting cancer stemness, metastasis, and drug resistance via regulating met/Src signaling pathway. BMC Cancer 18, 609-609 (2018).
52. H. Pan et al., Interferon-Induced Protein 44 Correlated With Immune Infiltration Serves as a Potential Prognostic Indicator in Head and Neck Squamous Cell Carcinoma. Front Oncol 10, 557157 (2020).
53. H. Wang et al., Long Noncoding RNA LINC01116 Contributes to Gefitinib Resistance in Non-small Cell Lung Cancer through Regulating IFI44. Mol Ther Nucleic Acids 19, 218-227 (2020).
54. Y. Wang, Y. Chen, B. Zhu, L. Ma, Q. Xing, A Novel Nine Apoptosis-Related Genes Signature Predicting Overall Survival for Kidney Renal Clear Cell Carcinoma and its Associations with Immune Infiltration. Front Mol Biosci 8, 567730 (2021).
55. D. Ou, Y. Wu, The prognostic and clinical significance of IFI44L aberrant downregulation in patients with oral squamous cell carcinoma. BMC Cancer 21, 1327 (2021).
56. Y.-J. Yap et al., The clinical utility of CD163 in viral diseases. Clinica Chimica Acta 541, 117243 (2023).
57. A. Droste, C. Sorg, P. Hogger, Shedding of CD163, a novel regulatory mechanism for a member of the scavenger receptor cysteine-rich family. Biochem Biophys Res Commun 256, 110-113 (1999). 58. H. J. Moller, Soluble CD163. Scand J Clin Lab Invest 72, 1-13 (2012).
59. A. Etzerodt et al., Soluble ectodomain CD163 and extracellular vesicle-associated CD163 are two differently regulated forms of 'soluble CD163' in plasma. Scientific Reports 7, 40286 (2017).
60. M. Kohyama et al., Role for Spi-C in the development of red pulp macrophages and splenic iron homeostasis. Nature 457, 318-321 (2009).
61. K. D. Poss, S. Tonegawa, Heme oxygenase 1 is required for mammalian iron reutilization. Proceedings of the National Academy of Sciences 94, 10919-10924 (1997).
62. Z. Zhang et al., Ferroportin1 deficiency in mouse macrophages impairs iron homeostasis and inflammatory responses. Blood 118, 1912-1922 (2011).
63. W. Nahrendorf, A. Ivens, P. J. Spence, Inducible mechanisms of disease tolerance provide an alternative strategy of acquired immunity to malaria. Elife 10, (2021).
64. A.-M. Sponaas et al., Migrating monocytes recruited to the spleen play an important role in control of blood stage malaria. Blood 114, 5522-5531 (2009).

65. K. Deroost et al., Tissue macrophages and interferon-gamma signalling control blood-stage *Plasmodium chabaudi* infections derived from mosquito-transmitted parasites. Current Research in Immunology 2, 104-119 (2021).
66. A. Ferreira, J. Balla, V. Jeney, G. Balla, M. P. Soares, A central role for free heme in the pathogenesis of severe malaria: the missing link? Journal of Molecular Medicine 86, 1097-1111 (2008).
67. M. Haldar et al., Heme-mediated SPI-C induction promotes monocyte differentiation into iron-recycling macrophages. Cell 156, 1223-1234 (2014).
68. G. Kovtunovych, M. A. Eckhaus, M. C. Ghosh, H. Ollivierre-Wilson, T. A. Rouault, Dysfunction of the heme recycling system in heme oxygenase 1-deficient mice: effects on macrophage viability and tissue iron distribution. Blood 116, 6054-6062 (2010).
69. Q. Wu et al., Renal control of life-threatening malarial anemia. Cell Reports 42, 112057 (2023).
70. W. Li et al., Identification and transcriptome analysis of erythroblastic island macrophages. Blood 134, 480-491 (2019).
71. J. A. Chasis, N. Mohandas, Erythroblastic islands: niches for erythropoiesis. Blood 112, 470-478 (2008).
72. R. N. Jacobsen et al., Mobilization with granulocyte colony-stimulating factor blocks medullar erythropoiesis by depleting F4/80(+)VCAM1(+)CD169(+)ER-HR3(+)Ly6G(+) erythroid island macrophages in the mouse. Exp Hematol 42, 547-561.e544 (2014).
73. C. Liao, K. S. Prabhu, R. F. Paulson, Monocyte-derived macrophages expand the murine stress erythropoietic niche during the recovery from anemia. Blood 132, 2580-2593 (2018).
74. G. C. Bullock et al., Iron control of erythroid development by a novel aconitase-associated regulatory pathway. Blood 116, 97-108 (2010).
75. L. T. Goodnough, E. Nemeth, T. Ganz, Detection, evaluation, and management of iron-restricted erythropoiesis. Blood 116, 4754-4761 (2010).
76. A. Kim, E. Nemeth, New insights into iron regulation and erythropoiesis. Curr Opin Hematol 22, 199-205 (2015).
77. P. Slusarczyk, K. Mleczko-Sanecka, The Multiple Facets of Iron Recycling. Genes (Basel) 12, (2021).
78. I. Theurl et al., On-demand erythrocyte disposal and iron recycling requires transient macrophages in the liver. Nature Medicine 22, 945-951 (2016).
79. T. Ulyanova, S. R. Phelps, T. Papayannopoulou, The macrophage contribution to stress erythropoiesis: when less is enough. Blood 128, 1756-1765 (2016).
80. R. S. Riley, J. M. Ben-Ezra, R. Goel, A. Tidwell, Reticulocytes and reticulocyte enumeration. J Clin Lab Anal 15, 267-294 (2001).

81. E. R. Meier, E. C. Wright, J. L. Miller, Reticulocytosis and anemia are associated with an increased risk of death and stroke in the newborn cohort of the Cooperative Study of Sickle Cell Disease. Am J Hematol 89, 904-906 (2014).
82. T. H. Lee et al., Peroxiredoxin II is essential for sustaining life span of erythrocytes in mice. Blood 101, 5033-5038 (2003).
83. S. J. Dixon et al., Ferroptosis: an iron-dependent form of nonapoptotic cell death. Cell 149, 1060-1072 (2012).
84. F. F. Dutra et al., Hemolysis-induced lethality involves inflammasome activation by heme. Proceedings of the National Academy of Sciences 111, E4110-E4118 (2014).
85. L. A. Youssef et al., Increased erythrophagocytosis induces ferroptosis in red pulp macrophages in a mouse model of transfusion. Blood 131, 2581-2593 (2018).
86. H. S. Kain et al., Liver stage malaria infection is controlled by host regulators of lipid peroxidation. Cell Death Differ 27, 44-54 (2020).
87. S. Li et al., Ferroptosis plays an essential role in the antimalarial mechanism of low-dose dihydroartemisinin. Biomed Pharmacother 148, 112742 (2022).
88. M. J. Finelli, P. L. Oliver, TLDc proteins: new players in the oxidative stress response and neurological disease. Mammalian Genome 28, 395-406 (2017).
89. M. J. Finelli, L. Sanchez-Pulido, K. X. Liu, K. E. Davies, P. L. Oliver, The Evolutionarily Conserved Tre2/Bub2/Cdc16 (TBC), Lysin Motif (LysM), Domain Catalytic (TLDc) Domain Is Neuroprotective against Oxidative Stress. The Journal of biological chemistry 291, 2751-2763 (2016).
90. M. R. Volkert, N. A. Elliott, D. E. Housman, Functional genomics reveals a family of eukaryotic oxidation protection genes. Proc Natl Acad Sci U S A 97, 14530-14535 (2000).
91. S. Klössel et al., Yeast TLDc domain proteins regulate assembly state and subcellular localization of the V-ATPase. The EMBO Journal 43, 1870-1897-1897 (2024).
92. K. X. Liu et al., Neuron-specific antioxidant OXR1 extends survival of a mouse model of amyotrophic lateral sclerosis. Brain 138, 1167-1181 (2015).
93. M. G. Williamson et al., Neuronal over-expression of Oxr1 is protective against ALS-associated mutant TDP-43 mislocalisation in motor neurons and neuromuscular defects in vivo. Hum Mol Genet 28, 3584-3599 (2019).
94. M. J. Finelli, K. X. Liu, Y. Wu, P. L. Oliver, K. E. Davies, Oxr1 improves pathogenic cellular features of ALS-associated FUS and TDP-43 mutations. Hum Mol Genet 24, 3529-3544 (2015).
95. M. J. Finelli et al., The epilepsy-associated protein TBC1D24 is required for normal development, survival and vesicle trafficking in mammalian neurons. Human Molecular Genetics 28, 584-597 (2018).
96. R. A. Oot, S. Wilkens, Human V-ATPase function is positively and negatively regulated by TLDc proteins. Structure, (2024).

97. A. F. Eaton, D. Brown, M. Merkulova, The evolutionary conserved TLDc domain defines a new class of (H(+))V-ATPase interacting proteins. Sci Rep 11, 22654 (2021).
98. T. Doyle et al., The interferon-inducible isoform of NCOA7 inhibits endosome-mediated viral entry. Nat Microbiol 3, 1369-1376 (2018).
99. M. Merkulova et al., Mapping the H+ (V)-ATPase interactome: identification of proteins involved in trafficking, folding, assembly and phosphorylation. Scientific Reports 5, 14827 (2015).
100. K. E. Finberg et al., The B1-subunit of the H+ ATPase is required for maximal urinary acidification. Proceedings of the National Academy of Sciences 102, 13616-13621 (2005). 101. Y. Yu et al., Hepatic transferrin plays a role in systemic iron homeostasis and liver ferroptosis. Blood 136, 726-739 (2020).
102. R. S. Ohgami et al., Identification of a ferrireductase required for efficient transferrin-dependent iron uptake in erythroid cells. Nat Genet 37, 1264-1269 (2005).
103. C. White et al., HRG1 is essential for heme transport from the phagolysosome of macrophages during erythrophagocytosis. Cell Metab 17, 261-270 (2013).
104. C. Delaby et al., Subcellular localization of iron and heme metabolism related proteins at early stages of erythrophagocytosis. PLoS One 7, e42199 (2012).
105. K. M. O'Callaghan et al., Heme-binding protein HRG-1 is induced by insulin-like growth factor I and associates with the vacuolar H+-ATPase to control endosomal pH and receptor trafficking. J Biol Chem 285, 381-391 (2010).
106. X. Xue et al., Protein regulation strategies of the mouse spleen in response to Babesia microti infection. Parasit Vectors 14, 61 (2021).
107. I. Sebina, A. Haque, Effects of type I interferons in malaria. Immunology 155, 176-185 (2018).
108. X. He, L. Xia, K. C. Tumas, J. Wu, X. Z. Su, Type I Interferons and Malaria: A Double-Edge Sword Against a Complex Parasitic Disease. Front Cell Infect Microbiol 10, 594621 (2020).
109. S. K. Wideman et al., Cellular iron governs the host response to malaria. PLoS Pathog 19, e1011679 (2023).
110. M. A. Clark et al., Host iron status and iron supplementation mediate susceptibility to erythrocytic stage *Plasmodium falciparum*. Nat Commun 5, 4446 (2014).
111. A. Neuberger, J. Okebe, D. Yahav, M. Paul, Oral iron supplements for children in malaria-endemic areas. Cochrane Database Syst Rev 2, Cd006589 (2016).
112. E. Jentho et al., Trained innate immunity, long-lasting epigenetic modulation, and skewed myelopoiesis by heme. Proc Natl Acad Sci U S A 118, (2021).
113. S. Caielli et al., Erythroid mitochondrial retention triggers myeloid-dependent type I interferon in human SLE. Cell 184, 4464-4479.e4419 (2021).
114. S. Giannouli, M. Voulgarelis, P. D. Ziakas, A. G. Tzioufas, Anaemia in systemic

lupus erythematosus: from pathophysiology to clinical assessment. Ann Rheum Dis 65, 144-148 (2006).
115. Y. Lu, X. M. Huang, Autoimmune hemolytic anemia as an initial presentation in children with systemic lupus erythematosus: two case reports. J Int Med Res 50, 3000605221115390 (2022).
116. C. C. Murdoch, E. P. Skaar, Nutritional immunity: the battle for nutrient metals at the host–pathogen interface. Nature Reviews Microbiology 20, 657-670 (2022).
117. I. Ullah, M. Lang, Key players in the regulation of iron homeostasis at the host-pathogen interface. Front Immunol 14, 1279826 (2023).
118. M. P. Soares, G. Weiss, The Iron age of host-microbe interactions. EMBO Rep 16, 1482-1500 (2015).
119. K. M. Robinson, J. K. Kolls, J. F. Alcorn, The immunology of influenza virus-associated bacterial pneumonia. Current Opinion in Immunology 34, 59-67 (2015).
120. C. Cillóniz et al., Bacterial co-infection with H1N1 infection in patients admitted with community acquired pneumonia. J Infect 65, 223-230 (2012).
121. G. T. Ellis et al., TRAIL+ monocytes and monocyte 2010;related cells cause lung damage and thereby increase susceptibility to influenza 2013; *Streptococcus pneumoniae* coinfection. EMBO reports 16, 1203-1218-1218 (2015).
122. Y. Wang et al., *Rig-I*$^{-/-}$ mice develop colitis associated with downregulation of G alpha i2. Cell Res 17, 858-868 (2007).
123. L. Liu et al., Commensal viruses maintain intestinal intraepithelial lymphocytes via noncanonical RIG-I signaling. Nature Immunology 20, 1681-1691 (2019).
124. H. Zhu et al., RNA virus receptor Rig-I monitors gut microbiota and inhibits colitis-associated colorectal cancer. J Exp Clin Cancer Res 36, 2 (2017).
125. J. Rehwinkel et al., SAMHD1-dependent retroviral control and escape in mice. Embo j 32, 2454-2462 (2013).

Supplementary Information

Supplementary Figures

The following are a list of Supplementary Figures referred to in the earlier chapters.

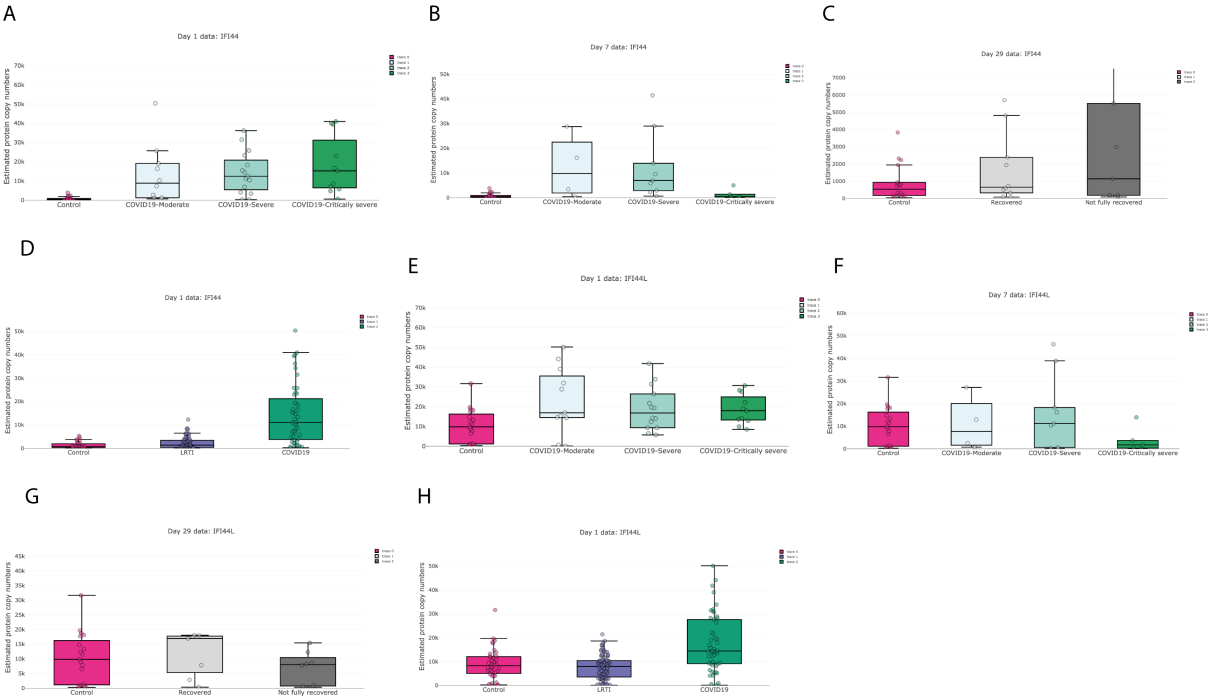


Figure S1: ImmPres Database.

A-H. Plots were generated online using the ImmPRes Database (33).

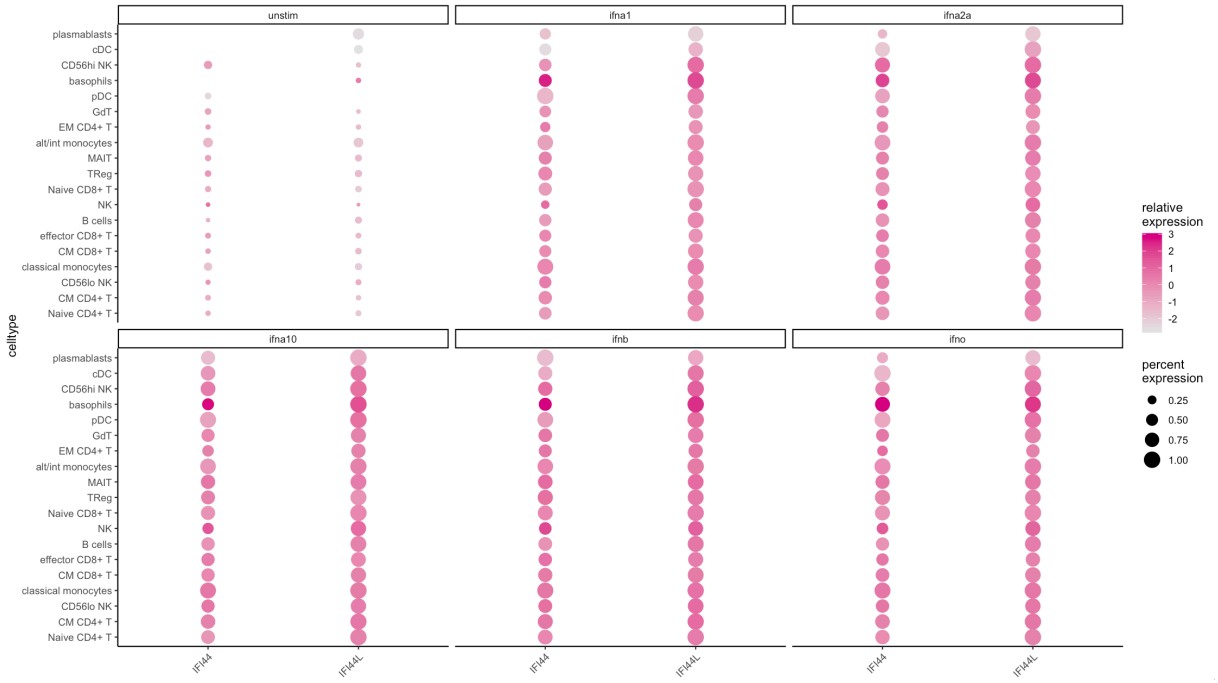


Figure S2: *IFI44* and *IFI44L* are highly expressed in most cell types in response to all subtypes of type I IFN.

Dot plot accompanying Figure 3.1A.

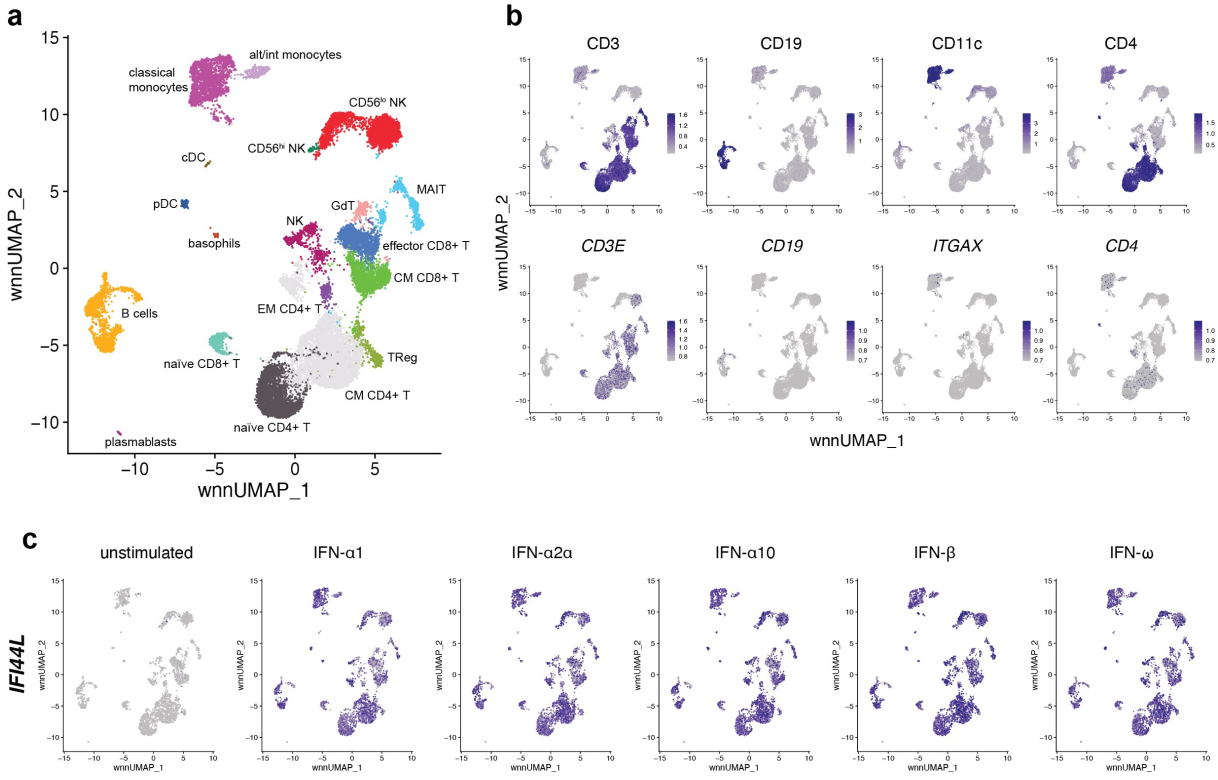


Figure S3: Single-cell expression of *IFI44L* in PBMCs.

Single-cell RNA sequencing of PBMCs after 24-hours of stimulation with 250U/mL of recombinant type I IFN. Dataset available via the IFN Resource Database.

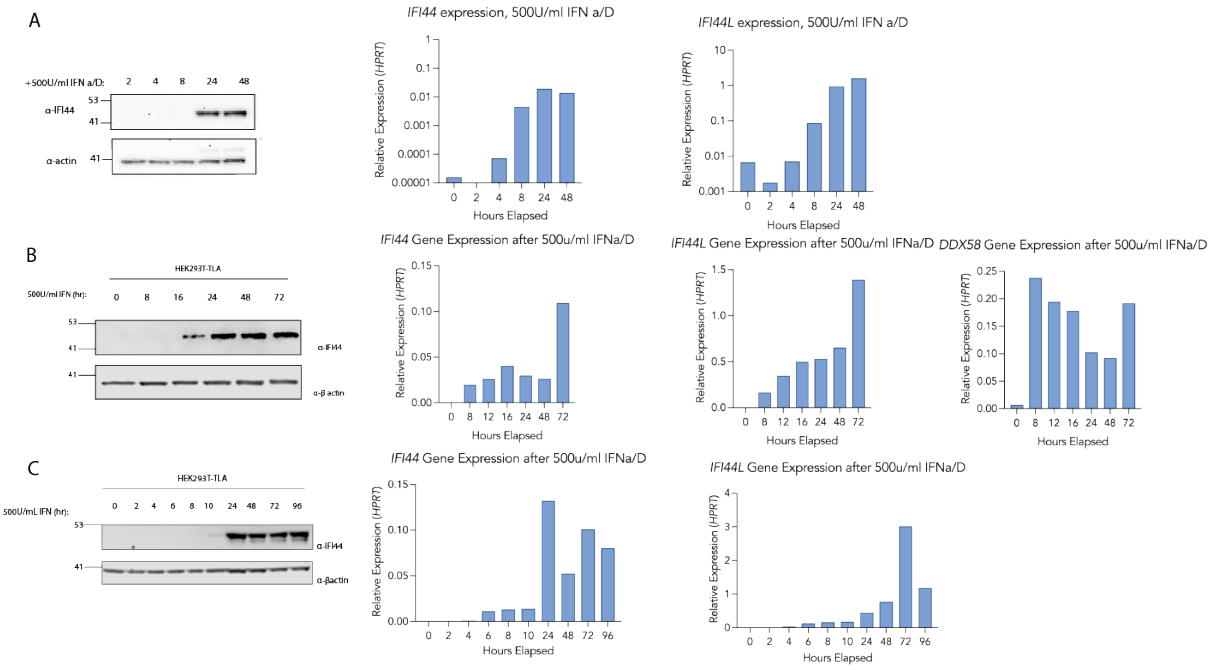


Figure S4: *IFI44* and *IFI44L* are late ISGs.

A-C. HEK293T cells were stimulated with 500U/mL of recombinant universal type I IFN, and lysed in RIPA buffer or Buffer RLT plus at 0 hr, 8 hr, 16 hr, 24 hr, 48 hr and 72 hr. Expression of IFI44 was detected through western blot using an endogenous α-IFI44 antibody, or through RT-qPCR with Taqman probes for the indicated genes. Each panel A-C demonstrates one independent repeat, with three total.

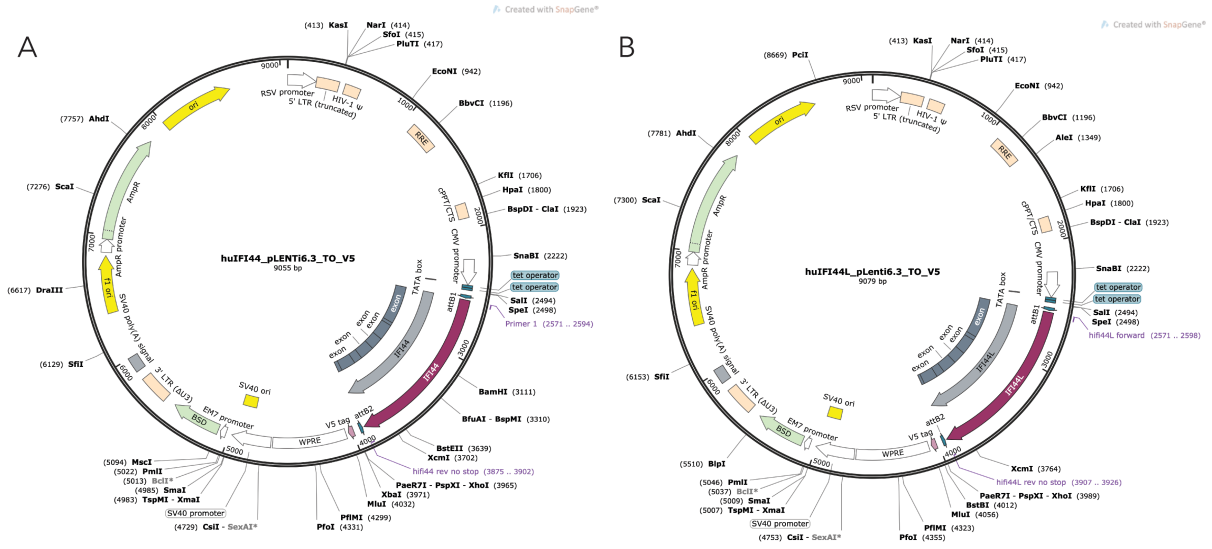


Figure S5: Plasmid maps for pLenti6.3 constructs.

A. Plasmid map for pLenti6.3/IFI44. **B.** Plasmid map for pLenti6.3/IFI44L. (A-B) Created with SnapGene.

Genes Downregulated in the spleen and liver of *Ifi44*$^{-/-}$ mice

Enbp1l1	EH Domain Binding Protein 1 Like 1. Predicted to be involved in actin cytoskeleton organization.
Cenpf	Centromere protein F. Associates with the centromere-kinetochore complex in the late G2 phase until anaphase, then to the spindle midzon in late anaphase and telophase, respectively.
Ifi44	Interferon-induced protein 44.
Stmn1	Involved in the regulation of the microtubule (MT) filament system by destabilizing microtubules.
Mki67	Encodes a nuclear protein required to maintain individual mitotic chromosomes, preventing the disassembly into chromatin.
Aspm	Assembly factor for spindle microtubles. Involved in mitotic spindle regulation.
Kif15	Kinesin-like protein. Plus-end directed kinesin-like motor enzyme involved in mitotic spindle assembly.
Ckap2	Cytoskeleton-associated protein 2. Possesses microtubule stabilizing properties. Involved in regulating aneuploidy, cell cycling, and cell death in a p53/TP53-dependent manner.
Ide	Insulin-degrading enzyme. Plays a role in intracellular signalling through degrading insulin and similar molecules such as APP peptides.
H2ac24	H2A clustered histone 24.

Figure S6: Differentially expressed genes in *Ifi44*$^{-/-}$ mice shared between spleens and livers. Top ten differentially expressed genes shared between spleens and livers in *Ifi44*$^{-/-}$ mice.

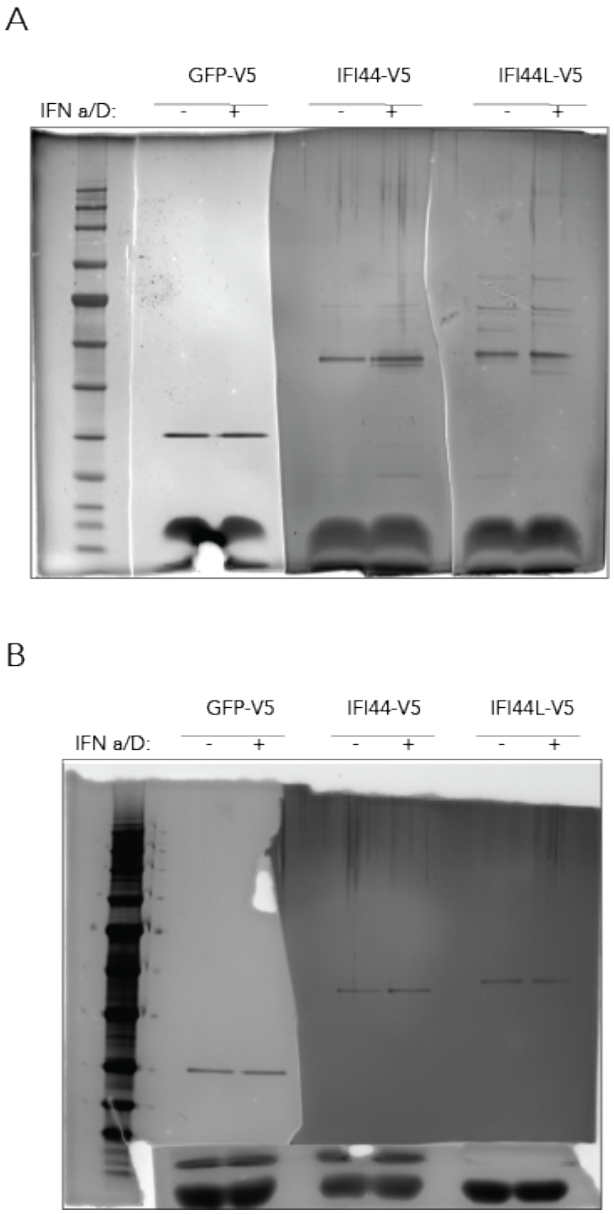


Figure S7: Immunoprecipitation of IFI44 and IFI44L with gentle NP40-based lysis buffer gives rise to inconsistent results.

A, B. HEK293T cells transiently transfected with IFI44, IFI44L or GFP were stimulated with 500 U/mL IFN a/D or media for 19 hours and then lysed and incubated with protein G Dynabeads conjugated to V5 antibody. Input, unbound and bound fractions were collected for downstream processing. Silver nitrate staining in two separate repeats in which cells were lysed with a gentle NP40 lysis buffer (the third repeat is shown in Figure 3.9 C).

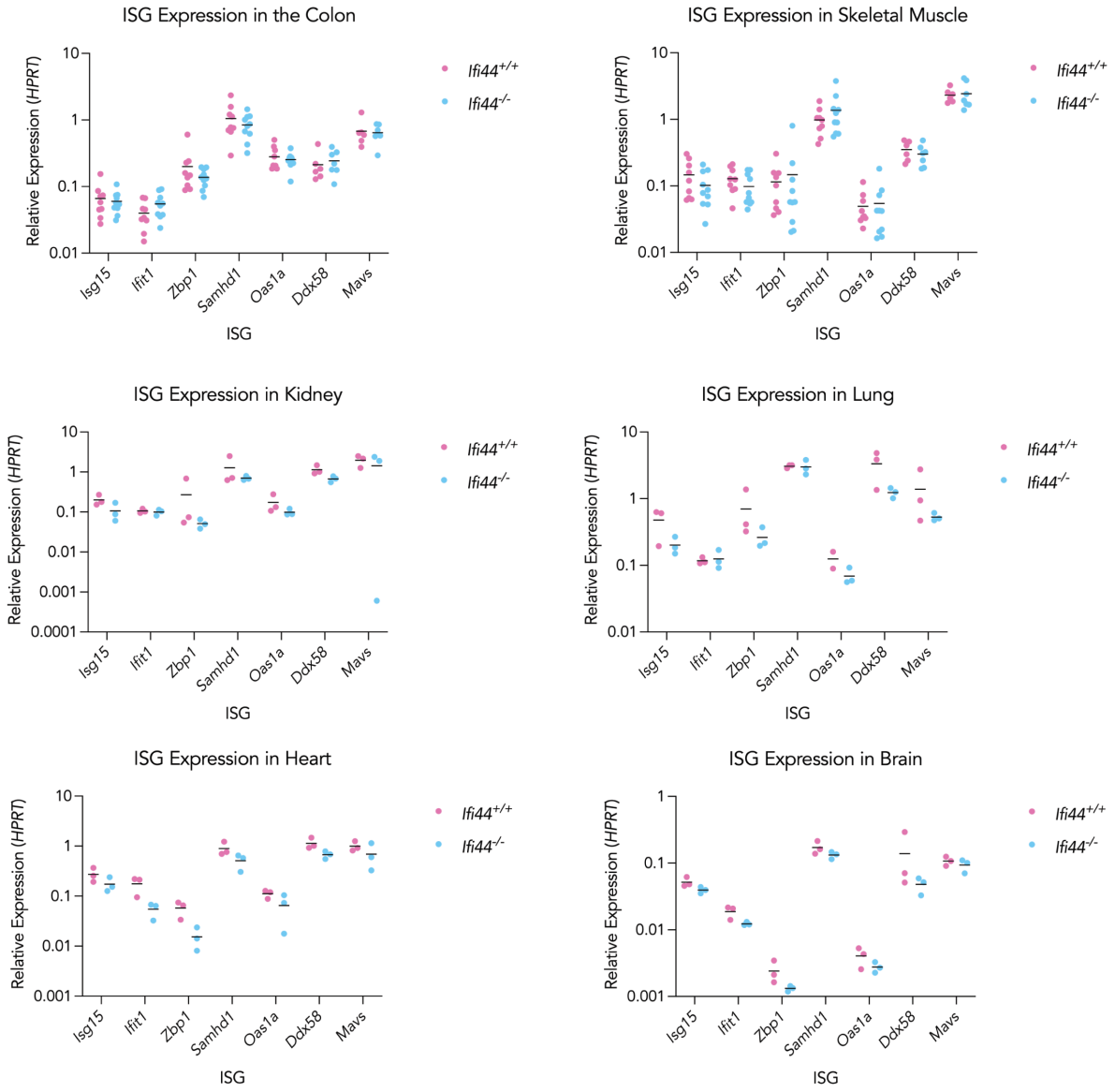


Figure S8: *Ifi44*$^{-/-}$ organs do not display an ISG signature.

RNA was isolated from *Ifi44*$^{+/+}$ and *Ifi44*$^{-/-}$ organs and RT-qPCR performed for the indicated genes. Each data point represents an individual biological replicate and is the average of two technical replicates.

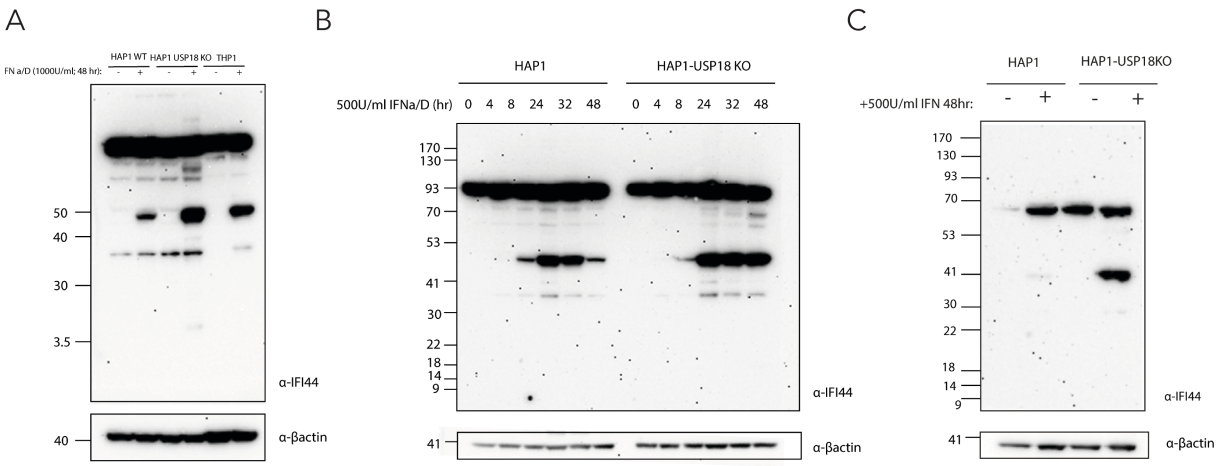


Figure S9: IFI44 is ISGylated.

All three repeats from Figure 4.2 are depicted here.

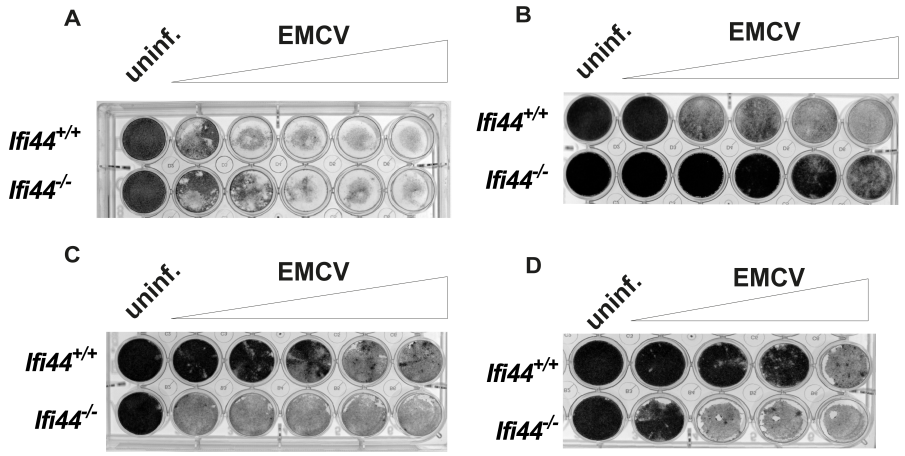


Figure S10: The role of mouse *Ifi44* in EMCV infection is inconclusive.

A-D. *Ifi44*$^{+/+}$ and *Ifi44*$^{-/-}$ immortalised MEFs were pre-treated with 0 U/mL or 100 U/mL of recombinant universal type I IFN (IFN a/D) for 24 hours and then infected with a 5-fold dilution series of EMCV, from 0.01 MOI to 1.6x10-5 MOI. After 24 hours, cells were fixed with 1:4 formaldehyde and stained with 0.05% crystal violet (CV), then plates were washed, dried and imaged. (A-D) each represent one independent experiment, culminating to four biological repeats.

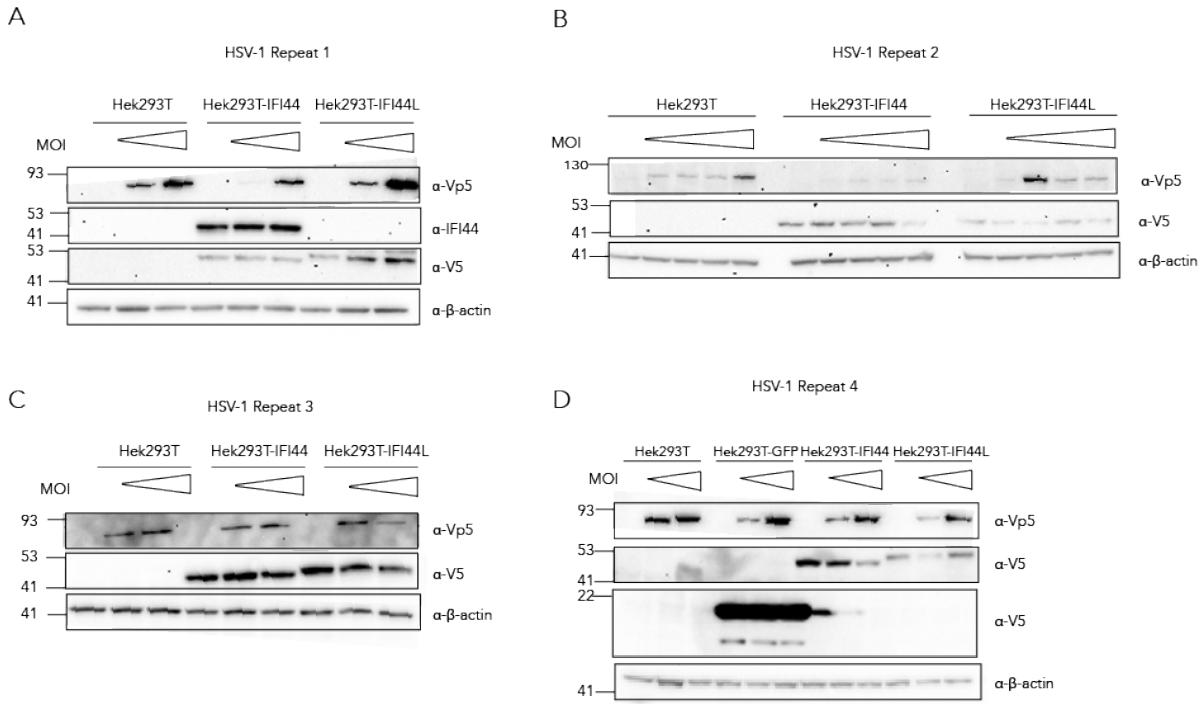


Figure S11: Overexpression of IFI44/L does not affect HSV-1 viral protein expression.

A-D. HEK293T cells stably overexpressing IFI44, IFI44L or GFP via lentiviral transduction and blasticidin selection were infected with HSV-1 at MOI 0.01 or 0.02, or uninfected cells underwent a media change. After 48 hours, cells were lysed in RIPA buffer and protein expression of viral proteins were detected by western blot using antibodies detecting endogenous proteins. (A-D) each represent one independent experiment, culminating to four biological repeats.

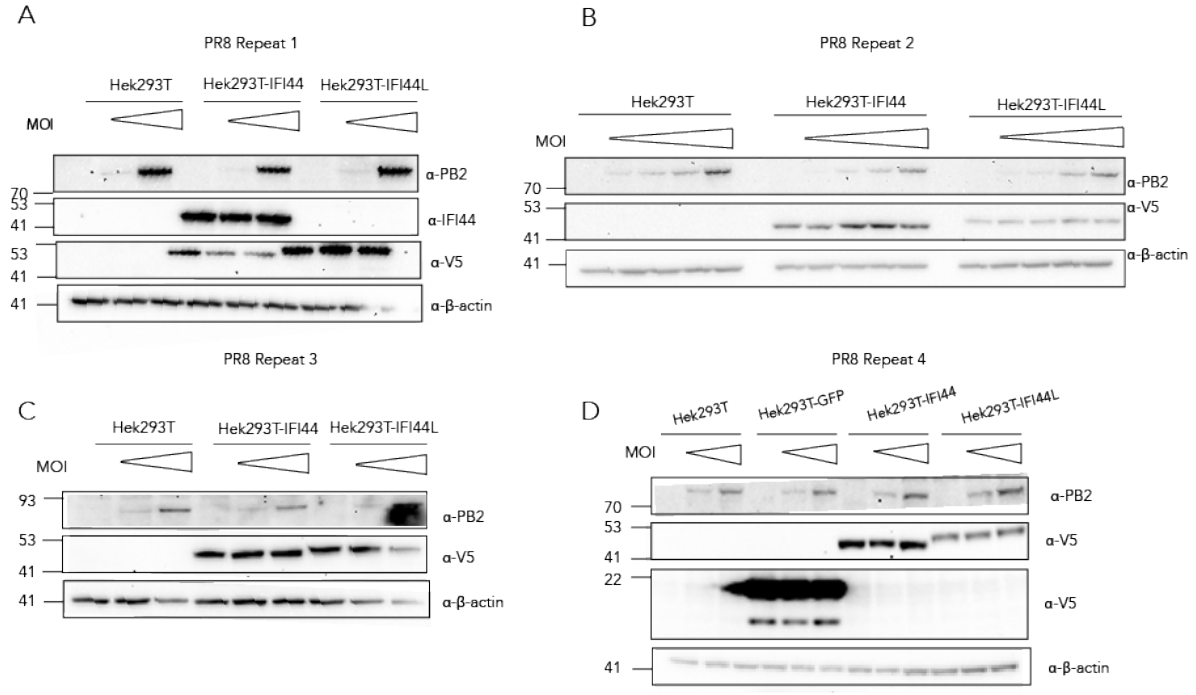


Figure S12: Overexpression of IFI44/L does not affect PR8 viral protein expression.

A-D. HEK293T cells stably overexpressing IFI44, IFI44L or GFP via lentiviral transduction and blasticidin selection were infected with PR8 at MOI 1 or 10, or uninfected cells underwent a media change. After 48 hours, cells were lysed in RIPA buffer and protein expression of viral proteins were detected by western blot using antibodies detecting endogenous proteins. (A-D) each represent one independent experiment, culminating to four biological repeats.

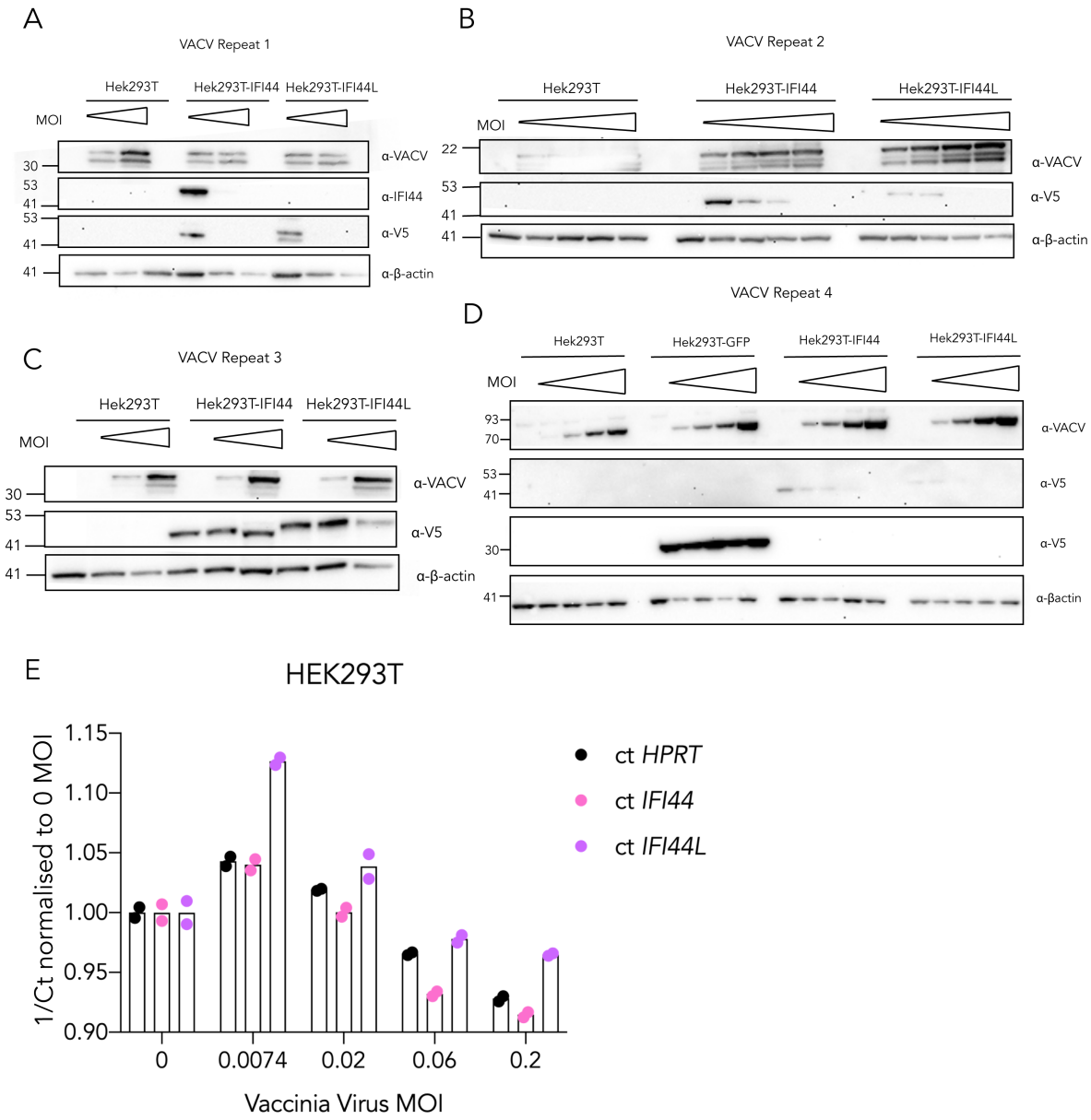


Figure S13: VACV degrades IFI44 and IFI44L.

A-D. HEK293T cells stably overexpressing IFI44, IFI44L or GFP via lentiviral transduction and blasticidin selection were infected with VACV WR at MOI 0.02 or 0.2, or uninfected cells underwent a media change. After 48 hours, cells were lysed in RIPA buffer and protein expression of viral proteins were detected by western blot using antibodies detecting endogenous proteins. **E.** Matched RNA samples were isolated from the experiment in (D), and RT-qPCR performed for the indicated probes. (A-D) each represent one independent experiment, culminating to four biological repeats. (E) One independent experiment.

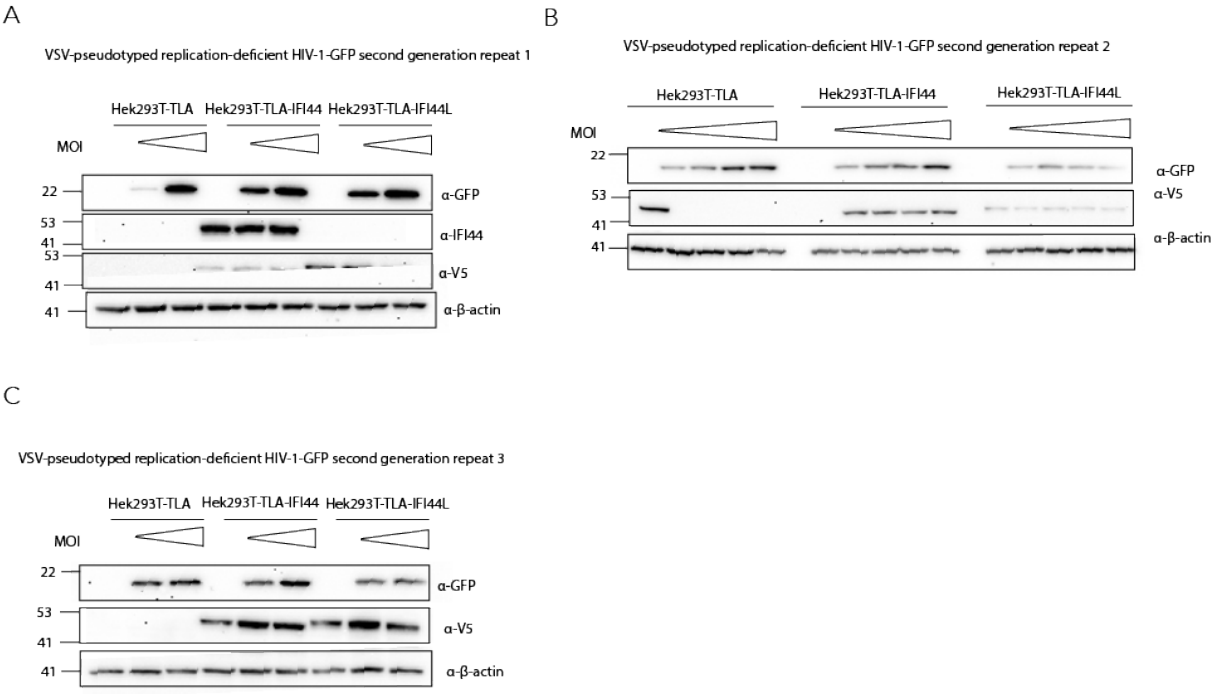


Figure S14: Overexpression of IFI44/L does not affect HIV-1 viral protein expression.

A-C. HEK293T cells stably overexpressing IFI44, IFI44L or GFP via lentiviral transduction and blasticidin selection were infected with VSV-pseudotyped HIV-1-GFP at 1:500 or 1:250, or uninfected cells underwent a media change. After 48 hours, cells were lysed in RIPA buffer and protein expression of viral proteins were detected by western blot using antibodies detecting endogenous proteins. (A-C) each represent one independent experiment, culminating to three biological repeats.

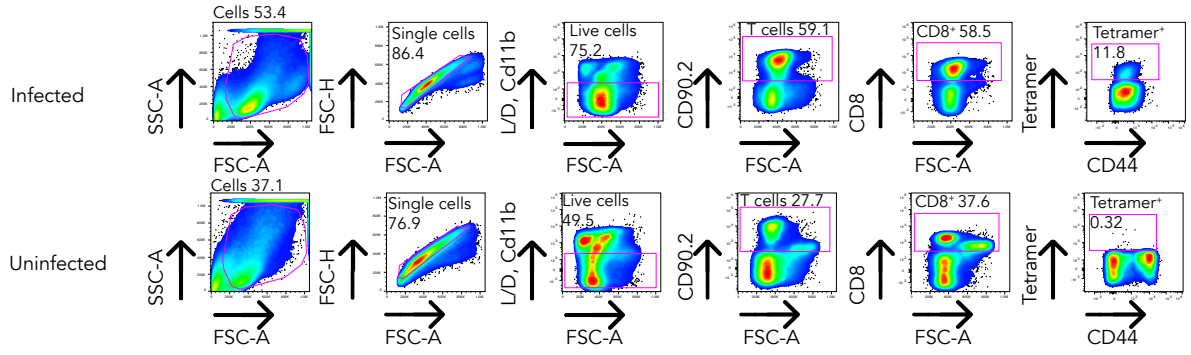


Figure S15: Gating strategy in murine lung and spleen samples for tetramer-specific CD8$^+$ T cells.

Gating strategy for Figure 4.9D, E.

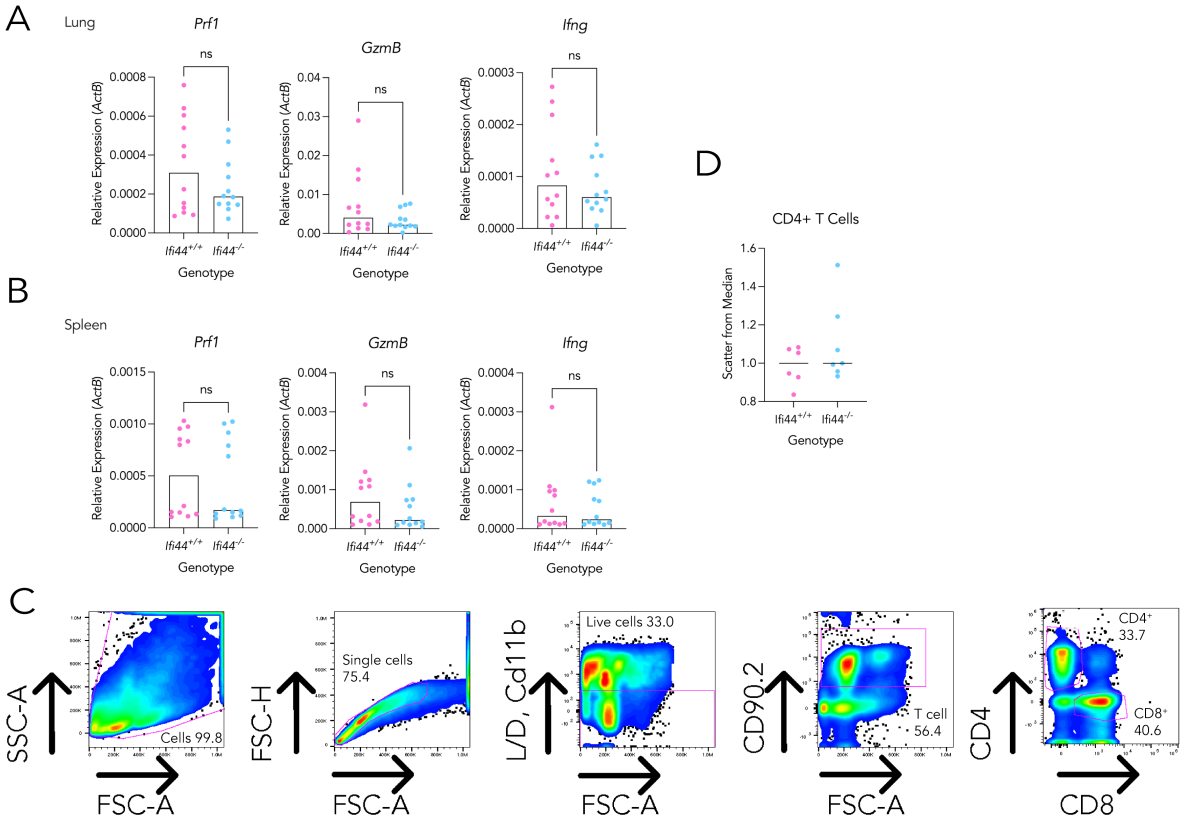


Figure S16: X-31 infected *Ifi44*$^{-/-}$ mice show no differences in the T cell compartment.

Mice were infected intranasally with 0.04 HAU IAV/X-31 or PBS and sacrificed at day 10 post infection. **A-B.** RNA was extracted from lung and spleen samples, and RT-qPCR performed for the indicated genes. **C.** Gating strategy for determining CD4^{+} T cells. **D.** CD4^{+} T cell abundance. (A-B) Each data point represents one biological replicate and the average of two technical replicates. Data represents two independent experiments, pooled. (D) Each data point represents one biological replicate.

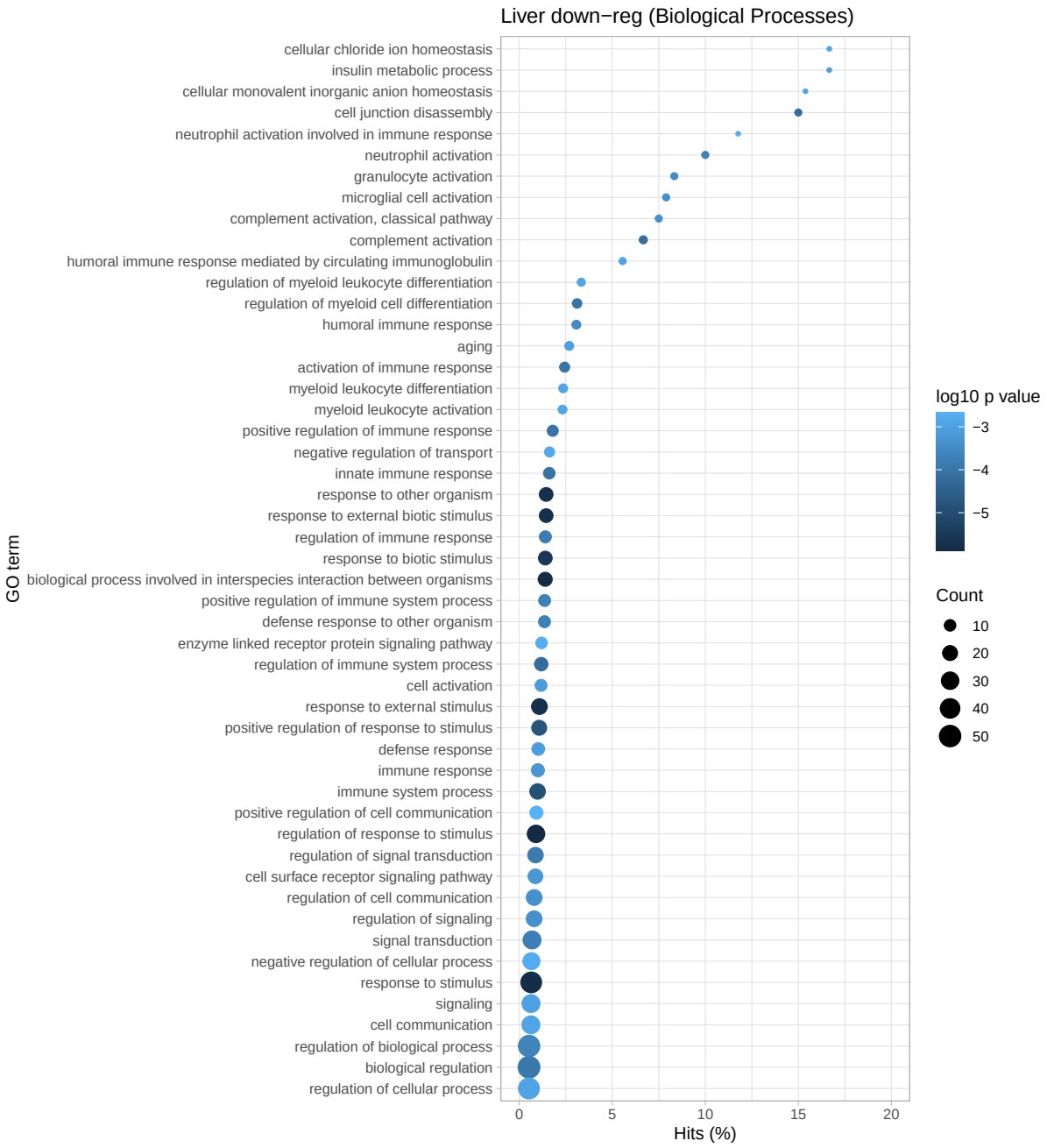


Figure S17: Gene ontology analysis on downregulated genes in *Ifi44*$^{-/-}$ livers.

A. Gene ontology analysis was performed on differentially expressed genes as identified by RNA sequencing using the gprofiler package (56), by Rachel Rigby. These were then filtered to only include categories containing more than 10 genes. The Y-axis shows the biological process GO term, while the X-axis annotates the % of genes present in the GO category that are differentially expressed in *Ifi44*$^{-/-}$ mice. The colour of the circle represents how significant the differential expression is, and the size of the circle denotes how many genes in the GO category are present.

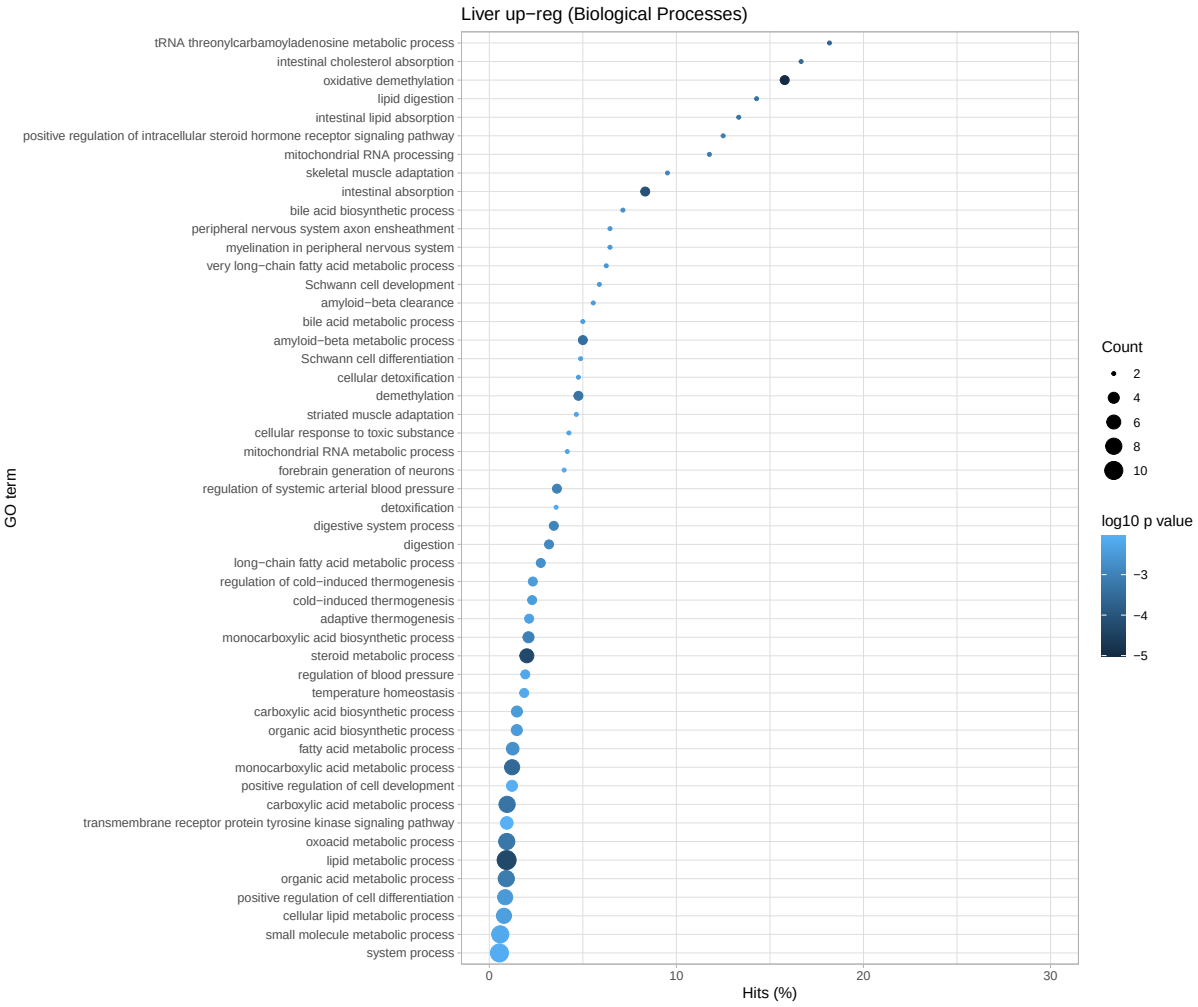


Figure S18: Gene ontology analysis on upregulated genes in *Ifi44*$^{-/-}$ livers.

Analysis performed as in Figure S17.

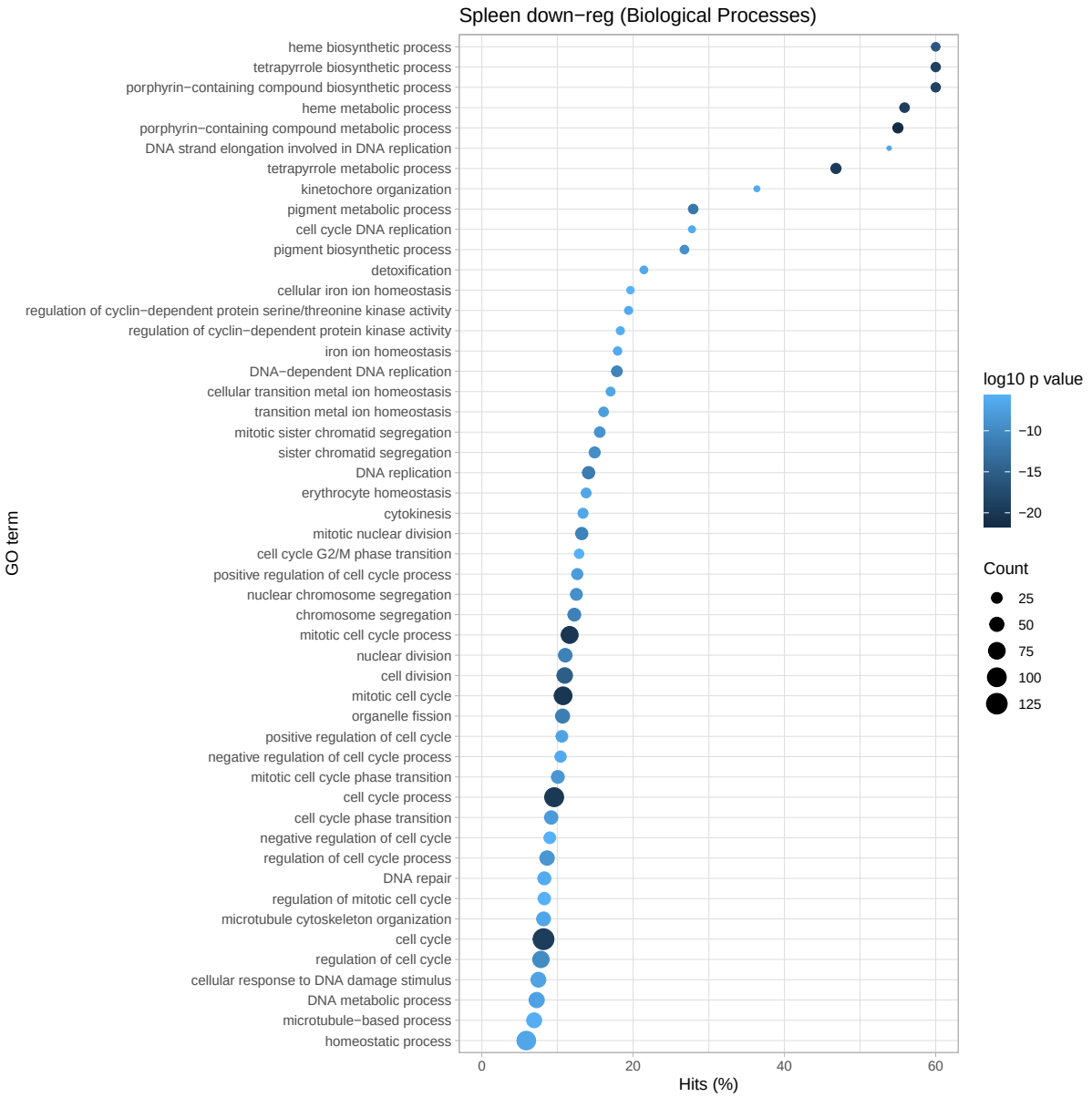


Figure S19: Gene ontology analysis on downregulated genes in *Ifi44*$^{-/-}$ spleens.

Analysis performed as in Figure S17.

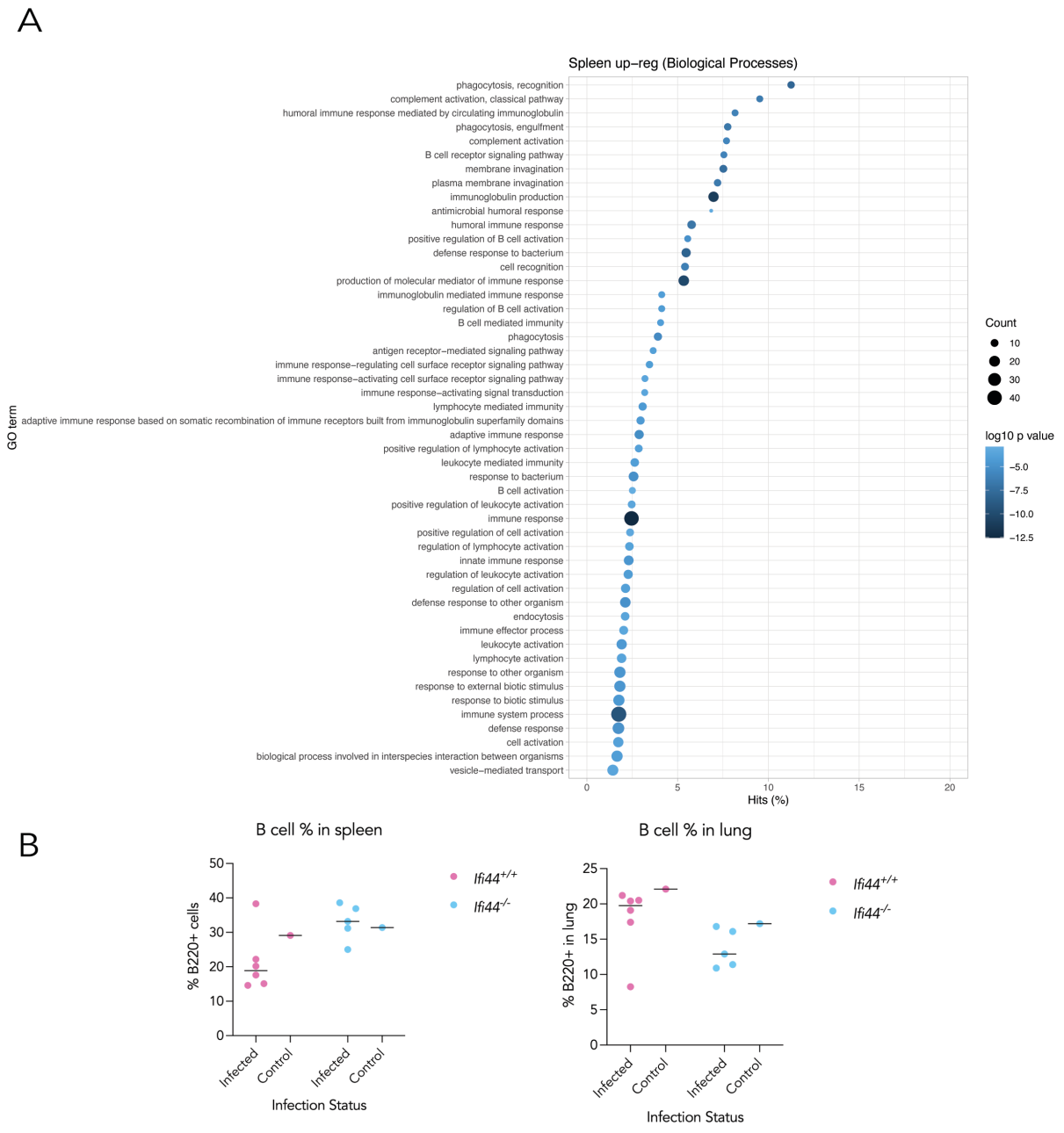


Figure S20: Gene ontology analysis on upregulated genes in *Ifi44*$^{-/-}$ spleens.

A. Analysis performed as in Figure S17. **B,C.** *Ifi44*$^{+/+}$ and *Ifi44*$^{-/-}$ mice were infected intranasally with 0.04 HAU IAV/X-31 or PBS and sacrificed 3 days post-infection. Lungs and spleens were enzymatically digested, and resulting cellular suspensions stained and fixed for flow cytometry. Cellular populations were analysed on an Attune flow cytometer. (B, C) Each data point represents one biological replicate.

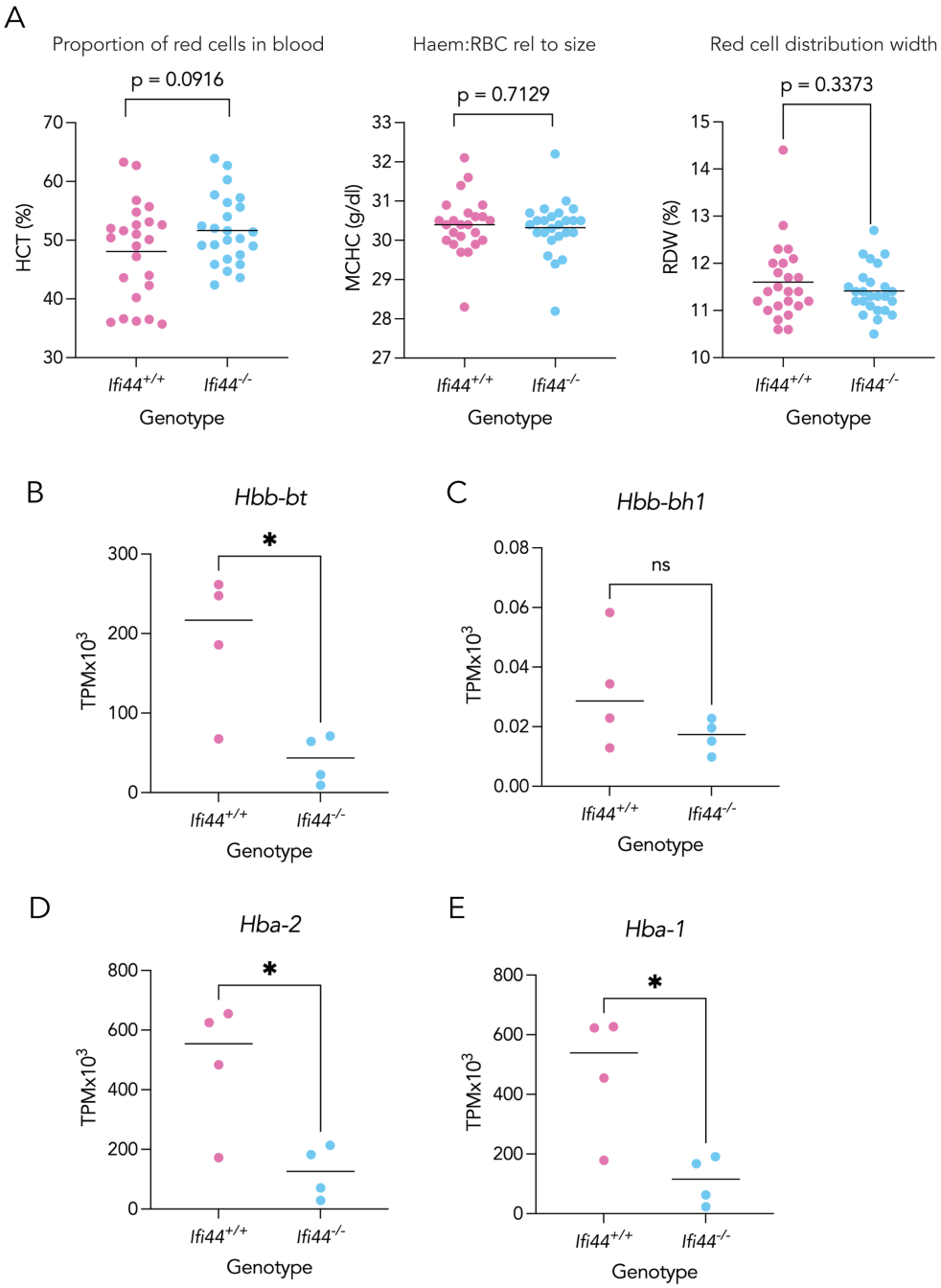


Figure S21: Haemoglobin genes are downregulated in *Ifi44*$^{-/-}$ spleens, but RBCs are loaded with similar levels of haem relative to their size.

A. *Ifi44*$^{+/+}$ and *Ifi44*$^{-/-}$ mice were sacrificed through exsanguination under terminal anaesthesia, and blood collected into EDTA-coated microtainers to prevent clotting. Blood was then analysed using a Pentra ES-60 machine. **B-E.** Analysis performed as in Figure S17. (A) Data is pooled from six independent experiments have been pooled. (A-E) Statistical analysis was performed using unpaired T-test. *=p<0.05, **=p<0.01, ***=p<0.001, ****=p<0.0001, ns=not significant.

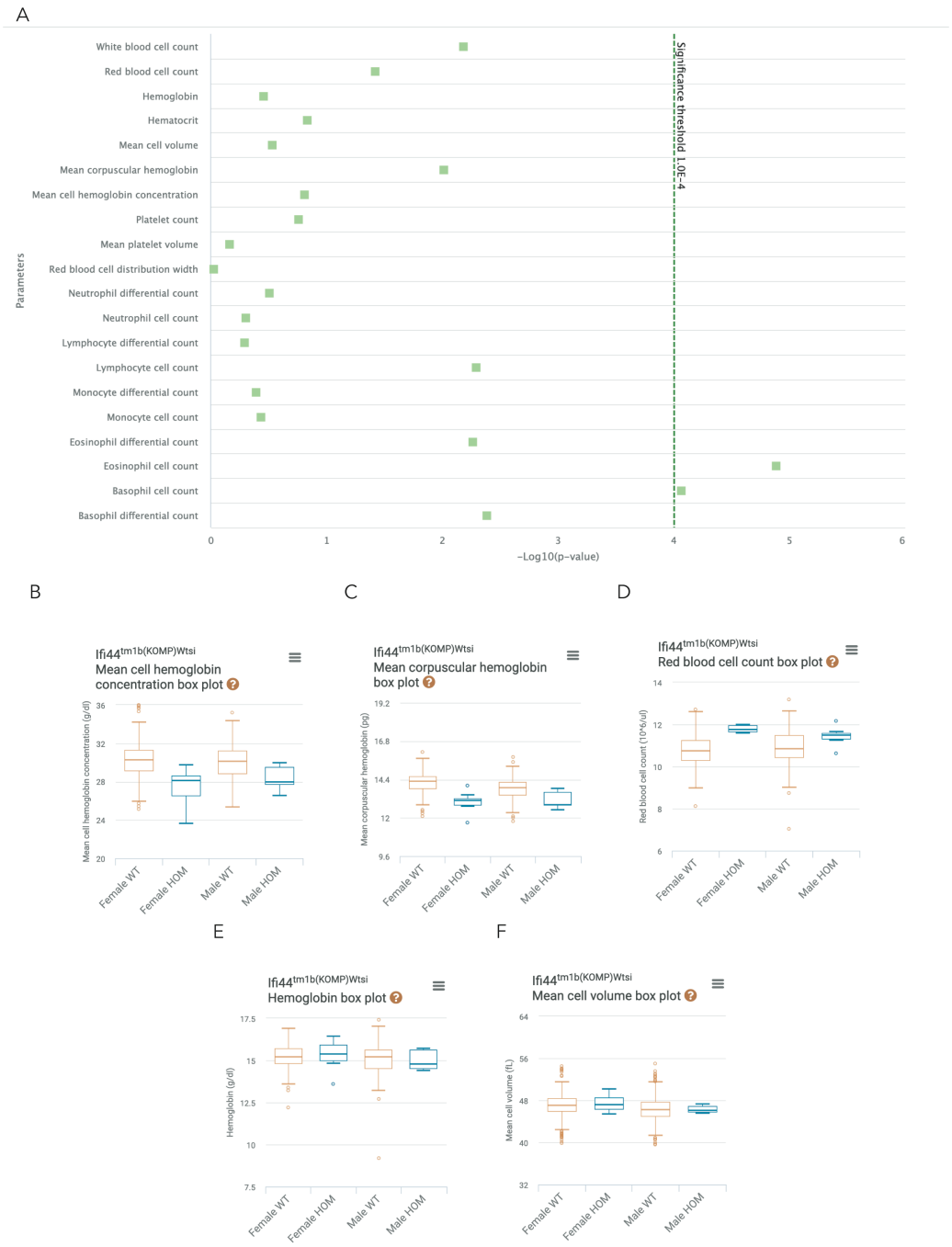


Figure S22: The International Mouse Phenotyping Consortium.

A. *Ifi44*$^{-/-}$ mice were generated on a C57 BL/6 background and phenotyped by the International Mouse Phenotyping Consortium (8, 9). **B-F.** Blood parameters for 7F, 7M *Ifi44*$^{-/-}$ mice vs 401F and 352M controls.

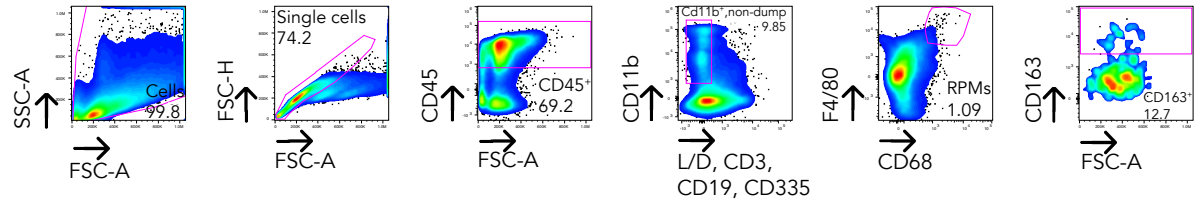


Figure S23: Gating strategy for RPMs.

Representative gating strategy for identifying RPMs.

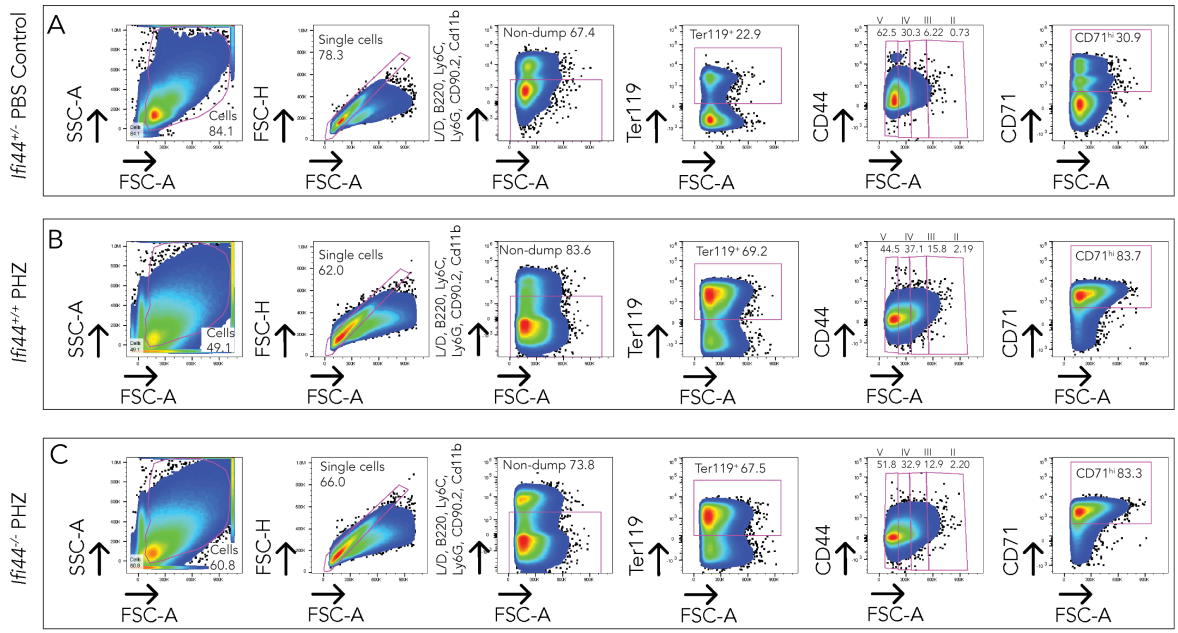


Figure S24: Splenic erythropoiesis gating strategy.

A-C. *Ifi44*$^{+/+}$ and *Ifi44*$^{-/-}$ mice were injected intraperitoneally with 0.08 mg/ g body weight PHZ on day 0 and day 2. On day 6, mice were sacrificed through exsanguination under terminal anaesthesia, and their spleens harvested. Spleens were enzymatically digested, and cell populations determined using an LSR Fortessa X50 flow cytometer.

Supplementary Table

The following is a Supplementary Table showing all reagents used in this study.

Table 6.1: Reagents used in this study

Reagent	Supplier	Cat. Number
10X Trypsin	ThermoFischer	15090046
3X FLAG ekution peptide	Cambridge Bioscience Ltd	4046200
8-well µslide chambers	Ibidi	80806
Amber microtainers	BD Biosciences	12937656
ATP	New England Biolabs	p0756L
BD Cytofix/Cytoperm™	BD Biosciences	554714
Blasticidin S HCl	ThermoFischer	A1113903
BLUeye Prestained Protein Ladder	Sigma Aldrich	94964
BSA	Sigma Aldrich	A7906
Cell Titre Glo Kit	Promega	G7571
Chloroform	SERVA	39543.01
CMC	Sigma Aldrich	21902
Collagen from calf skin	Sigma Aldrich	C8919
Collagenase type II	Rockland	MB-123-0050
Compensation Particles Set	BD Biosciences	552845
Crystal Violet Stain	Sigma Aldrich	HT90132
dATP	Promega	U1201
DMEM, GlutaMAX supplement	Gibco	31966047
DMSO	Sigma Aldrich	D8418
DNase I Bovine Pancreas	Sigma Aldrich	D4263
dNTP Mix	ThermoFischer	R0191
DMEM	Gibco	11965092
Dynabeads™ Protein G	Invitrogen	10004D
eBioscience™ Foxp3 / Transcription Factor Staining Buffer Set	Invitrogen	0052300
EDTA-coated microtainers	BD Biosciences	10346134
ELISA Stop Solution	ThermoFischer	SS03
ezDNase	ThermoFischer	11766051

Table 6.1: Reagents used in this study

Reagent	Supplier	Cat. Number
FastAP Thermosensitive Alkaline Phosphatase	ThermoFischer	FD0454
FastDigest BsmBI	ThermoFisher	C737303
Ferrostatin-1	Sigma Aldrich	SML0583
Fixation Buffer	Biolegend	420801
Foetal Calf Serum	Biosera	FB1001/500; batch 018BS695
Formaldehyde	Sigma Aldrich	252549
Fugene 6	Promega	E2692
Geneticin G418 Sulfate	Gibco	10131035
GO Taq DNA polymerase	Promega	M712B
Hemin	Sigma-Aldrich	H9039-1G
Herculase II fusion DNA polymerase	Aglient Technologies	600677
IL-1β ELISA	Thermo Fischer	88-7013-22
Iodoacetamide	Promega	VB1010
Iron Assay Kit	Sigma Aldrich	MAK025-1KT
L-Glutamine	Gibco	25030081
LDH Release Assay	Promega	J2380
Lipofectamine-2000	Invitrogen	11668019
LIVE/DEAD™ Fixable blue cell stain kit	Invitrogen	L34961
LIVE/DEAD™ Fixable far red stain kit	Invitrogen	L34973
LIVE/DEAD™ Fixable NIR stain kit	Invitrogen	L34975
LIVE/DEAD™ Fixable violet cell stain kit	Invitrogen	L34964
LPS	Sigma Aldrich	L7770
LR clonase II enzyme mix	Invitrogen	12538120
MEM Non Essential Amino Acids Solution 100X	ThermoFischer	11140050
MG132	Sigma Aldrich	M8699
Midiprep kit	Qiagen	12643
Miniprep kit	Qiagen	27106

Table 6.1: Reagents used in this study

Reagent	Supplier	Cat. Number
Mounting medium with DAPI	Ibidi	50011
Mouse IL-1β Uncoated ELISA Kit	Invitrogen	88701322
NEB Stable Competent *E. coli*	New England Biolabs	C3040H
Neutral buffered formalin	Sigma Aldrich	HT501128
Nitrocellulose membrane	Bio-Rad	1620112
NuPAGE LDS Sample Buffer	Invitrogen	NP0007
NuPAGE MOPS-SDS Running Buffer	Invitrogen	NP000102
NuPAGE Novex 4-12% Bis-TRIS gel	Invitrogen	NP0321BOX
OligodT	ThermoFischer	18418012
Pen/Strep	Sigma Aldrich	P0781
Phenylhydrazine Hydrochloride	Invitrogen	114715
Pierce BCA Protein Assay Kit	Invitrogen	23228
Pierce Silver Stain for Mass Spectrometry	Invitrogen	24600
Ponceau	Sigma-Aldrich	P7170
Precellys homogenising tubes	Precelleys	4310170
Propidium Iodide	Sigma Aldrich	P4170
Protease Inhibitor Cocktail	Cell Signalling Technology	5871S
Proteinase K	ThermoFischer	EO0491
Puromycin Dihydrochloride	ThermoFischer	A1113803
QIAquick gel extraction kit	Qiagen	28704
QIAshredder	Qiagen	79656
R848	InvivoGen	r183731
Random Hexamers	Invitrogen	79236
Red Blood Cell Lysis Buffer	Sigma Aldrich	R7757

Table 6.1: Reagents used in this study

Reagent	Supplier	Cat. Number
RNA ScreenTape devices	Aglient Technologies	50675576
RNA ScreenTape Ladder	Aglient Technologies	50675578
RNA ScreenTape Sample Buffer	Aglient Technologies	50675577
RNA later	Invitrogen	R0191
RNase A	Sigma Aldrich	R4642
RNeasy mini Kit	Qiagen	74136
ROS Glo Kit	Promega	G8820
RPMI	Gibco	11875093
RSL3	Invitrogen	SML2234
S-Trap	Profiti	NC1828287
Skimmed milk powder	Sigma Aldrich	70166
SOCS media	ThermoFischer	15544034
Stbl3 bacteria	Invitrogen	C737303
Superscript III reverse transcriptase	Invitrogen	18080044
T4 DNA ligase	New England Biolabs	M0202S
T4 Polynucleotide kinase	New England Biolabs	M0201L
TaqMan Fast PCR Master Mix	Applied Biosystems	4444557
Tetramer for IAV NP (ASNENMETM)	NIH Tetramer facility	366-374
Triton-X 100	ThermoFischer	BP151100
TRIzol reagent	Invitrogen	15596026
Trypsin-EDTA (0.25%)	Gibco	25200056
Tween-20	Sigma-Aldrich	P9416
UltraPure DNase/RNase-Free Distilled Water	ThermoFischer	10977049
UltraPure PBS pH 7.4	ThermoFischer	10010056
Universal Type I IFN (IFN a/D)	Bio-Techne	112002
V5 synthetic peptide	Stratech Scientific	PP100378
Western blotting filter paper 8.5 cm	ThermoFischer	88610

Table 6.1: Reagents used in this study

Reagent	Supplier	Cat. Number
Western Lightening Plus ECL	PerkinElmer	NEL104001EA
YoYo3 Iodide	Invitrogen	Y3606